UNIVERSITY OF BIRMINGHAM

NEGATIVE IMPEDANCE CONVERTERS FOR ANTENNA MATCHING

By

Oluwabunmi O. Tade

A Thesis submitted to the College of

Engineering and Physical Sciences, University

of Birmingham, for the degree of

DOCTOR OF PHILOSOPHY

School of Electronics, Electrical, & Computer Engineering,

University of Birmingham, Edgbaston,

Birmingham, B15 2TT,

U.K.

ABSTRACT

This thesis describes research into Negative Impedance Converters (NIC) for antenna matching. There are many applications that require small wideband antennas, from mobile phones and devices which are being required to cover larger frequency bands to cognitive radios that are expected to operate within any frequency band with minimum reconfiguration. However there are fundamental limits on antennas such as the Chu-Harrington and Bode-Fano that restrict the available bandwidths obtainable from small antennas and antennas matched using conventional reactive elements that obey Foster's theorem. However, non-Foster elements have been shown to provide wideband matching of antennas independent of frequency. Non-Foster elements can be realised using NICs.

In this thesis, a non-Foster element is designed based on Linvill's model. One of the drawbacks on NICs is stability and this has limited the top achievable frequency. A new stability analysis is developed and reported in this thesis, and it is shown that this makes it possible to predict correctly the frequency of oscillation. It also leads to the development of a means via which stable NICs can be developed for any frequency range, which is demonstrated in the thesis. With the aid of the new stability analysis, a 1.5GHz NIC prototype is developed, operating up to 15 GHz, which is the highest frequency reported to date. Its performance in terms of noise and linearity are also characterised. Another novel NIC schematic is also introduced in the thesis; it makes use of a single transistor and a pair of coupled lines. Because of its use of a single transistor, stability is less critical and hence it is able to achieve a working frequency of 6GHz. It is also characterised for noise and linearity and its performance compared with the NIC based on Linvill's model. Reducing the stability concern makes it possible for the coupled line NIC to be integrated into a monopole. The experimental prototype described in the thesis shows the expected performance in terms of wideband matching at much lower frequency without loss of performance in gain. System implications of using NICs within an antenna system are also discussed.

DEDICATIONS

To God and my parents

ACKNOWLEDGEMENTS

I would like to say a special thank you to my supervisors Dr. Peter Gardner, Reader in Microwave Engineering and Professor Peter S. Hall for their supervision throughout my studies and their kind words of encouragements and support when the going got tough. I would also like to thank them for letting me sharing in their wealth of experience.

I would also like to thank all members of the Communication Engineering Research Group for their help and support over the last three years. Special thanks also goes to my other brilliant colleagues and very nice friends Dr. Yuriy Nechayev, Dr. Rijal Hamid, Dr. Zhen Hu, Dr. Ghaith Mansour, Fatemeh Norouzian, Jin Tang, Donya Jasteh, Mohammed Milani, Vahid Behzadan, Farid Zubir etc. With all your support and encouragement, my study life becomes happy in all respects!

I am also very grateful to Mr. Alan Yates for providing all the technical support in using the equipment and fabricating the PCBs for the active circuits and the integrated antenna and Mr. Warren Hay for workshop support.

Finally, I would like to give my deepest gratitude to my family; Engr. and Mrs. Tade, my sisters; Bukola and Funmilola; and Sandra for their unconditional support and love. Thank you for believing in me. Your generous support and boundless love mean the most to me.

PATENTS AND PUBLICATIONS

Publications

1) **O.O. Tade**, P. Gardner and P.S. Hall, “Antenna Bandwidth Broadening with a Negative Impedance Converter”. Accepted for publication in International Journal of Microwave and Wireless technologies, 2013.

2) P. Gardner, A. Feresidis, P. Hall, T. Jackson, **O. Tade**, M. Mavridou, Y. Kabiri and X. Gao, “Frequency Reconfiguration in Single and Dual Antenna Modules”, European Conference on Antennas and Propagation, April 2013.

3) **O. O. Tade**, P. Gardner and P. S. Hall, “Negative Impedance Converters for Broadband Antenna Matching”, European Microwave Conference, November, 2012.

4) **O.O. Tade**, P. Gardner and P.S. Hall, “1.5GHz Negative Impedance Converter”. IET 2nd Annual Active RF Devices, Circuits and Systems Seminar. 2012

5) **O. O. Tade**, P. Gardner and P. S. Hall, “Broadband Matching of Small Antennas using Negative Impedance Converters”, IEEE International Symposium on Antenna and Propagation and USNC-URSI National Radio Science meeting, July, 2012.

6) **O. O. Tade**, Z. H. Hu, P. Gardner and P. S. Hall, “Small antennas for cognitive radio using negative impedance converters”, 12th Annual Post Graduate Symposium on the Convergence of Telecommunications, Networking and Broadcasting (PGNet2011), Liverpool, UK. 2011.

TABLE OF CONTENT

LIST OF FIGURES

LIST OF TABLES

CHAPTER 1

INTRODUCTION

1.1 Background

There is a relationship between antenna size and the realisable bandwidth as defined by the Chu limits in [1]. The Chu limit gives the relationship between the radius of the circle that completely circumscribes an antenna and the Q of the antenna. However, McLean in [2] redefined how the Q of an antenna should be calculated, this is given in eq. 1.1.

$$Q = \frac{1}{(k^3a^3)} + \frac{1}{(ka)} \tag{1.1}$$

Where k is the wave number and a is the radius of a sphere that completely circumscribes the antenna as shown in Fig.1.1.

McLean's equation is a derivation from the original Chu Limits equations. There has also been a lot of research into means of improving the gain of an antenna through the use of matching networks but this is also bounded by the Harrington limits [3] on antenna as given in

$$\mathrm{G} = (\mathrm{ka})^2 + 2\mathrm{ka} \tag{1.2}$$

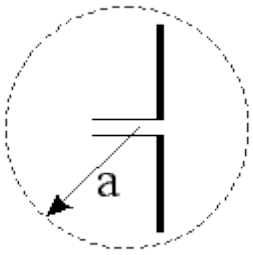

Fig.1 1 Antenna dimensioning using Chu's Limit

The Chu limit can be related to the antenna bandwidth by rewriting the Q of the antenna as shown in equation 1.3

$$Q = \frac{f_c}{\Delta f} = \frac{1}{\left(k^3 a^3\right)} + \frac{1}{(ka)} \qquad 1.3$$

Where f_c is the antenna centre frequency at resonance and Δf is the bandwidth if the antenna.

Comparing equation 1.1 with equation 1.3, it can be seen that reducing the radius of the sphere which translates to a physical reduction in the antenna size, the antenna bandwidth also reduces. The reducing in size means that the antenna radiation resistance also reduces and this in turn leads to a reduction the antenna efficiency. From eq. 1.2, it is clear that antenna gain is also proportional to the antenna size (a).

These two fundamental limits on antenna make it tough to have a small antenna with a low Q (wideband). However, there are existing and future applications that requires the use of wideband small antenna. These fundamental limits were defined for Foster elements but with the use of non-Foster elements as would be shown and discussed later in this thesis, it is possible to overcome these limitations.

1.1.1 Mobile phones – need for small antennas

Current mobile phones are required to work over increasingly large frequency bands from 470MHz to 2.4GHz covering a host of communications standards such as DVB-H, GSM 900, 1800, Wi-Fi, Bluetooth etc. There is also the size constraint in mobile devices which necessitates the use of small antennas and where possible the smallest number of antennas in a particular device to cover as much bandwidth as possible. With the current trends, it has been suggested that future mobile devices could have as many as 20 different antennas to cover the different required bands [4]. Prior methods for covering the increasing number of frequency bands include either the use of different antennas to cover the individual bands or a single antenna made reconfigurable with different matching networks like [5-6]. Manteuffel and Arnold in [6] used 17 different matching networks to match an antenna between 0.1GHz to 2.5GHz. The multiple matching networks however provide narrow instantaneous bandwidths. A better solution would be to have a small antenna which can cover these wide bandwidths and the transceiver frontend can then be made reconfigurable or be the ultimate software defined radio (SDR). SDRs are seen as a practical version of the Software radio (SR) first proposed by Mitola in [7]. His ideal SR would not include any analogue frontend component but will ultimately have the antenna and an Analogue to Digital Converter (ADC) in the receive chain and the transmit chain would consist of the Digital to Analogue Converter (DAC) and power amplifiers (PA) as shown in Fig.1.2. This meant that RF signals would have to be digitized without any down conversion. Digitizing at RF poses a high demand on the ADC therefore there is a need for some analogue signal processing such as down conversion from RF to baseband and some form of reconfigurable filtering [8].

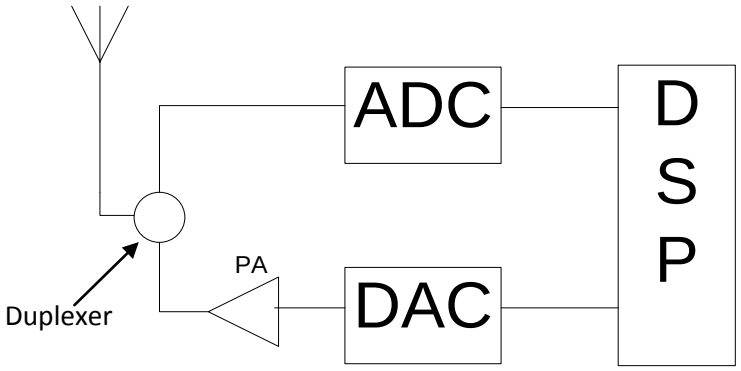

Fig.1.2 Software radio as envisioned by Mitola [6,8]

1.1.2 Cognitive radio – need for small antennas

Cognitive Radios (CR) resulted from an FCC frequency survey carried out between 30MHz and 3000MHz. This survey showed that within the licensed frequency bands, the spectrum was underutilised whereas the unlicensed bands showed high utilisation [9]. Therefore it was proposed to have transceivers which would opportunistically use these underutilised licensed frequency bands but will not cause harmful interference to the licensed user also referred to as Primary user (PU). In [10], a CR node is described as a wireless device that was aware of its surrounding and can adjust its operating parameters autonomously. In [8, 11], CR nodes are described as Software defined radio (SDR) that can additionally sense their environment. A block architecture of what a CR transceiver should look like is shown in Fig.1.3 [14]. The CR architecture shows two chains, the spectrum sensing chain and the transceiver chain. One of the primary requirements of CR is not to cause harmful interference to the PU. The Wireless Regional Area Network (IEEE 802.22) specifies that a CR node would need to detect the PU within two seconds of the PU becoming active [9].

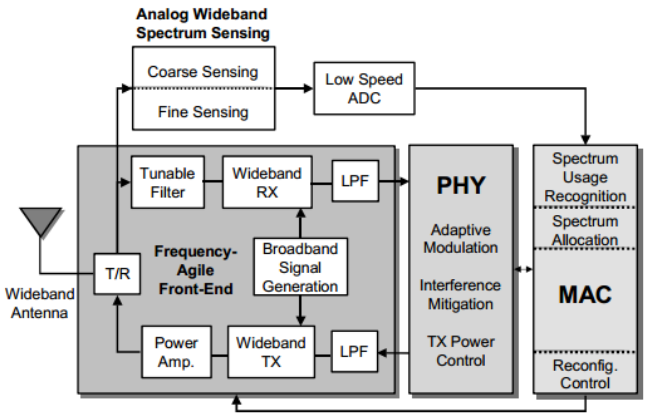

Fig.1.3 Cognitive Radio architecture [14]

From the definitions and requirements of CR nodes, it is clear that one of the key requirements is spectrum sensing. There have been numerous suggestions about how to perform spectrum sensing. One of the methods suggested involves all nodes performing spectrum sensing individually and then pooling the results together in a central node, which then redistributes the spectrum availability within the CR network [12]. This method requires extra complexities within the CR nodes as there is a need to either employ a stop and search mechanism or have a dedicated spectrum sensing chain. Ref [13] suggests spectrum sensing being performed by CR nodes not actively involved in communications but this could breakdown when all the nodes within the network becomes active. Alternatively, the central node could be the only node with spectrum sensing ability and other nodes relying on it for spectrum availability information [12]. This is a good solution but there is a higher possibility of interference with PU users because of the hidden terminal problem. The hidden terminal problem occurs when a terminal is visible from a wireless access point (AP), but not from other terminal communicating with that AP. This leads to difficulties in media access control and can also leads to interference between the two nodes. Therefore, there is still a need for

spectrum sensing being performed by individual terminals to avoid the hidden terminal problem and for CR nodes in ad hoc networks with no central node [12].

To perform spectrum sensing, wideband antennas are preferred because they give the ability to utilise the advances made in Digital Signal Processing (DSP) with concurrent baseband signal processing. Also the current social trend lends credence to the fact that CR nodes would ultimately be mobile and handheld hence they would also require small broadband antenna to function optimally. Therefore in Cognitive radio networks, there is definitely a great need for small wideband antennas.

1.2 Objectives

The objective of this research is to investigate means of achieving broad band small antennas for use either in mobile devices or in mobile cognitive radio nodes. Because these mobile devices are to operate over a wide frequency range, there is a need to have the matching networks operate over a wide frequency with high frequency cut-off points. CR nodes are known to be frequency nomadic therefore they do not benefit from frequency planning, hence they need highly linear CR nodes. With linearity a major challenge for CR nodes [14], the linearity of matching networks is important as these nodes would have to operate adjacent to other signals and not to cause any harmful interference as well as being immune to other signals.

1.3 Layout

The thesis consists of nine relatively short chapters. Overviews of the content of the chapters are given below. Chapter 1 contains the introduction and motivations for the research and the

need for small broadband antennas. It is also states the fundamental limitations of the small antennas and how this impacts on the state of antenna design. Chapter 2 contains a literature review into antenna matching, the use and limitation of passive antenna matching. It also highlights the use of non-Foster elements based matching networks, how these elements are realised using Negative Impedance Converters (NIC), the theory behind the NIC and the major limitation of the NIC which is stability. It also reviews the prior work into NICs and non-Foster matching network. Chapters 3, 4 and 5 present original simulation, design and measurement work to demonstrate and access: the potential of NICs achieved using the Linvill's two transistor schematic; the stability problems associated with the schematic; a new stability analysis method which can predict the oscillations in the Linvill's schematic and how the analysis helps in the design of stable NIC circuits. It also shows a realised Linvill's NIC prototype with the highest reported top frequency. Linearity and noise measurements were performed on this prototype. A new NIC circuit schematic is introduced in chapter 6, it makes use of a pair of coupled lines along with a transistor to realise an NIC. A stability analysis was done on the NIC. This NIC prototype was fully characterised with noise and linearity measurements. Because it is more stable when compared to the Linvill NIC and its layout design is simpler, it was possible to integrate it with an antenna. This NIC and antenna integration is described in chapter 7. The NIC matched antenna is compared with passively matching the same antenna and the antenna itself and it can be seen that the NIC matched antenna performs better than the alternatives without adverse effect on the gain. Chapter 8 described the possible means of integrating the NIC based matching network into a transceiver front end highlighting the different requirements and suggesting possible solutions. Chapter 9 has the conclusions of the thesis and the future work plans.

References

[1] L. J. Chu, "Physical limitations of omnidirectional antennas," *Journal of Applied Physics,* vol. 19, p. 13, December 1948.

[2] J. S. McLean, "A re-examination of the fundamental limits on the radiation Q of electrically small antennas," *Antennas and Propagation, IEEE Transactions on,* vol. 44, p. 672, 1996.

[3] R. F. Harrington, "Effect of Antenna Size on Gain, Bandwidth and Efficiency," *Journal of Research of the National Bureau of Standards - D. Radio Propagation,* vol. 64D, p. 12, june 29, 1959 1959.

[4] P. Vainikainen, J. Holopainen, C. Icheln, O. Kivekas, M. Kyro, M. Mustonen, S. Ranvier, R. Valkonen, and J. Villanen, "More than 20 antenna elements in future mobile phones, threat or opportunity?," in *Antennas and Propagation, 2009. EuCAP 2009. 3rd European Conference on*, 2009, pp. 2940-2943.

[5] Z. H. Hu, C. T. P. Song, J. Kelly, P. S. Hall, and P. Gardner, "Wide tunable dual-band reconfigurable antenna," *Electronics Letters,* vol. 45, pp. 1109-1110, 2009.

[6] D. Manteuffel and M. Arnold, "Considerations for Reconfigurable Multi-Standard Antennas for Mobile Terminals," in *Antenna Technology: Small Antennas and Novel Metamaterials, 2008. iWAT 2008. International Workshop on*, 2008, pp. 231-234.

[7] J. Mitola, "The software radio architecture," *Communications Magazine, IEEE,* vol. 33, pp. 26-38, 1995.

[8] F. K. Jondral, "Software Defined Radio - Basics and Evolution to Cognitive Radio," *EURASIP Journal on Wireless Communications and Networking,* pp. 275-283, 2005.

[9] C. Cordeiro, K. Challapali, D. Birru, and N. Sai Shankar, "IEEE 802.22: the first worldwide wireless standard based on cognitive radios," in *New Frontiers in Dynamic*

Spectrum Access Networks, 2005. DySPAN 2005. 2005 First IEEE International Symposium on, 2005, pp. 328-337.

[10] H. Harada, "A Software Defined Cognitive Radio Prototype," in *Personal, Indoor and Mobile Radio Communications, 2007. PIMRC 2007. IEEE 18th International Symposium on*, 2007, pp. 1-5.

[11] S. Haykin, "Cognitive radio: brain-empowered wireless communications," *Selected Areas in Communications, IEEE Journal on*, vol. 23, pp. 201-220, 2005.

[12] B. A. Fette, *Cognitive Radio Technology*, 1 ed.: Academic Press, 2009.

[13] S. H. Song, K. Hamdi, and K. B. Letaief, "Spectrum sensing with active cognitive systems," *Wireless Communications, IEEE Transactions on*, vol. 9, pp. 1849-1854, 2010.

[14] P. Marshall, *Quantitative Analysis of Cognitive Radio and Network Performance*: Artech House, 2010.

Chapter 2

LITERATURE REVIEW

2.1. Background

In recent years, the use of a matching network to resonate an antenna has become common practice. These matching networks usually involve the use of passive elements to resonate the antenna's reactive part. These passive elements are usually capacitors or inductors depending on whether the antenna is capacitive or inductive. Using these elements always results in narrow matched bandwidths. An example of an attempt to match an antenna passively is described in [1]. It had an antenna made up of coupling elements used to excite a PCB as shown in Fig.2.1. This PCB can act as the chassis of a mobile device and it uses different matching networks to optimize the coupling at different frequencies. The location of the matching network is also shown in Fig.2.1. To improve the total efficiency of the antenna beyond the estimated minimum requirement for different applications, 17 different matching networks were used to match the antenna between 0.1GHz and 2.5GHz. Figure.2.2 shows the antenna efficiency at the frequency bands and compares it to what is obtainable by the antenna itself without the different matching networks. This shows that the matched antenna not only require multiple matching networks but also requires the use of either tuneable elements and or switches within the antenna. The instantaneous bandwidths available are also very small as can be seen in Fig.2.2.

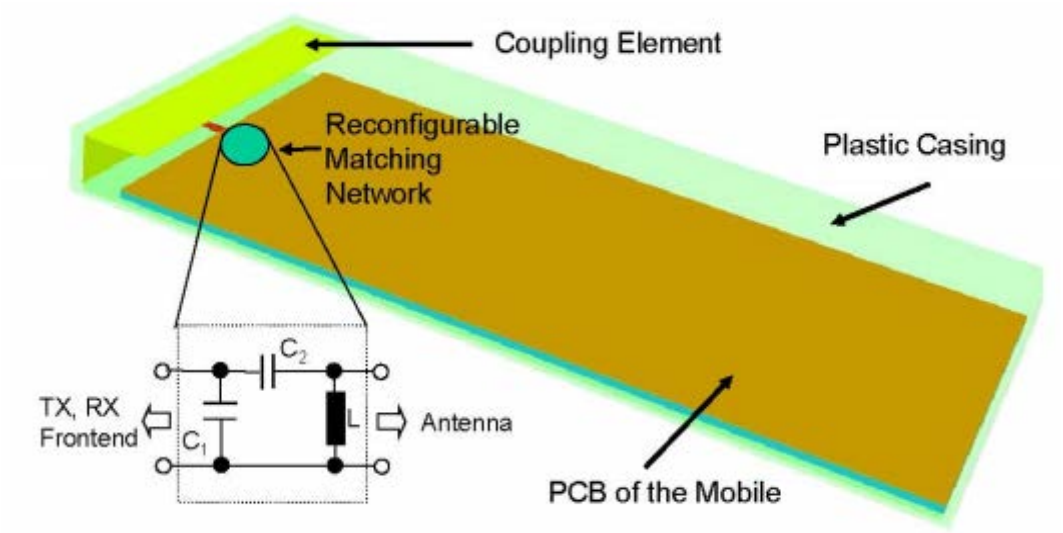

Fig.2. 1 Antenna schematic with reconfigurable tuning matching network [1]

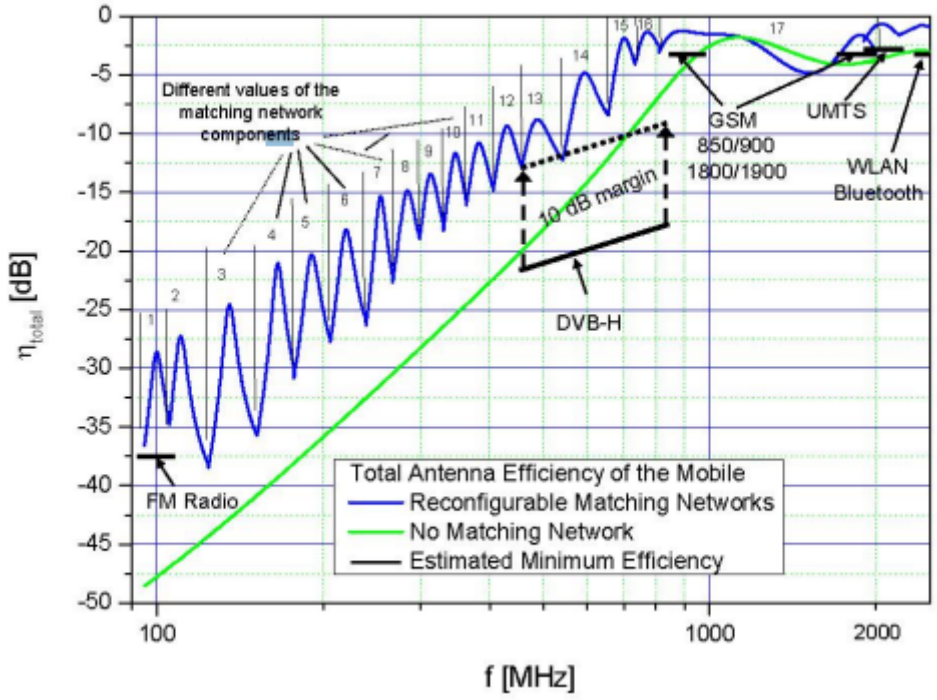

Fig.2.2 Total efficiency of antenna in Fig.2.1 with different matching networks compared with antenna alone and estimated minimum efficiency for different standards [1]

Ref [2-3], describes a two-port chassis antenna which has been matched on either or both of its two ports with passive matching networks. With switchable or tuneable passive matching networks, only small instantaneous bandwidths are achievable especially at the lower end of

the frequency bands as shown in Fig.2.3. The exact matched instantaneous bandwidths are not given in the paper but by observation, the matched bandwidths are very narrow. To cover between 0.7GHz to 3GHz, multiple matching networks or tuneable matching networks are required.

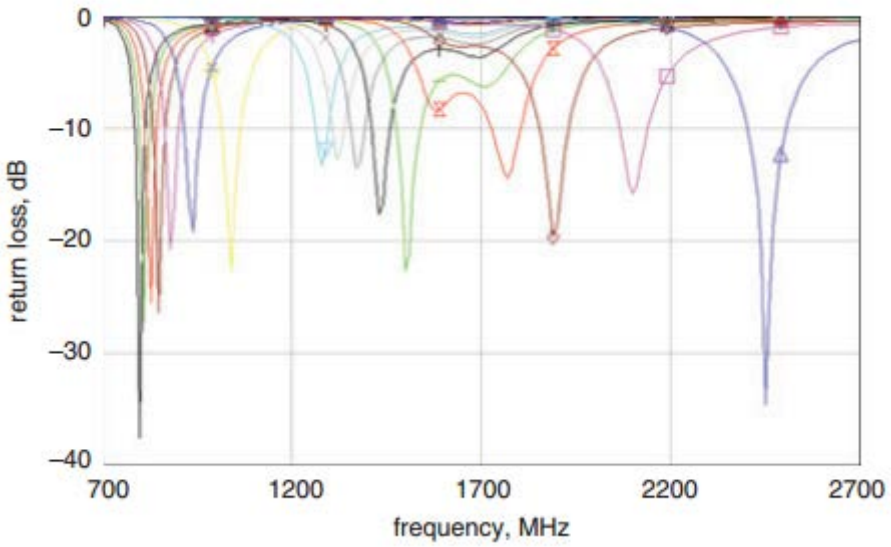

Fig.2.3 Simulated antenna return loss of chassis antenna using tuneable matching network [3]

Alternative means of achieving broadband matching uses active devices and the co–design of the antenna and the RF-front end. The usual method is to connect the antenna and frontend through 50Ω ports. This procedure usually requires the use of multiple matching networks in both the antenna and frontend. In the co-design methodology however, the antenna impedance is matched directly to the input impedance of the LNA. This not only relaxes the matching constraints but also reduces the component count of the overall matching network and achieves a better power transfer. Reference [4] describes an example of an antenna-LNA co-design as shown in Fig.2.4. In this work two LNAs are designed. One of which is matched to 50Ω with passive elements and another which has been co-designed with an antenna. In

both cases, the transistors and bias conditions are the same. The LNAs are designed for operation between 3.1GHz to 5.1GHz. The antenna in this work is a printed triangular monopole. Figure.2.5 shows the performance comparison between the co-designed antenna and LNA against the standard 50Ω method. It can be seen that the gain of the co-designed antenna is better by at least 7dB. Although this paper has only published simulated results, however, it shows the potential of using active matching networks to improve the maximum power transfer. Other examples using this method of active matching can be found in [5-6]. GTumax is the unilateral transducer gain for a two port device, the second port this case is a wideband antenna in the far-field.

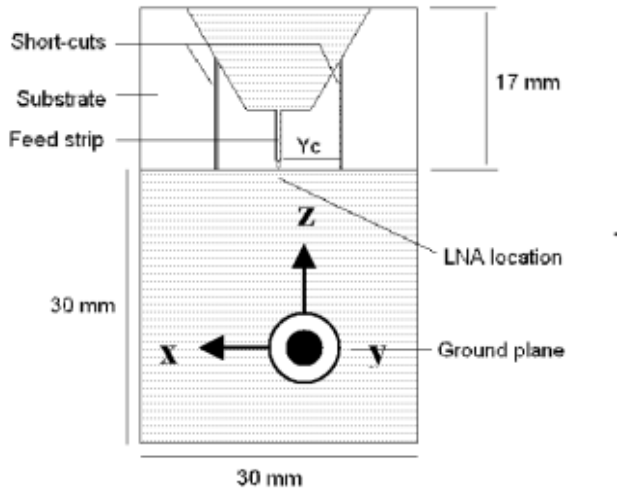

Fig.2. 4 Triangular monopole antenna schematic [4]

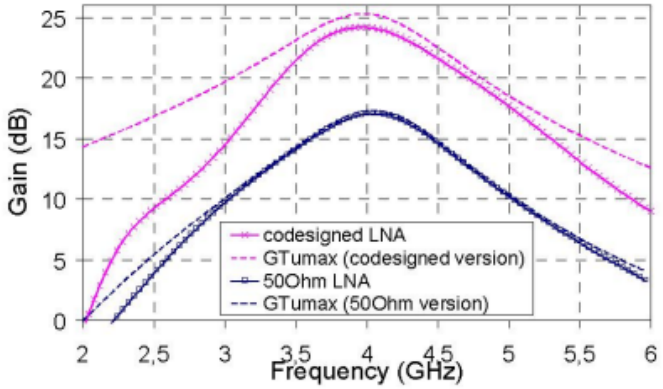

Fig.2. 5 Power gain and GTumax for 50 ohms and co-designed antenna RF frontend configuration [4]

GTumax shown in Fig. 2.5 is the maximum transducer unilateral gain of a two port network.

$$G_{T,max} = \left|\frac{S_{21}}{S_{12}}\right| \left(K - \sqrt{(K^2 - 1)}\right)$$

Where K is the stability K-factor.

However, this method has some flaws, one of which is that the antenna becomes non-reciprocal. Another is that almost in all cases the return loss of the co-designed antenna is always worse than that which is obtainable with the standard 50Ω connections.

Figure.2.6 indicates why passive matching networks are only able to cancel the reactance of an antenna over a narrow frequency band. Passive elements have Foster properties as the Foster theorem states that the reactance of a passive lossless network increases monotonically with frequency [7]. Therefore to cancel the capacitive reactance of an antenna would require an inductor and a capacitor to cancel the inductive reactance of an antenna, Fig.2.6a. However, if there is an element whose reactance decreases with frequency, it would be possible to cancel the reactance of any element or antenna completely as shown in Fig.2.6b. These elements are non-Foster elements and they are usually negative capacitors or negative inductors.

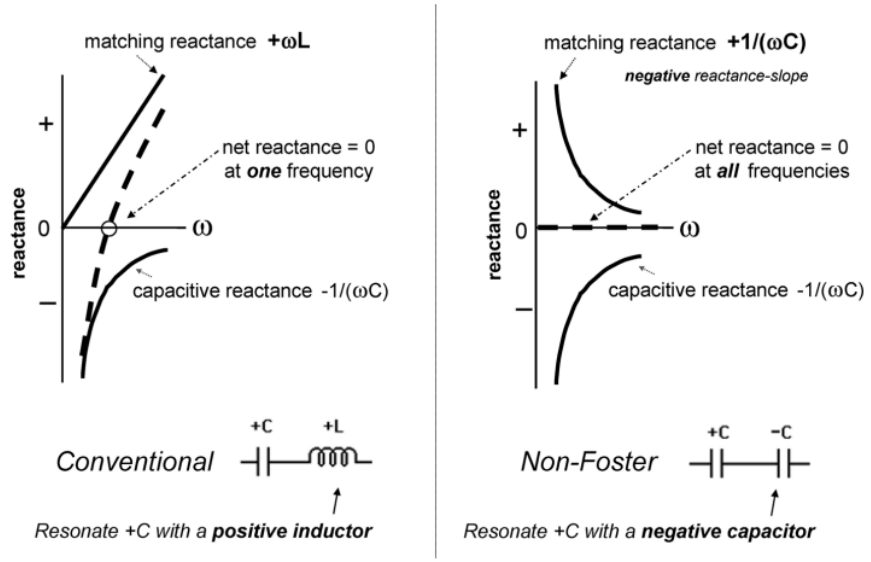

(a) (b)

Fig.2. 6 (a) Conventional matching (b) vs non-Foster matching [8]

2.2. Non-Foster matching

Reference [9] gives a comparison between matching an antenna passively and matching using non-Foster elements. The antenna is a cylindrical monopole mounted on an infinite ground plane which is 0.6m long and 0.01m diameter. It is operational between 30MHz to 90MHz. The input impedance of the antenna was simulated using Antenna Model®[9].

Using an L – shaped matching network consisting of two inductors 477nH and 51.9nH, it was possible to obtain a perfect match at 60MHz. To compute the radiation efficiency of the passively matched antenna, a two-port model representation of the antenna was developed [9]. In the two-port model the antenna input impedance Z_a is given as

$$Z_a = R_a + jX_a = R_r + R_l + jX_a \qquad (2.1)$$

Where R_r and R_l are radiation and loss resistances respectively and jX_a is the antenna reactance. The radiation resistance, R_r, is then represented by a transformer which transforms the radiation resistance to a 50Ω system impedance (Z_0). The turns ratio, N, of the transformer is given in equation 2.2. The equivalent two port representation of the antenna is shown in Fig.2.7. It should be noted that this representation is only valid at a single frequency.

$$N = \sqrt{\frac{R_r}{Z_0}} \tag{2.2}$$

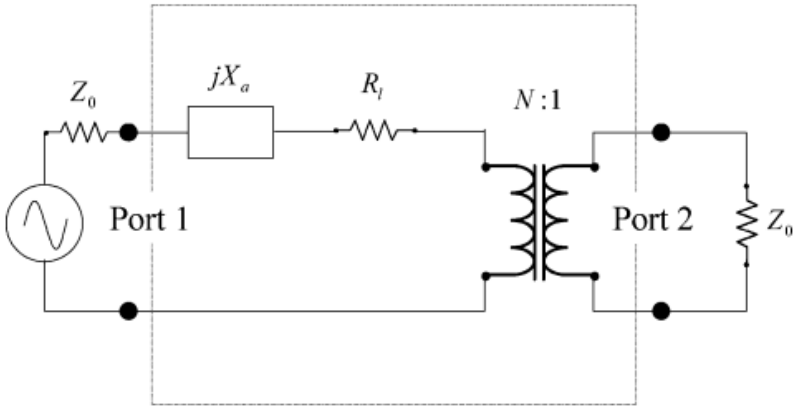

Fig.2. 7 Two port representation of an antenna [9]

Using the two port representation shown in Fig.2.7, the simulated return loss and total efficiency of the antenna when passively matched is shown in Fig.2.8. At 60MHz, where the antenna is matched, the efficiency peaks at approximately 80% but outside this frequency, the efficiency of the antenna drops rapidly with a 3dB bandwidth of just 3MHz. Using the equivalent circuit, the reactive part of the antenna can be cancelled by negating the reactive elements in the antenna equivalent circuit using a series combination of -8.657pF and -234.17nH. It was possible to match the antenna completely between 36MHz to 90MHz as

shown in Fig.2.9 with a total efficiency of better than 95% across the matched frequency band. This shows a better efficiency bandwidth product than obtained with Foster matching alone. This comparison amongst others like [10] highlights the potential of non-Foster elements in obtaining wideband matching without degrading the antenna efficiency.

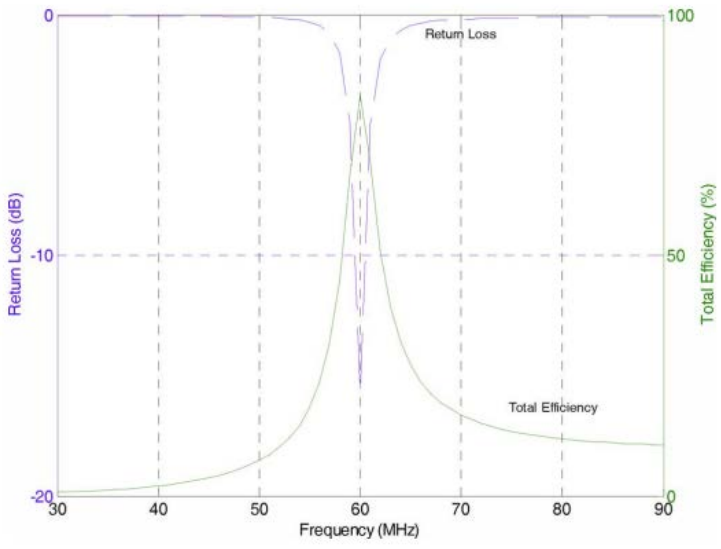

Fig.2. 8 Return loss and total antenna efficiency of the passively matched antenna [9]

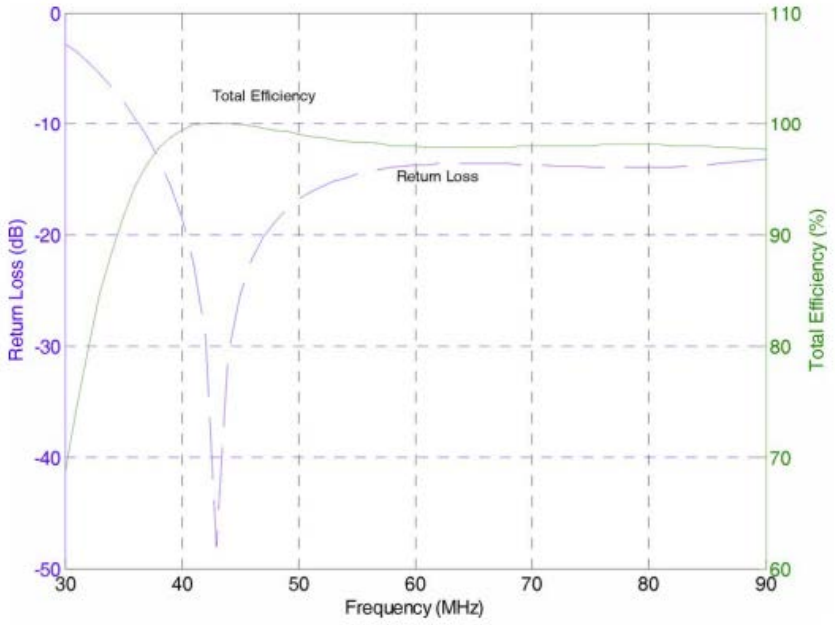

Fig.2. 9 Return loss and total antenna efficiency of the non-Foster matched antenna [9]

2.3. Negative Impedance Converter

The previous section (2.2) showed the potential of non-Foster elements. These elements are however not available in reality. To realise a non-Foster element, a Negative Impedance Converter (NIC) is required.

The idea of using negative impedance converters for realising non-Foster elements with a transistor was first shown by Linvill [11] in 1953. Non-Foster elements had been used within the telephone networks to generate negative impedance repeaters but these NICs used vacuum tubes [11-12]. These designs were limited by the bulkiness and relatively short life-cycle associated with vacuum tubes. They were also not rugged and deteriorated rapidly with age. The ideal Linvill NIC had a conversion factor of between -0.9 to -0.98 and this conversion factor is dependent on the alpha (α, current gain) of the transistors.

The Linvill NIC consists of two transistors connected as shown in Fig.2.10. There exist feedback connections between the two transistors. The base of transistor 1 is connected to the collector of transistor 2 and the base of transistor 2 is connected to the base of transistor 1. The impedance to invert (Z_{load}) is connected between the two collector terminals which in this case are the two 510Ω resistors. When Fig.2.10 is considered, then the voltage from the emitter of transistor 1 is presented at point B via the feedback connection between the two transistors. The same rule applies to the voltage at the emitter of transistor 2 which is presented at point A. Computing the impedance seen across the two emitter terminals, Z, would give a negative fraction of the impedance connected between the two feedback paths, Z_{load}.

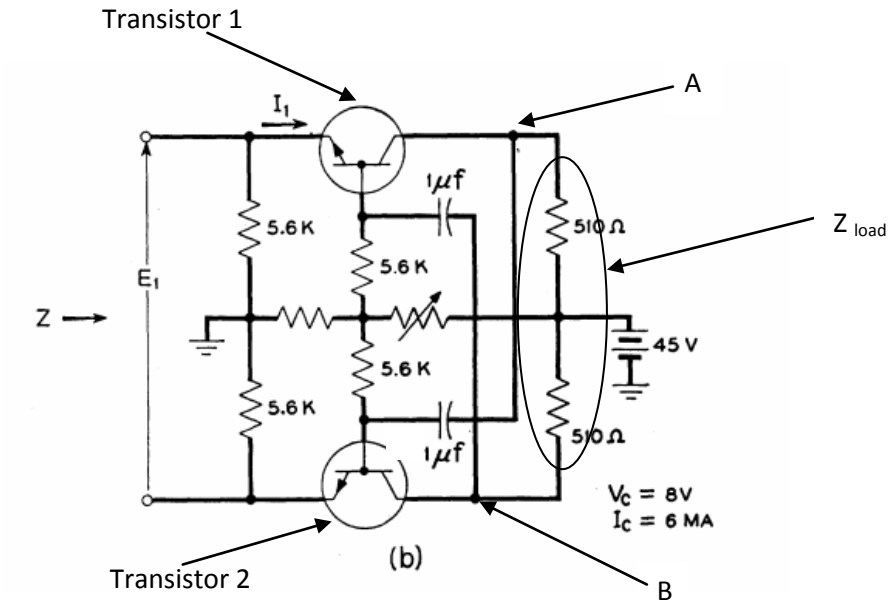

$$Z = -\gamma Z_{load}$$

Fig.2.10 Linvill's Negative Impedance Converter [9, 11]

2.3.1. Theory of NICs

Linvill in [11] gives a schematic by which the analysis of the NIC can be done. The two junction transistors are represented by the emitter and base terminal resistances, r_e, r_b and the collector is represented by a current dependent current source in parallel with the collector resistance r_c (T- model of a transistor shown in Fig.2.11a). The dc blocking capacitor required on the feedback path is represented by Z_d and the base current setting resistances are represented by Z_g. Using this schematic, shown in Fig.2.11b, it is possible to prove the impedance inversion analytically.

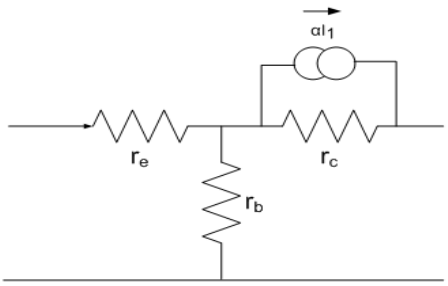

(a)

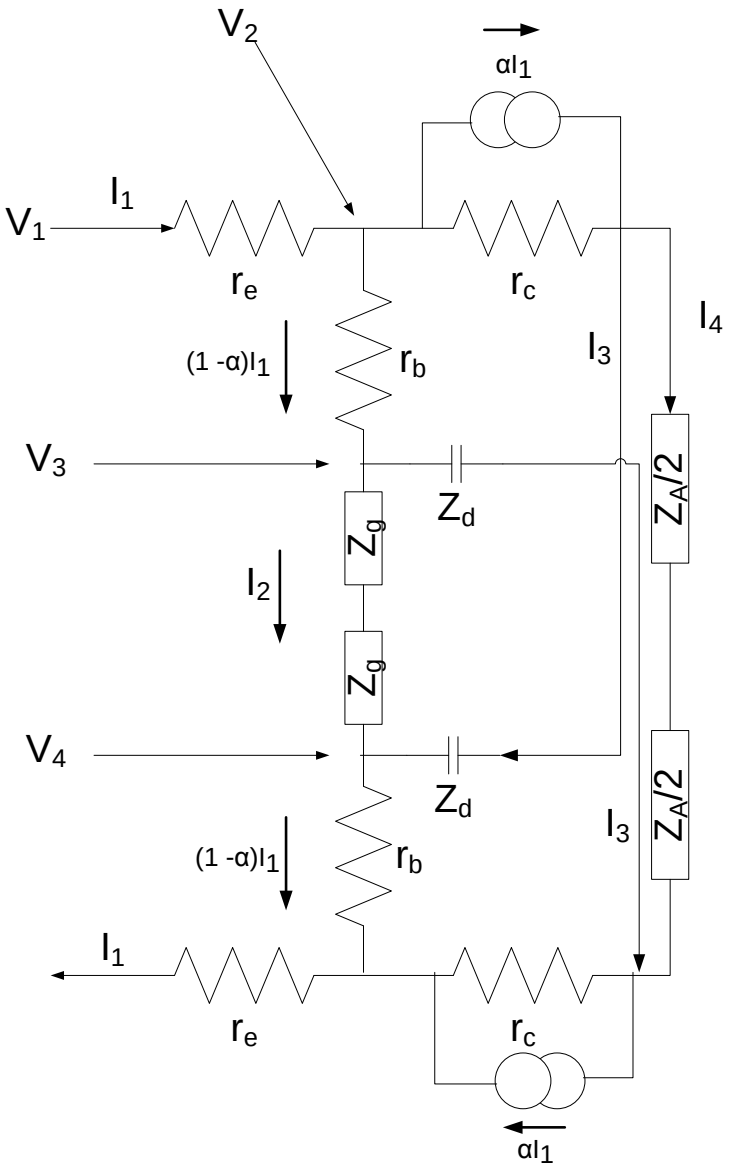

(b)

Fig.2. 11 (a) The T- model of a transistor (b)Equivalent circuit of the Linvill's NIC [11]

$$V_2 = V_1 - I_1 r_e \tag{2.3}$$

$$V_3 = V_2 - (1-\propto) I_1 r_b \tag{2.4}$$

Substituting equation 2.3 into 2.4

$$V_3 = V_1 - I_1 r_e - (1-\propto) I_1 r_b \tag{2.5}$$

$$V_4 = r_e I_1 + (1-\propto) I_1 r_b \tag{2.6}$$

$$I_2 = \frac{V_2 - V_4}{2Z_g} \tag{2.7}$$

Therefore,

$$I_2 = \frac{V_1 - 2I_1 r_e - 2(1-\propto) I_1 r_b}{2Z_g} \tag{2.8}$$

$$I_3 = (1-\propto) I_1 - I_2 \tag{2.9}$$

$$I_3 = (1-\propto) I_1 - \frac{V_1 - 2I_1 r_e - 2(1-\propto) I_1 r_b}{2Z_g} \tag{2.10}$$

$$I_4 = \frac{V_4 + I_3 Z_d - (V_3 - I_3 Z_d)}{Z_A} \tag{2.11}$$

And also

$$I_4 = \propto I_1 - I_3 \tag{2.12}$$

Equating equations 2.11 and 2.12

$$V_4 + 2I_3Z_d - V_3 = \propto I_1Z_A - Z_AI_3 \tag{2.13}$$

then

$$V_4 - V_3 + (2Z_d + Z_A)I_3 = \propto I_1Z_A \tag{2.14}$$

Substituting the variables,

$$r_eI_1 + (1-\propto)I_1r_b - V_1 + I_1r_e + (1-\propto)I_1r_b + (2Z_d + Z_A)(1-\propto)I_1 - \frac{2Z_d + Z_A}{2Z_g}(V_1 - 2I_1r_e - 2(1-\propto)I_1r_b) = \propto I_1Z_A \tag{2.15}$$

Then

$$I_1\left(r_e + (1-\propto)r_b + r_e + (1-\propto)r_b + (2Z_d + Z_A)(1-\propto) + \left(\frac{2Z_d + Z_A}{Z_g}\right)r_e + \left(\frac{2Z_d + Z_A}{Z_g}\right)(1-\propto)r_b - \propto Z_A\right) = V_1\left(1 + \frac{2Z_d + Z_A}{2Z_g}\right) \tag{2.16}$$

$$I_1\left(2r_e + 2(1-\propto)r_b + \frac{2Z_d + Z_A}{Z_g}\left((1-\propto)Z_g + r_e + (1-\propto)r_b\right) - \propto Z_A\right) = V_1\left(\frac{2Z_g + 2Z_d + Z_A}{2Z_g}\right) \tag{2.17}$$

Then

$$\frac{V_1}{I_1}$$

$$= \frac{2r_e + 2(1-\propto)r_b + \frac{2Z_d + Z_A}{Z_g}\left((1-\propto)Z_g + r_e + (1-\propto)r_b\right) - \propto Z_A}{1 + \frac{2Z_d + Z_A}{2Z_g}} \quad (2.18)$$

$$\frac{V_1}{I_1} = 2r_e + 2(1-\propto)r_b + \frac{2(2Z_d + Z_A)(1-\propto)Z_g}{2Z_g + 2Z_d + Z_A} - \frac{2 \propto Z_A Z_g}{2Z_g + 2Z_d + Z_A} \quad (2.19)$$

When $Z_d = 0$

$$\frac{V_1}{I_1} = 2r_e + 2(1-\propto)r_b + \frac{2Z_A Z_g(1-\propto)}{2Z_g + Z_A} - \frac{2 \propto Z_A Z_g}{2Z_g + Z_A} \quad (2.20)$$

$$\frac{V_1}{I_1} = 2r_e + 2(1-\propto)r_b + Z_N(1 - 2 \propto) \quad (2.21)$$

Where $Z_N = \frac{2Z_A(Z_d + Z_g)}{2Z_d + 2Z_g + Z_A}$

2.4. Realisations of Negative Impedance Converters

There have been a number of attempts to demonstrate the use of NICs and non-Foster elements in providing broadband matching. These can be broadly divided into two; previous works that have shown demonstrations of non-Foster elements for matching antennas in

simulations only and work that has shown the potential of non-Foster elements and also shown and demonstrated prototypes.

Reference [13] shows the use of non-Foster elements to match an antenna. The authors introduced an additional port into the antenna. The port was added in order to have a point via which input impedance of the antenna can be controlled with the appropriate addition of loads to the second port to help improve the real part of the antenna and bring it closer to the system impedance and as well as giving an opportunity to include non-Foster elements into the antenna which would help bring the reactive part of the antenna close to zero. It was expected that these two actions would inevitably result in a wideband antenna with better efficiency especially at lower frequency ranges.

This was applied to a 6 inch loop antenna as shown in Fig.2.12 which is resonant at 690MHz (red curve in Fig.2.12), below this frequency the real part of antenna impedance is low. It has 10dB return loss bandwidth of 60MHz and a 6dB return loss bandwidth of 120MHz. A non-Foster element based matching network, which consisted of -1.2pF capacitor and -27nH inductor, was added in series and there was an improvement in the 6dB simulated return loss bandwidth from 120MHz to 400MHz between 450MHz to 850MHz and 10dB return loss bandwidth increase of 120MHz from 60MHz to 180MHz. The non-Foster elements have been able to improve the match of the antenna lower than its original resonant frequency. This work however showed only simulated results of the antenna return loss and does not show any result for antenna efficiency or gain.

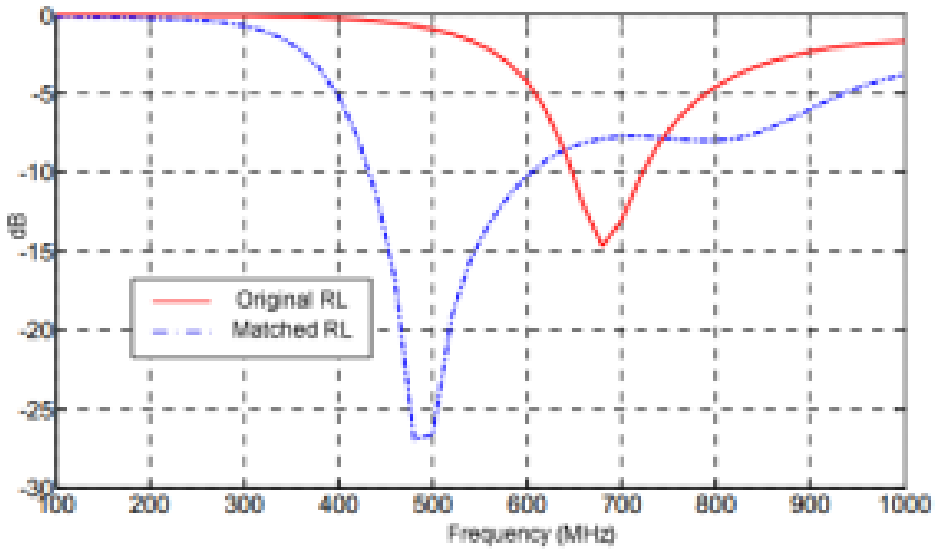

Fig.2. 12 Matched input return loss comparison between the unmatched antenna and the antenna matched with non-Foster network. [13]

Reference [14], showed the prospects of improving the matched bandwidth of a meta-material antenna. The meta-material antenna is compact, multi-frequency but has a high Q. Its high Q can be attributed to the composite right left hand (CRLH) transmission lines that make-up the antenna. The antenna in this case is a microstrip patch partially filled with left-handed structures (Fig.2.13) and it has multiple resonances at 1GHz, 1.5GHz and 2GHz as shown by its return loss in Fig.2.14. The figure also shows that the antenna has low instantaneous bandwidths when resonant. Simulating an equivalent circuit of the antenna, it was possible to determine the values of the negative elements required to match the antenna. Though the values of the elements in the non-Foster matching network were not given in the paper, it showed that by introducing an NIC at the output of the antenna, the NIC would match the antenna at a lower frequency; 807MHz with a 10dB return loss bandwidth of approximately 400MHz (Fig.2.15). It also stated that one of the challenges of a practical NIC was its stability which is a direct result of the parasitic which are worse at higher frequencies.

Fig.2. 13 Antenna partially filled with LH structures [14]

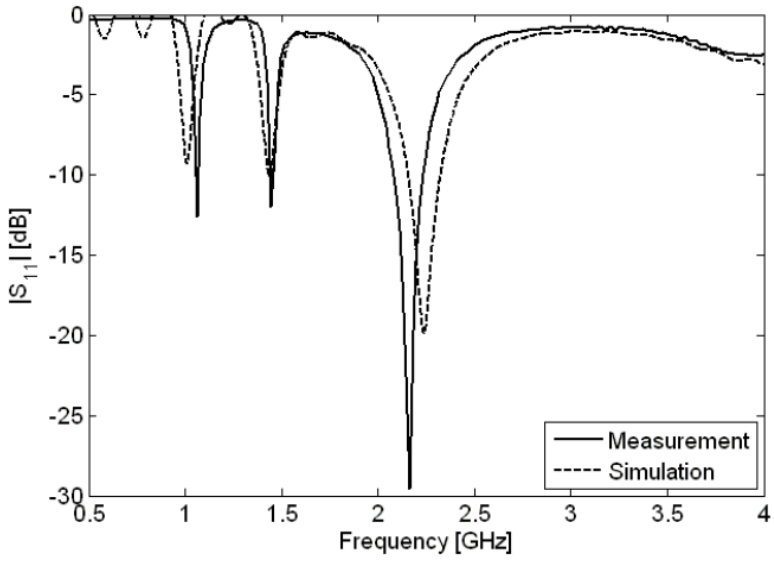

Fig.2. 14 Return loss of the multi frequency antenna [14]

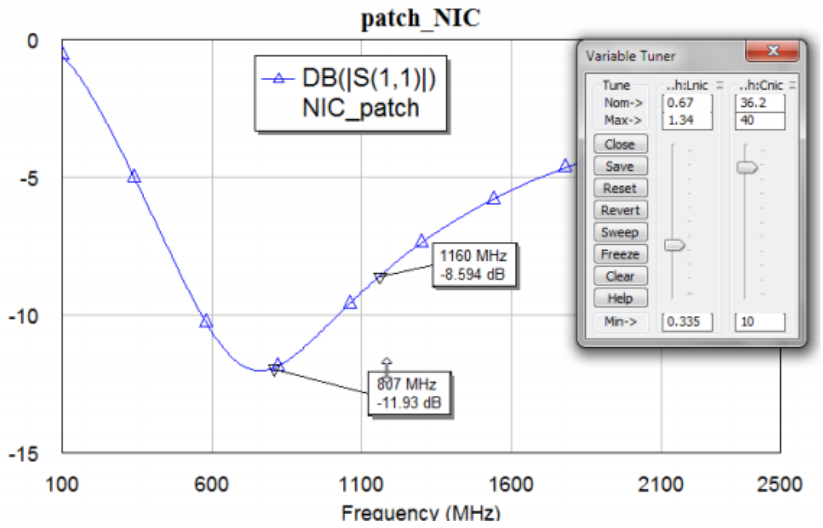

Fig.2. 15 Return loss of the antenna matched with NIC [14]

Another example of an antenna matched with non-Foster element realised using NIC is described in [15]. In this paper, a three inch monopole was mounted on a 9 in^2 square ground plane. The simulated antenna input impedance plot is shown in Fig.2.16. From Fig.2.16 it is clear that the antenna is not matched anywhere between 1MHz and 1000MHz. Before the first series resonance of the antenna, the antenna can be seen to be highly capacitive and hence it is possible to cancel the reactive part of the antenna by having a matching network which consists of a negative capacitance in series with the antenna.

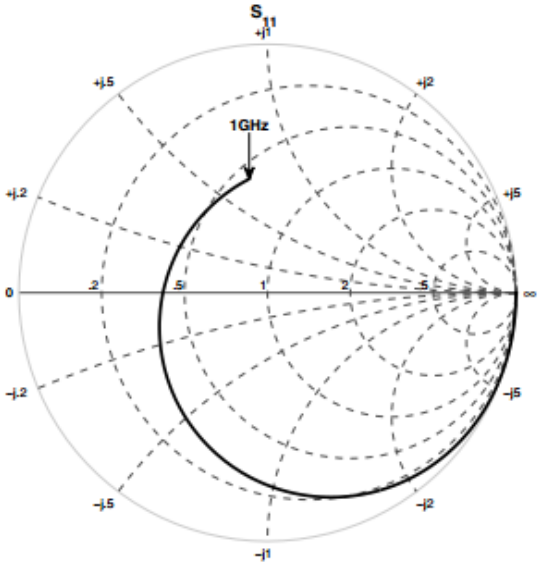

Fig.2. 16 Antenna impedance plot of the 3in monopole [15]

Figure 2.17 shows the net reactance of the NIC matched antenna, it is clear that the antenna with non-Foster matching has a lower reactance when compared with the antenna alone. Its reactance is also almost zero between 350MHz and 600MHz. Fig.2.18 shows the simulated transducer gain of the antenna with and without non-Foster matching network and it can be seen that there is gain improvement between 50MHz to 650MHz. If the gain plot in Fig. 2.18 is compared with the impedance plot in Fig.2.17, it would be seen that the gain improvement occurs when the addition of non-Foster elements causes a change in the reactance of the matched antenna. The antenna described has been fabricated and the antenna gain improvement trend simulated has been confirmed though the maximum gain improvement with the non-Foster matching network is 6dB. The authors also pointed out the need to perform a signal to noise ratio (SNR) measurement as this is an important performance parameter for receiving antennas. The effects of noise from the active devices and the associated non-linearity have not been quantified.

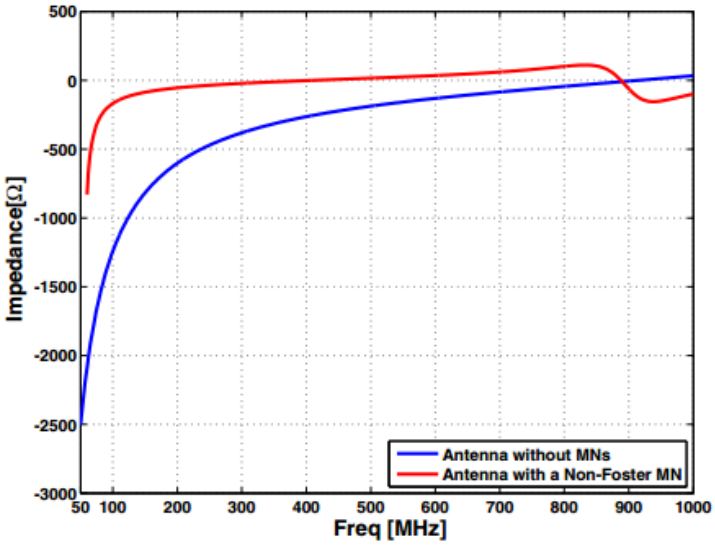

Fig.2. 17 Input reactance comparison between the antenna alone and antenna with non-Foster matching [15]

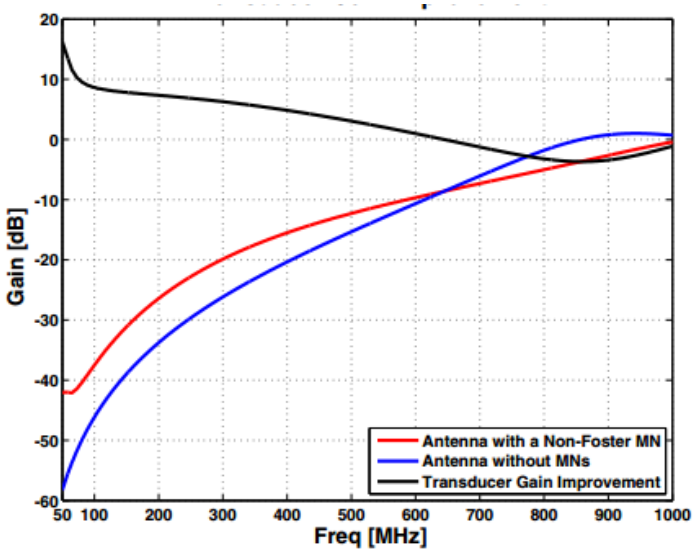

Fig.2.18 Transducer gain improvement of the antenna with non-Foster matching [15]

Sussman-Fort in [8] described a fabricated NIC and performed some measurement on the prototype, including the SNR measurement. During the initial work, a six inch monopole is matched using a series non-Foster element realised with the Linvill architecture using a SiGe BJT transistor. The element is connected in series with the antenna. Using a transmitter set to broadcast between 20MHz to 100MHz, the gain advantage of an NIC matched antenna is

compared to what is obtainable with the antenna alone when connected to an 8dB noise figure receiver. The noise added due to the NIC matched antenna is also compared with that due to the antenna alone. In the case of the receiver, the noise level recorded by the spectrum analyser is due to the environmental noise and the noise of the analyser while with the NIC matched antenna, the recorded noise by the spectrum analyser is a combination of the environmental noise, the noise of the spectrum analyser and the noise due to the non-Foster circuit. Therefore, the SNR advantage of the NIC matched antenna over the antenna alone is given by equation (2.22) and shown in Fig.2.19. Figure.2.19 shows a maximum SNR improvement of approximately 9dB at 30MHz with the NIC. The reduction in SNR improvement with frequency can be attributed to the fact that the difference between the simulated transducer gain of the antenna alone and the antenna with NIC is reducing with frequency as can be deduced from Fig.2.20.

$$\mathrm{SNR_{adv}} = \mathrm{Gain_{adv}} - \mathrm{Noise_{adv}} \qquad (2.22)$$

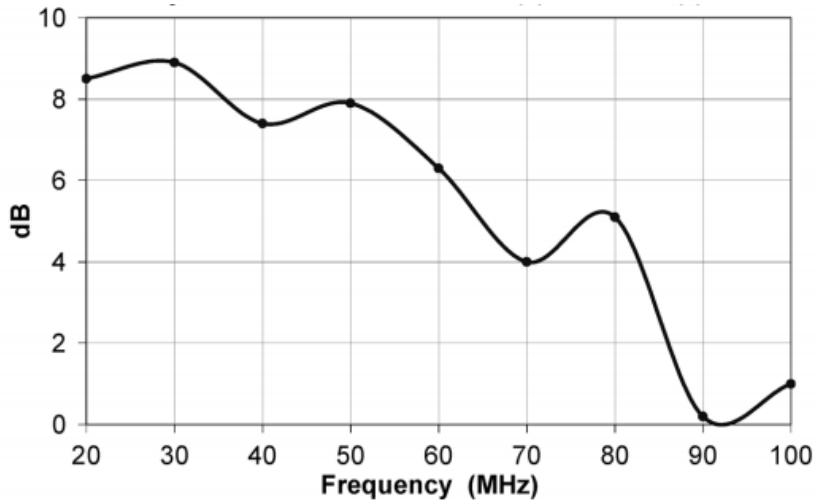

Fig.2. 19 Improvement in SNR of the NIC matched antenna over the antenna alone [8]

Figure.2.20 shows the simulated transducer gain comparison between the antenna alone, the antenna matched with non-Foster matching and with different matching passive matching networks. It is clear that passive matching out-performs the antenna without matching but only within given frequency bands, and outside these bands, the antenna by itself is often a better option. However, the non-Foster matched antenna performs fairly well across the entire frequency band and in some case out performs the passively matched antenna except at higher frequencies where the antenna is almost resonant due to its end loading.

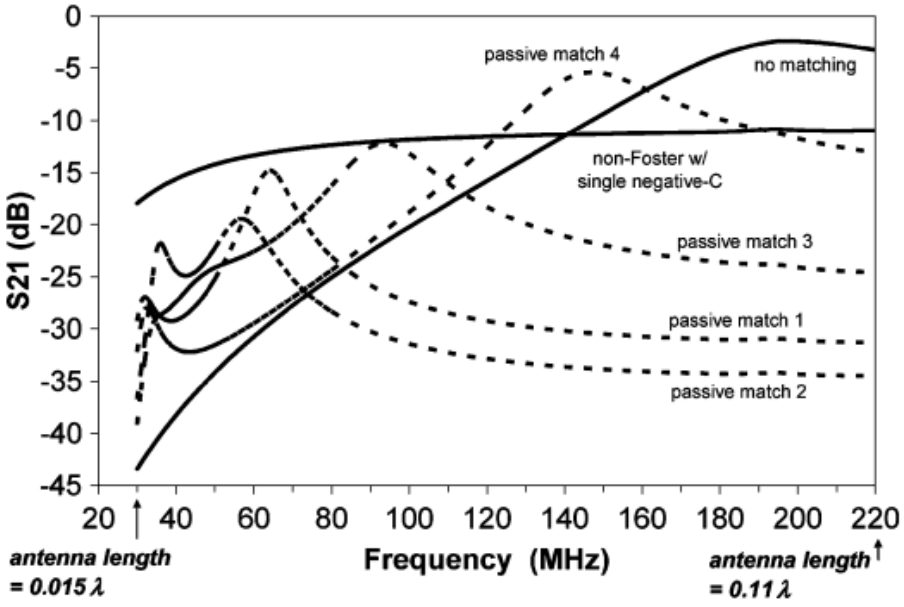

Fig.2. 20 Simulated S21 comparison between passive , non-Foster and no matching [8]

A 12 inch dipole was also matched using an NIC based matching network. The SNR performance of this antenna was compared with a 12 inch lossy matched blade antenna. Figure.2.21 shows the measured SNR advantage of the NIC matched antenna over the lossy blade equivalent. The measurement setup is similar to that used for the 6 inch monopole characterisation. It was observed that there is at least a 10dB advantage with using the NIC matched antenna over using the lossy blade antenna. This enhanced SNR advantage is very useful in the overall system architecture especially when it is used in the receive mode. The 6

inch antenna and the 12 inch dipole had top frequencies of 220MHz and 120MHz, respectively. The notches at 28MHz and 63MHz in Fig.2.21 were attributed to noise spikes from other transmitters within the antenna range. This paper showed the advantages of using NIC to match an antenna; it is also the first publication to show the effect of noise from the active devices with the SNR measurements but did not show any results for linearity and also has a top frequency of 220MHz.

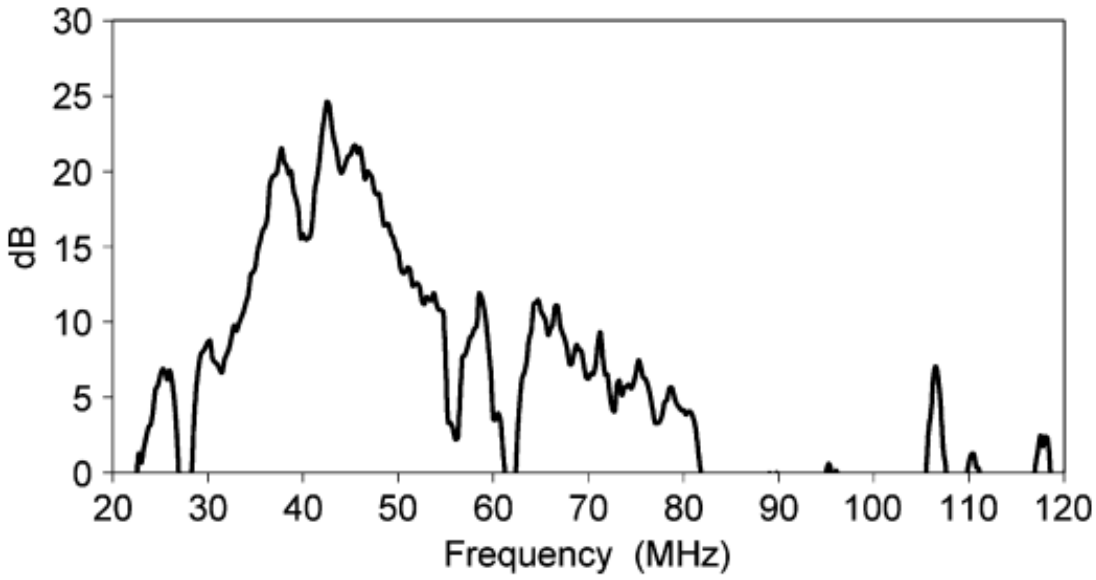

Fig.2. 21 Measured SNR advantage of NIC matched antenna over lossy matched blade [8]

Ref [16] is another paper that tries to apply NIC to meta-materials. Though the paper has the term meta-material and the initial parts of the paper allude to applying NIC to meta-material antenna, the eventual application was a loop antenna. The NIC was designed using the one port equivalent of the Linvill's NIC, the schematic is shown in Fig.2.22.

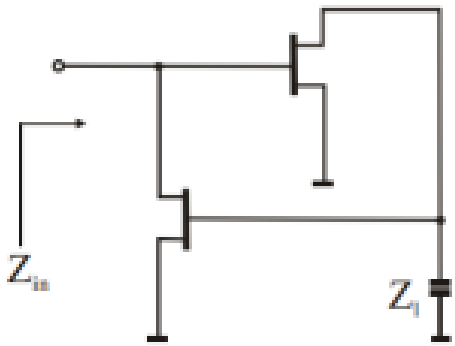

Fig.2. 22 A modified one port Linvill NIC schematic [16]

The element to invert is a capacitor, Z_l and the transistors are FETs. When compared to the Linvill NIC, the second port of the standard Linvill circuit has been grounded. The prototype of the NIC is shown in Fig.2.23. Measured and simulated results of the NIC are shown in Fig.2.24. It can be seen that the inverted reactance is consistent with a -60nH inductor especially at lower frequencies (up to 40MHz).

Fig.2. 23 The fabricated single port NIC [16]

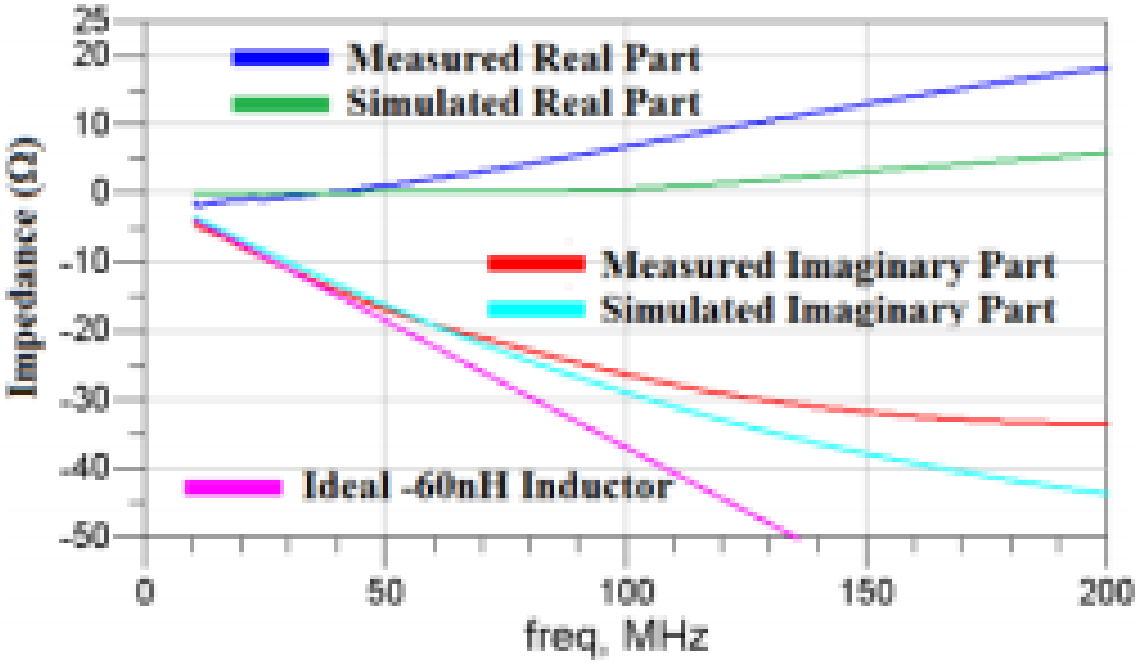

Fig.2. 24 The simulated and measured impedance plots of the modified one port NIC [16]

The built NIC was used as load on a simple small loop antenna. The antenna is made of a 2mm diameter copper wire formed into a 50mm diameter loop and this forms an active replica of a split ring resonator (SRR). An additional positive capacitor was connected in parallel with the inductor in order to achieve the MNZ (mu-near-zero: when the permeability is near zero) behaviour. This active SRR was put between two loops connected to a network analyser and its transmission coefficient was measured. The measured S_{21} is shown in Fig.2.25 and compared to similar antenna loaded with a 140pF capacitor.

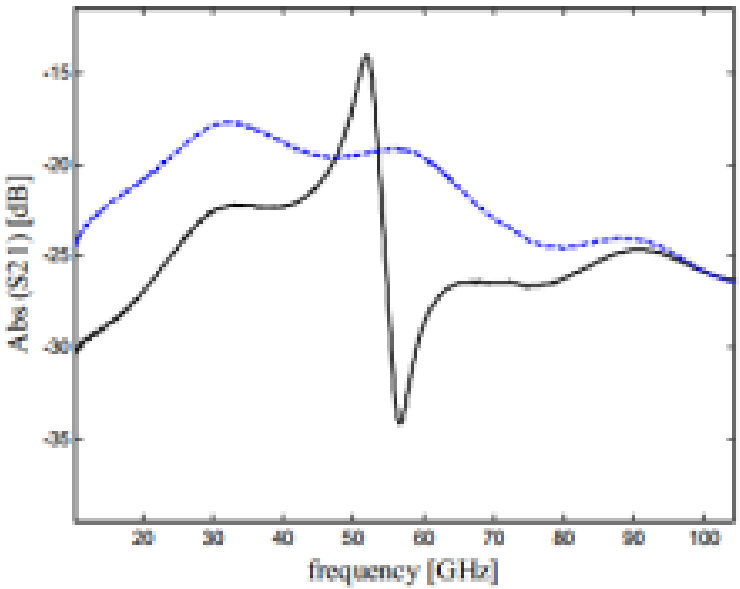

Fig.2. 25 Measured S21 of the loop load in capacitor (solid line) and the negative inductance (dashed line) [16]

Fig.2.25 shows he measured S_{21} of the antenna loaded with a capacitor, the units on the frequency axis is labelled in GHz but within the literature and in other results, it is clear that this is a typographical error and it should have read MHz. Therefore, when referring to this graph, the units shall be assumed to be in MHz. From Fig.2.25, it is clear that the S_{21} of the antenna loaded with 140pF capacitor does have a higher peak S_{21} at 50MHz but this degrades rapidly outside this frequency point. The antenna loaded with a negative inductance however does perform better over the entire frequency band except at 50MHz. This paper however does not discuss or show any results for noise and linearity; neither does it fully explain how an inverted capacitor leads to a negative inductance. Also the title maybe misleading as the eventual and demonstrated application was not a meta-material antenna as the title suggested. This paper therefore does not show any improvement on the results shown in [8].

Ref [17] also shows a prototype antenna with an integrated NIC. The paper alluded to the fact that the antenna was meta-material inspired because of the reactive loading. This paper is a

follow on from an initial publication [18] from one of the authors where a dual band monopole was realised. The monopole by itself is resonant between 5.15 – 5.80GHz but when loaded with inductors and capacitors, it can also be made resonant between 2.40 – 2.48GHz. The capacitor was realised as an inter-digital capacitor. A T shape slot is also cut into the monopole and it is this slot that is primarily responsible for the lower frequency resonance. For the purpose of integration with an NIC, the antenna was redesigned for 300MHz and some modifications were made to allow for embedding active circuit's requirements such as DC bias as depicted in Fig.2.26b while its original size and dimensions are also shown in Fig.2.26a. Another reason the authors gave for scaling down was because it relaxes the design requirements of the NIC which shows the difficult in realising NICs at high frequencies.

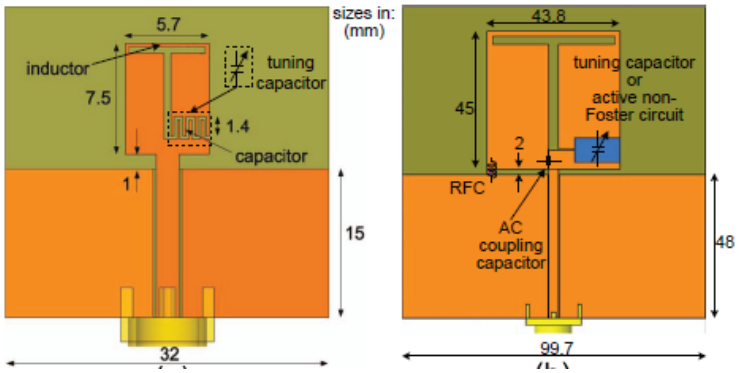

(a) (b)

Fig.2. 26 Antenna schematic, (a) shows original dimensions for Wi-Fi and (b) shows scaled version [17]

In the scaled version of the antenna, the capacitor is replaced with non-Foster elements L_{nf} and C_{nf}. With the non-Foster elements, it was possible to match the antenna continuously between 280MHz and 450MHz. The antenna return loss was sensitive to the values of L_{nf} and C_{nf}, therefore it was decided in the implementation to use a trimmer capacitor during the

fabrication process for extra control and flexibility. The integrated antenna and NIC is shown in Fig.2.27. The NIC integrated antenna was achieved on two layers with the active elements on the top side of the antenna and the trimmer capacitor on the bottom layer. The measured matched bandwidth of the prototype at different C_{nf} values is shown in Fig.2.28. It can be seen that the 10dB return loss bandwidth is much smaller (20MHz, 30MHz and 40MHz) than the simulated return loss bandwidth of 170MHz, though the matched bandwidths are still larger than was is obtainable with Foster matching. The authors believe that the reduced return loss bandwidths are due to the interaction between the antenna resonance and the frequency dependence of the non-Foster elements. It can also be noted that the magnitude of S_{11} is greater than 0dB at frequencies below the operation ranges, the authors however believe this would not result in instabilities. Though this paper demonstrated integration between an antenna and the NIC, however, measurements on gain, noise and linearity were not reported. There is also a remarkable difference between the expected simulated results and the measured results shown. The use of the term meta-material is not clearly justified as there are examples of antennas loaded with reactive elements which are not meta-material. It is also not clear the need and use for the T shaped slot in the antenna at this frequency because in the initial publication this was used to make the antenna dual band. It is however very simple and planar and this makes it easy to incorporate with the RF frontend.

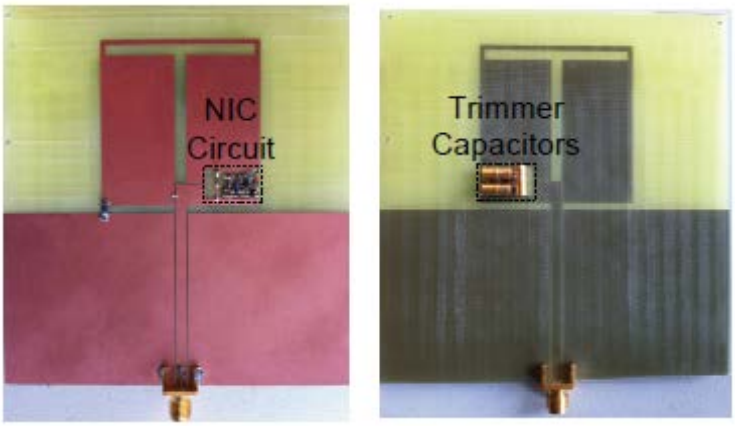

Fig.2. 27 Fabricated NIC matched antenna showing both the top and bottom views [17]

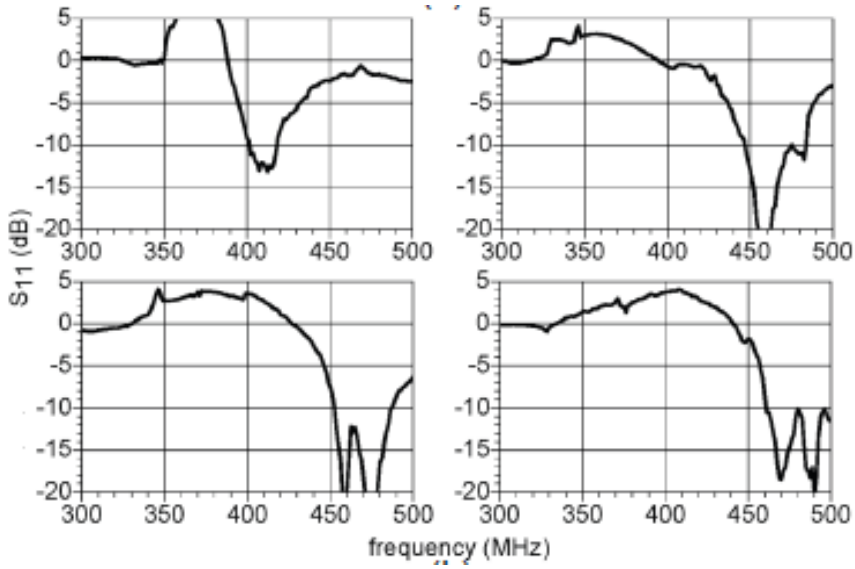

Fig.2. 28 Measured antenna return loss at different capacitance [17]

Another example of an NIC implementation with complete integration with an antenna can be found in [19]. Here the authors describe a non-Foster circuit (NFC) which is based on the Linvill architecture. Because of the instability associated with non-Foster elements, a 3pF fixed capacitor was included between the NIC and the measurement ports as shown in Fig.2.29. This is to ensure a net positive reactance at the measurement ports. Also because of the frequency variation of the capacitance obtainable from the NIC, a varactor was included in parallel with the NIC (Fig.2.30) for additional control on the overall capacitance seen at the two measurement ports.

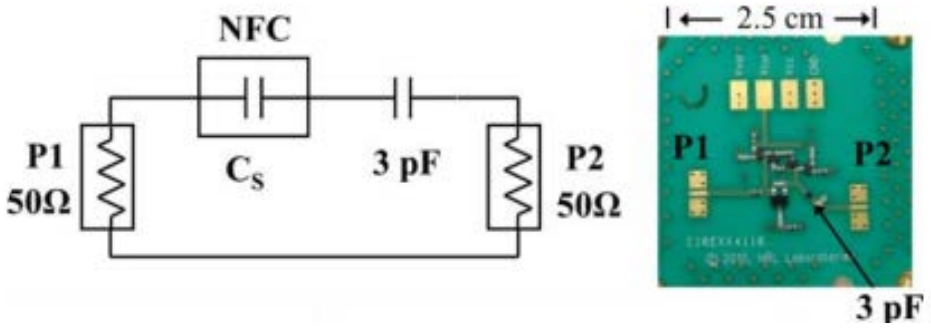

(a) (b)

Fig.2.29. (a) NIC circuity and (b) Fabricated NIC prototype circuit [19]

The NIC circuit is shown in Fig.2.30 and transistors Q1 and Q2 are the two transistors used in the NIC. They are biased at 15V, 10mA. The transistors Q3 and Q4 form part of the active biasing network. In order to reduce the possibility of oscillation from the resonant circuit that would occur if an RF choke inductor was used as part of the biasing network, high value resistors, R_{CC2} were used to set the voltage at the collector of transistors Q1 and Q2. The elements to invert are the 4.7pF capacitor and 45.4Ω resistor.

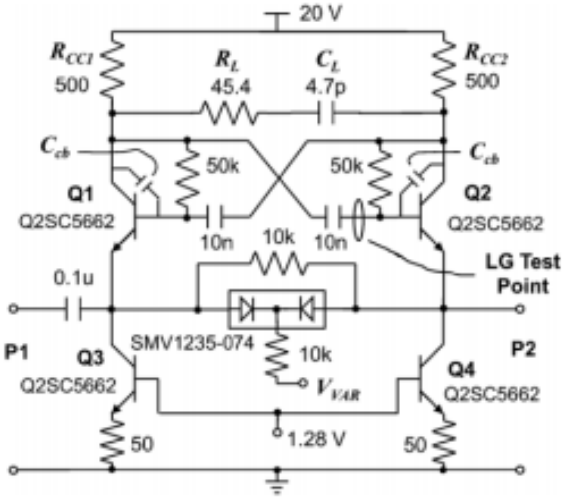

Fig.2. 30 Schematic of the non-Foster circuit [19]

Figure 2.31 shows the measured S_{11} and S_{21} of Fig.2.29(b) at different bias voltages and that of a fixed 3pF capacitor. It is clear that the S_{21} through the NIC is improved by 22dB between

1 – 10MHz whereas between 10MHz and 100MHz, the improvement is bias voltage dependent. The peak in S_{11} is also noted and this indicates the presence of a net negative resistance. This NIC has also been incorporated into an antenna. The antenna is a 15cm long monopole, with 5mm diameter on 1.44mm^2 ground plane. The antenna is fed through the NIC as shown in Fig.2.32. The measured input impedance through NIC matched monopole is shown in Fig.2.33. It is clear when compared with the antenna alone that the net reactance is close to zero with a variation between -20Ω to 80Ω whereas the reactance of the antenna alone without matching varies between -1200Ω and 0Ω. It is clear that the NIC circuit is cancelling the reactance of the antenna over a wide frequency range. The comparison between the measured S_{21} of the NIC matched antenna and an arbitrary antenna against the antenna by itself is shown in Fig.2.34. It can be seen that the NIC matched antenna improves the S_{21} by at least 10dB between 30MHz and 200MHz irrespective of the bias condition.

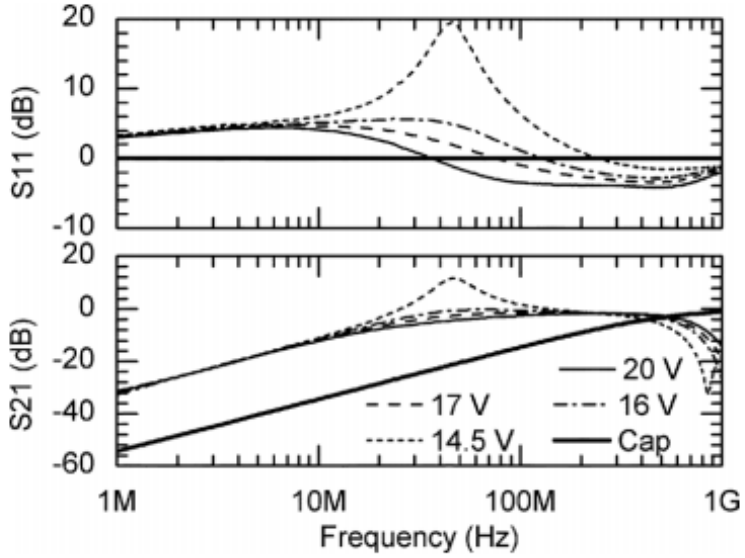

Fig.2. 31 Measured S_{11} and S_{21} of non-Foster circuit [19]

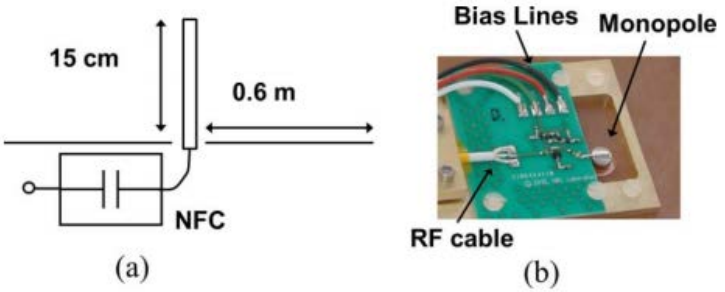

Fig.2. 32 (a) Schematic of the non-Foster enhanced monopole and (b) the fabricated non-Foster enhanced monopole [19]

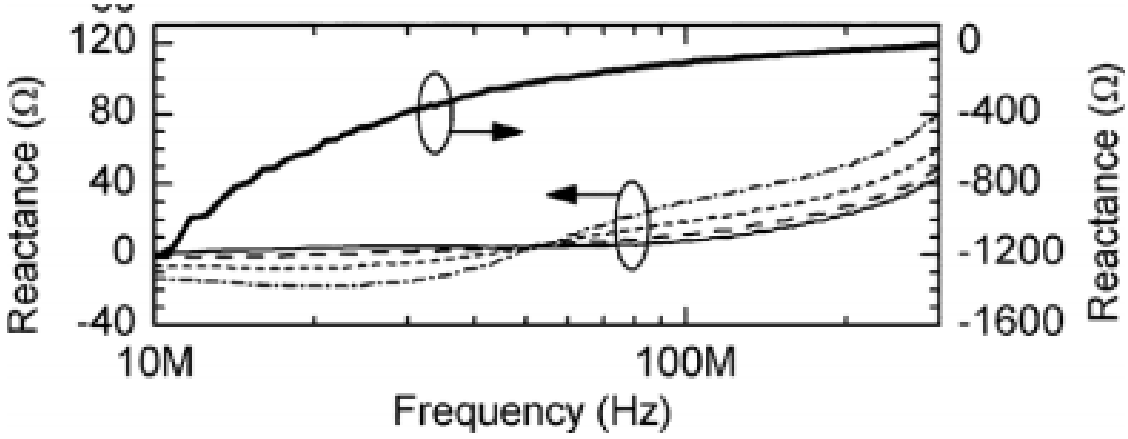

Fig.2. 33 Measured input reactance of non-Foster enhanced monopole compared with an unmatched antenna. [19]

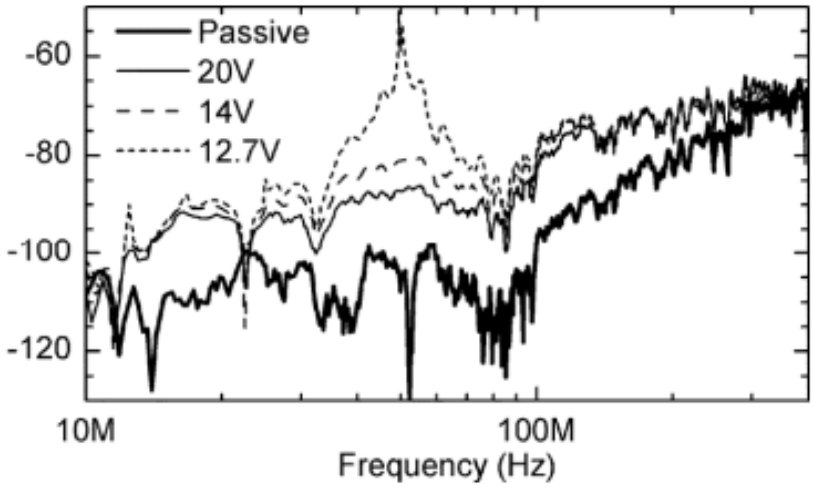

Fig.2. 34 Measured S_{21} of non-Foster enhanced monopole at different bias conditions compared to passive antenna [19]

One of the recurrent themes with most of the previous work into NICs is stability. This has led to designs being scaled down or in some cases they are limited to simulations only. Hence, the top frequency of reported prototype is limited to 500MHz. In [19], the NIC was demonstrated at 1GHz but the integration with the antenna showed only results up to 200MHz.

The problem of stability is therefore a major hindrance to the successful demonstration and implementation of NICs, especially at higher order frequency.

Table 2.1 shows a summary of the reviewed publications on NICs detailing the key parameters such as top frequencies, NIC circuit type, antenna used and whether it was realised physically or just via simulations. Also included in the table are details on noise and linearity measurements.

Table 2.1 Summary on NICs

Ref	Max Freq. (MHz)	Type of NIC circuit	Antenna type	Simulated or Measured	Stability analysis (Type)	Noise measurement	Linearity measurement

[8]	220	Linvill two transistor model	6 inch monopole and 12 inch dipole	Measured	None	Yes	No
[9]	90	Linvill two transistor model	Monopole (Equivalent circuit)	Simulated	Yes (Stability circles)	No	No
[10]	2500	Ideal non-Foster elements	PIFA	Simulated	None	No	No
[13]	1000	Ideal non-Foster elements	6 inch loop	Simulated	None	No	No
[14]	5000	Linvill two transistor model	Microstrip patch antenna with Left hand structures	Simulated	None	No	No
[15]	600	Linvill two transistor model	3 inch monopole	Measured	None	No	No
[17]	500	Linvill two transistor model	Dual band metamaterial inspired antenna	Measured	None	No	No
[16]	100	Modified Linvill two transistor model	Loop antenna	Measured	None	No	No
[19]	200	Modified Linvill two transistor model	15cm monopole	Measured	None	No	No

2.5. Stability within NICs

There are available means of testing stability in active circuits. Examples are the K – factor test, the B1 auxiliary stability factor, the use of stability circles and the normalised determinant function (NDF). The theory behind these stability methods are widely available

in literature and have been used extensively to determine the stability of amplifiers and to check the start-up conditions of the oscillators.

Some of these test methods have also been included into some simulators like K-factor, B1 and stability circles or μ stability factor, but as described in [20], the K- factor tests do not correctly predict the instability associated with NICs. One flaw of the K - factor test can be seen in its definition. Ref [21] gives the definition of the Rollett K stability factor as shown in Eq.2.23 below. The condition for stability is that K >1.

$$K = \frac{1 - |s_{11}|^2 - |s_{22}|^2 + |\Delta|^2}{2 \times |s_{12}| \times |s_{21}|} \tag{2.23}$$

where Δ is the determinant of the circuit's S – matrix.

Stability factor, μ, computes the geometric stability factor of a 2-port. The geometric stability factor computes the distance from the center of the Smith Chart to the nearest unstable point of the input source plane. The necessary and sufficient condition for unconditional stability of the two port is that μ > 1. Likewise, the μ stability factor is also dependent on the S – matrix

$$\mu = \frac{1 - |s_{11}|^2}{|s_{22} - s_{11}{}^{*}\Delta| + |s_{21}s_{12}|} \tag{2.24}$$

B1 is the auxiliary stability factor for a two-port, defined as Eq.2.25 and the condition for stability is that B1 > 0.

$$B1 = 1 + |s_{11}|^2 - |s_{22}|^2 - |\Delta|^2 \qquad 2.25$$

$$\Delta = s_{11}s_{22} - s_{12}s_{21}$$

NDF is considered a rigorous method of predicting the stability of an N-port network structure. It is defined as the ratio of the determinants of the network function when all the generators are on and when there are off.

$$NDF = \frac{\Delta(s)}{\Delta_o(s)} \qquad 2.26$$

Where Δ(s) is the corresponding network function (impedance) when all the generators and active elements are on and $\Delta_o(s)$ is the same network function when all the generators and active elements are off. It can be seen that the NDF also rely on network impedances at measurement ports which would lead to missing the hidden mode of oscillation.

It can be observed that Eq. 2.23 -2.25 are based on the corresponding S – matrix (appendix D) of the NIC. The S - matrix is a port based parameter and it is possible for it to miss out the other sources of instability. References [22-23] point to unstable hidden modes of oscillation in linear systems which are not apparent from the input and output ports. The use of a stability method based on state space representation of a linear system to predict the instability of active circuits would not fully reveal instabilities as they are usually dependent on the time domain behaviour of the NIC circuit. It has also been suggested that complex non-Foster elements (trying to invert more than one element per NIC) have a higher probability of instability. This is one of the reasons why most of the prototypes available involve simple non-Foster elements.

Other methods available in the literature regarding stability of non-Foster elements involves computing the stability of the NIC based on loads applied, open or short circuit [8, 11]. These methods also do not give useful information because they inherently depend on measurements from the ports of the NIC.

2.6. Other NIC configurations

Asides from the use of transistors and the Linvill's schematic to realise non-Foster elements, there are other means of realising these elements. Herold, in [24], lists a variety of devices that can be used to realise negative resistances but they almost all require the use of vacuum electron tubes. The use of vacuum tubes was also suggested by [11].

Another NIC method makes use of an amplifier. This was also suggested in [24] in which the impedance to invert, which in this case is a resistor, is connected to the output of the amplifier. Feedback lines then connect the two terminals of the resistor to the input terminals of the amplifier. Sussman-Fort and Rudish in [8] showed a slightly different schematic. In this case, the impedance to invert is connected along the feedback path as shown in Fig.2.35

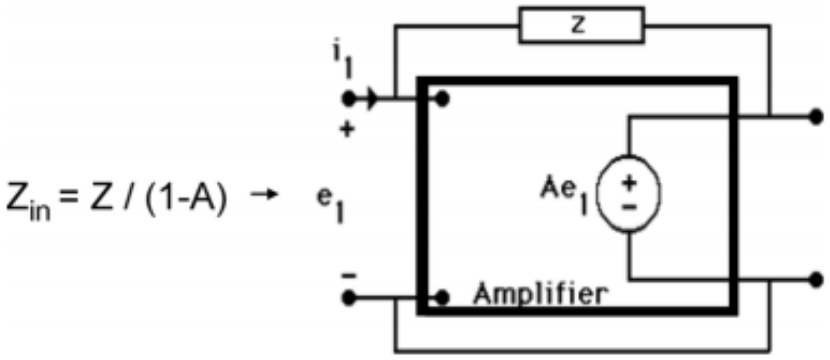

Fig.2. 35 Amplifier based NIC [8]

Reference [8] also suggested another schematic for achieving non-Foster elements. The authors used a transformer to achieve the phase inversion required to achieve the impedance inversion. The value of the negative impedance is dependent on the turning ratio of the transformer. Fig.2.36 shows the transformer based NIC.

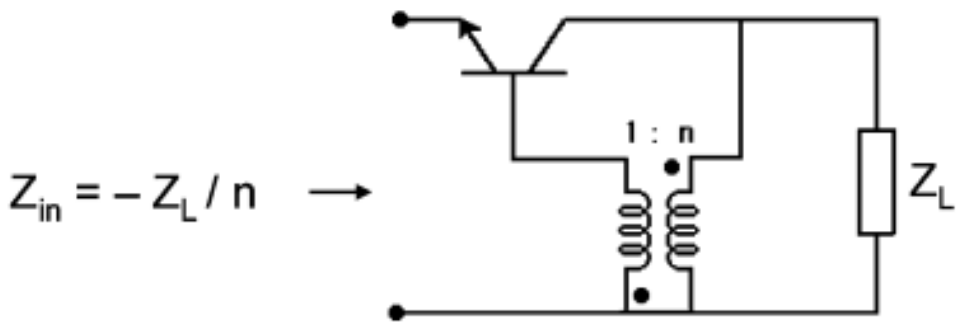

Fig.2. 36 Transformer based NIC [8]

2.7. Other application of NIC

Asides from impedance matching, to which most of the NIC demonstrations are aimed, there are other applications which use NICs although these have only been demonstrated analytically. Reference [25] showed the use of NICs as a capacitance multiplier for use in integrated low pass filters. There is a need for high value capacitors when designing filters especially at very low frequencies. In this work, the authors use the operational amplifier based NIC to obtain a negative capacitor. They were able to demonstrate, by simulation, the inverting of a 100pF capacitor to yield approximately -100nF between 500mHz to 500kHz as shown in Fig.2.37. The authors then replace the 100pF with a similar NIC (double inversion) and this results in a higher positive capacitance, which ranged from 4µF to 10nF, depending on the values of other NIC parameters. Using this active high value capacitor, a low pass filter was designed and its response is shown in Fig.2.38. Varying the simulated capacitor value, by varying other NIC parameters, a low pass filter was designed which had a response whose cut-off frequency varies between 400mHz to 159Hz.

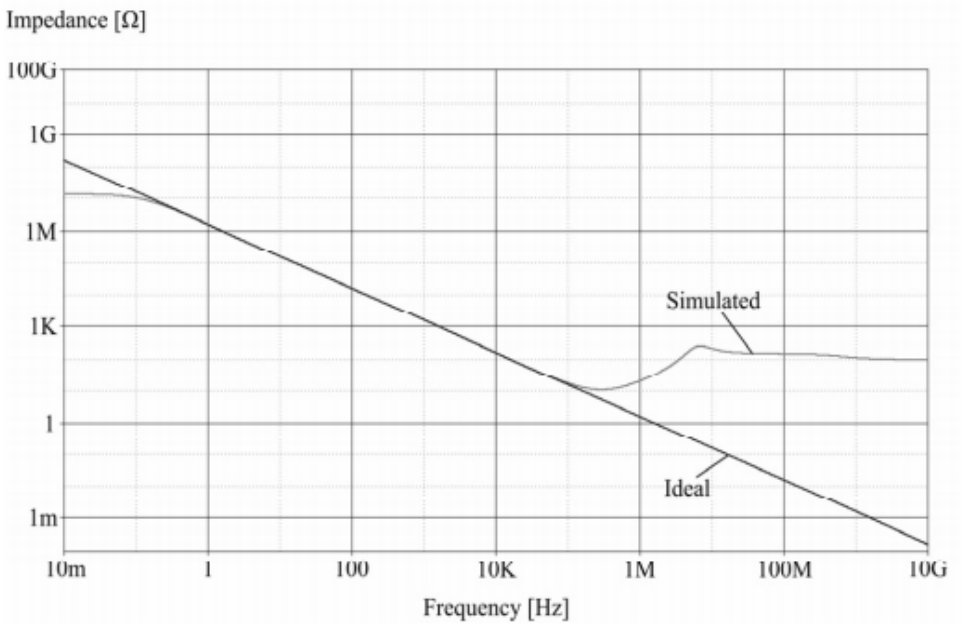

Fig.2. 37 Simulated comparison of NIC reactance and ideal -100nF [25]

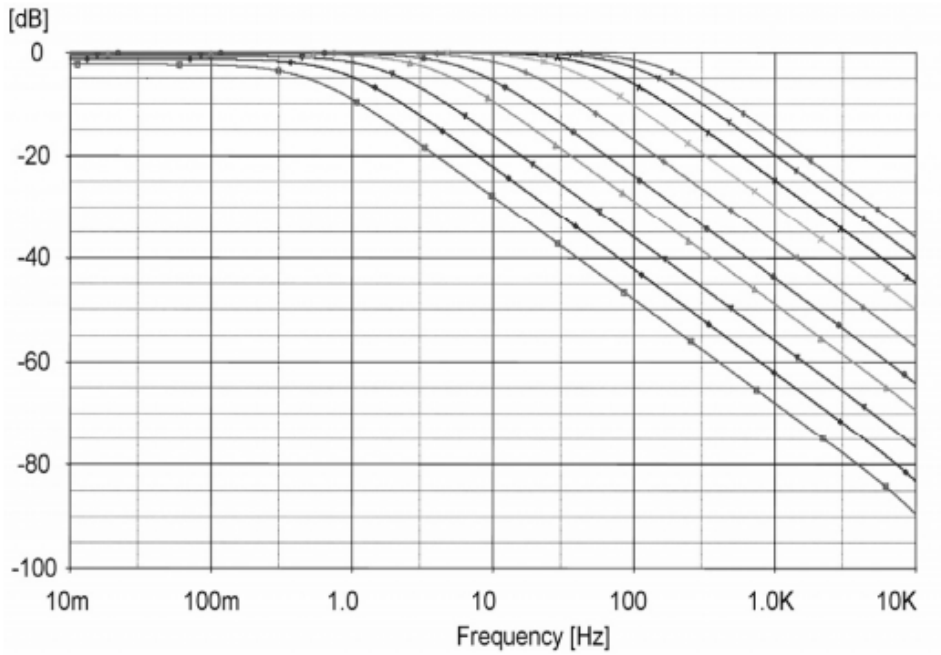

Fig.2. 38 Low pass filter response with active capacitors [25]

In another example provided in Ref.[26], the proposed NIC in [25] is employed to increase the temperature sensitivity in a bridge sensor and an error spread of less than $\pm 1\%$ was reported.

2.8. Conclusion

In this chapter, a review into the state of art in non-Foster matching has been discussed. It has also been shown how non-Foster elements help provide broadband matching of antennas and complete impedance cancellation.

Schematics for non-Foster element realisation and a few examples have been discussed. The common problem associated with NICs and non-Foster elements is stability. The current stability analysis methods have been discussed and the reasons why these methods fail to correctly predict instability within the NICs has been highlighted. Other means and schematics of achieving non-Foster elements have also been discussed and the uses of NIC in applications other than impedance matching are also discussed.

Of all the examples of the realisation of an NIC discussed, the highest frequency achieved by an integrated prototype is 500MHz [17]. But this did not discuss the effect of noise and linearity and also had some results that might suggest instability within the NIC. Ref [8] was the only reference to date to show the effect of noise within the NIC and its effect on an integrated NIC antenna but this also did not show any results on linearity and its top frequency was 200MHz. On the whole, NICs have been viewed and an accepted method for making small broadband antennas but the instability and complexity of the Linvill schematic have limited the highest frequency and the fabrication of prototypes.

The use of NICs within other applications just like other alternatives to the Linvill NIC have not really got any traction at the moment as prior efforts have all been focused on making broadband antennas using the two transistor Linvill's schematic.

Reference

[1] D. Manteuffel and M. Arnold, "Considerations for Reconfigurable Multi-Standard Antennas for Mobile Terminals," in *Antenna Technology: Small Antennas and Novel Metamaterials, 2008. iWAT 2008. International Workshop on*, 2008, pp. 231-234.

[2] C. T. P. Song, Z. H. Hu, J. Kelly, P. S. Hall, and P. Gardner, "Wide tunable dual-band reconfigurable antenna for future wireless devices," in *Antennas & Propagation Conference, 2009. LAPC 2009. Loughborough*, 2009, pp. 601-604.

[3] Z. H. Hu, C. T. P. Song, J. Kelly, P. S. Hall, and P. Gardner, "Wide tunable dual-band reconfigurable antenna," *Electronics Letters*, vol. 45, pp. 1109-1110, 2009.

[4] M. Pelissier, F. Demeestere, F. Hameau, D. Morche, and C. Delaveaud, "LNA-antenna codesign for UWB systems," in *Circuits and Systems, 2006. ISCAS 2006. Proceedings. 2006 IEEE International Symposium on*, 2006, p. 4 pp.

[5] D. Ueo, H. Osabe, K. Inafune, M. Ikebe, E. Sano, M. Koutani, M. Ikeda, and K. Mashiko, "7-GHz Inverted-F Antenna Monolithically Integrated with CMOS LNA," in *Intelligent Signal Processing and Communications, 2006. ISPACS '06. International Symposium on*, 2006, pp. 259-262.

[6] S. Bories, M. Pelissier, C. Delaveaud, and R. Bourtoutian, "Performances Analysis of LNA-Antenna Co-Design for UWB System," in *Antennas and Propagation, 2007. EuCAP 2007. The Second European Conference on*, 2007, pp. 1-5.

[7] W. R. MacLean, "The Reactance Theorem for a Resonator," *Proceedings of the IRE*, vol. 33, pp. 539-541, 1945.

[8] S. E. Sussman-Fort and R. M. Rudish, "Non-Foster Impedance Matching of Electrically-Small Antennas," *Antennas and Propagation, IEEE Transactions on,* vol. 57, pp. 2230-2241, 2009.

[9] J. T. Aberle, "Two-Port Representation of an Antenna With Application to Non-Foster Matching Networks," *Antennas and Propagation, IEEE Transactions on,* vol. 56, pp. 1218-1222, 2008.

[10] G. Bit-Babik, C. Di Nallo, J. Svigelj, and A. Faraone, "Small Wideband Antenna with non-Foster Loading Elements," in *Electromagnetics in Advanced Applications, 2007. ICEAA 2007. International Conference on,* 2007, pp. 105-107.

[11] J. G. Linvill, "Transistor Negative-Impedance Converters," *Proceedings of the IRE,* vol. 41, pp. 725-729, 1953.

[12] L. C. Verman, "Negative Circuit Constants," *Radio Engineers, Proceedings of the Institute of,* vol. 19, pp. 676-681, 1931.

[13] S. Koulouridis, "Non - foster circuitry design for antennas," in *Antennas and Propagation (EUCAP), Proceedings of the 5th European Conference on,* 2011, pp. 237-239.

[14] D. Segovia-Vargas, V. Gonzalez-Posadas, J. L. Jimenez, M. Ugarte, x00F, E. oz, J. Herraiz-Martinez, M. Garcia, and L. E. oz, "Negative impedance converters (NICs) in the design of small and multifrequency antennas," in *Antennas and Propagation (EUCAP), Proceedings of the 5th European Conference on,* 2011, pp. 2724-2728.

[15] K.-S. Song and R. G. Rojas, "Electrically small wire monopole antenna with Non-Foster impedance element," in *Antennas and Propagation (EuCAP), 2010 Proceedings of the Fourth European Conference on,* 2010, pp. 1-4.

[16] S. Hrabar, I. Krois, I. Bonic, and A. Kiricenko, "Non-foster elements - new path towards broadband ENZ and MNZ metamaterials," in *Antennas and Propagation (EUCAP), Proceedings of the 5th European Conference on*, 2011, pp. 2674-2677.

[17] H. Mirzaei and G. V. Eleftheriades, "A wideband metamaterial-inspired compact antenna using embedded non-Foster matching," in *Antennas and Propagation (APSURSI), 2011 IEEE International Symposium on*, 2011, pp. 1950-1953.

[18] J. Zhu and G. V. Eleftheriades, "Dual-band metamaterial-inspired small monopole antenna for WiFi applications," *Electronics Letters*, vol. 45, pp. 1104-1106, 2009.

[19] C. R. White, J. S. Colburn, and R. G. Nagele, "A Non-Foster VHF Monopole Antenna," *Antennas and Wireless Propagation Letters, IEEE*, vol. 11, pp. 584-587, 2012.

[20] J. L. Jimenez-Martin, V. Gonzalez-Posadas, A. Parra-Cerrada, A. Blanco-Campo, E. Ugarte-Munoz, and D. Segovia-Vargas, "Full conditions for the stability analysis of negative impedance converters," in *Antennas and Propagation (EUCAP), 2012 6th European Conference on*, 2012, pp. 135-138.

[21] D. V. Krstic, G. Jovanovic, and A. Vasic, "Linvill and Rollett Stability Factor and Condition of Feedback Oscillator Design," in *Telecommunications in Modern Satellite, Cable and Broadcasting Services, 2007. TELSIKS 2007. 8th International Conference on*, 2007, pp. 639-640.

[22] S. D. Stearns, "Non-foster circuits and stability theory," in *Antennas and Propagation (APSURSI), 2011 IEEE International Symposium on*, 2011, pp. 1942-1945.

[23] S. D. Stearns, "Incorrect stability criteria for non-foster circuits," in *Antennas and Propagation Society International Symposium (APSURSI), 2012 IEEE*, 2012, pp. 1-2.

[24] E. W. Herold, "Negative Resistance and Devices for Obtaining It," *Radio Engineers, Proceedings of the Institute of*, vol. 23, pp. 1201-1223, 1935.

[25] A. De Marcellis, G. Ferri, and V. Stornelli, "NIC-based capacitance multipliers for low-frequency integrated active filter applications," in *Research in Microelectronics and Electronics Conference, 2007. PRIME 2007. Ph.D.*, 2007, pp. 225-228.

[26] A. J. Lopez-Martin, J. I. Osa, M. Zuza, and A. Carlosena, "Analysis of a negative impedance converter as a temperature compensator for bridge sensors," *Instrumentation and Measurement, IEEE Transactions on*, vol. 52, pp. 1068-1072, 2003.

CHAPTER 3

POTENTIAL OF BROADBAND ANTENNA MATCHING USING NEGATIVE IMPEDANCE CONVERTERS

3.1. Background

The need for physically small antennas is quite evident in the mobile handset industry but with the restriction in size comes a limit in the matched bandwidth of the antenna. Chu [1], gives a relationship between antenna size and Q, indicating that bandwidth and volume are proportional as shown in equation 3.1.

$$Q = \frac{1}{(k^3a^3)} + \frac{1}{(ka)} \qquad (3.1)$$

where a is the radius of the sphere that completely circumscribes the antenna, $k = 2\pi/\lambda$ and $Q = \frac{f_c}{\Delta f}$ where fc is the antenna centre frequency and Δf is the bandwidth if the antenna.

The use of passive matching networks has been explored, but this is also limited by the trade-off specified by the Bode-Fano limit. With the advent of cognitive radios (CR) and IEEE 802.22, the standard for wireless regional area networks (WRAN) which use the white spaces in television frequency spectrum, there will be a need for mobile CR nodes; these nodes will require small antennas that are wideband for either communication or spectrum sensing. The conventional means of matching antennas to yield broadband performances are limited by the Chu and Bode-Fano limits. This is mainly due to the need to resonate the antenna with passive positive reactances (Foster elements), but this only results in net zero reactance at spot (resonant) frequencies. Any change either side of this spot frequency causes the net

reactance to change and the antenna losses it match. This then leads to a compromise between match quality and bandwidths. However, as described in chapter 2, if an element with a negative impedance slope is used, then it is possible to have a net zero reactance continuously within the whole or part of the bandwidth. These elements with negative slopes are called non-Foster elements and they are usually negative capacitors and inductors.

As previously discussed in chapter 2, a negative impedance converter (NIC) can be used to realise a non-Foster element (see Fig.2.10). Linvill, in 1957, showed how to realise non-Foster elements with NICs [2]. This involved the use of transistors connected in a feedback path arrangement with the impedance to invert connected between the two drain or collector terminals. A simple circuit schematic of the Linvill NIC without the DC bias network is shown in Fig. 3.1a. This circuit provides a negative capacitive reactance across the emitter terminals. One of the advantages of Linvill's NIC is that it is reciprocal and symmetric and this makes it usable in the duplex mode of operation, though this is dependent on the transistor choice in terms of its power handling capability.

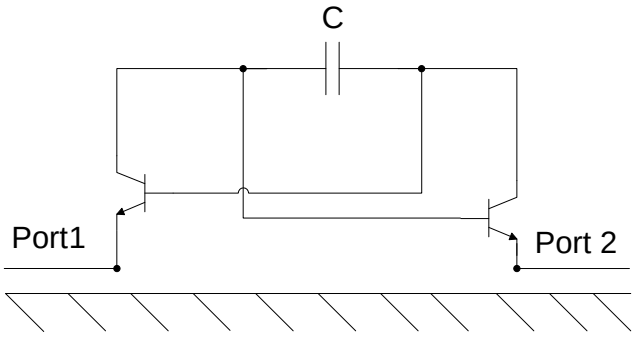

(a)

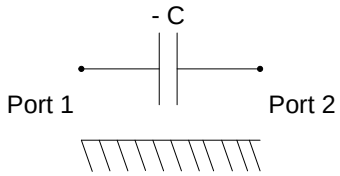

(b)

Fig.3.2 (a) Linvill's Negative Impedance Converter Circuit and (b) Ideal negative capacitance

3.2. Simulation with ATF54143 transistor

Using the Linvill's NIC shown in Fig 3.1a, a negative capacitor was simulated using the Microwave Office simulator by Applied Wave Research.

The heterojunction FET, Avago ATF 54143, was chosen because it is wideband, has a low noise figure and good 3rd order intercept point (IP3) as seen in the datasheet in the appendix A. Using s-parameter files of an Avago ATF 54143 transistor biased at 3V, 60mA, connected as in the Linvill's configuration with a 3.9pF AVX capacitor, simulation showed a negative capacitance appears at the output. The datasheets for the transistor and the capacitor used in this simulation are in the appendix A. This was then compared with what was obtained when an ideal negative capacitor was connected between two 50Ω measurement ports in the same simulator as shown in Fig. 3.1b. Figures. 3.2 and 3.3 show the results.

From the input and output impedance plots shown on the Smith chart, Fig.3.2, and its impedance against frequency plots, Fig.3.3, the basic properties of a non-Foster element can be seen:

1. Anticlockwise rotation around the Smith chart with increasing frequency (fig. 3.2)

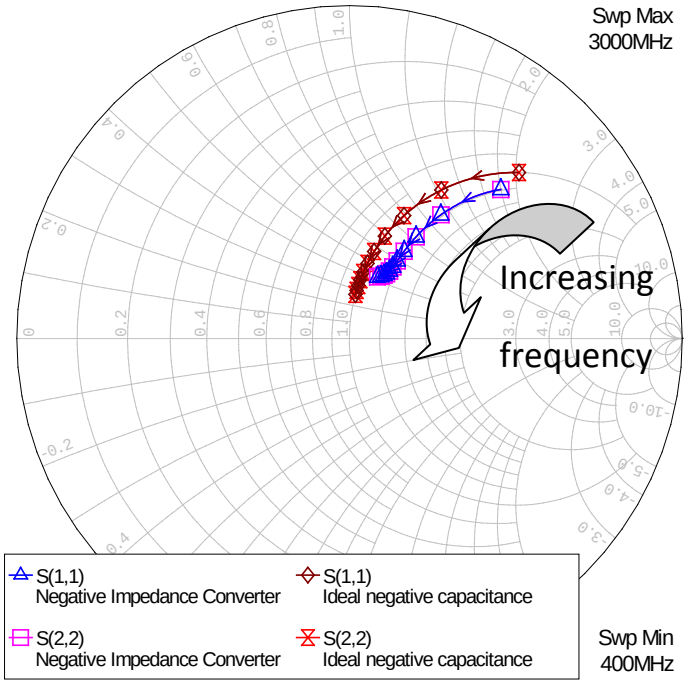

Fig.3.3 S - parameter plots of NIC of Fig.3.1 and ideal negative capacitance

2. Negative slope of impedance to frequency curve (fig. 3.3)

The reactance of a positive capacitance can be represented by equation 3.2

$$X_c = \frac{-1}{\omega C} \qquad 3.2$$

When the capacitance C is negative, the reactance equation becomes

$$X_c = \frac{-1}{-\omega C} = \frac{1}{\omega C} = \frac{1}{2\pi f C} \qquad 3.3$$

This implies that

$$X_c \propto \frac{1}{f} \qquad 3.4$$

This results in an inverse proportionality between capacitive reactance and frequency which is seen in Fig.3.3

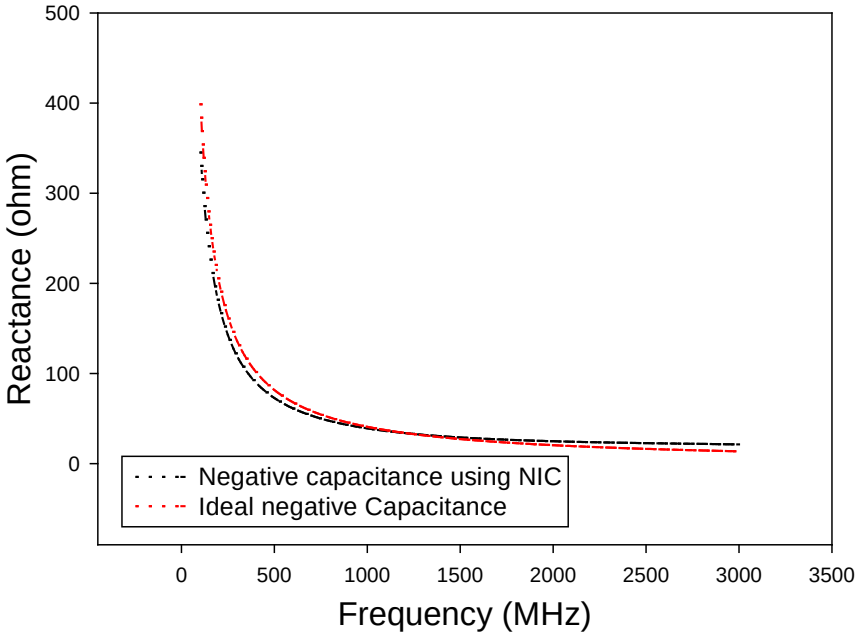

Fig.3.4 Simulated Impedance vs Frequency of NIC and ideal negative capacitance.

Figure 3.4 shows the capacitance vs frequency plot extracted from the reactance found in the simulator. It can be seen that there is a frequency dependence in the case of the negative capacitor realised using the NIC, unlike that obtainable from the ideal capacitance. This dependence is primarily due to the transistors. Equation 3.5 shows a relationship between the output Z_{out} impedance and the impedance to invert Z_{in} [2].

$$Z_{out} = (1\text{-}2 \propto)Z_{in} + 2r_e + (1 - \propto)2r_b \qquad (3.5)$$

where, Z_{out} is impedance seen across the terminals of the NIC, Z_{in} is the capacitor being inverted, α is the current gain of the transistor in common base mode, r_e and r_b are emitter and base resistance respectively.

The proof of eq. 3.2 is given in chapter 2 (eqs. 2.3 – 2.21). The equivalent circuit of the NIC used in this analysis is shown in ref [2].

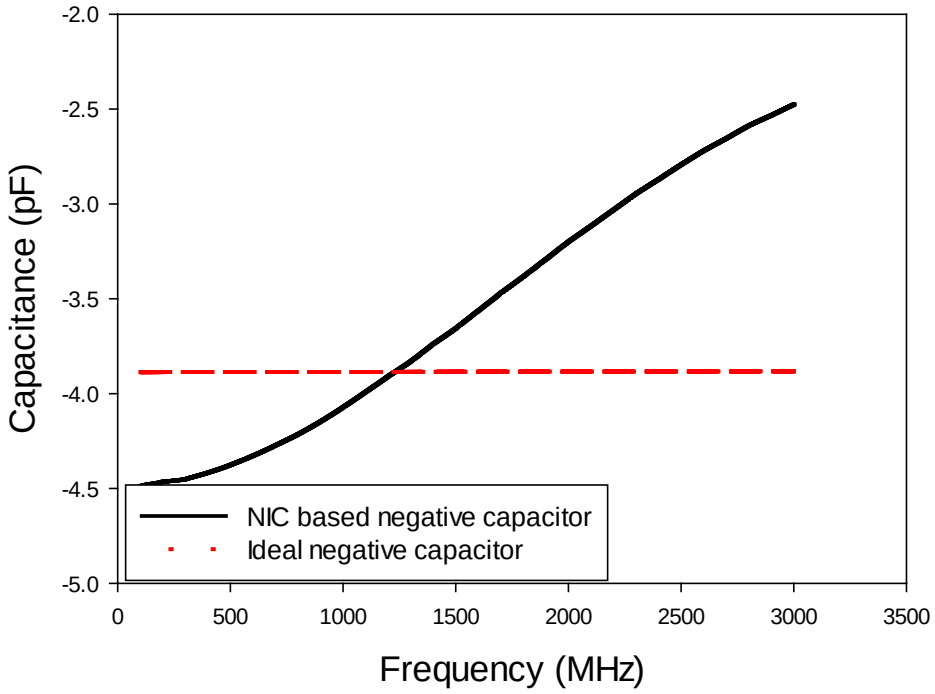

Fig.3.5 Simulated capacitance against frequency.

The first term of the expression above is most significant as the second and third terms r_e and r_b are relatively small but also contribute to the overall resistance in the inverted impedance, hence in Fig. 3.2, the overall resistance seen through the NIC based capacitor is larger than that through the ideal negative capacitor. It should be noted that because S-parameters are being measured, there is always a 50Ω load at the other port. Therefore, the impedance seen on the Smith chart is the inverted impedance in series with a 50Ω load from the ports. The parameter in the first term which leads to negative impedance is α, the current gain of the transistor in the common base mode, and this is frequency dependent. Its dependence can be expressed as [2]

$$\propto = \frac{\propto_0}{1 + j\frac{f}{f_{cutoff}}} \tag{3.6}$$

where f_{cutoff} is the alpha cut-off frequency, $\propto_0$ is the current gain at DC. Variation of α with frequency thus leads to a frequency dependence in the negative capacitance seen in Fig.3.4.

3.3 Antenna matching with Negative Impedance Converters

3.3.1 The Antenna

To demonstrate the use of non-Foster elements in antenna matching, an antenna which is electrically small was chosen. This was then matched with both conventional passive and non-Foster elements. The antenna chosen is the chassis antenna, this antenna was designed within the University of Birmingham AAEL research group and the results of this antenna has been reported the literature [3-5]. Figure 3.5 shows the antenna. It consists of a mobile sized ground plane and a coupling element on the left hand end of the ground plane. The coupling element is displaced from the edge of the ground plane by 6mm and has dimensions 40mm × 5mm × 7mm. The ground plane forms the primary radiating element. It can also serve as the chassis of a mobile or handheld device. Its size is 40mm × 100mm. The ground plane and coupling elements are fabricated from copper with thickness of 0.5mm. They are held together by a Rohacell^{TM} block with ε_r of 1.08 as shown in the photograph in Fig.3.6. The Q of the antenna is 19 at 900MHz. The antenna was simulated using CST which uses a finite integral full wave method (appendix C). Its S_{11} is shown in Fig 3.7. It is clear that the antenna is matched nowhere in the frequency range shown. It is therefore normal to use a matching circuit to permit operation in any given frequency band.

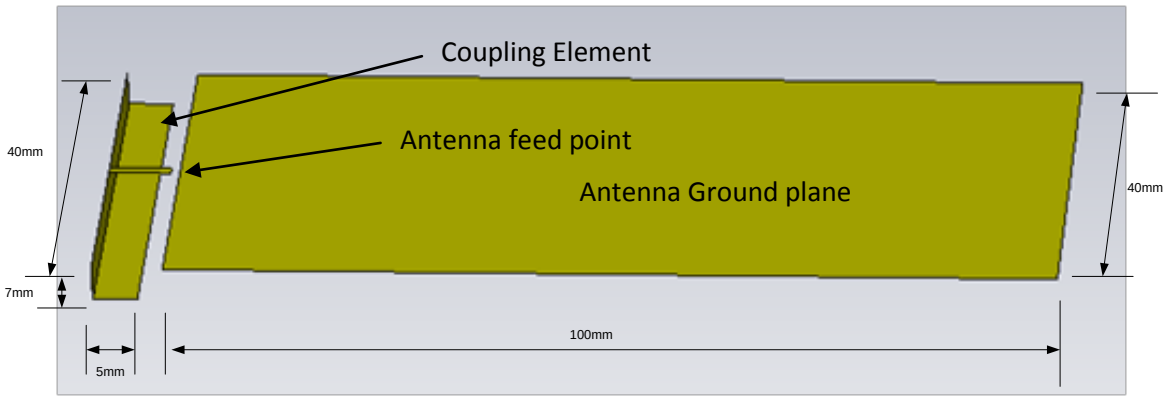

Fig.3.6 The chassis antenna structure layout schematic

Fig.3 7 The chassis antenna structure: the fabricated prototype

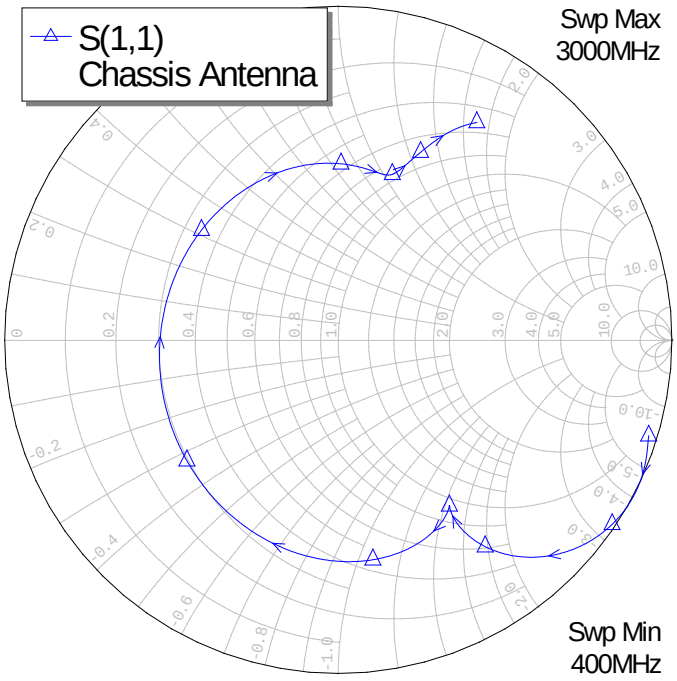

Fig.3 8 Simulated return loss, S11, of Chassis antenna

3.3.2 Matching Network

3.3.2.1. Ideal Negative Reactance Component Matching

To match this antenna, there is a need to find an approximate equivalent circuit of the antenna, in the form of an RLC network. To obtain the non-Foster matching network, the reactive part of the equivalent RLC circuit of the antenna is negated. The resultant negative LC network is then optimised in AWR which then forms the final non-Foster matching network. The resultant matching network is an L-shaped network of negative inductor and capacitor in series and a shunt negative capacitor, as shown in Fig 3.8.

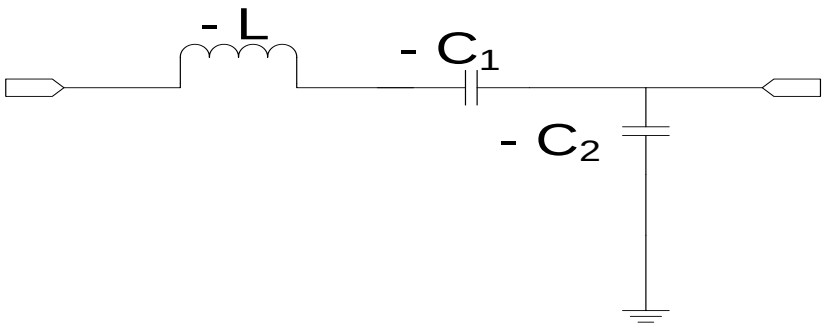

Fig.3 9 Non-Foster matching network

The return loss of the antenna matched with ideal negative elements is shown in Fig 3.9. This shows a wideband performance, with a return loss better than -10dB between 0.8GHz – 2.4GHz. This is a significant improvement from that which is obtainable when the same antenna is matched using passive elements. The Q of the antenna can also be seen to improve from 19 without matching to 1 after non-Foster matching.

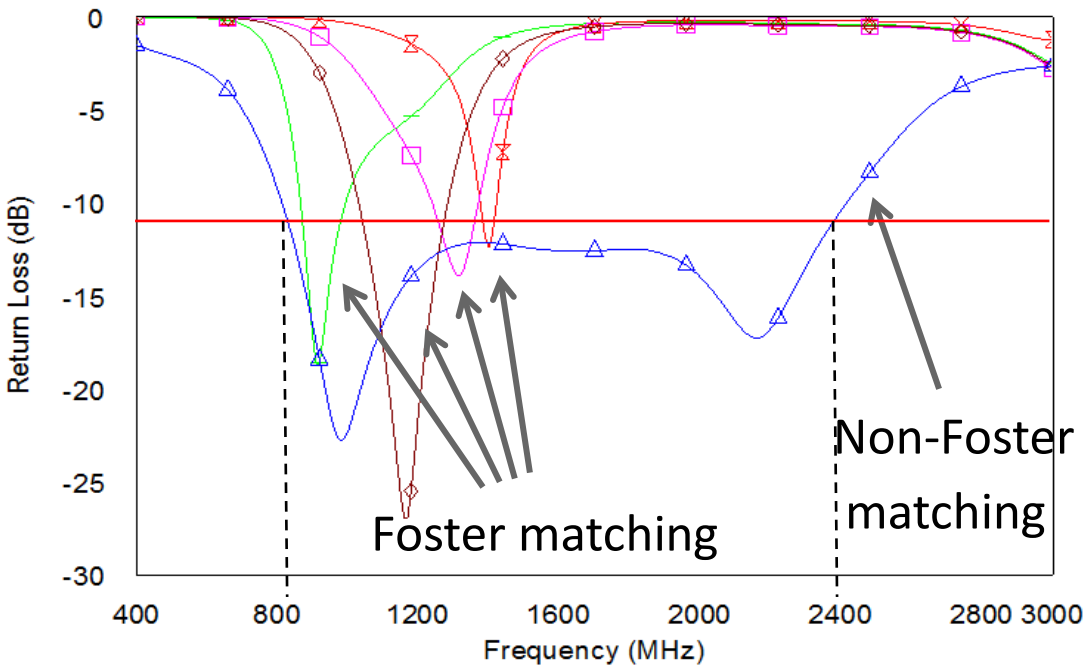

Fig.3 10 Simulated matched antenna return loss

This wideband matching is possible because the matching network shown in Fig 3.8 is non-Foster as can be seen in the anti-clockwise rotation around the Smith chart with increasing frequency in Fig 3.10.

Despite the ability of non-Foster elements to cancel the reactance of an element completely, independent of frequency, Fig.3.9 shows this is not the case, as the antenna is not matched completely over the entire bandwidth. This can be attributed to the fact that the non-Foster matching network whose S_{11} is shown in Fig.3.10 does not completely represent the conjugate of the antenna and also a simple LC matching network cannot fully represent the antenna. To obtain complete matching over the antenna frequency band, there is a need to increase the number of non-Foster elements and the complexity of the matching network.

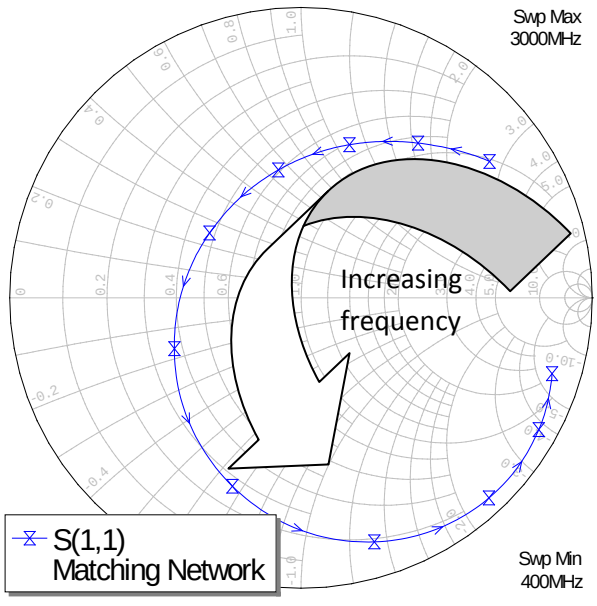

Fig.3 11 Simulated input impedance of the Non-Foster matching network.

3.3.2.2. Realistic Negative Impedance Matching

In order to simulate negative elements using the Linvill NIC model as practically possible, there is a need to include the required DC bias network and transmission lines. This practical schematic is shown in Fig.3.11a and it was simulated using AWR design environment. Fig.3.11a shows the schematic of the NIC which is used to realise the shunt element in the non-Foster element in the matching network. For the series elements, the capacitor indicated in Fig.3.11a is replaced by the corresponding inductor and capacitor. The S – parameters of the series and shunt elements are then combined along with the simulated antenna. It can be seen from Fig 3.11b that the overall achievable -10dB matched bandwidth is reduced from 1.6GHz (Fig.3.9 blue curve) to 1.1GHz (Fig.3.11b). This is due to the parasitics in the lumped elements, the bias network and the transmission lines. It should also be noted that there is a positive return loss between 2GHz and 2.7GHz. This is a sign of potential instability and could set the transistors into oscillations making them uncontrollable and unresponsive.

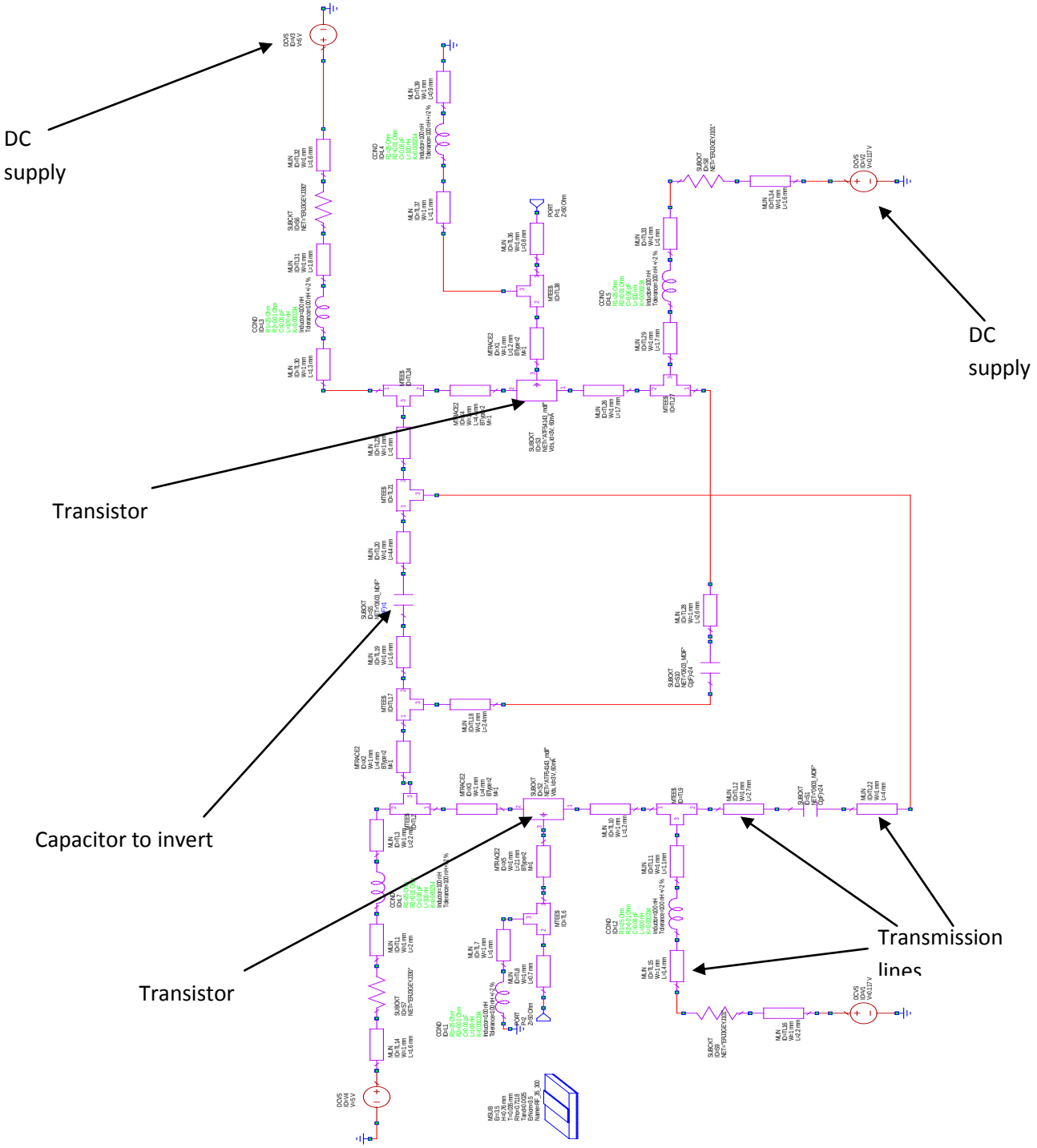
DC
supply
DC
supply
Transistor
Capacitor to invert
Transistor
Transmission
lines

(a)

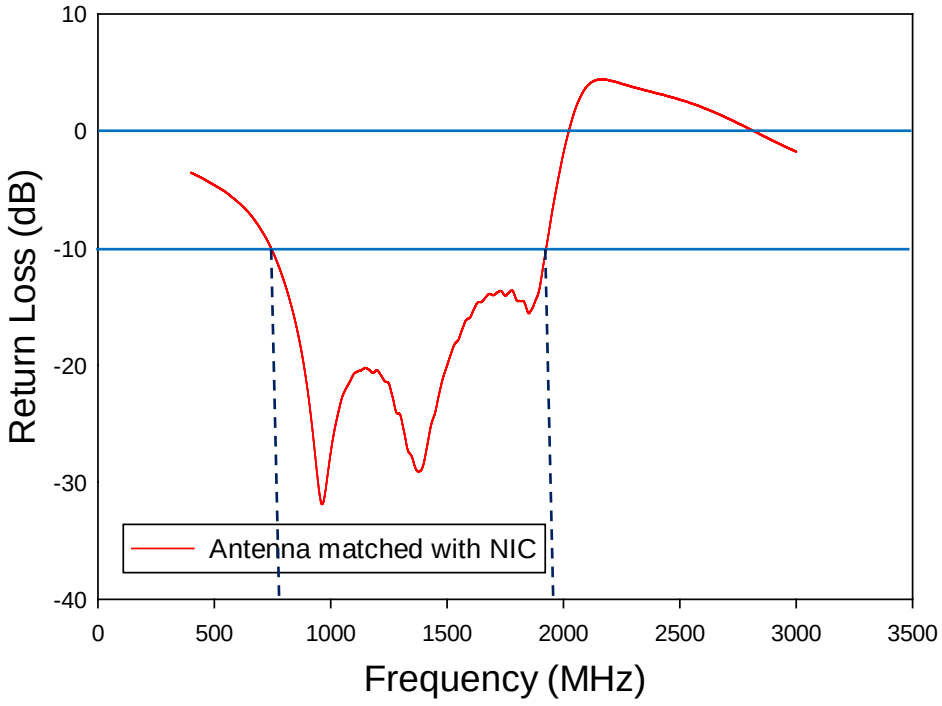

(b)

Fig.3 12 Simulated NIC matched antenna return loss with biasing and feedback paths.

The simulated non-Foster elements' S- parameters were combined with the simulated antenna in CST Microwave Studio and simulated realised gain, radiation and total efficiency were obtained. The definitions of antenna parameters and how they are calculated are in appendix D. These results were then compared with what is obtainable when the same antenna is matched passively to resonante at 1.8GHz. Table 3.1 shows the comparison between these simulated results. Table 3.2 shows that the NIC matched antenna has a better gain bandwidth product when compared to simulating the antenna with passive elements only.

Table 3 1: Simulated antenna performance.

Frequency (MHz)	Radiation Efficiency (dB)		Total Efficiency(dB)		Gain (dBi)	
	NIC matching	Passive matching	NIC matching	Passive matching	NIC matching	Passive matching
0.7	-3.086	-12.31	-3.508	-27.25	-1.407	-24.85
0.8	-2.503	-6.938	-2.647	-20.61	-0.6902	-18.88
1	-1.57	-2.435	-1.724	-12.63	0.505	-10.61
1.2	-1.61	-1.502	-1.851	-9.512	0.8724	-7.021
1.4	-1.998	-1.24	-2.041	-8.018	1.298	-4.971
1.6	-1.886	-0.7043	-1.948	-3.975	2.428	0.03442
1.8	**-0.9752**	**-0.2629**	**-1.158**	**-0.3037**	**3.771**	**4.325**
2	-0.2484	-0.0695	-0.2489	-2.6	4.658	2.156
2.2	-1.857	-0.2002	-2.951	-4.12	1.84	0.608
2.4	-6.858	-0.2461	-10.18	-4.295	-5.343	0.5358
2.6	-15.37	-0.1835	-19.95	-4.471	-15.01	0.6678

Table 3 2: Simulated gain-bandwidth product

	NIC matching	Passive matching
Gain bandwidth product (dBi)	1.86	0.96

All the above simulation results shows that non-Foster elements help achieve broad bandwidths without having adverse effects on the antenna gain and efficiency. It also indicates that there is an undesirable potential for oscillation when using NICs. This point is discussed later in chapter 4.

3.4 Tuning Range Enhancement Using NICs

Another potential application of an NIC is its use in enhancing the tuning range of a varactor tuned antenna by allowing the total capacitive reactance to tune pass zero reactance [6-7]. To demonstrate this, the chassis antenna described in Section 3.3 has been matched with a network consisting of a series varactor and a shunt 5.9nH inductor as shown in Fig.3.12a. This matching network provided a tuning range of 514MHz between 1777MHz and 2291MHz as shown in Fig.3.13. When this antenna is matched with a matching network that consists of a non-Foster element, realised using the NIC with an effective negative capacitance of -1.7pF, in series with a varactor and a shunt 5.9nH inductor as shown in Fig.3.12b, it is possible to match the antenna between 1381MHz and 2050MHz. This is because the net capacitance in series with the antenna using the NIC varies from -2.879pF to 1.248pF as against 0.72pF to 4.15pF with the varactor alone. Fig.3.13 also shows that the instantaneous bandwidths with the NIC and varactor. These bandwidths are larger especially at the lower frequency when compared with that of the varactor alone matching network which is synonymous with non-Foster matching. There is also another advantage of being able to switch easily from positive capacitance to negative capacitance by just varying the bias conditions of the varactor and enjoy the benefit of both non-Foster matching and Foster matching.

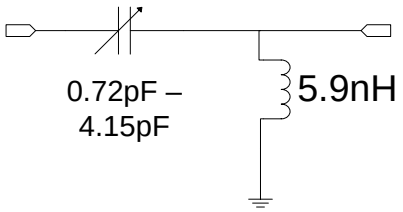

(a)

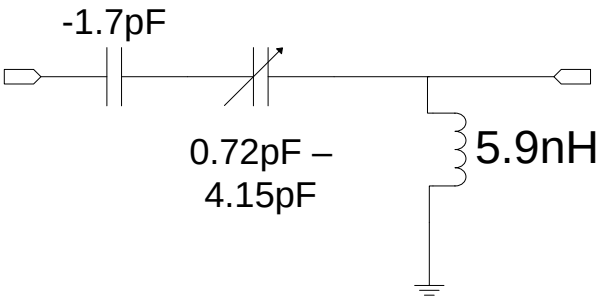

(b)

Fig.3 13 (a) Varactor matching network and (b) NIC and Varactor matching network.

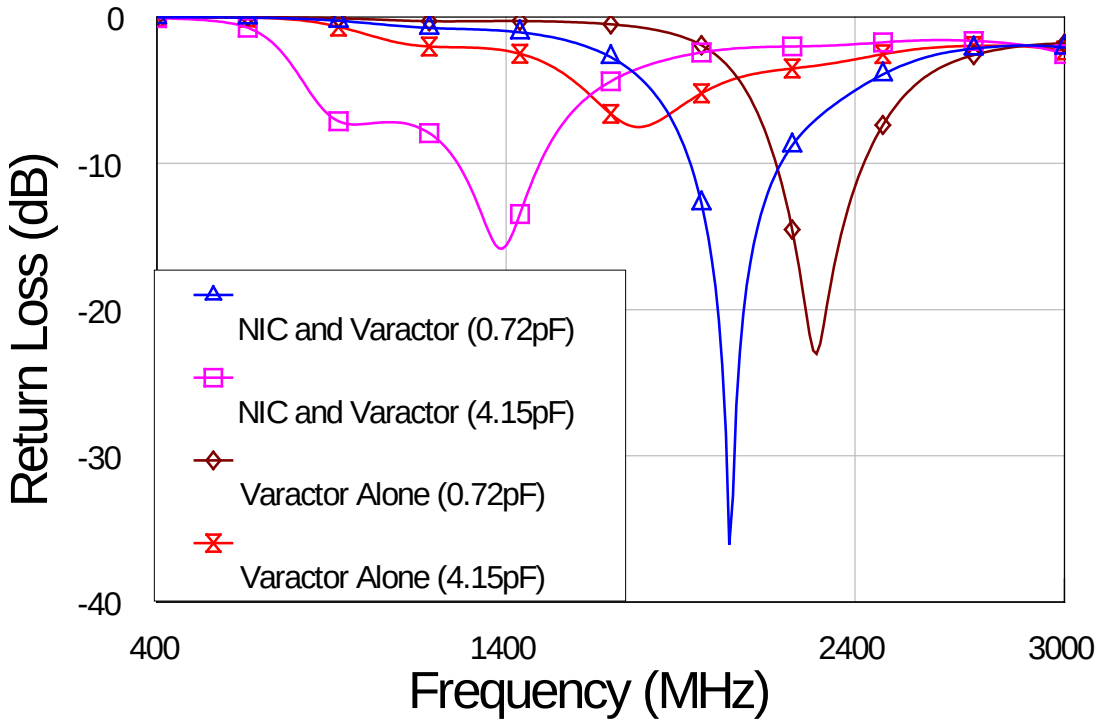

Fig.3 14. Simulated antenna return loss of tunable antenna with and without NIC

3.5. Conclusion

In this chapter, the need for non-Foster matching and its use in obtaining wideband matching has been discussed. A simulated antenna has been matched with both passive and non-Foster matching networks to demonstrate the potential of non-Foster elements and NICs. The use of NIC to achieve non-Foster elements have also been discussed and demonstrated with simulation and the potential difference between non-Foster elements realised using NICs and ideal negative elements have also been shown. And finally the use of non-Foster elements realised using NICs to match an antenna have been shown and the resultant wide bandwidth match is shown and its potential for increasing the tuning range of varactors. The potential for instability was also pointed out with a matched S_{11} begin greater than 0dB.

Reference

[1] L. J. Chu, "Physical Limitations of OmniDirectional Antennas," *Journal of Applied Physics,* vol. 19, pp. 1163-1175, 1948.

[2] J. G. Linvill, "Transistor Negative-Impedance Converters," *Proceedings of the IRE,* vol. 41, pp. 725-729, 1953.

[3] Z. H. Hu, J. Kelly, C. T. P. Song, P. S. Hall, and P. Gardner, "Novel wide tunable dual-band reconfigurable chassis-antenna for future mobile terminals," in *Antennas and Propagation (EuCAP), 2010 Proceedings of the Fourth European Conference on*, 2010, pp. 1-5.

[4] Z. H. Hu, C. T. P. Song, J. Kelly, P. S. Hall, and P. Gardner, "Wide tunable dual-band reconfigurable antenna," *Electronics Letters,* vol. 45, pp. 1109-1110, 2009.

[5] Z. H. Hu, C. T. P. Song, J. Kelly, P. S. Hall, and P. Gardner, "Novel reconfigurable dual-port UWB chassis-antenna," in *Antennas and Propagation Society International Symposium (APSURSI), 2010 IEEE*, 2010, pp. 1-4.

[6] Oluwabunmi O. Tade, Zhen H. Hu, Peter Gardner and Peter S. Hall, "Small antennas for cognitive radio using negative impedance converters," *The 12th Annual Post Graduate Symposium on the Convergence of Telecommunications, Networking and Broadcasting (PGNet2011),* 2011 2011.

[7] P. Gardner, A. Feresidis, P. Hall, T. Jackson, O. Tade, M. Mavridou, Y. Kabiri and X. Gao, "Frequency Reconfiguration in Single and Dual Antenna Modules," presented at the 7th European Conference on Antennas and Propagation Sweden, 2013.

CHAPTER 4

STABILITY IN PRACTICAL NIC CIRCUIT

4.1. Physical Realisation of NIC

As a first step in achieving an NIC matched antenna, a single negative capacitor was designed and built [1-4]. The schematic is shown in Fig 4.1 below. The components in the schematic include the Avago 54143 transistors, the bias network and other elements required to achieve a standalone negative element. There are passive elements (resistor,R, and capacitor,C,) and transmission lines, TX LINE, between the measurement ports and the collectors of the Avago ATF54143 transistors used which are the terminals of the NIC. The capacitors, C, ensures a circuit with an overall positive capacitance. As the capacitor to invert, C_{inv}, has some inherent parasitic resistances, if there are no positive elements between the measurement ports and the NIC, the circuit will be unstable and unmeasurable because the arising negative parasitic resistances would lead to instabilities. The effects of these added elements (R and C) and transmission lines would then be de-embedded from the measured result to obtain the actual NIC performance. Details of the de-embedding process are described later in chapter 5. Capacitors C_{DC} are DC blocking capacitors required to correctly bias the transistors that make up the NIC circuit.

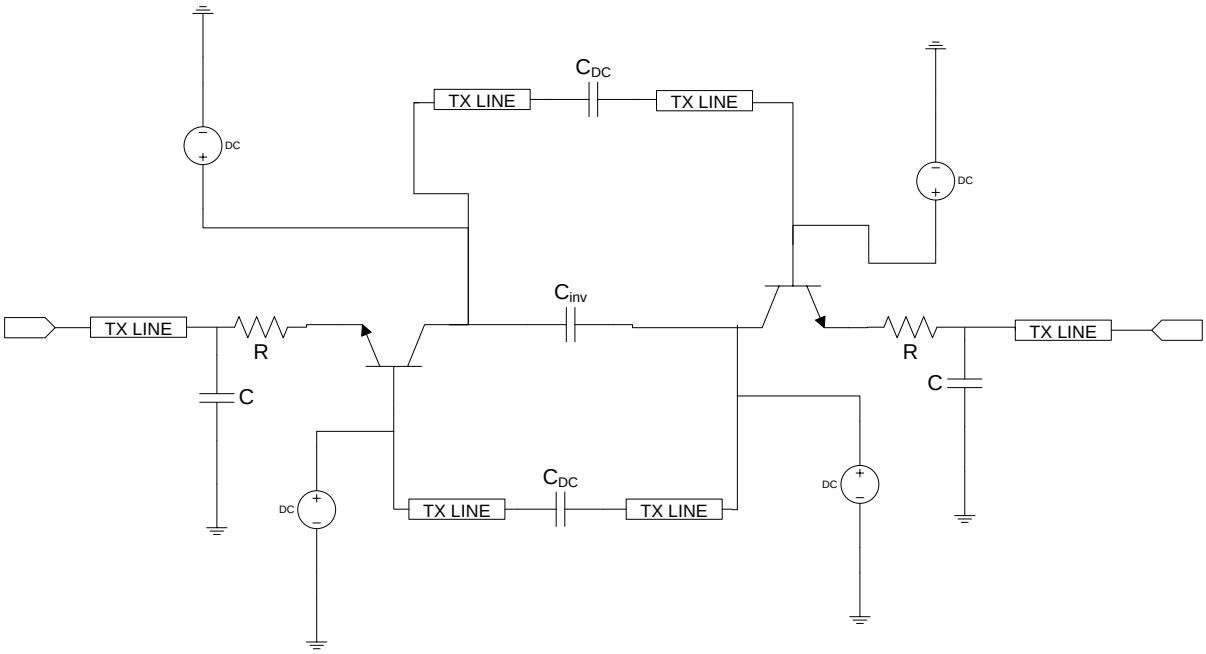

Fig.4 .1 AWR Circuit schematic for single element standalone negative impedance converter

R and C are the stability resistor and capacitor respectively, C_{DC} are the dc blocking capacitor, TXLINE are the coplanar waveguide (CPW) lines, C_{inv} is the capacitor to invert.

Because of the potential for instability noted in previous chapter (Fig. 3.11), it was necessary to check the stability of the circuit before it was fabricated. The standard methods and tools available for predicting and testing for stability of a circuit rely on test methods based on two port networks, such as the K stability factor and the B1 auxiliary stability factor test. These two methods provide the necessary and sufficient conditions for unconditional stability [5]. These two stability test methods were chosen because they are the two widely used and quoted methods and they can be simulated in AWR. The two conditions are:

$$K > 1 \text{ and } B1 > 0 \qquad (4.1)$$

where $$K = \frac{1-|s_{11}|^2-|s_{22}|^2+|\Delta|^2}{2|s_{12}s_{21}|}$$

and $$B1 = 1 + |s_{11}|^2 - |s_{22}|^2 - |\Delta|^2$$

$$\Delta = s_{11}s_{22} - s_{12}s_{21}$$

Appendix D contains how the component s – parameters can be calculated. The simulated magnitudes of K and B1 stability tests on the above circuit schematic were done using AWR and are shown in Fig. 4.2. The results show that the Linvill based circuit should be unconditionally stable as the two conditions are met.

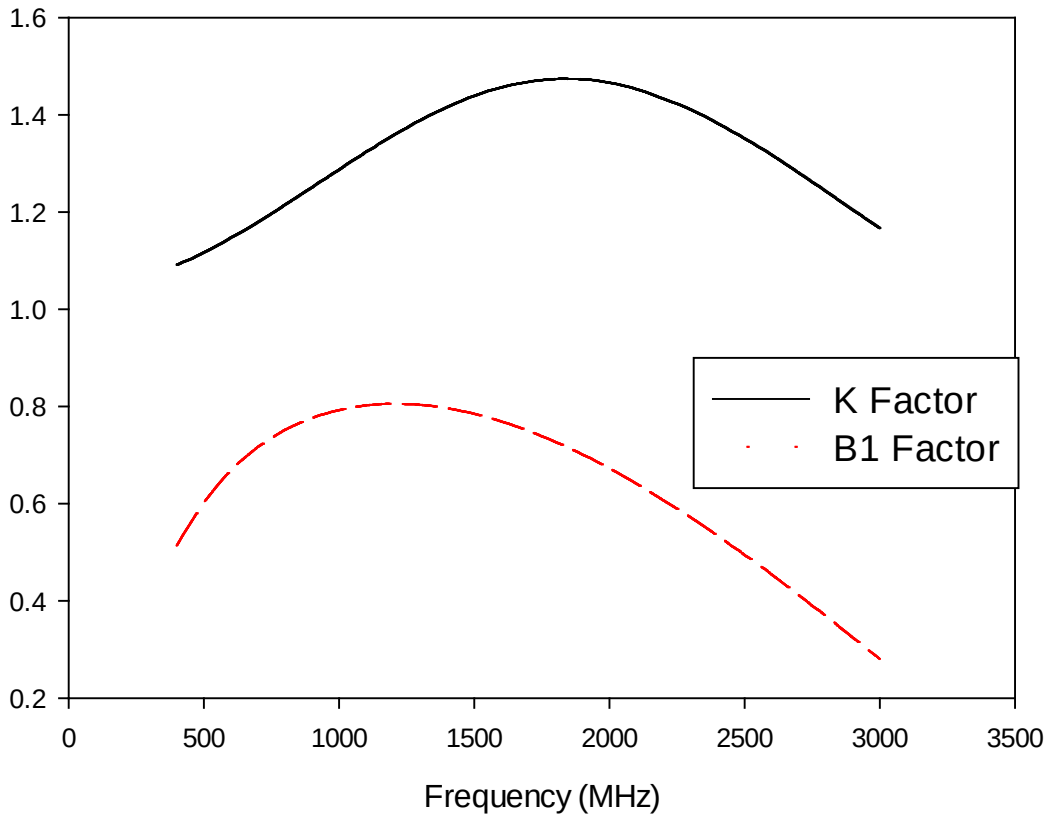

Fig.4 2 Simulated K-factor and B1 auxiliary stability factor

R = 10Ω, C = 2pF, C_{dc} = 0.1pF and C_{inv} = 3.9pF

When this simulated circuit was built as described later in chapter 5, it was found that they were unstable, with oscillation at 1.9GHz and at higher order harmonics. Clearly this was not predicted by the K-factor and B1 auxiliary stability factor tests.

The simulator was unable to correctly predict the instability because these stability prediction methods rely only on measurements of the two port S – parameters. It is known that there are hidden modes which can also cause instability, and these modes may not be observable from the ports. Hence, any prediction method that relies on the port measurements alone will not always indicate these instability modes [6].

Therefore, in order to realise a stable NIC, a further stability analysis was done, as described in the following section.

4.2. Stability Analysis

An approximate stability analysis based on the pole locations on the complex s-plane [7] has been developed. This analysis reveals how instabilities within the NIC can be predicted, though these instabilities may not be observable from the measurement ports.

4.2.1 Transfer Function

To determine the location of the poles of the NIC, it is necessary to first find the transfer function of the NIC. Also because a numeric analysis is being performed it is possible to determine the transfer function of the NIC away from the measurement ports. The ratio of the Laplace transforms of the response of a circuit, Y(s), and the input, X(s), is called the transfer function and this is expressed in equation 4.2 below [8],

$$H(s) = \frac{Y(s)}{X(s)} \qquad 4.2$$

The roots of the numerator of the transfer function are called the zeros of the transfer function and the roots of the denominator are called the poles of the transfer function. The location of the zeros and poles of the transfer function on the complex s- plane determine the stability or otherwise of a system according to Nyquist.

For a given driving voltage or impulse the response of the system can be derived from its transfer function. The response can be obtained by re-writing equation 4.2.

$$Y(s) = H(s)X(s) \qquad 4.3$$

And the time domain response of the system is obtained by inverse Laplace transforms of equation 4.3

$$y(t) = \mathcal{L}^{-1}\{H(s)\}x(t) \qquad 4.4$$

The inverse transform of the transfer function will show how stable the system is. If the poles of the transfer function are negative or negative complex, they would be on the left hand side of the complex s-plane, the response of the system in time domain will result in a decaying exponential while if the poles are positive or positive complex, they would be on the right hand side of the complex s-plane, the time domain response will have a growing exponential which would then lead to oscillation with increasing amplitude. If the poles are purely imaginary, this would also lead to oscillation but with constant amplitude.

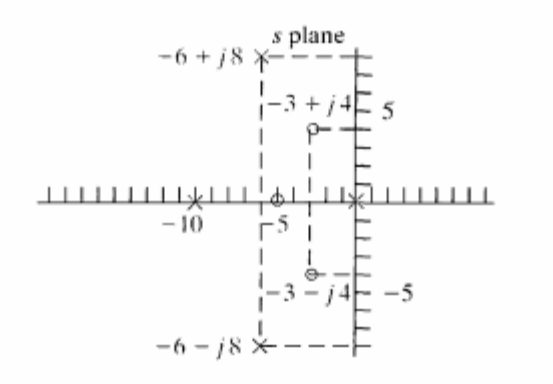

Fig.4 3 Complex S-plane and location of poles

The stability analysis proceeds by noting the symmetry of the circuit and splitting the analysis into the even and odd modes respectively.

4.2.2 Even mode

Figure 4.4 shows the development of the circuit model. Fig 4.4a shows the Linvill's NIC circuit model without the complete bias network with the required DC blocking capacitors C_{B1} and C_{B2} and the capacitor, C, being inverted. Figure 4.4b shows the circuit with capacitors split into two. In the even mode, the currents flow out of the transistors into the capacitor C are equal but opposite directions. Hence an open circuit occurs in the middle of this capacitor [9]. This implies that the element to invert, C, does not play a part in this analysis. However, in the feedback paths, the currents out of the transistors are equal and flow in the same (clockwise) direction around the feedback path. Splitting the circuit along its line of symmetry, gives Fig. 4.4c. The capacitor to invert has an open circuit on its terminal while the path through the DC blocking capacitors can be combined and closed off because

of the symmetric and reciprocal property of the NIC circuit, giving Fig.4.4d. C_1 in the figure is the series combination of $2C_{B1}$ and $2C_{B2}$.

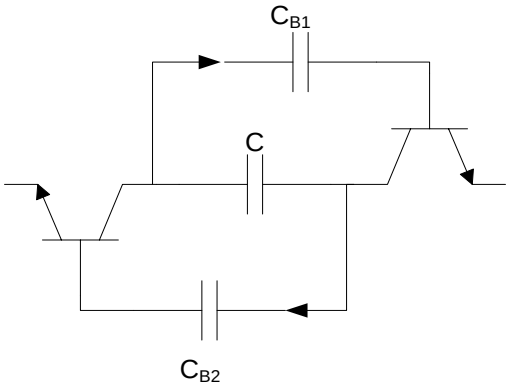

(a)

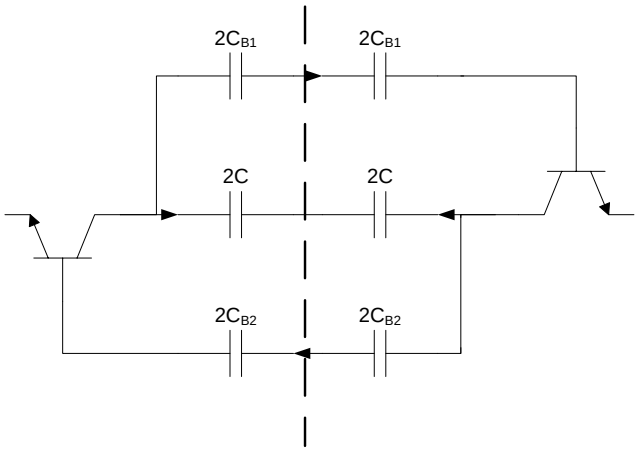

(b)

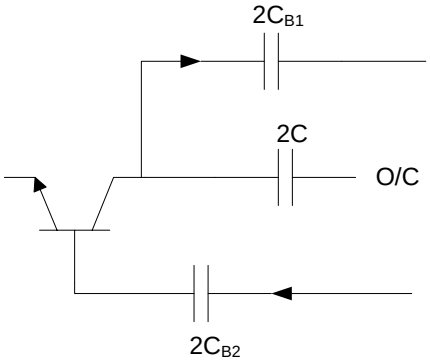

(c)

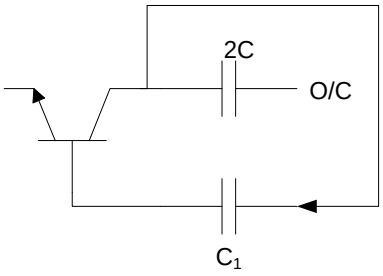

(d)

Fig.4 4 Development of the NIC circuit in even mode operation

(a) The NIC schematic (b) NIC in even mode operation (c) NIC after split along its line of symmetry and (d) NIC with closed up feedback path.

The equivalent circuit of NIC, with a transistor equivalent circuit, operating in the even mode is shown in Fig. 4.5. The equivalent circuit of the transistor in common gate mode, capacitor C_1 and an input source voltage V_s and output voltage V_o have been added.

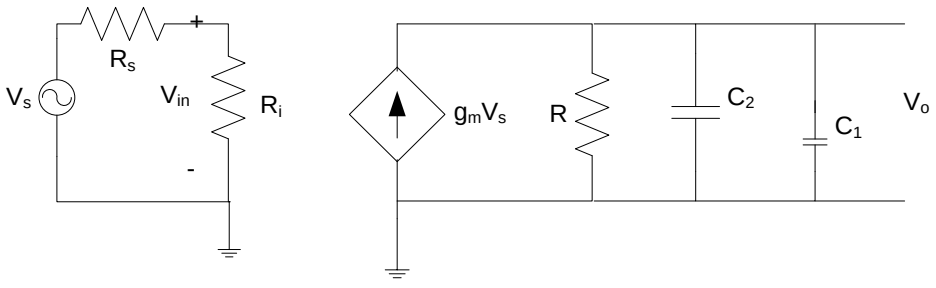

Fig.4 5 Equivalent circuit of the NIC in even mode (C_2 is the collector capacitance)

Now, let the reactance, X_A, be

$$X_A = R \,||\, C_2 \tag{4.5}$$

so that

$$X_A = \frac{R}{1 + sRC_2} \tag{4.6}$$

and let the reactance, X_T, be

$$X_T = X_A || C_1 \tag{4.7}$$

where

$$X_T = \frac{R}{1 + sR(C_1 + C_2)} \tag{4.8}$$

The output voltage, V_o, is given by

$$V_O = g_m V_s X_T \tag{4.9}$$

so that

$$\frac{V_o}{V_s} = \frac{g_m R}{1 + sR(C_1 + C_2)} \tag{4.10}$$

Equation 4.10 represents the transfer function of the NIC in the even mode. The poles, s, of the transfer function are:

$$s = -\frac{1}{R(C_1 + C_2)} \tag{4.11}$$

The poles are always going to be on the left-hand side of the complex s-plane, indicating unconditional stability, in the Nyquist stability criteria.

However, if the transmission lines forming the feedback paths are included in the above analysis, the even mode equivalent circuit becomes Fig. 4.6 with the inductor, L, which can be used to approximate a short transmission line that form the feedback path.

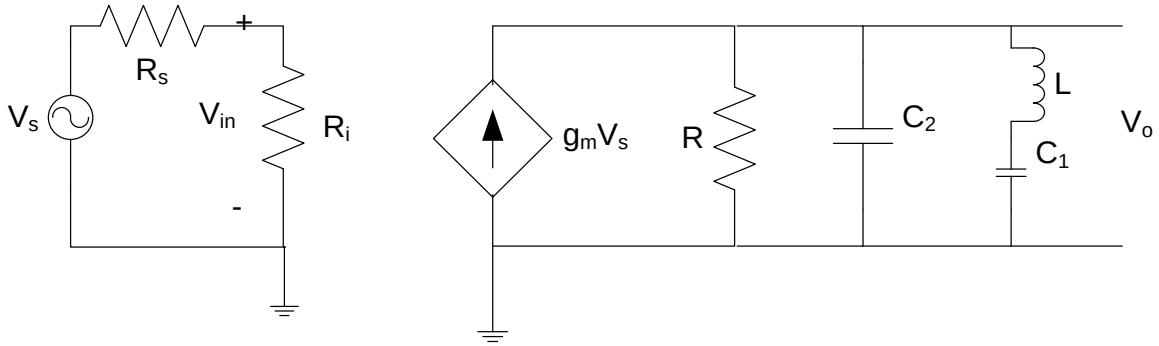

Fig.4 6 Equivalent circuit of NIC in even mode with feedback lines included

Now, let the reactance X_B be

$$X_B = \frac{1 + s^2LC_1}{sC_1} \tag{4.12}$$

and as before

$$X_A = \frac{R}{1 + sRC_2} \tag{4.13}$$

The reactance X_T becomes

$$X_T = X_A || X_B \tag{4.14}$$

where

$$\frac{1}{X_T} = \frac{1 + sRC_2}{R} + \frac{sC_1}{1 + s^2LC_1} \tag{4.15}$$

$$= \frac{(1 + sRC_2)(1 + s^2LC_1) + sRC_1}{R(1 + s^2LC_1)} \tag{4.16}$$

so that,

$$X_T = \frac{R(1 + s^2LC_1)}{1 + s^2LC_1 + sRC_2 + s^3RC_1C_2L + sRC_1} \tag{4.17}$$

The output voltage, V_o, is

$$V_O = i_O X_T \tag{4.18}$$

where

$$i_O = g_m V_s \tag{4.19}$$

so that

$$V_O = g_m V_{is} X_T \tag{4.20}$$

The voltage transfer function is given by

$$\frac{V_O}{V_s} = g_m X_T \tag{4.21}$$

$$= \frac{g_m R(1 + s^2 LC_1)}{s^3 RLC_1C_2 + s^2 LC_1 + sR(C_1 + C_2) + 1} \tag{4.22}$$

The roots of the denominator are the poles of the transfer function and their position on the complex s-plane determines the stability of the system. When the values of R and C_2 obtained from the AVAGO ATF 54143 transistors data sheet are used and the length of the feedback path is approximated by an inductor by using Eq. 4.23, the poles of the transfer function can be found. C_1 is the value of the DC blocking capacitor. L is given by

$$L = \mu \frac{dl}{w} \tag{4.23}$$

where L is the inductance per unit length, μ is the magnetic permeability, d is the conductor thickness, l is the conductor length and the w is the width of the conductor.

For R = 0.3Ω, L = 4.9nH, C_1 = 1pF and C_2 = 0.8pF the poles of $s^3 RLC_1C_2 + s^2 LC_1 + sR(C_1 + C_2) + 1$ are

$$\begin{aligned} s_1 &= -4.1166 \times 10^{+12} \\ s_2 &= 0.0142j \times 10^{+12} \\ s_{3=} &-0.0142j \times 10^{+12} \end{aligned} \tag{4.24}$$

Two of the poles, s_2 and s_3, are complex conjugates of each other and are on the imaginary axis of the complex s-plane. This implies that the system will oscillate with fixed amplitude at a given frequency. The frequency of oscillation, f, can be determined by using the following equations:

$$s = \sigma + \omega j \tag{4.25}$$

$$\omega = 2\pi f \tag{4.26}$$

$$f = \frac{0.0142 \times 10^{+12}}{2\pi}$$

$$= 2.26\text{GHz}$$

This frequency of oscillation is about 16% from the measured oscillation frequency, of 1.9GHz of the fabricated circuit described in the next chapter.

This even mode analysis shows that the feedback path is a critical factor in circuit stability. From the analysis, it can be deduced that using a transistor with a transition frequency lower the expected frequency of oscillation will help prevent the system from going into oscillation because after the transition frequency, the transistor has a gain lower than unity which would not start up an oscillation. The interdependence of feedback path length and stability puts a cap on the highest frequency achievable.

A parametric study on the effect of the length of the feedback path was done and the results are shown in Table 4.1. It can be seen that varying the length of the feedback path represented by the inductor causes the predicted frequency of oscillation to change. This therefore gives an ability to relate and quantify the relationship between the feedback path

length and the frequency of oscillation. Therefore, the stability and the maximum frequency attainable of an NIC circuit are greatly dependent on the feedback path length.

Table 4.1: Parametric study on feedback path length and frequency of oscillations

Inductance (nH)	Feedback Pathlength (mm)	Poles of transfer function			Frequency of oscillation (GHz)
		s1(x 10^12)	s2(x 10^12)	s3(x 10^12)	
1	3.75	-8.44	0.0032 + 0.0316i	0.0032 - 0.0316i	5.03
2	7.37	-1.69	0.022i	-0.022i	3.56
3	10.38	-2.53	0.018i	-0.018i	2.91
4	13.29	-3.37	0.016i	-0.016i	2.51
5	15.82	-4.22	0.014i	-0.014i	2.24
6	18.34	-5.06	0.013i	-0.013i	2.05
10	24.61	-8.44	0.01i	-0.01i	1.6
20	29.13	-1.69	0.0007i	-0.0007i	1.1
30	20.43	-2.53	0.0006i	-0.0006i	0.95

The stability analysis and the parametric study of the even mode not only confirms the intuition that reducing the feedback path length helps achieve a stable NIC and help achieve a higher cut-off frequency, but it also helps quantify this intuition. By this quantification, It is thus possible to know at what frequency a given structure will become unstable for a given feedback path length. This is very useful, as it helps in the choice of transistor. A transistor

should be chosen with a transition frequency that is lower than the predicted frequency of oscillation of the circuit with a given length of the feedback path.

4.2.2. Odd mode

An odd mode analysis has also been performed on the circuit. The current out of the two transistors through the feedback path are in the opposite directions around the feedback path, as shown in Fig 4.7a. and hence the simplification that was applied in the even mode is not applicable. In the odd mode, the current through the capacitor to invert, C, results in a virtual ground in the middle of that capacitor and this results in the circuit of Fig. 4.7b [9]. The capacitor C is split into a series connection of two capacitors of value 2C and a ground is placed between them.

The equivalent circuit of the transistor in the common-gate mode is shown in Fig.4.7c, with the parallel combination of C_2 and R forming X_T as seen in Fig.4.7d. When the closed circuit formed by the feedback paths and equivalent circuits of the transistor that make up the NIC in odd mode are analysed, the NIC equivalent circuit in odd mode is shown in Fig.4.7e is obtained and this forms the basis of the odd mode analysis.

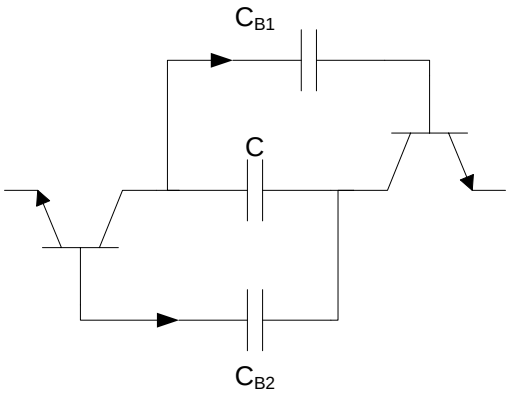

(a)

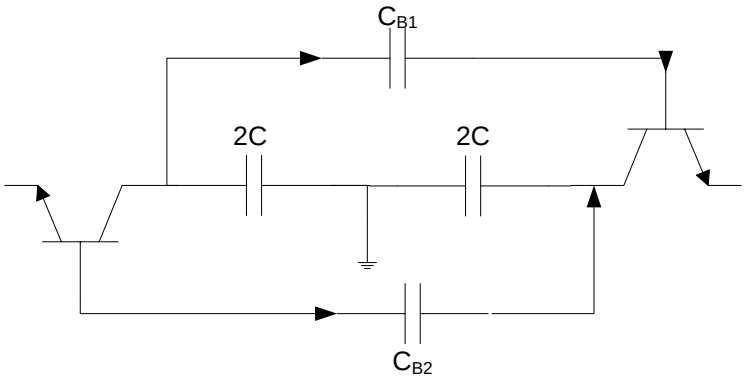

(b)

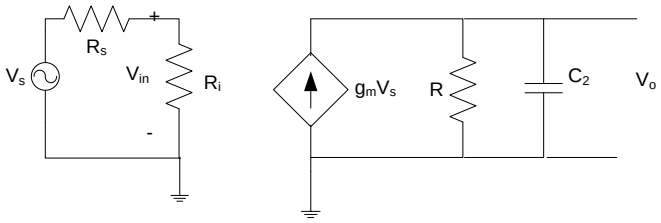

(c)

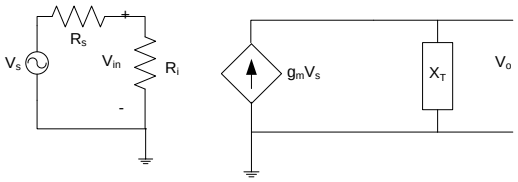

(d)

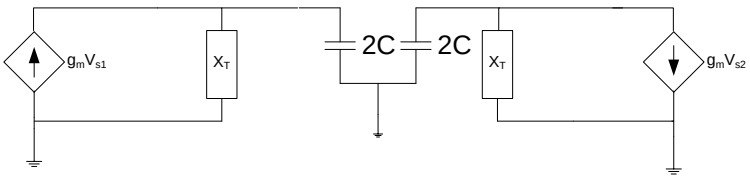

(e)

Fig.4 7 Development of the equivalent circuit of the NIC operating in the odd mode

The reactance X_T is given by

$$X_T = R || C_2 \tag{4.27}$$

where

$$X_T = \frac{R}{1 + sRC_2} \tag{4.28}$$

The reactance, X_{TT} is the parallel combination of $2X_T$ and 2C, and is given by

$$\frac{1}{X_{TT}} = \frac{1 + sRC_2}{2R} + \frac{2sC}{1} \tag{4.29}$$

$$= \frac{1 + sRC_2 + 4sRC(2 + 2sRC_1)}{2R} \tag{4.30}$$

Inverting the equation, gives

$$X_{TT} = \frac{2R}{1 + s(RC_2 + 4RC)} \tag{4.31}$$

The voltage V_0 is given by

$$V_o = g_m V_s X_{TT} \tag{4.32}$$

so that the transfer function, V_o/V_s is given by

$$\frac{V_0}{V_s} = \left(\frac{2R}{1 + s(RC_2 + 4RC)}\right) g_m \tag{4.33}$$

The poles of the transfer function are

$$s = \frac{-1}{R(C_2 + 4C)} \tag{4.34}$$

With an inductor representing the transmission line inserted into the equivalent circuit as before, the reactance X_{TT} becomes

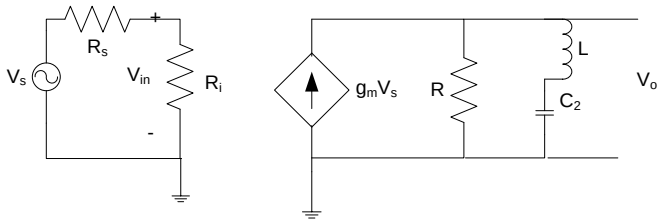

Fig.4 8 The equivalent circuit of the NIC including inductor representing the feedback in the NIC

$$X_T = R \,||\, (L + C_2) \tag{4.35}$$

$$X_T = \frac{R(s^2LC_2 + 1)}{s^2LC_2 + sRC_2 + 1} \tag{4.36}$$

$$\frac{1}{X_{TT}} = \frac{s^2LC_2 + sRC_2 + 1}{2R(s^2LC_2 + 1)} + \frac{2sC}{1}$$

$$= \frac{s^2LC_2 + sRC_2 + 1 + 4sRC\,(s^2LC_2 + 1)}{2R(s^2LC_2 + 1)} \tag{4.37}$$

Inverting, gives

$$X_{TT} = \frac{2R(s^2LC_2 + 1)}{s^2LC_2 + sRC_2 + 1 + 4sRC\,(s^2LC_2 + 1)} \tag{4.38}$$

The output voltage becomes

$$V_o = g_m V_s X_{TT} \tag{4.39}$$

and the transfer function becomes

$$\frac{V_o}{V_s} = \left(\frac{2R(s^2LC_2 + 1)}{4s^3LRCC_2 + s^2LC_2 + s(RC_2 + 4RC) + 1}\right) g_m \tag{4.40}$$

The poles of the transfer function can be determined by using the values of the variables from equation 4.24 and C = 3.9pF

$$s_1 = -2.1361 \times 10^{11}$$

$$s_2 = (-0.003 + 0.1597j) \times 10^{11}$$

$$s_3 = (-0.003 - 0.1597j) \times 10^{11}$$

The poles are on the left hand side of the complex s- plane. Therefore, in the odd mode, the NIC would be stable.

The above results agree with reasoning, in that, in the even mode, the currents from the different transistors flow in the same direction around the feedback path, (Fig. 4.9a). This represents a circulating current around the feedback path, which can be easily amplified and

hence start up an oscillation. Whereas, in the odd mode (Fig. 4.9b), because the currents in the feedback path are in opposite directions to one another, and assuming that the transistors are exactly similar, then these currents will be equal and effectively cancel each other out. This means that an oscillation will not start in the odd mode, when using similar transistors. The difference in the measured frequency of oscillation and that predicted in the even mode, can be attributed to the small differences in the actual transistor used. One of the major results from the stability analysis is the ability to predict the frequency of oscillation within the NIC to a reasonable level of accuracy and using this information in the choice of transistor.

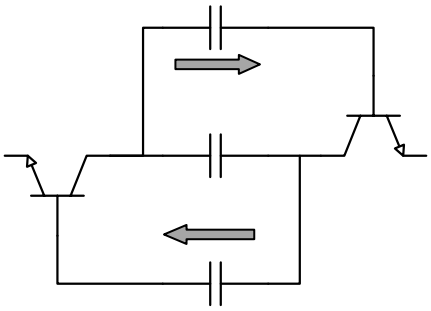

(a)

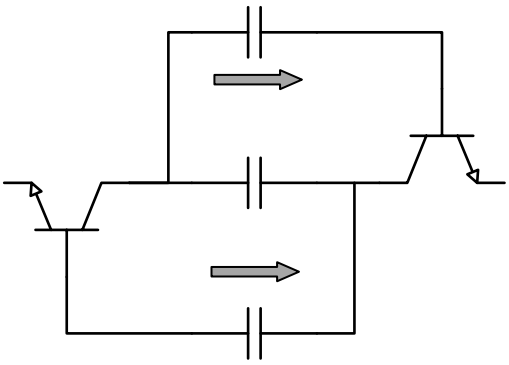

(b)

Fig.4 9 Current flow around the feedback path (a) Even mode and (b) Odd mode

4.3. Conclusion

This chapter shows a stability analysis for the NIC. The standard K factor and auxiliary B1 stability factor test performed using AWR did not predict the oscillation that was experienced when the NIC circuit was fabricated. This is because these tests are based on measurements made from the ports of the circuit; therefore hidden mode oscillations were not detected. Because of the inability of the standard test to be able to predict the instability, a new stability analysis was done. This analysis is based on the transfer function of circuit. It has been possible to predict the frequency of the oscillation to within 16% of that obtained by measurement. The analysis also reveals the critical part of the NIC circuit that leads to oscillation, the feedback path between the transistors. With a parameter study, it is possible to realise a stable NIC given a fixed feedback path length.

References

[1] Oluwabunmi O. Tade, Zhen H. Hu, Peter Gardner and Peter S. Hall, "Small antennas for cognitive radio using negative impedance converters," The 12th Annual Post Graduate Symposium on the Convergence of Telecommunications, Networking and Broadcasting (PGNet2011), 2011 2011.

[2] O. O. Tade, P. Gardner, and P. S. Hall, "Negative impedance converters for broadband antenna matching," in Microwave Conference (EuMC), 2012 42nd European, 2012, pp. 613-616.

[3] O. O. Tade, P. Gardner, and P. S. Hall, "Broadband matching of small antennas using negative impedance converters," in Antennas and Propagation Society International Symposium (APSURSI), 2012 IEEE, 2012, pp. 1-2.

[4] O.O. Tade, P. Gardner and P. S. Hall "1.5GHz Negative Impedance Converters," IET 2nd Annual Active RF Devices, Circuits and Systems Seminar, 2012 2012.

[5] G. Gonzalez, Microwave Transistor Amplifiers, Analysis and Design, 2nd Edition ed.: Prentice-Hall Inc, 1996.

[6] S. E. Sussman-Fort and R. M. Rudish, "Non-Foster Impedance Matching of Electrically-Small Antennas," Antennas and Propagation, IEEE Transactions on, vol. 57, pp. 2230-2241, 2009.

[7] A. S. Sedra and K. C. Smith, Microelectronic Circuits Revised Edition: Oxford University Press, Inc., 2007.

[8] J. W. Nilsson and S. Riedel, Electric Circuits: Prentice Hall, 2010.

[9] D. M. Pozar, Microwave Engineering, 3Rd Ed: Wiley India Pvt. Limited, 2009.

Chapter 5

REALISATION OF NIC ANTENNA MATCHING

5.1. Negative Impedance Converter Realisation

Using the information obtained from the stability analysis, a stable and oscillation free NIC was designed, using the inter-dependence between the choice of transistor and feedback path length. The NIC was realised as a two layer structure, with a common ground plane in between, as this gives the best method of realising a short feedback path.

The overall structure is shown in Fig. 5.1[1-3]. Its overall size is 50mm × 50mm. Fig.5.1a shows the cross-sectional view of the two layers, connected using 0.8mm diameter vias, made using rivets and soldered top and bottom. The top layer, Fig.5.1b, contains the transistors, the capacitor to invert and a part of the transistor DC bias network. The bottom layer, Fig.5.1c, contains the feedback path and a part of the DC bias network. The substrate used is Taconic TLY – 5 with thickness of 1.57mm, dielectric constant of 2.2 and loss tangent of 0.0009. The copper ground plane has a thickness of 0.07mm made from the combined ground plane of the two layers. Table 5.1 shows the list of elements used to realise this NIC and the datasheets of the elements are included in the appendix A.

The length of the feedback path is 13.4mm which is equivalent to an inductance of 4.9nH. Using the stability criteria from chapter 4, this implies that the circuit would oscillate at 2.26GHz. There is therefore a need to find a transistor whose F_T is lower than the calculated frequency of oscillation. Figure 5.2 shows the gain of the NXP BFS – 17 and Avago ATF 54143 (datasheet in appendix A). From the graph, it can be seen that the F_T of the BFS- 17 transistor, 1.9GHz, is lower than the expected frequency of oscillation, unlike the ATF 54143

transistor whose F_T is 12GHz and has a gain of 16dB at the predicted frequency of oscillation. This therefore makes the BFS – 17 transistor a suitable choice, but also limits the top frequency of the NIC. The effect of using the ATF – 54143 transistor is described in section 5.2.1.

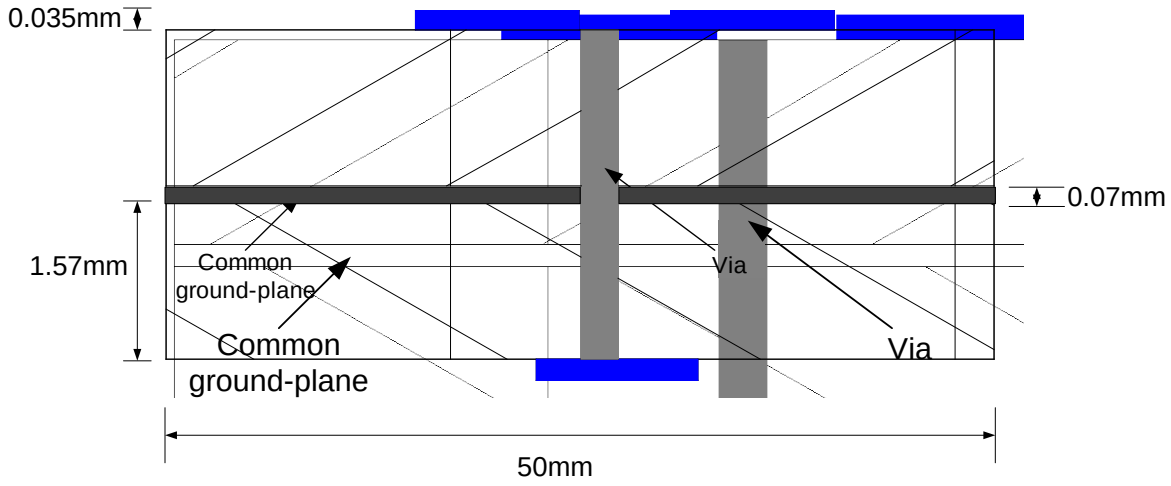

(a)

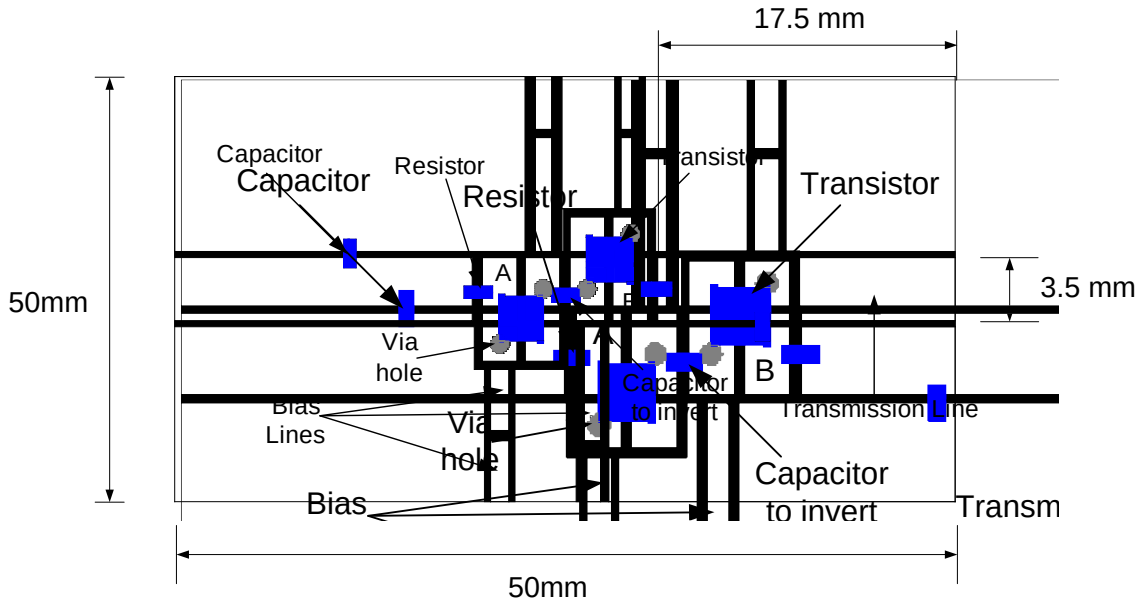

(b)

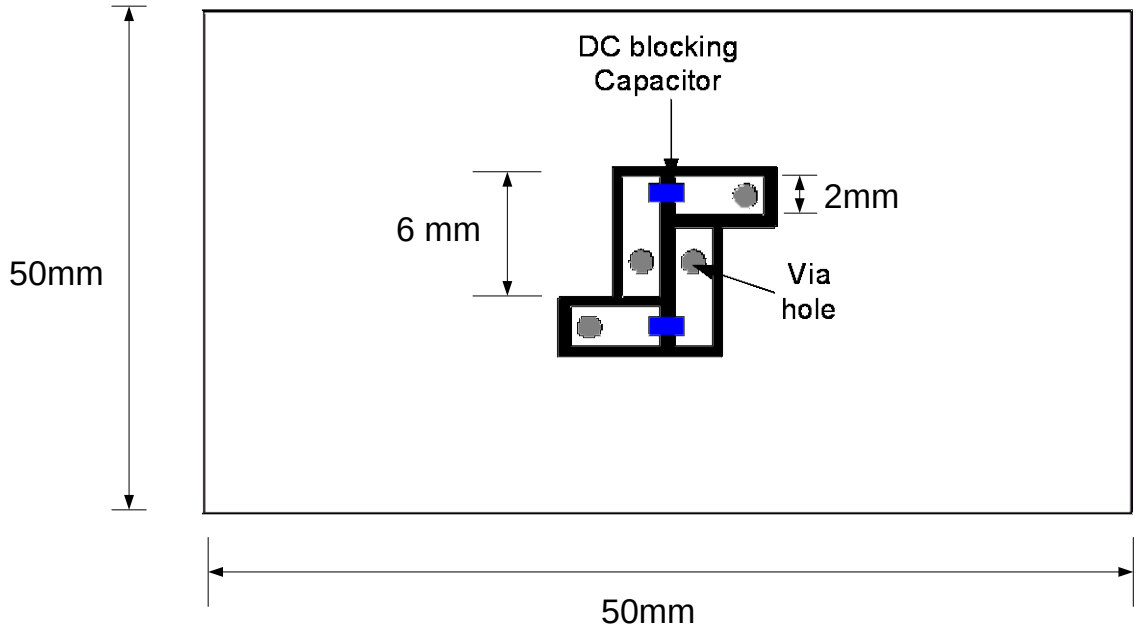

(c)

Fig.5 1 The Negative Impedance Converter structure (a)Top view (b) Reverse view and (c) the cross sectional view

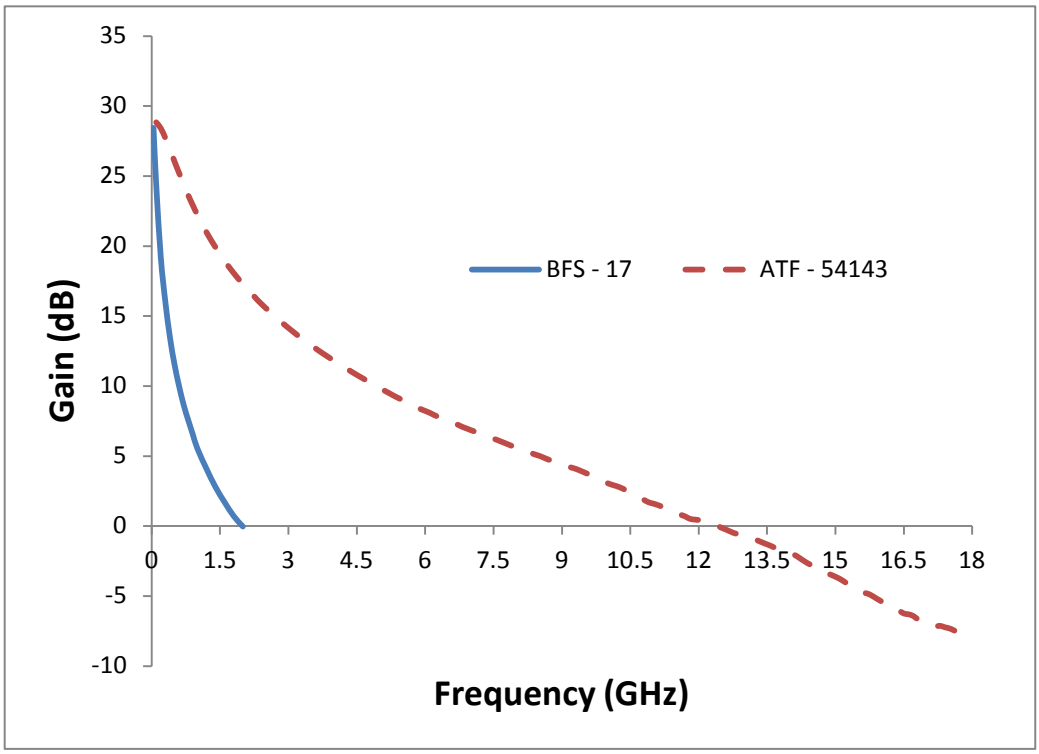

Fig.5 2 Transistor gain comparison of NXP BFS – 17 and Avago ATF 54143

Table 5 1 : Components used in the NIC

Component	Manufacturer	
Transistor	NXP	BFS-17
Capacitor	AVX	3.9pF
Inductor	Coilcraft	1.8nH
Resistor	Panasonic	33Ω
	Panasonic	10Ω
	Panasonic	10 kΩ
Substrate	Taconic	TLY-5

Negative impedances are inherently unstable; this is primarily due to the element being inverted having some inherent resistance, which also gets inverted. This inverted resistance is the primary source of the inherent instability within negative impedances. Therefore, to ensure the entire structure is stable and ultimately measurable, it is necessary to add positive components between the NIC ports and the measurement ports. This makes both the reactance and resistance measured at the measurement ports always positive and the NIC performance and characteristics are then de-embedded from the measured results. A 17.5mm co-planar waveguide (CPW) transmission line is added between the NIC terminal (points A and B in Fig.5.1b) and the measurement port to allow for SMA connections as shown in Fig.5.1b. There are also resistors in series with the NIC terminals to provide resistive damping and capacitors to ground to ensure that the net reactance measured in always

positive. These additional elements are de-embedded from the measured results to obtain the NIC performance.

The de-embedding is done using the NEG2 element in AWR design environment as shown in Fig.5.3. A circuit board containing the added positive elements and the CPW transmission line between the measurement port and the points A on the circuit (Fig 5.1b) was built and measured. The measured S – parameters (TXLineonly) are then loaded into the NEG2 block, which negates the transpose of the Y matrix of “TXLineonly”.

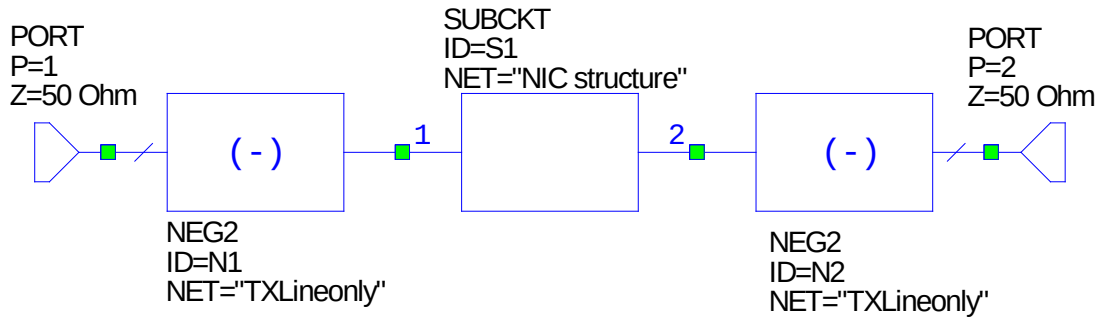

Fig.5 3 De-embedding in AWR

The NEG2 block was then connected in series at both ends with the S - parameter block of the measured NIC structure. The resultant s-parameters of the cascaded blocks are the de-embedded s-parameters of the NIC. The condition for validity of the NEG2 element approach is met, because the negated network consisting of the CPW transmission lines and the positive lumped elements is reciprocal.

The NIC circuit that was built is shown in Fig.5.4. The metal casing is for mechanical stability and to ensure that it is rugged. The NIC core, without the bias network and the other

elements added to ensure overall positive reactance before de-embedding, are indicated in Fig.5.4a and the feedback paths are also indicated in Fig.5.4b.

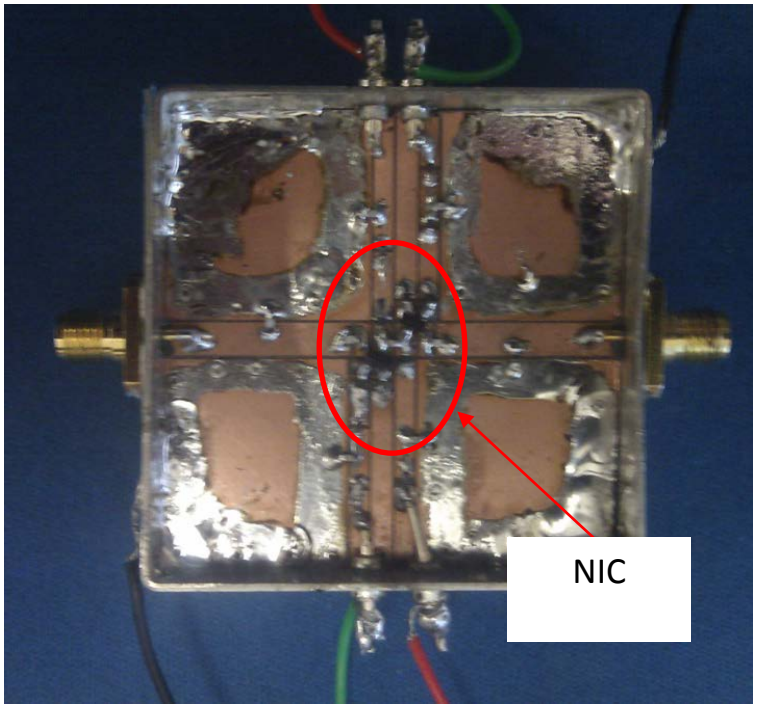

(a)

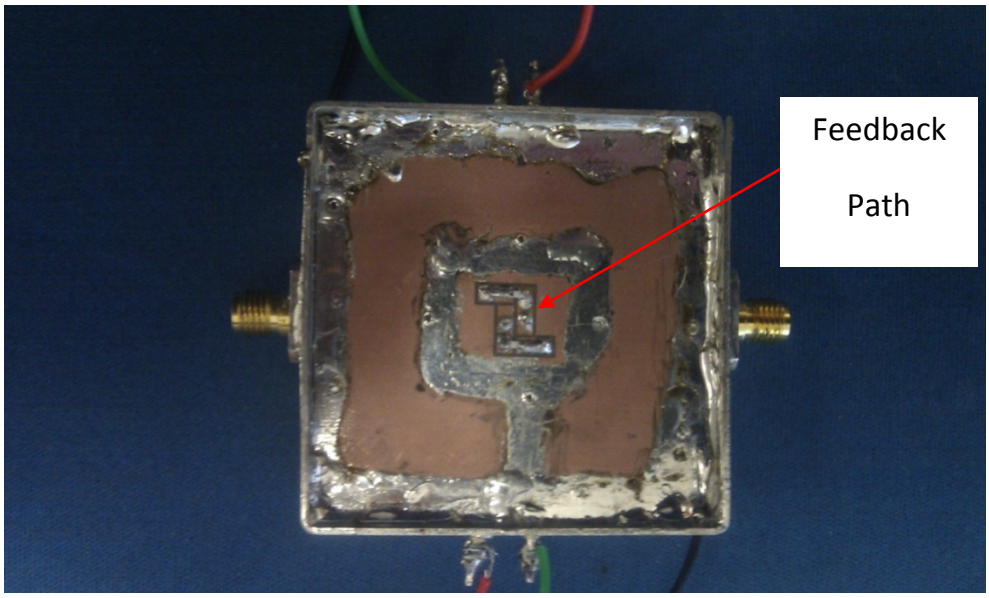

(b)

Fig.5 4 Built NIC structure (a) Top view and (b) Reverse view

5.2. Measured Results

5.2.1. Prototype 1

Initial attempts at fabricating the NIC involved the use of the Avago ATF 54143 with an F_T of 12GHz. The NIC layouts were similar to those discussed in Section 5.1. The two layer approach was taken because it was the only viable means through which the feedback paths could be routed on the PCB as well as making the NIC core physically small. The transistors were biased at 3V and 60mA. This prototype was found to oscillate at 1.9GHz. The first indication of instability occurs whenever the NIC is powered up. The powering sequence for the FET transistor is that the drain voltage in turned on first and then the gate voltage. Turning on the gate voltage usually helps control the current through the drain but because of the instability the DC control over the gate and drain are lost. Hence, it is never possible to bias the transistors to the required bias conditions. Connecting port two of the NIC structure to a spectrum analyser with port one terminated with a matched load shows spikes within the frequency band where the transistor is active as shown in Fig.5.5. Any attempt to damp the oscillation which includes adding a 100Ω resistor in series with the NIC core and using 2200nH inductors on the bias lines failed to bring the oscillation under control. Also the fact that the oscillation was not obvious within the circuit simulator when using the K and B1 stability test methods made it difficult to stop the oscillation.

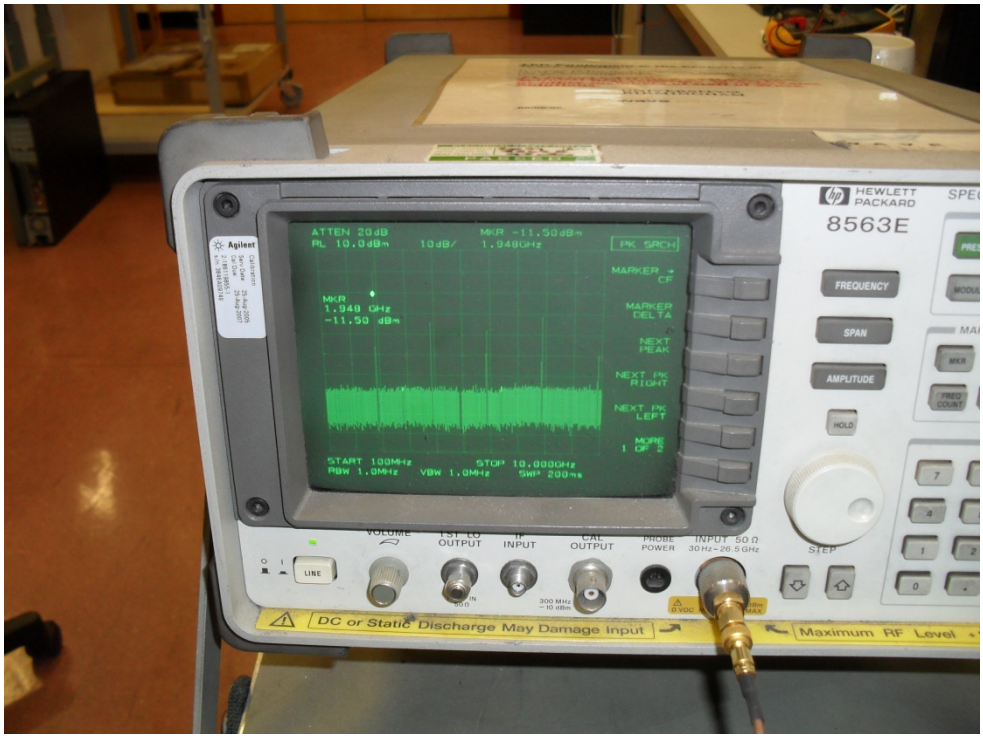

Fig.5 5 . Spectrum of oscillating NIC

5.2.2. Prototype 2

Prototype 2 used the NXP BFS 17 transistor and used the same structure as shown in Fig.5.4. The measured S_{11} and S_{22} of the structure at the measurement ports are shown in Fig.5.6. It should be noted that this still exhibits Foster performance as it rotates clockwise around the Smith chart. The clockwise rotation is due to the connecting transmission lines and additional elements added between the measurement port and the NIC terminals. Figure 5.7 shows the de-embedded NIC performance, which shows non-Foster performance by a section of the locus having anti-clockwise rotation around the Smith chart. The reactance against frequency, Fig.5.8, also shows a negative slope, which is characteristic of non-Foster elements.

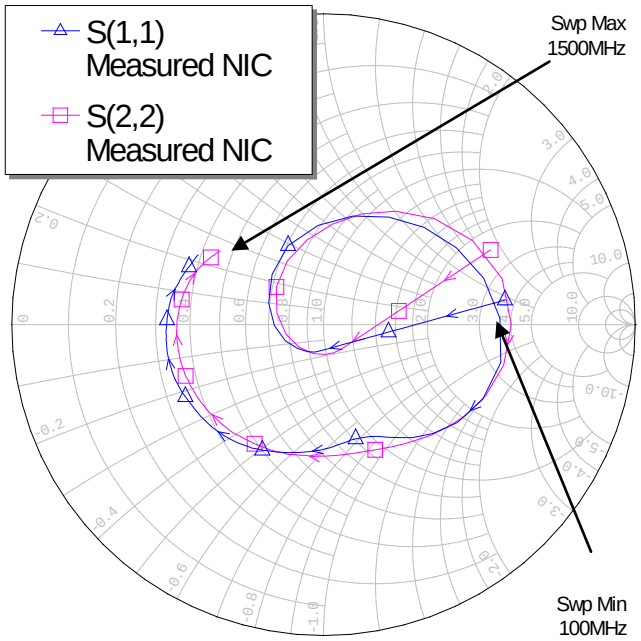

Fig.5 6 Measured input and output impedance plot of NIC structure

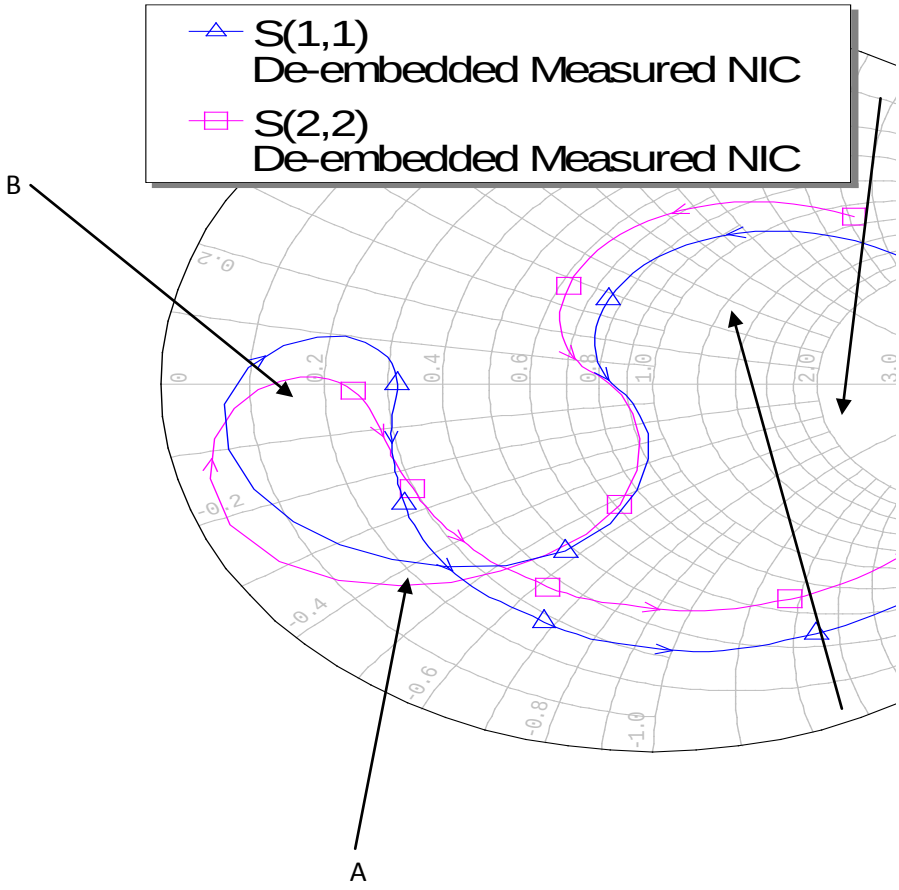

Fig.5 7 De-embedded Measured Impedance plot of the NIC

In Fig 5.7, between 480MHz and 595MHz, which are represented by points A and B respectively, it can be observed that the NIC does not exhibit the expected non-Foster performance, because of the clockwise rotation around the Smith chart. This can also be noticed in the impedance against frequency plot in Fig 5.8. This may be attributed to a series resonance observed within this frequency band. This can also be observed in Fig.5.10 where the negative capacitance across the terminals can be seen to go through a series resonance within this frequency band. The resultant values of the capacitance and inductance shown in Fig.5.10 were obtained from the de-embedded measured reactance of the NIC using eq 3.3. This also leads to a higher loss observed in the NIC within this frequency band as seen in Fig.5.9.

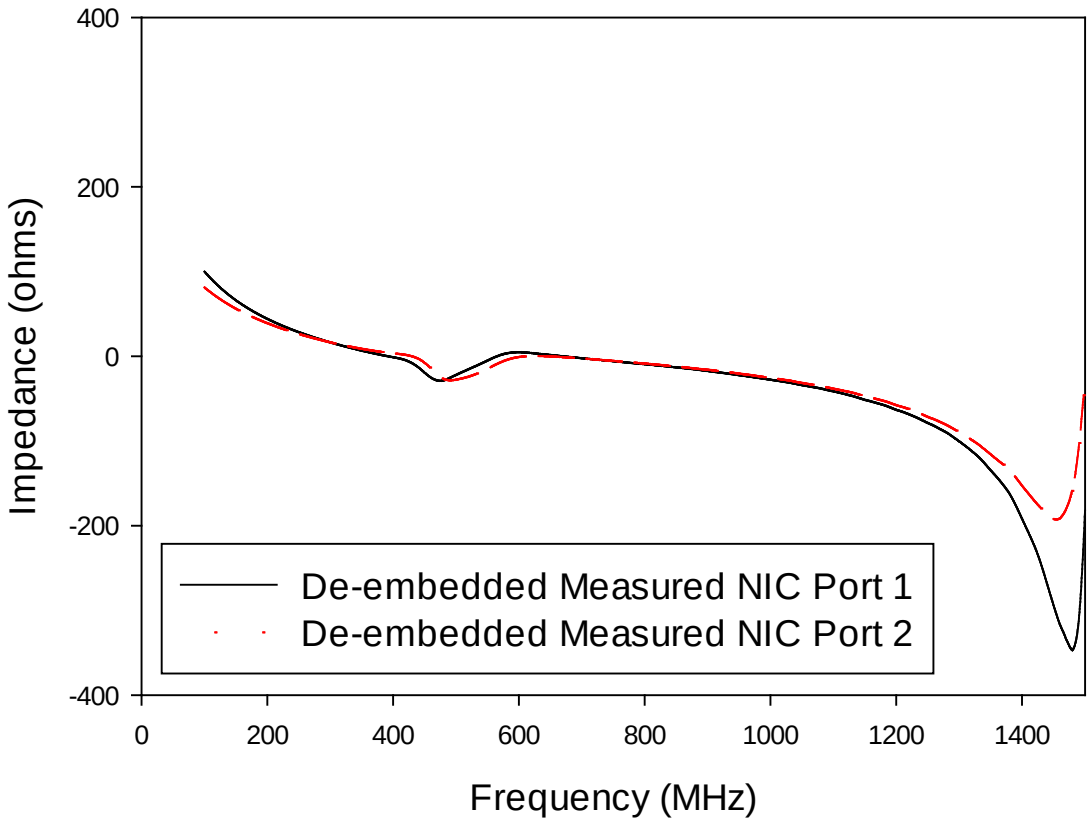

Fig.5 8 De-embedded reactance plot of the NIC

The insertion loss through the NIC is shown in Fig. 5.9. This is essentially the de-embedded S_{21} of the NIC circuit. It is seen that it is lossy within the frequency band where the negative capacitor goes through resonance. Outside this frequency band the loss is better than 7dB up to the cut off frequency of 1.5GHz.

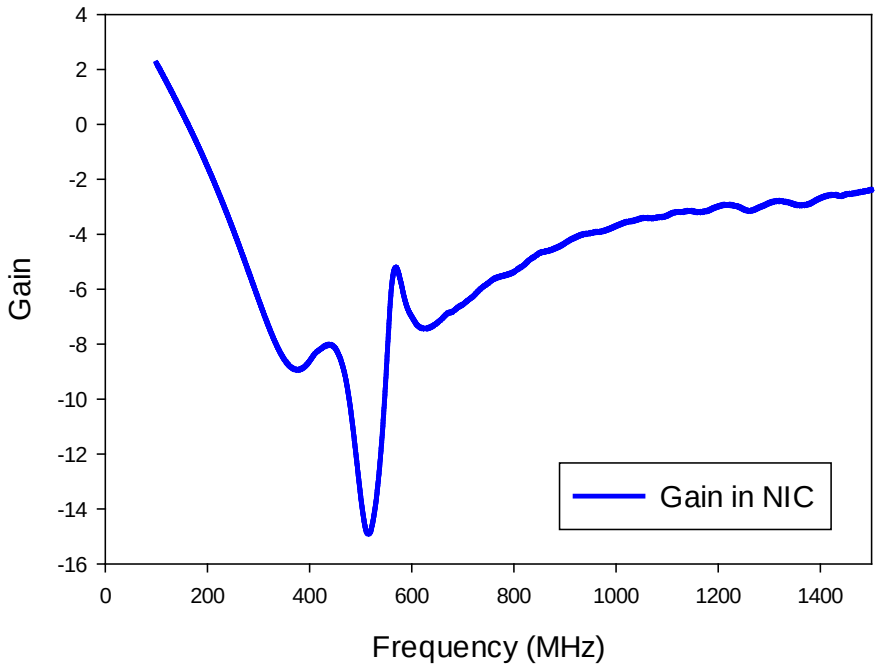

Fig.5 9 Gain through the NIC

The series capacitance and inductance seen between the ports of the NIC is shown in Fig.5.10. It can be noticed that the values changes with frequency as expected (Eq. 3.3 and Fig.3.4). It can be seen that at higher frequencies above 700MHz, the NIC is more inductive than capacitive. These values can be computed from the measured reactance of the de-embedded NIC using equations 3.2 – 3.4. This behaviour can also be observed by looking at the impedance plots on a Smith chart (Fig.5.7) where the locus crosses between the negative capacitive region into the inductive region. It should also be noted that the capacitance and inductance are frequency dependent. The Q of the resultant element is computed using Eq.

5.1 and is shown in Fig.5.11. The Q obtained is low when compared to commercially available reactance elements and this due to the high loss through the NIC. Improving the low of the NIC would definitely increase the Q value of the negative impedance.

$$Q = \frac{|X|}{R} \tag{5.1}$$

where X is the reactance of the NIC and R is its resistance.

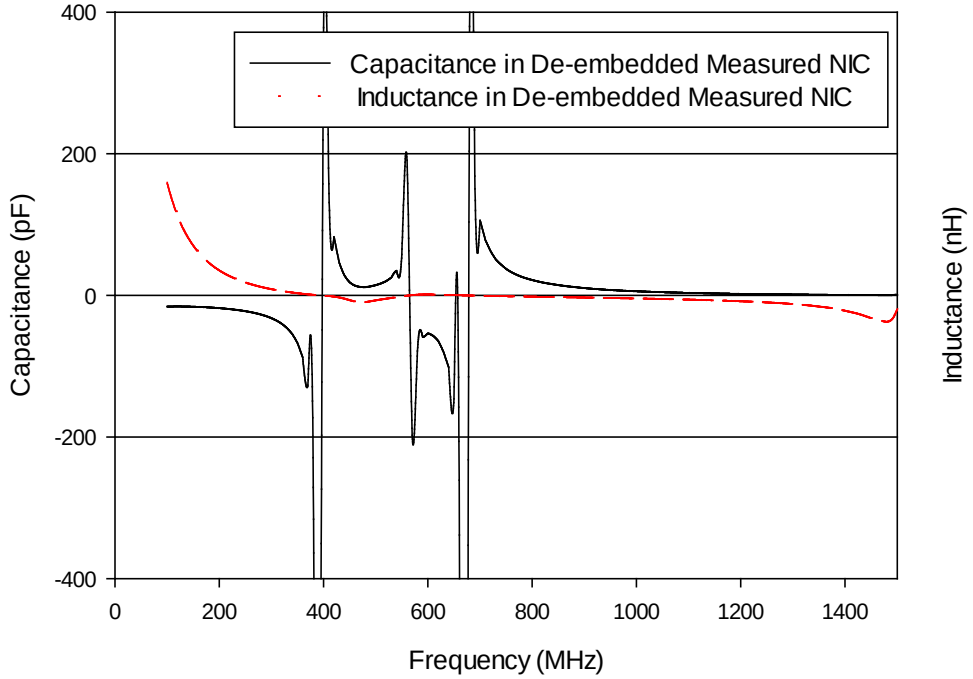

Fig.5 10 The capacitance and inductance of the de-embedded NIC

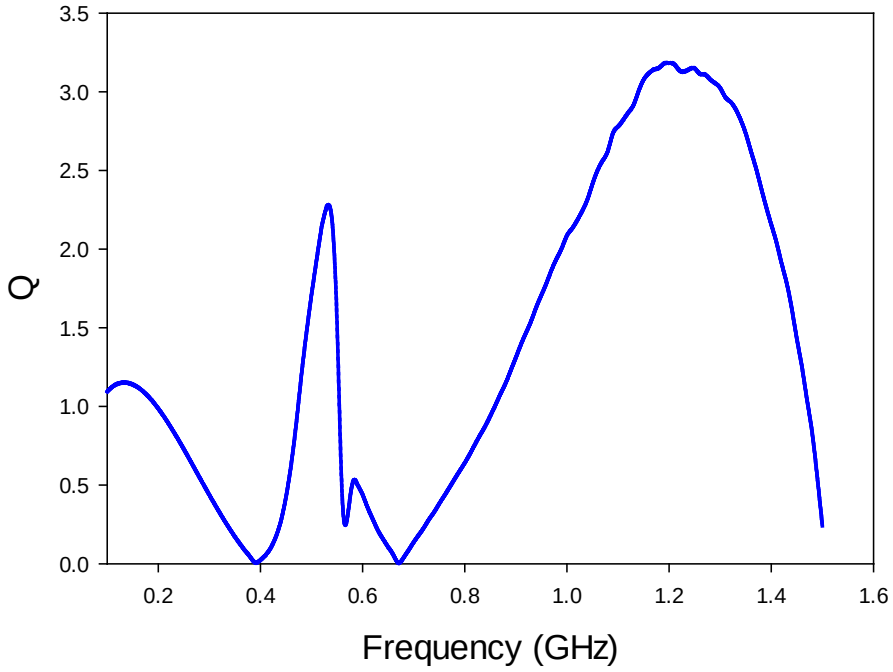

Fig.5 11 Q of the de-embedded NIC

5.3. Antenna and NIC matching

5.3.1 Simulation

Due to the complexity involved in realising a single element NIC, it was decided to revise the matching network earlier described in chapter 3 to a single negative element matching network. The de-embedded single NIC, prototype 2, was used to match the antenna described in section 3.2.1 (chassis antenna) along with a positive lumped element inductor. The revised matching network is shown in Fig. 5.12a. To simulate the performance, the S - parameters of the antenna is combined with the S - parameters of the measured and de-embedded NIC along with the S - parameters of the inductor.

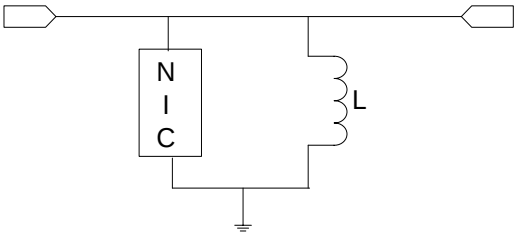

(L = 4.7nH)

(a)

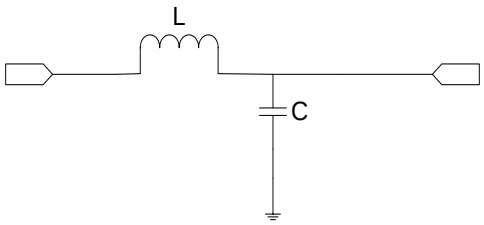

(b)

(L = 14.5nH and C = 7pF)

Fig.5 12 (a) The revised antenna matching network. (b) The passive matching network

The S parameters of the NIC and the inductor are imported into CST as s2p files. These are then combined with the simulated antenna in the circuit simulator in CST to generate the antenna return loss, shown in Fig.5.13. A better than -6dB return loss was obtained between 0.647GHz – 1.5GHz. For comparison, a passive matching network was also used to match the same antenna in CST. The passive matching network is shown in Fig.5.12b and it consists of a series inductor of 14.5nH and a shunt capacitor 7pF. The return loss obtained with the single NIC element matching network can be seen to be better than what is obtainable with passive matching as shown in Fig.5.13. The comparison shows that NIC can indeed provide wideband matching of an antenna.

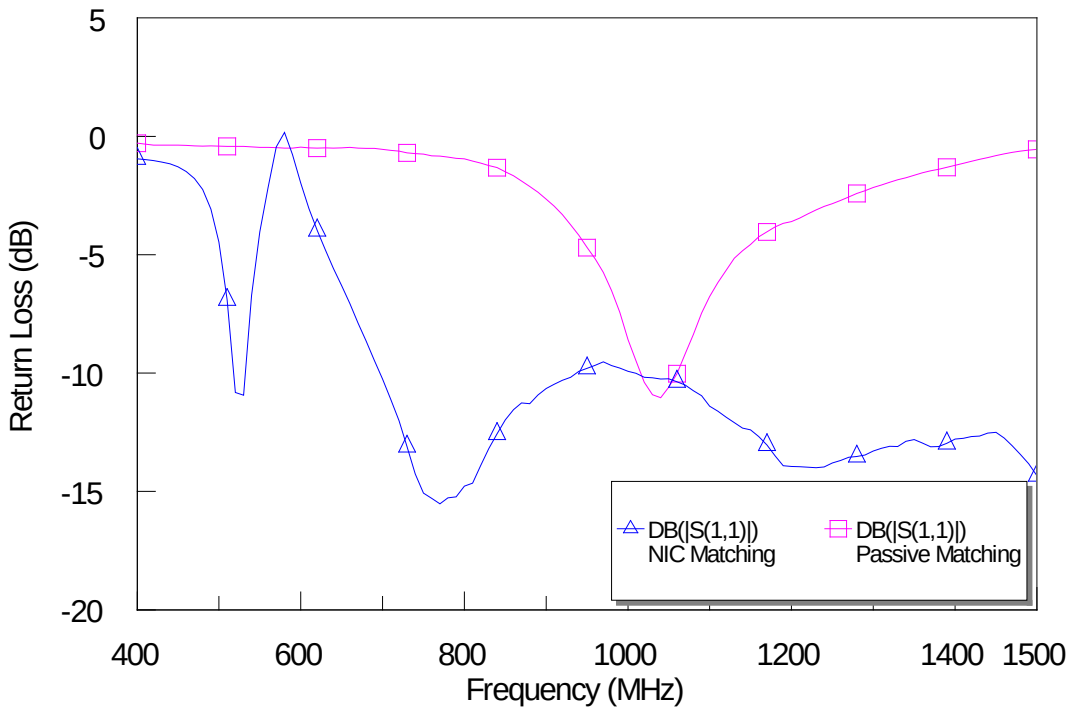

Fig.5 13 . Antenna return loss using revised NIC matching network and passive matching network

It is known that loss helps improve return loss [4], so the NIC matched antenna is also compared to a lossy passive matched antenna and a purely resistive matched antenna.

The lossy passive matching network consists of the matching network used in a purely reactive matching network, along with a resistor whose value is chosen to ensure that the return loss is similar to or better than that which is obtainable with the NIC based matching network. The matching network is shown in Fig.5.14.

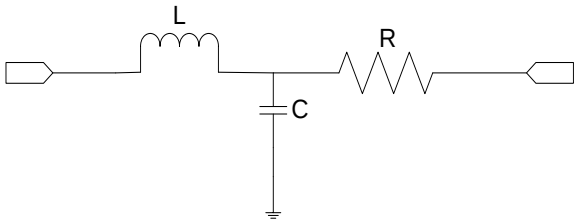

(L = 7.9nH. C = 6.1pF and R= 23Ω)

Fig.5 14 Lossy passive matching network

The purely resistive matching network consists of a resistor to ground as shown in Fig.5.15. The value of the resistor is also chosen to obtain similar or better return loss as compared with the NIC matched antenna.

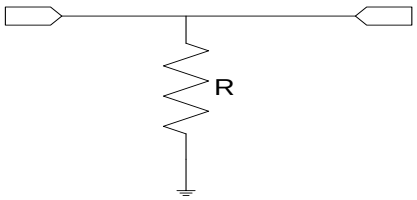

(R = 29Ω)

Fig.5 15. Resistive matching network.

The effect of different antenna matching methods on both antenna return loss and total efficiency are shown in Figs.5.16 and 5.17, respectively.

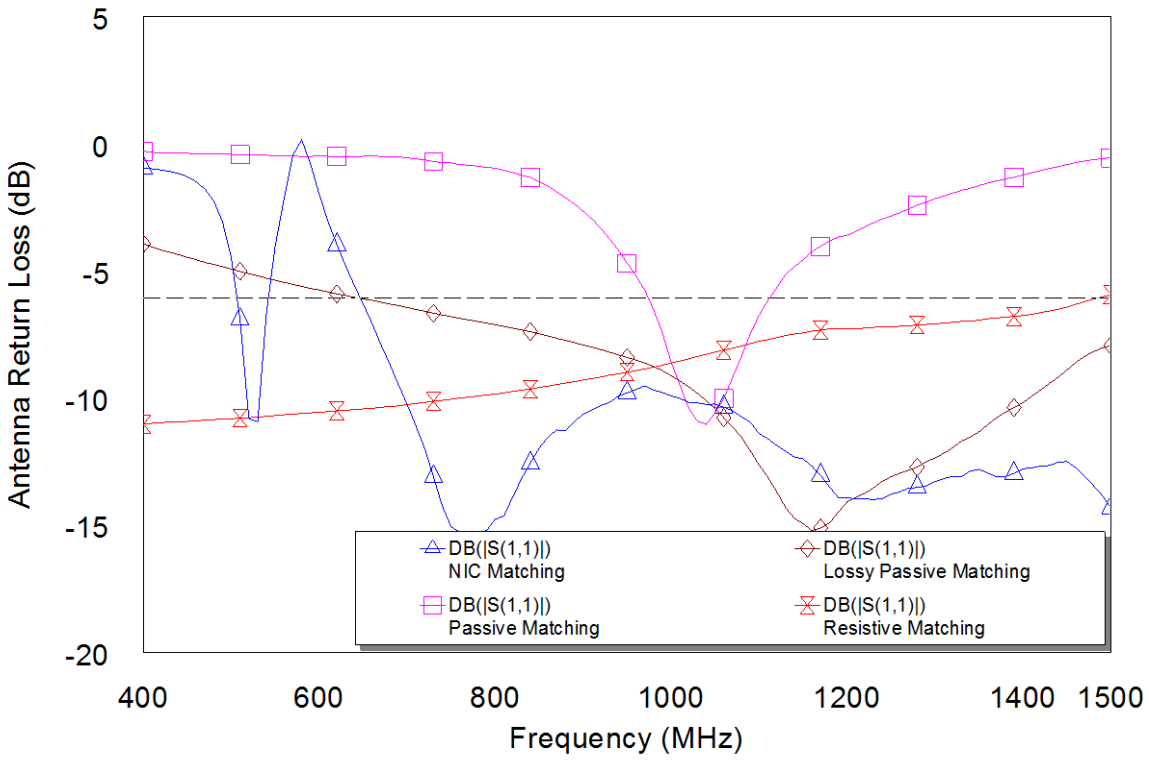

Fig.5 16 Simulated antenna return loss of the different matching networks

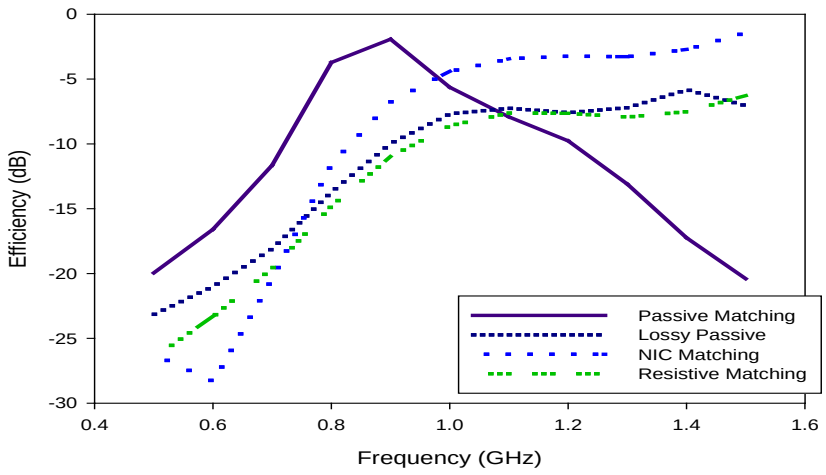

Fig.5 17 Simulated total efficiency of antenna with different matching networks

From the results, it can be observed that of the three different matching networks that yield broadband matching, namely lossy passive, NIC and resistive, the NIC matched antenna performs best by up to 5dB when compared to the lossy passive matched antenna. This means

that the loss through the NIC is not being used to improve the antenna return loss but the non-Foster performance has an impact on the antenna performance as expected. In Fig.5.17, the NIC matched antenna has a dip in total efficiency at 0.6GHz, this is due to the almost total reflection experienced at this frequency indicated by the S_{11} of close to 0dB (Fig.5.16).

When the antenna efficiency of the NIC matched antenna is compared with the passively matched antenna, it is clear that the passively matched antenna achieves a higher peak efficiency of -2dB at 0.85GHz but it degrades rapidly at frequencies outside a relatively narrow band whereas the NIC matched antenna has a better total efficiency over a wide frequency range. Therefore, the NIC matched antenna would have a better efficiency-bandwidth ratio when compared to the passively matched antenna. The passively matched antenna would clearly serve best in a narrow band scenario.

5.3.2 Measurements

The feasibility of integrating the NIC matching circuit was considered in order to validate the simulations and to investigate the practical difficulties. To use the matching network in Fig.5.12, it is important to locate the upper terminal of the NIC a distance from the inductor and antenna that is small compared to a wavelength. In prototype 2, the terminal is accessible if the connector and transmission lines are removed but not sufficiently to enable a shunt connection to earth. Figure5.18 shows the difficulty of shorting the second terminal of the NIC while still maintaining a connection to the antenna and the associated bias networks. For this reason, this was not attempted.

Also, implementing a single element NIC with the required bias network using the current fabrication methods would require more than 20% of the ground plane as can be seen from

Fig.5.18. In practice, as this antenna is geared for use in a mobile or handheld device, this amount of space would not be available for the antenna. Hence, it would be necessary to look at alternate means of fabrication that reduces the overall size of the NIC circuit and makes it easier to implement on the chassis antenna. The ground plane of the chassis antenna is also the radiating element because the surface current on the antenna is primarily on the ground plane. Therefore by etching in the NIC into the ground plane would disrupt the surface current and effectively change the antenna impedance and this makes it difficult to simply integrate the NIC and this antenna together.

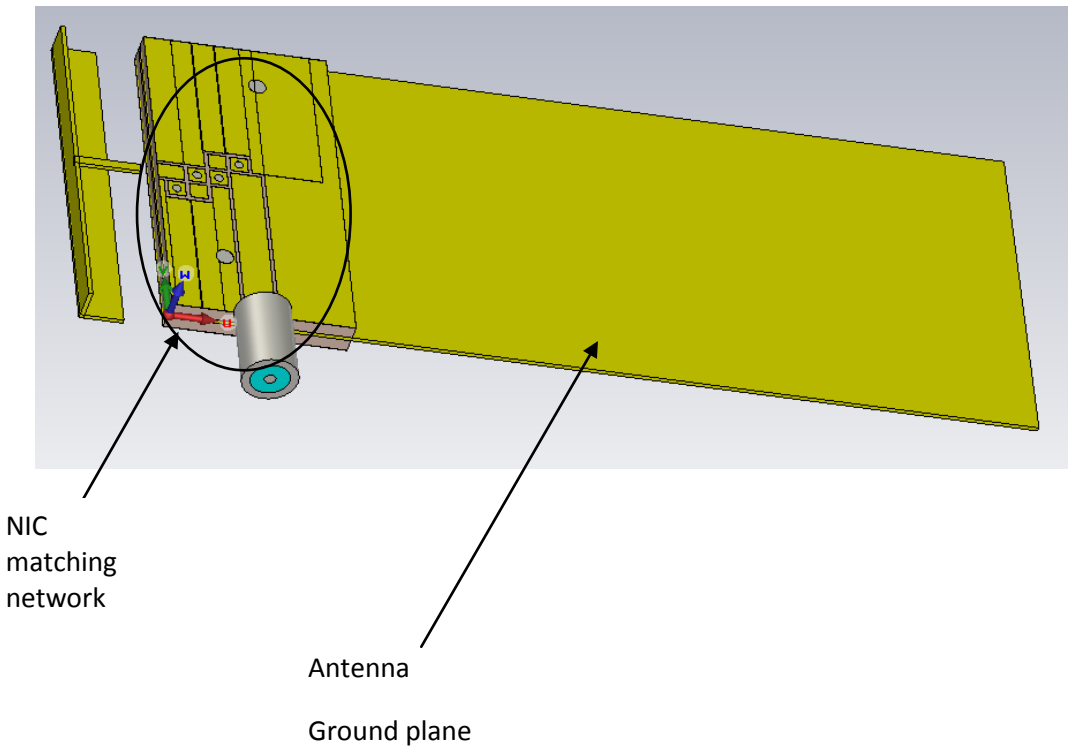

Fig.5 18. Proposed NIC matched chassis antenna

5.4. Noise and Linearity Measurement

5.4.1. Antenna Equivalent Circuit

Fabricating a fully integrated NIC matched chassis antenna is difficult as noted in the previous section. Because of these difficulties, it was decided to design an equivalent circuit which represents the antenna between 0.7 GHz - 1 GHz. The equivalent circuit comprises of a CPW line, a capacitor in series with an inductor in shunt as shown in Fig. 5.19 with the corresponding values of the elements that make up the equivalent circuit. The equivalent circuit aims to transforms a 50Ω port impedance into what the simulated antenna impedance would be at its feed point through a CPW transmission line and the three lumped elements. The magnitude and phase plots of the equivalent circuit's S_{22} is compared with the simulated antenna's s-parameters and shown in Fig. 5.20. In Fig.5.20, it can be seen that there is agreement between the simulated antenna and the equivalent circuit in terms of return loss magnitude especially within the frequency range of interest (700MHz – 1000MHz). The values of the elements within the equivalent circuit were obtained by curve fitting.

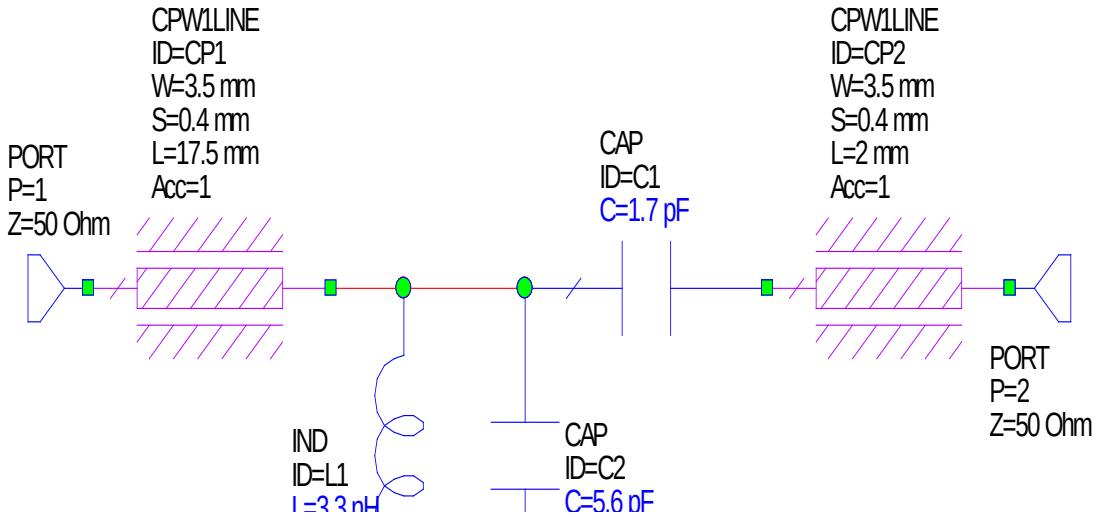

Fig.5 19 Antenna equivalent circuit

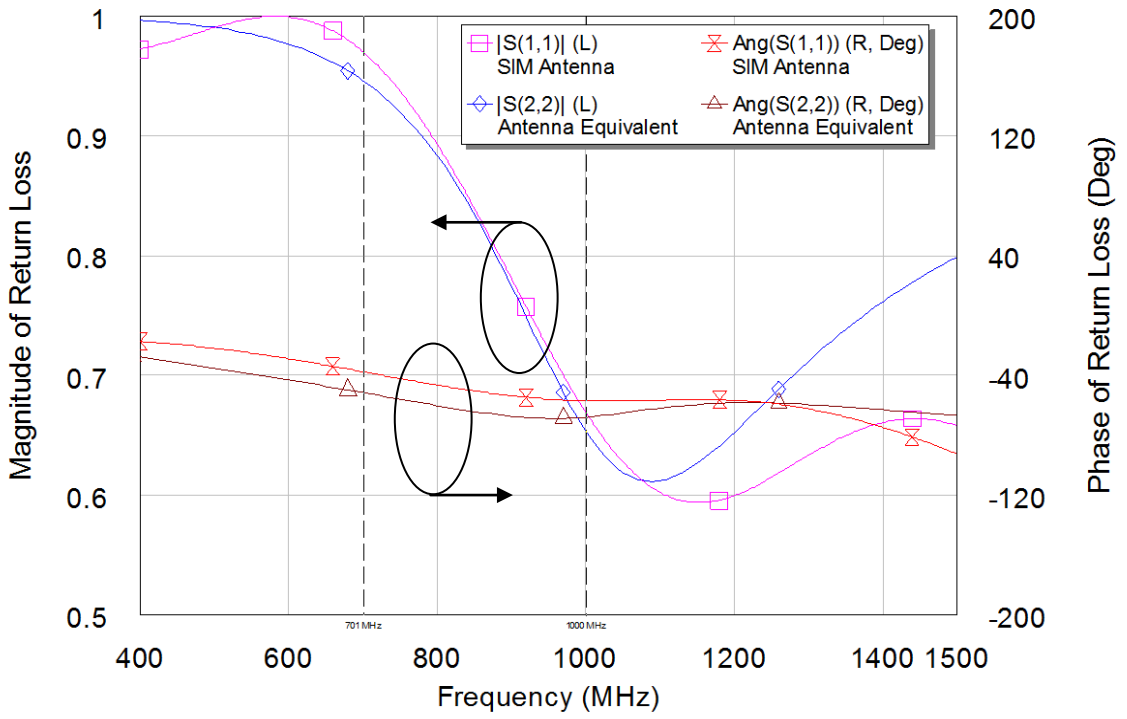

Fig.5 20 Magnitude and phase plot of antenna equivalent circuit and measured antenna

The equivalent antenna circuit is realised like the standalone NIC described in section 5.1. It is double layered, with a common ground plane in between. Vias connect the two layers together. The 50Ω port termination is transformed to the impedance seen at the feed point of the chassis antenna through a 17.5mm CPW line, a series capacitance of 1.7pF and a capacitor and an inductor of 5.6pF and 3.3nH to ground. The impedance measured at port 2 is comparable to that of the chassis antenna at the feed point.

The equivalent circuit described above was combined with the NIC based matching network as shown in Fig.5.21a. The measured S_{22} of this equivalent NIC matched antenna circuit is shown in Fig. 5.21b. It shows a match of better than -10dB within the frequency range of 0.7GHz – 1GHz. This frequency range is chosen because there is reasonable agreement between the antenna and the equivalent circuit between 0.7GHz and 1GHz as seen in Fig.5.20. Outside this range, it can be seen that there is a significant difference between the

antenna and the equivalent circuit. Therefore the decision was made to characterise the noise and linearity of the NIC matched antenna within this frequency range.

(a)

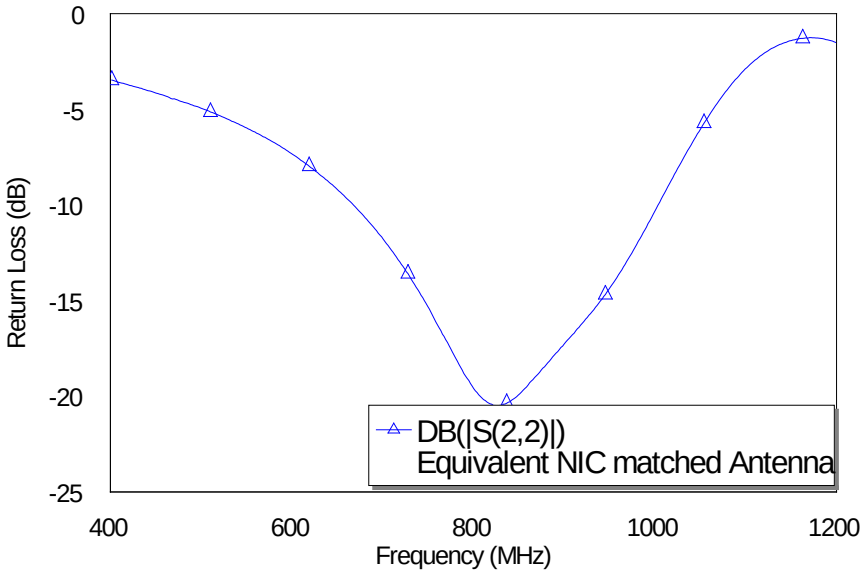

(b)

Fig.5 21 (a) Equivalent antenna matched with NIC matching network and (b) Measured S22 of equivalent antenna matched with NIC matching network

5.4.2. Noise measurement

The antenna noise temperature is a measure that describes the noise power received by the antenna at a given frequency. It can be obtained by integrating the product of the antenna directivity and the brightness temperature distribution of the environment over the entire space. The brightness temperature of the environment is dependent on many noise sources: cosmic, atmospheric, man-made and ground. The noise power received at the antenna terminals is [5]:

$$N = KT_aB \qquad 5.2$$

Where K is Boltzmann coefficient, T_a is the antenna noise temperature and B is the bandwidth of the system receiver. In this case the antenna noise temperature within an NIC matched antenna would consist of all the above noise sources as well noise coming from the use of active devices, transistors. This section shows the result of the added noise from using the NIC.

The equivalent circuit in section 5.4.1 is used to measure the noise performance of the representative NIC matched antenna. This is compared with using a purely resistive matching network.

For this measurement, we used the Y – factor measurement technique [6]. A pre-calibrated noise source with a known Excess Noise Ratio (ENR) which can be turned on and off is required, and a source from Noise Com Inc was used. This requires a DC voltage supply of 28V.

The ENR of the noise source is given by [6]:

$$\mathrm{ENR} = \frac{T^{s}_{ON} - T^{s}_{OFF}}{T_0} \tag{5.3}$$

where,

T^{s}_{ON} is the noise temperature of the noise source when it is ON and

T^{s}_{OFF} is the noise temperature of the noise source when it is OFF

T_0 is the reference temperature

In the case of pre-calibrated noise sources,

$$T^{s}_{OFF} = T_0 = 290\mathrm{K} \tag{5.4}$$

The measurement setup is shown in Fig. 5.22. It can be seen that the noise source is connected to port 1of the DUT (Device under test) which is the equivalent circuit, whilst the output port of the DUT is connected to a LNA (Low Noise Amplifier). The output of the LNA is connected to the spectrum analyser which is used to measure the noise power as the noise source is turned ON and OFF. The LNA is optional and it is only required to amplify the noise power beyond the noise floor of the spectrum analyser. If the option to use the LNA is chosen, there is a need to calibrate the measurement set up to determine the exact noise contribution of the LNA prior to use in the noise measurement setup.

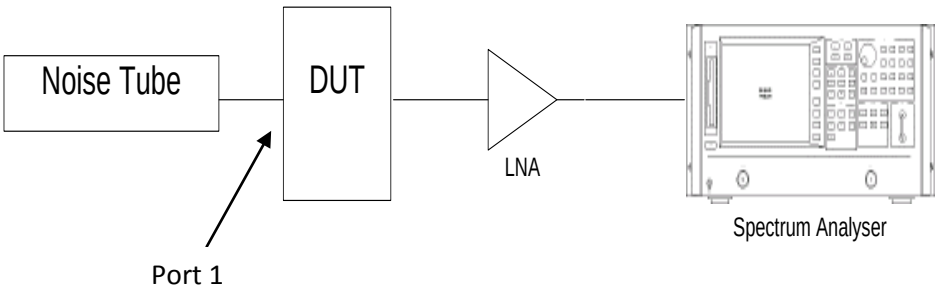

Fig.5 22 Setup for noise measurement.

The ratio of the measured noise power in the spectrum analyser when the noise source is switched on and off is the Y- factor. This is also equivalent to the ratio of noise temperature.

$$Y = \frac{N_{ON}}{N_{OFF}} = \frac{T_{ON}}{T_{OFF}} \tag{5.5}$$

where

N_{ON} = Measured noise power when noise source is ON,

N_{OFF} = Measured noise power when noise source is OFF,

T_{ON} = Measured noise temperature when noise source is ON and

T_{OFF} = Measured noise temperature when noise source is OFF

Now,

$$T_{ON} = T_{sys} + T^{s}_{ON}$$
$$T_{OFF} = T_{sys} + T^{s}_{OFF} \tag{5.6}$$

where,

T_{sys} is the noise temperature of the measurement set up.

Power measurements were taken at frequencies in steps of 0.01GHz, between 0.7GHz and 1GHz. The noise factor of the measurement system, F_{sys}, is found from the noise temperature of the measurement system by [6]

$$F_{sys} = 1 + \frac{T_{sys}}{T_0} \tag{5.7}$$

Because the measurement set-up involves multiple components which eventually contribute to the overall measured noise, it is necessary to have a second stage correction via which the noise factor of the DUT is extracted. This second stage correction is based on the noise contribution seen for a cascaded system of noise and it is done using the Friis formula for noise factor [7].

$$F_{cascade} = F_1 + \sum_{i=2}^{n} \frac{F_i - 1}{G_1 G_2 \dots \dots . G_{n-1}} \tag{5.8}$$

Where F_i and G_i are the noise factor and gain of the i^{th} stage in a cascaded system

The extracted noise figure of the DUT given by

$$NF_{DUT}(dB) = 10 \log F_{DUT} \tag{5.9}$$

From Fig.5.22, the DUT is the 2^{nd} stage of the system, therefore, F_2 extracted from F_{sys} using eq. 5.8 is the F_{DUT}.

The noise figure of the DUT is then used to calculate the signal to noise ratio (SNR) of the DUT. This is compared with the SNR obtained from a purely resistive matching network, which gives a similar antenna return loss within the same frequency band. The SNR advantage (SNR_{adv}) of the NIC matched antenna over the lossy matched antenna is computed using the eq. 5.10 [6] and shown in Fig 5.23.

$$SNR_{adv} = (S_{NIC} - S_{lossy}) - (NF_{NIC} - NF_{lossy}) \tag{5.10}$$

where,

S_{NIC} is the gain with NIC matching and

S_{lossy} is the gain with purely resistive matching

It can be seen that in Fig. 5.23, there is a significant SNR advantage over a wide frequency range, with a peak advantage of 17dB at 750MHz. This can be compared with the result in Fig.5.17 which showed an antenna efficiency improvement of the order of 5dB. Also this means that there is less noise generated from the NIC when compared to the purely resistive matching network. From the initial results in Fig.5.17, it is clear that the NIC would have a better gain when compared to the purely resistive matching network (Appendix D for relationship between gain and efficiency). In transistors, the noise increases with frequency, this therefore explains the downward slope with increasing frequency (Appendix A). This result is similar to that obtained by Sussman-Fort and Rudish [8] in which they showed a peak SNR advantage of 25dB at 40MHz and a useful advantage over the frequency range of 30MHz and 60MHz.

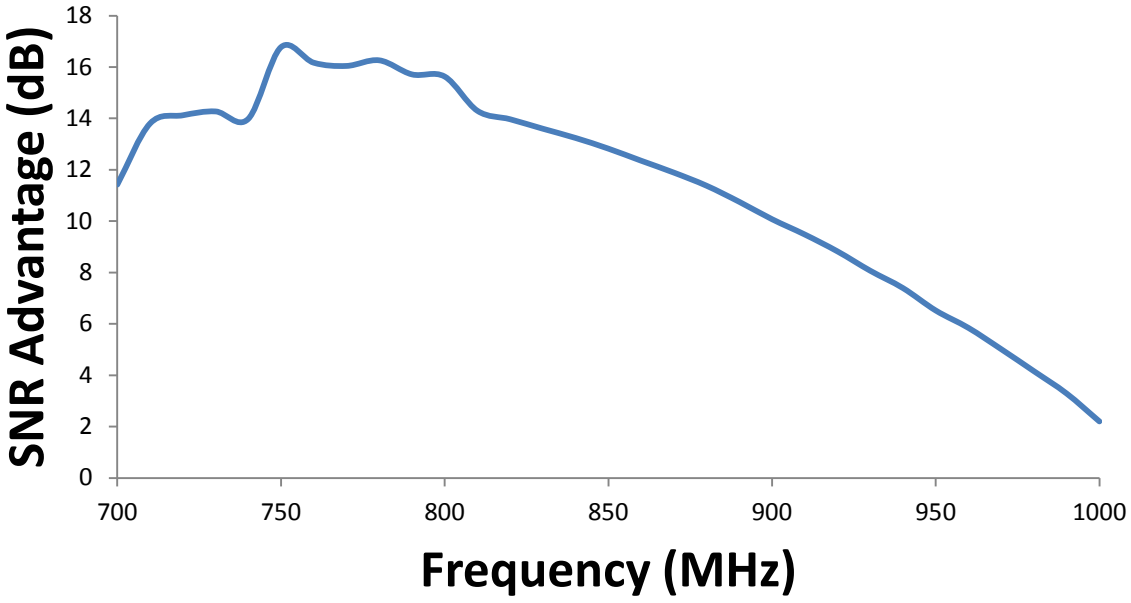

Fig.5.23 SNR advantage of a NIC matched equivalent antenna over a resistive matched equivalent antenna

5.4.3. Linearity measurements

NIC consists of transistors, which are inherently non-linear devices. There is therefore a need to check the linearity performance. This is likely to be particularly important in cognitive radio (CR) nodes because of their wideband nature. CR nodes may have to operate at frequencies next to high power signals. As the nodes become more prominent in future deployments the need for highly linear nodes will increase.

Linearity measurements usual involve the use of two independent tones separated in frequency. These two tones are then fed into the DUT. In a non-linear device, the two tones and other harmonics are generated at the output of the DUT. Figure 5.24 illustrates this concept.

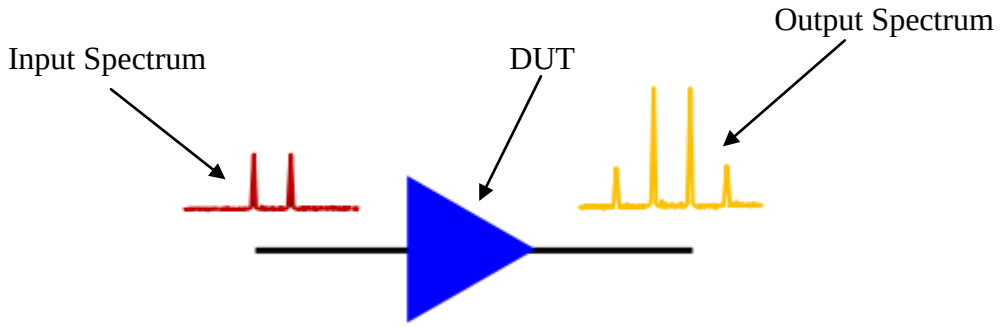

Fig.5 24 Effects of non-linearity in amplifier on two tones

The fundamental tones at the output of the DUT have a 1:1 relationship with the input power of the fundamental tones where as the 3rd order products have a 3:1 relationship with the input power. In active devices, there exist a saturation point at which the linear 1:1 relationship between the input power and the output power ceases. If the response of the output power is extrapolated beyond the saturation point then the intercept point between the 3rd order product and the extrapolated fundamental response is called the third order intercept point (IP3). This point is shown in Fig. 5.25 below.

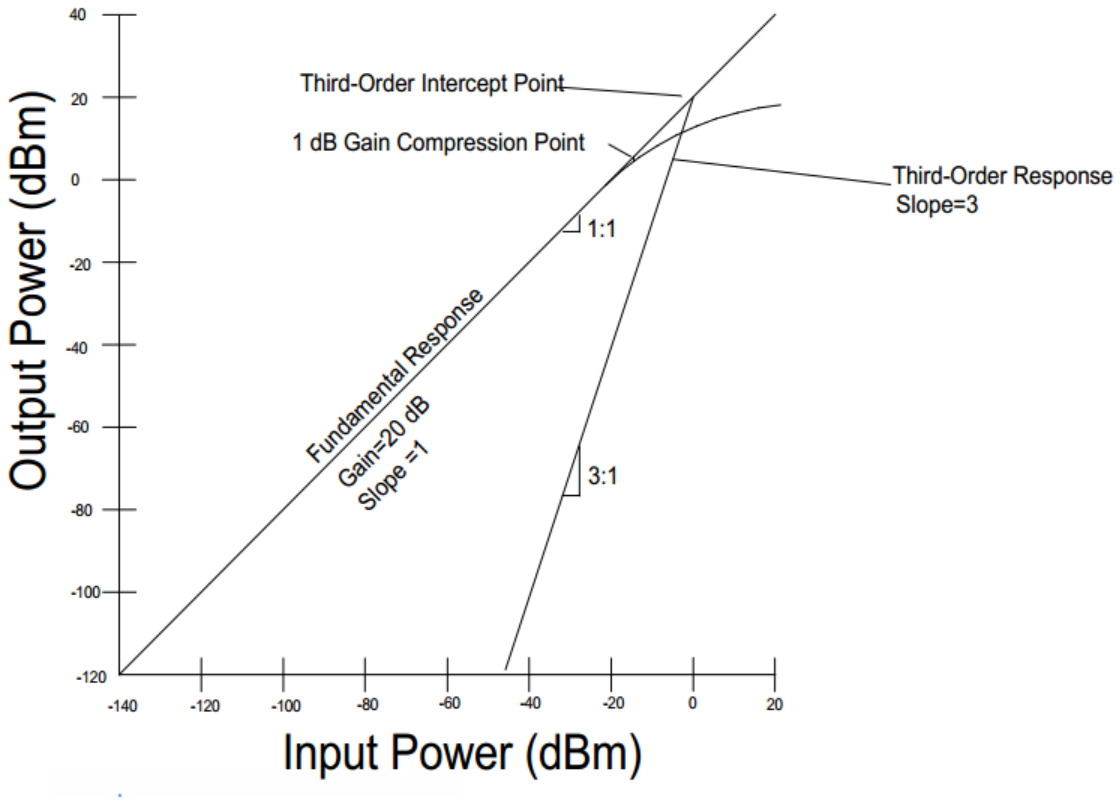

Fig.5 25 Third order intercept point [5]

The standard measure of linearity is the 3rd order intercept point (IP3). For this measurement, two independent signal tones separated in frequency are generated by a Rohde & Schwarz, ZVA 67, Vector Network Analyser (VNA) which has four ports with two independent generators. The measurement setup is shown in Fig. 5.26. It consists of the VNA generating two independent tones with frequency separation of 1MHz. The two tones are then combined in ZAPD-2-21-3W-S+ power splitter before being fed into the DUT. The output of the DUT is then fed back through one of the other ports into the VNA where the output power of the fundamental tones and the intermodulation signals are measured. The IP3 is then computed using the following equations .

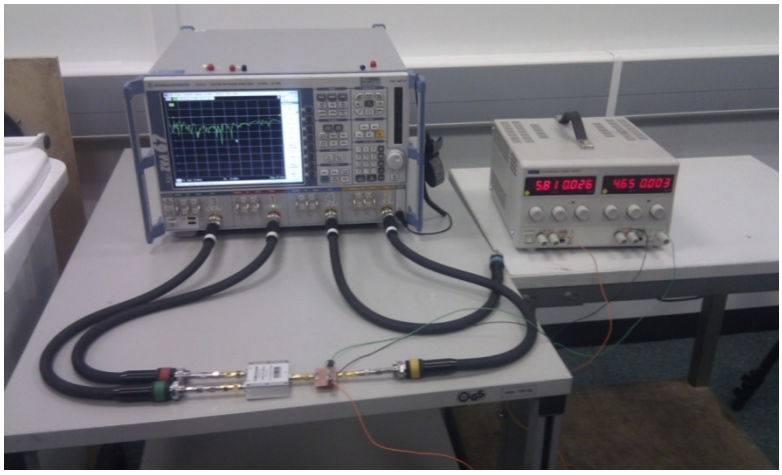

Fig.5 26 Inter-modulation measurement set-up

$$\mathrm{IP3} = \mathrm{P_{out}} + \frac{\Delta \mathrm{IM}}{2} - \mathrm{G} \qquad (5.11)$$

where, ΔIM is the difference between the power levels of the output fundamental signal (P_{out}) and the 3rd order product, and G is the gain of the DUT.

The DUT in this measurement is the prototype 2 NIC matched equivalent antenna. The power spectrum plot at a fixed frequency of 900MHz with constant stimuli is shown in Fig. 5.27.

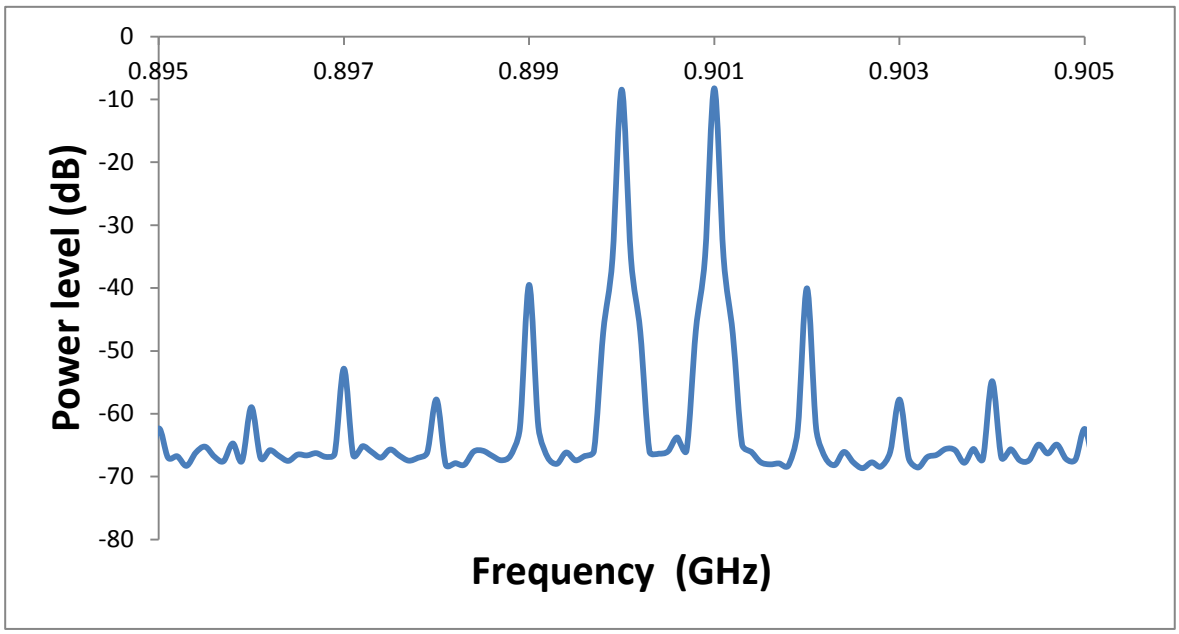

Fig.5 27 Output power spectrum

Third order products can be seen, as well as the 5^{th} and 7^{th} order products. When the measurement described above is done with a frequency sweep between 700MHz to 1000MHz, the 3^{rd} order intercept points across the 300MHz frequency span were computed and the IP3 is shown in Fig. 5.28.

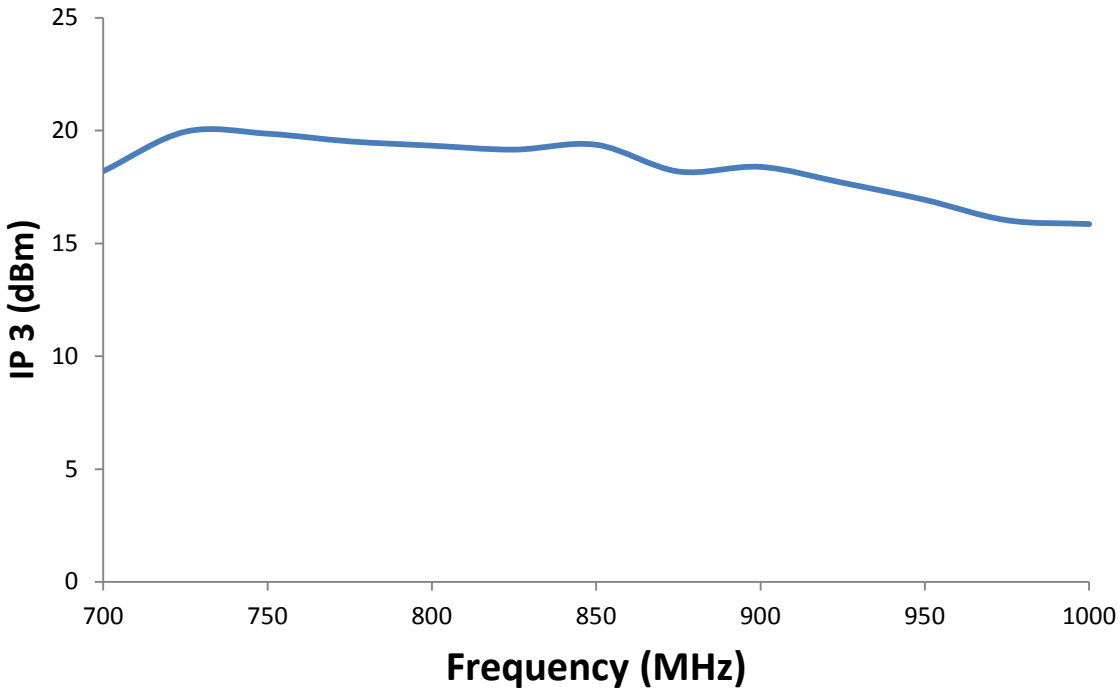

Fig.5 28. 3rd Order Intercept point.

The measured IP3 was found to be within the range of similar components of other available RF front-end devices. Using the cascaded system IP3 equation, Eq.5.12, it can be seen that the impact of an NIC matched antenna will be minimal as the overall IP3 of a receive chain is dominated by the linearity of the later stages. The impact in the transmit mode would be higher but because the IP3 value is within the range of other devices in the chain, the impact is also expected to be manageable.

$$\frac{1}{IP3_{sys}{}^2} = \frac{1}{IP3_1{}^2} + \sum_{i=2}^{n} \frac{G_1{}^2 G_2{}^2 G_3{}^2 \dots\dots\dots G_{n-1}{}^2}{IP3_i{}^2} \qquad (5.12)$$

Where n = number of stages and G is the gain of the stage

5.5. Conclusion and summary

An NIC with an upper frequency cut-off of 1.5GHz has been shown. The measured NIC has been combined in a simulator with a chassis antenna and the wideband performance has been achieved. This also showed a better performance than a resistively and lossy matched antenna. An equivalent circuit has been built to represent the antenna within a frequency band and it is with this equivalent circuit combined with an NIC that the noise and linearity performance of the NIC is investigated. It can be seen that the NIC matched antenna shows a Signal to Noise ratio advantage when compared with a resistively matched antenna. It terms of linearity, it can be seen that the NIC's IIP3 of 18dBm is within range of commercially available RF front end components. Also because the cascaded IP3 of a system is dominated by the later stages also helps limit any impact the IP3 of the NIC matched antenna might have on the overall receiver system performance.

Reference

[1] O. O. Tade, P. Gardner, and P. S. Hall, "Negative impedance converters for broadband antenna matching," in *Microwave Conference (EuMC), 2012 42nd European*, 2012, pp. 613-616.

[2] O. O. Tade, P. Gardner, and P. S. Hall, "Broadband matching of small antennas using negative impedance converters," in *Antennas and Propagation Society International Symposium (APSURSI), 2012 IEEE*, 2012, pp. 1-2.

[3] O. O. Tade, P. Gardner, and P. S. Hall, "Antenna bandwidth broadening with a negative impedance converter," *International Journal of Microwave and Wireless Technologies*, vol. 5, pp. 249-260, 2013.

[4] J. T. Aberle, "Two-Port Representation of an Antenna With Application to Non-Foster Matching Networks," *Antennas and Propagation, IEEE Transactions on,* vol. 56, pp. 1218-1222, 2008.

[5] D. M. Pozar, *Microwave Engineering, 3Rd Ed*: Wiley India Pvt. Limited, 2009.

[6] Agilent Technologies. Noise Figure Measurement Accuracy - The Y-Factor Method [Online]. Available: http://cp.literature.agilent.com/litweb/pdf/5952-3706E.pdf

[7] H. T. Friis, "Noise Figures of Radio Receivers," *Proceedings of the IRE,* vol. 32, pp. 419-422, 1944.

[8] S. E. Sussman-Fort and R. M. Rudish, "Non-Foster Impedance Matching of Electrically-Small Antennas," *Antennas and Propagation, IEEE Transactions on,* vol. 57, pp. 2230-2241, 2009.

CHAPTER 6

COUPLED LINE NEGATIVE IMPEDANCE CONVERTER

6.1. Background

The use of negative impedance converters (NIC) in broad band matching of antennas has been shown in the previous chapter. There are however some disadvantages and limitations with using an NIC that uses the Linvill's two transistor model. Some of these limitations are listed below:

1. The Linvill's NIC is based on the use of two transistors, and as a consequence there is the possibility of a build up of current in the feedback paths between the two transistors which will ultimately lead to oscillation, as the two transistors have gain. The frequency of oscillation is dependent on the length of the feedback path as discussed in chapter 4.
2. The use of two active devices also makes biasing more complicated. The bias network occupies a large area and hence practical implementation of an NIC matched antenna using the Linvill's model is very difficult using standard PCB (Printed Circuit Board) technology.
3. The use of two active devices (transistors) is likely to be a source of high noise levels and low linearity. Reducing this number could improve the noise and linearity.

The common characteristic with all the above mentioned limitations is the use of active devices, which in this case is the transistor. If there was a means of achieving non-Foster elements without active devices or reducing the active device count, then it might be possible to reduce these complexities and limitations. Therefore, there is a need to find an alternative method of realising non-Foster elements with less complexity.

Sussman-Fort in [1], introduces an alternative to the two transistor Linvill NIC. He used a transistor along with a transformer to realise non-Foster elements. This new circuit does offer an alternative, but the use of a transformer means that it is difficult to implement at higher frequencies and on PCBs. The schematic of the transformer based NIC is shown in Fig. 6.1, in the form of a single terminal NIC. The element to invert, Z_L, is connected between the collector of the transistor and one of the terminals of the secondary winding in the transformer. It should also be noted that the secondary windings have been flipped in order to achieve the phase inversion required for realising the non-Foster element. The resultant impedance seen at the terminal of the NIC (Z_{in}) is a ratio of the impedance to invert to the turn ratio, $-\frac{Z_L}{n}$.

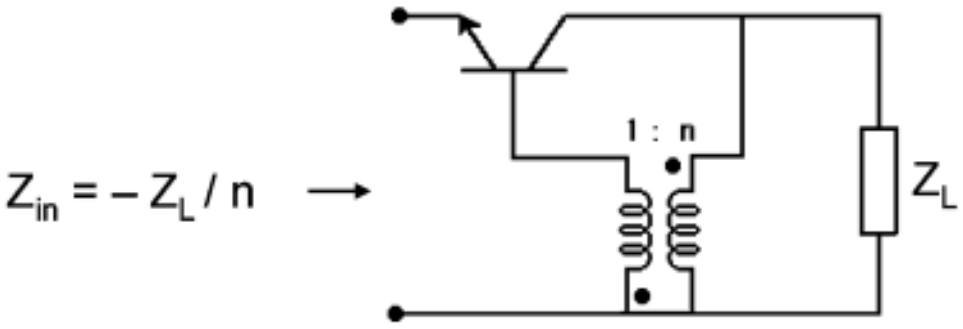

Where Z_L is the impedance to invert and n is the turns ratio of the transformer

Fig. 6. 1 Transformer based NIC [1]

In this chapter, a new NIC circuit is proposed. It uses a single transistor and a pair of coupled transmission lines. It is expected that this new circuit, henceforth referred to as the coupled line NIC, would address the limitations of the two transistor NIC such as noise and linearity. It may not completely solve the problem as there are still active devices within the circuit but

because the active element count has been halved, it is expected that there would be significant improvements. It is also expected that the use of a single active device would make it easier to implement a fully integrated NIC matched antenna because of less demand on space by the circuit and its associated bias network.

6.2. The Coupled Line NIC

The basic idea behind the NIC is the ability to present the voltages from one end of the NIC circuit to the opposing side of the impedance to invert. With Linvill's NIC, this is achieved with the use of the feedback paths. Using the coupled lines in the coupled line NIC, it is possible to achieve this same impedance inversion although in a different and subtle way as shown by the analysis given in section 6.2.1. The schematic of the coupled line NIC is shown in Fig.6.2. It consists of a transistor and pair of CPW coupled line.

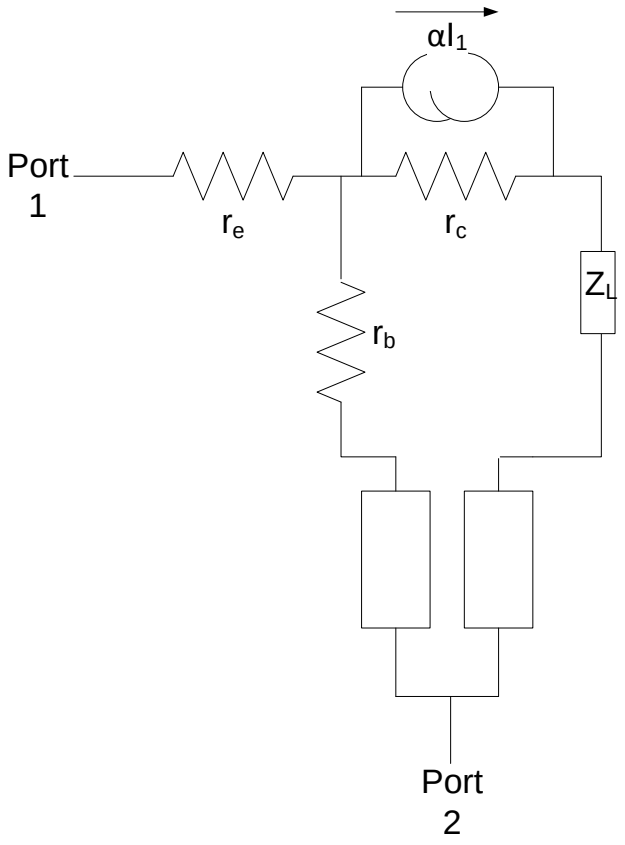

Fig. 6. 2 The coupled Line NIC schematic

6.2.1 Coupled line equivalent circuit

In order to analyse this schematic, the coupled line has been replaced with a simple “T” network equivalent as shown in Fig.6.3. A typical lossless transmission line can be approximated by an L shaped network consisting on impedance in series and another shunt to ground as shown in Fig.6.3b [2]. Therefore in the case of a coupled line whose ends are joined together and grounded, Fig.6.3c can be used to represent the grounded coupled lines.

Also to simplify the coupled line NIC analysis, the coupled line NIC would be analysed as a single port device thereby grounding port 2 in Fig.6.2. The grounded coupled line section in Fig.6.3a can be represented by an equivalent “T” network as shown in Fig.6.3b. The impedances Z_s and Z_p are inductors and their values can be obtained by using the following equations and analysis. The shunt impedance is represented as two $2Z_p$ impedances in parallel in order to maintain the symmetry of the equivalent circuit structure.

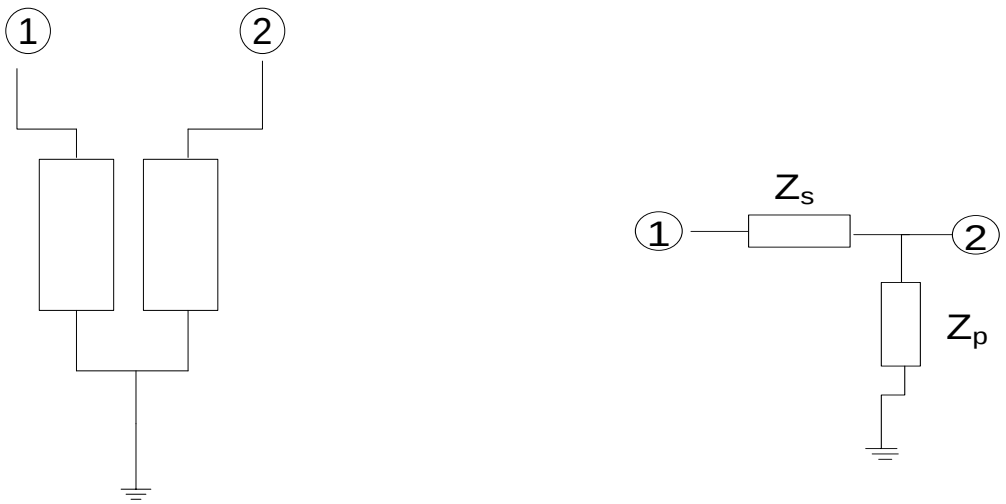

(a) (b)

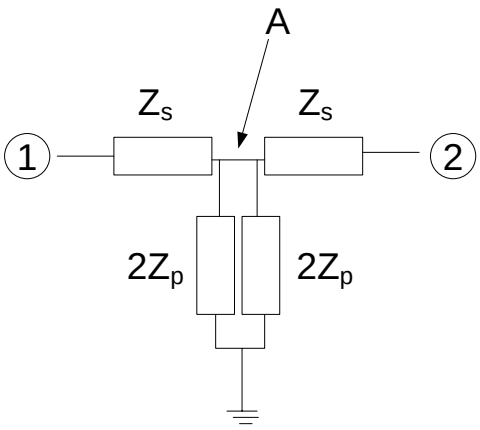

(c)

Fig. 6. 3 (a) The grounded coupled line section (b) Equivalent circuit of a transmission line (c) The equivalent T network

In odd mode, Fig.6.3b reduces to Fig.6.4a because there is a virtual ground created at point A in the middle of the equivalent circuit. While in the even mode, Fig.6.3b reduces to Fig.6.4b because of the open circuit that develops at point A in the equivalent circuit.

(a) (b)

Fig. 6. 4 (a) Equivalent T network in odd mode and (b) Equivalent T network in even mode.

Therefore,

$$Z_s = Z_{in\ odd} \text{ and } Z_{in\ even} = Z_s + 2Z_p \quad (6.1)$$

However,

$$Z_{in\ odd} = jZ_{odd} \tan \theta_{odd} \quad (6.2)$$

and

$$Z_{in\ even} = jZ_{even} \tan \theta_{even} \quad (6.3)$$

Therefore,

$$\omega L_s = Z_{in\ odd} = jZ_{odd} \tan \theta_{odd} \quad (6.4)$$

$$\omega L_p = Z_p = \frac{Z_{in\ even} - Z_{in\ odd}}{2} \quad (6.5)$$

$$\omega L_p = Z_p = \frac{j}{2} (Z_{even} \tan \theta_{even} - Z_{odd} \tan \theta_{odd}) \quad (6.6)$$

The values of Z_{even}, $\tan \theta_{even}$, Z_{odd} and $\tan \theta_{odd}$ are the impedance and electrical length of the coupled line section in even and odd mode. These values were obtained via simulation of the coupled line and the values of the corresponding inductors L_p and L_s are calculated using equations 6.4 and 6.5 at spot frequencies. The computed values of Lp and Ls are then optimised using AWR for best results. The resultant equivalent circuit has L_p = 0.57nH and L_s = 1.234nH. Fig.6.5 shows S_{21} magnitude and phase comparison between the coupled line and the equivalent circuit, the S_{21} was compared because it shows the transmission characteristics of the circuit and schematic. There is a reasonable agreement between the two schematics. The lack of perfect agreement is due to the fact that the values of the inductors

were computed at specific frequency (1 GHz) and these inductors are also frequency independent.

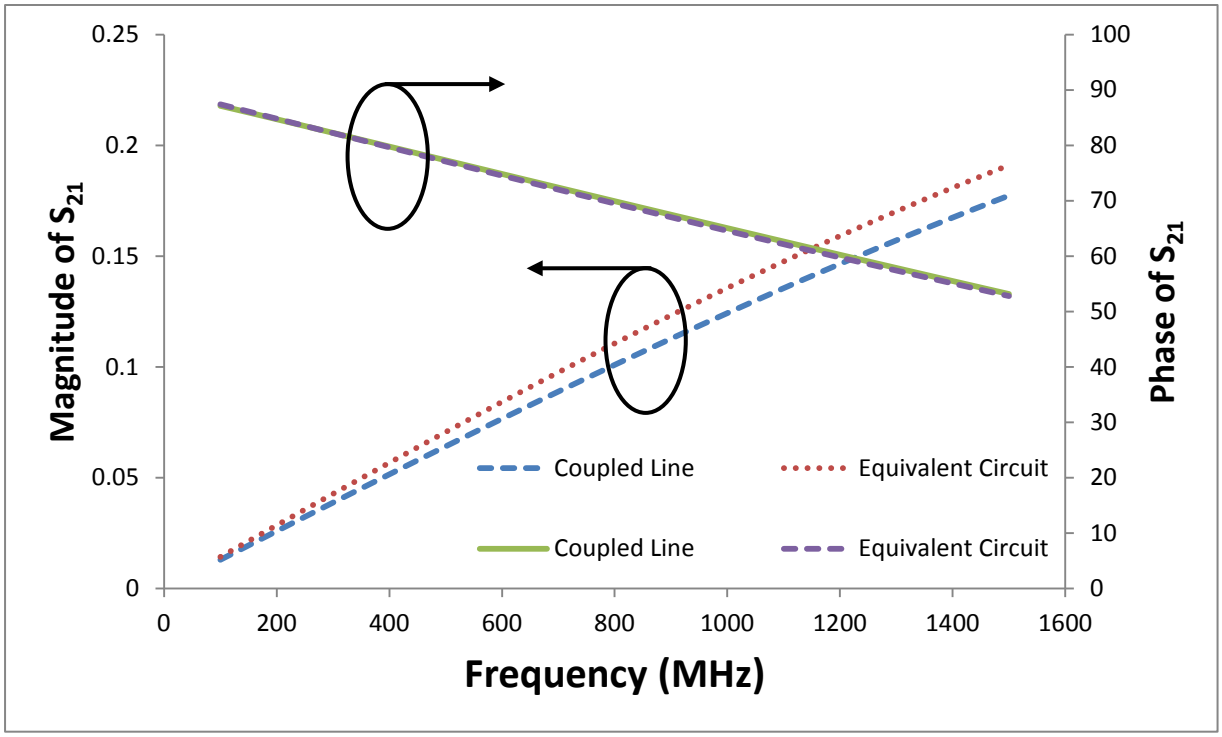

Fig. 6. 5 Comparison of simulated S_{21} of grounded coupled line section and equivalent circuit

6.2.2 Coupled Line NIC Analysis

The current source in Fig.6.2 representing the collector terminal of a transistor can be transformed into a voltage source as shown in Fig.6.6. Given that there is agreement between the coupled line section and its equivalent T network as shown in Fig.6.5, the coupled line section can also be replaced by its element equivalent in the analysis in order to be able to perform a circuit analysis.

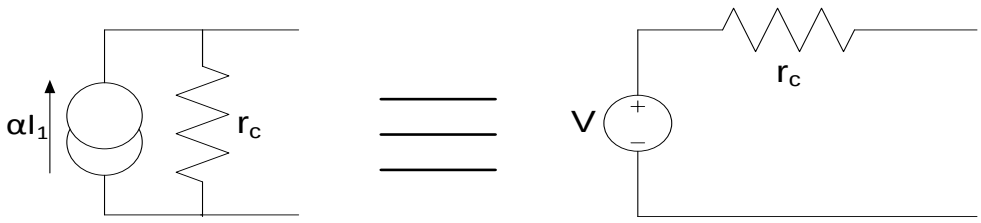

Fig. 6. 6 The transformation between a current source into a voltage source.

Where

$$V = \alpha I_1 r_c \tag{6.7}$$

Replacing the current source with its equivalent voltage source and the coupled line with its equivalent circuit, the coupled line NIC can be represented as shown in Fig.6.7 and it is this schematic on which the analysis is based.

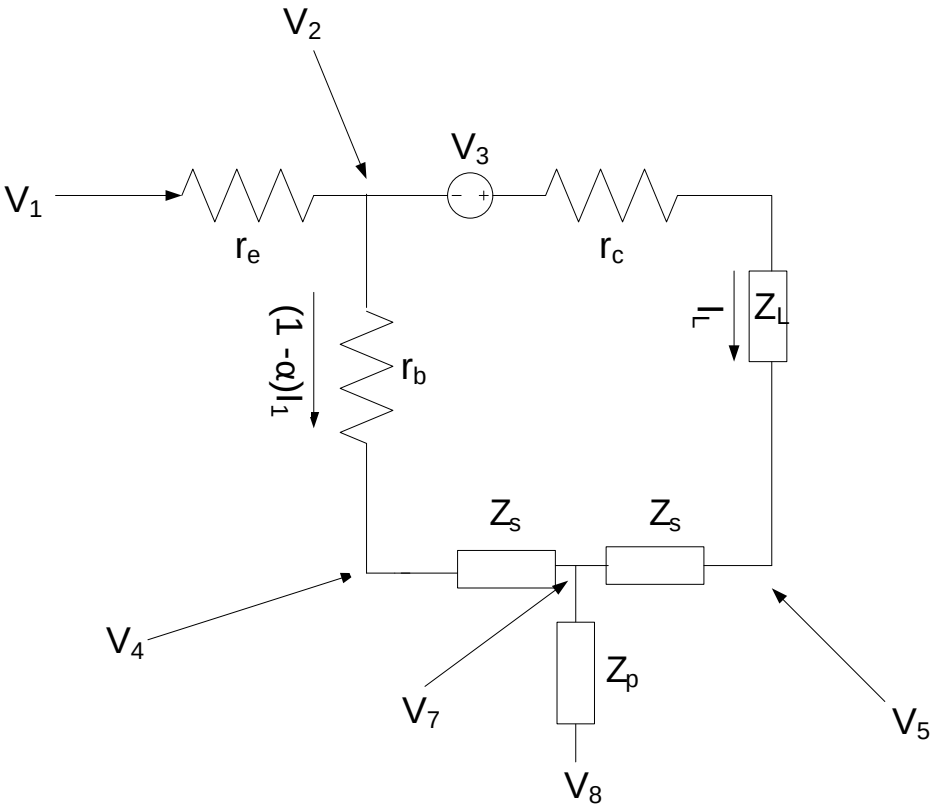

Fig. 6. 7 Equivalent circuit for the coupled line NIC

From Fig.6.7,

$$V_2 = V_1 - I_1 r_e \tag{6.8}$$

$$V_4 = V_2 - (1- \propto) I_1 r_b = V_1 - I_1 r_e - (1- \propto) I_1 r_b \tag{6.9}$$

$$V_4 - V_7 = (1- \propto) I_1 Z_s \tag{6.10}$$

$$I_L = \frac{V_2 + V_3 - V_7}{r_c + Z_L + Z_s} \tag{6.11}$$

$$I_L = \frac{V_1 - I_1 r_e + \propto I_1 r_c - (V_4 - (1- \propto) I_1 Z_s)}{r_c + Z_L + Z_s} \tag{6.12}$$

$$I_L = \frac{V_1 - I_1 r_e + \propto I_1 r_c - V_1 + I_1 r_e + (1- \propto) I_1 r_b + (1- \propto) I_1 Z_s}{r_c + Z_L + Z_s} \tag{6.13}$$

$$I_L = \frac{\propto I_1 r_c + (1- \propto) I_1 r_b + (1- \propto) I_1 Z_s}{r_c + Z_L + Z_s} \tag{6.14}$$

$$V_7 = V_8 + Z_p (I_L + (1- \propto) I_1) \tag{6.15}$$

$$V_7 = V_8 + Z_p I_1 \left(\frac{\propto r_c + (1- \propto) r_b + (1- \propto) Z_s}{r_c + Z_L + Z_s} + (1- \propto) \right) \tag{6.16}$$

$$V_7 = V_4\text{-}(1\text{-}\ \propto)I_1Z_s \tag{6.17}$$

$$V_7 = V_1\text{-}\ I_1r_e\text{-}(1\text{-}\propto)I_1r_b\text{-}(1\text{-}\ \propto)I_1Z_s \tag{6.18}$$

Equating 6.16 and 6.18

$$\begin{aligned} V_1\text{-}\ I_1r_e\text{-}(1\text{-}\propto)I_1r_b\text{-}(1\text{-}\ \propto)I_1Z_s \\ = V_8 \\ + Z_pI_1\left(\frac{\propto r_c + (1\text{-}\propto)r_b + (1\text{-}\ \propto)Z_s}{r_c + Z_L + Z_s} + (1\text{-}\ \propto)\right) \end{aligned} \tag{6.19}$$

$$\begin{aligned} \frac{V_1\text{-}V_8}{I_1} = r_e + (1\text{-}\propto)r_b + (1\text{-}\propto)Z_s \\ + Z_p\left(\frac{\propto r_c + (1\text{-}\propto)r_b + (1\text{-}\ \propto)Z_s}{r_c + Z_L + Z_s} + (1\text{-}\ \propto)\right) \end{aligned} \tag{6.20}$$

$$\begin{aligned} Z_{in} = r_e + (1\text{-}\propto)r_b + (1\text{-}\propto)Z_s \\ + \left(\frac{\propto r_cZ_p + (1\text{-}\propto)r_bZ_p + (1\text{-}\propto)Z_sZ_p}{r_c + Z_L + Z_s}\right) \\ + (1\text{-}\propto)Z_p \end{aligned} \tag{6.21}$$

If the collector impedance r_c is represented as a complex impedance Z_c then, equation 6.21 becomes

$$Z_{in} = r_e + (1- \propto)r_b + (1- \propto)Z_s + \left(\frac{\propto Z_c Z_p + (1- \propto)r_b Z_p + (1- \propto)Z_s Z_p}{Z_c + Z_L + Z_s}\right) + (1- \propto)Z_p \quad (6.22)$$

$$Z_{in} = r_e + (1- \propto)r_b + (1- \propto)Z_s + \left(\frac{Z_c Z_p + (1- \propto)Z_p(r_b + 2Z_s + Z_L)}{Z_c + Z_L + Z_s}\right) \quad (6.23)$$

Assume that $\alpha \cong 1$

This implies that

$$Z_{in} = r_e + \frac{Z_p Z_c}{Z_c + Z_L + Z_s} \quad (6.24)$$

$$Z_{in} \cong r_e + Z_p\left(\frac{1}{1 + \frac{Z_L + Z_s}{Z_c}}\right) \quad (6.25)$$

Applying binomial theorem equation 6.25 can be approximated as

$$Z_{in} = r_e + Z_p\left(1- \frac{Z_L + Z_s}{Z_C}\right) \cong r_e + Z_p - \frac{Z_p}{Z_c}Z_L - \frac{Z_p}{Z_c}Z_s \quad (6.26)$$

In the case where the collector impedance is purely imaginary and inductive then equation 6.26 becomes

$$Z_{in} \cong r_e + Z_p - \beta Z_L - \beta Z_s \quad (6.27)$$

Where β is constant $= \frac{Z_p}{Z_c}$

The input impedance seen across the terminals of the coupled line NIC has been shown to exhibit anti-Foster behaviour at specific conditions (when the collector impedance is reactive). In order to demonstrate this further, a simulation of the NIC structure using the s – parameters of the transistor is necessary as this would give the chance to utilise the transistor in its real state where the other parasitics within the transistor and the rest of the structure can be introduced into the analysis.

6.3. Simulations of Coupled Line NIC

To prove this concept, the coupled line NIC was simulated in AWR design environment. It consists of a single transistor and an edge coupled co-planar waveguide (CPW) line. Each transmission line that makes the coupled line section is 2mm wide and 6mm long. The gap between the two conductors is 0.4mm. These values were chosen to make the coupled line shorter than $\lambda/4$ and then optimised for best performance. The circuit schematic is shown in Fig 6.8. The impedance to invert is between the drain or collector of the transistor and the coupled line section. The negative element occurs between the source or emitter of the transistor and the two ends of the coupled line which have been joined together to form the other terminal of the coupled line NIC. Measurement ports are attached to the ends of these terminals to measure the S- parameters.

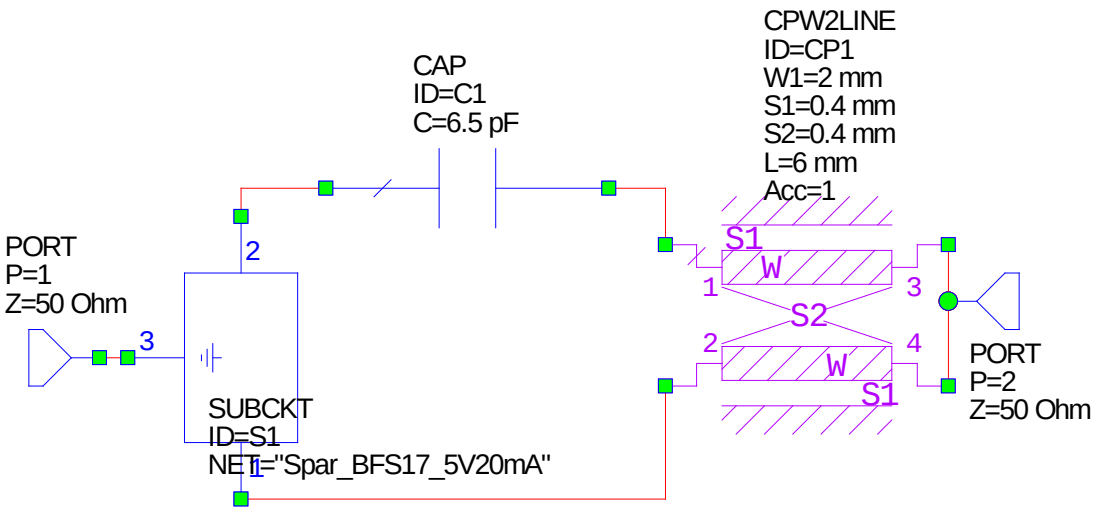

Fig. 6. 8 Schematic for the coupled line NIC

For the simulation, the S – parameters of NXP BFS17 transistor was used. The circuit is connected as shown in Fig 6.8 and the capacitor to invert is 6.5pF. The transistor is biased at 5V and 20mA. Fig 6.9 shows the input and output impedance plots of the coupled line NIC on a Smith chart. It can be seen to exhibit the non-Foster characteristics with the anti-clockwise rotation along the Smith chart. The resultant locus of the non-Foster element is observed to go outside the Smith chart. This shows that the resultant negated capacitor includes an inherent resistance. Sources of the resistance include losses from the coupled line section and the terminal resistances of the transistor. Therefore, during measurement, positive elements would be added between the NIC and the measurement ports to make the NIC measureable and these added elements would be de-embedded as previously done and explained in chapter 5.

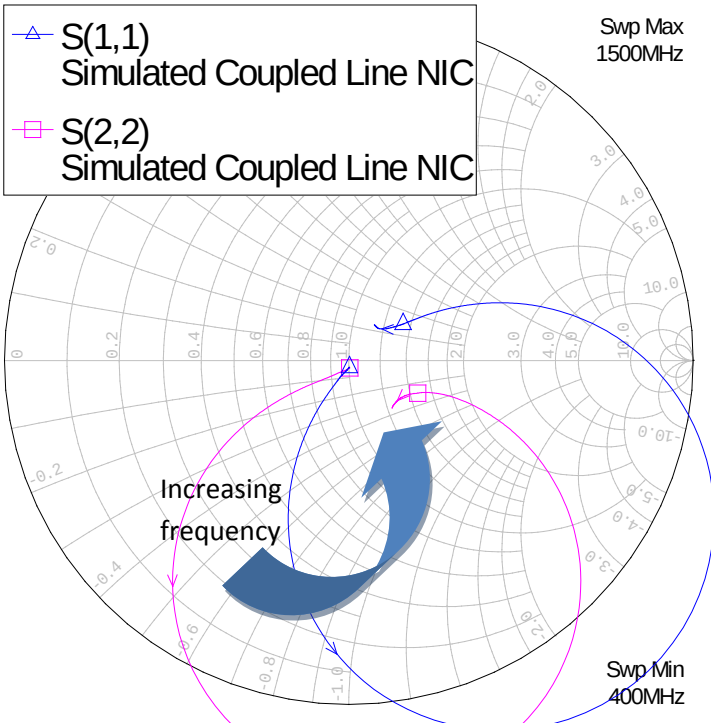

Fig. 6. 9 Simulated S11 and S22 of coupled line NIC

The negative reactance slope that characterises non-Foster elements is also evident as shown in Fig.6.10. The coupled line NIC structure is asymmetric unlike the Linvill's NIC but it is reciprocal as can be seen in its S_{21} and S_{12} plots shown in Fig 6.11.

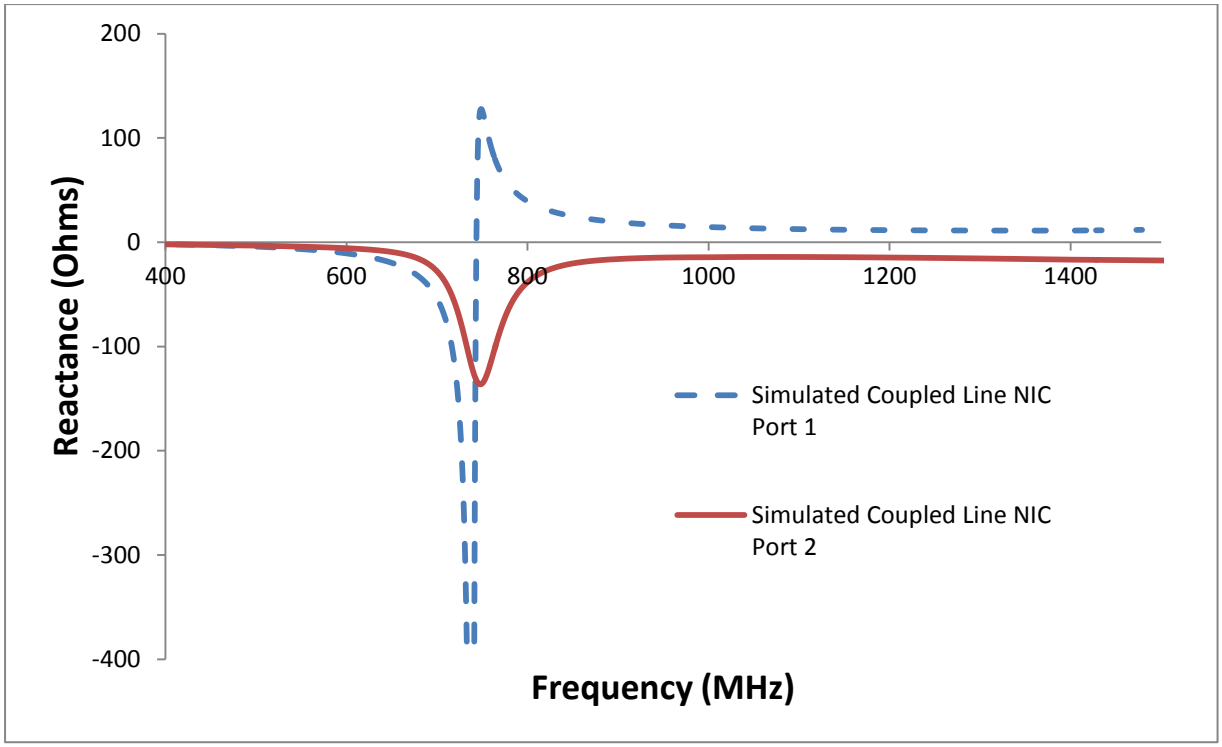

Fig. 6. 10 Simulated reactance of coupled line NIC of Fig. 6.8

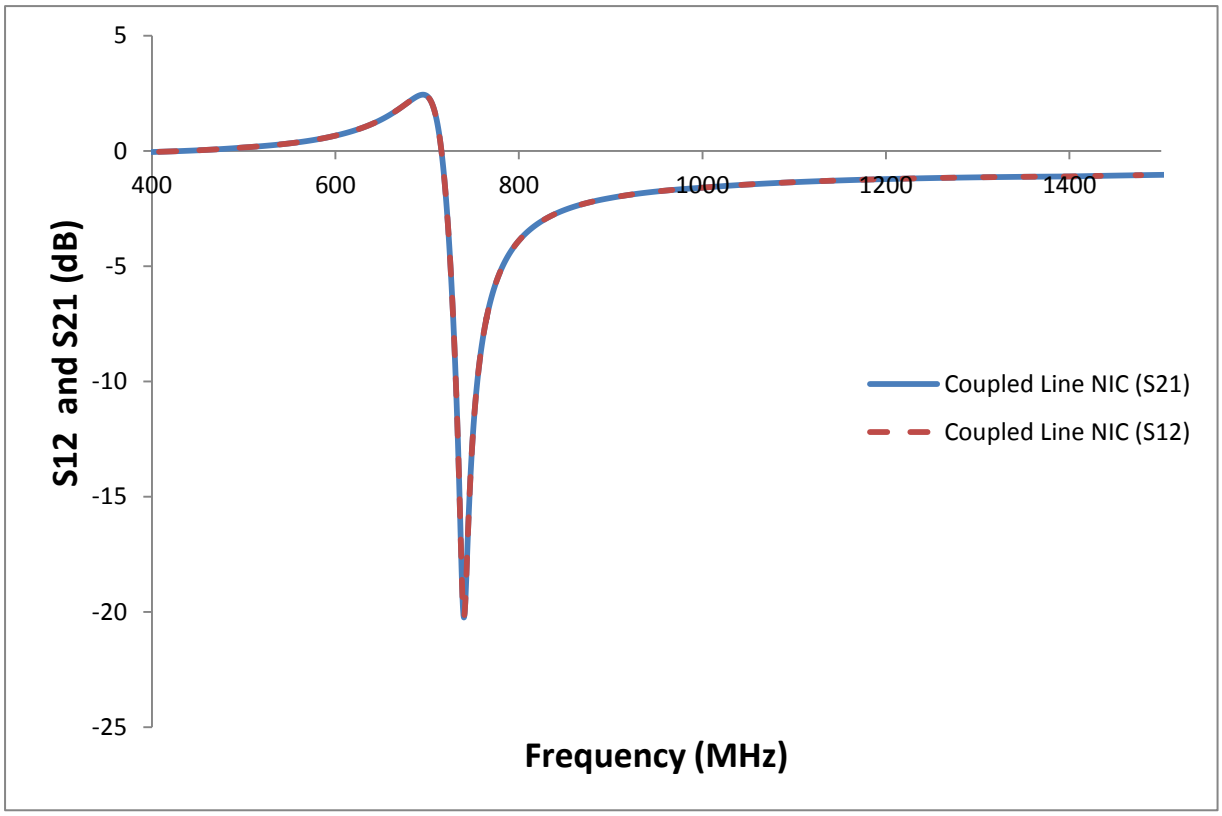

Fig. 6. 11 Simulated S_{21} and S_{12} of coupled line NIC of Fig. 6.8.

The capacitance against frequency plot is also shown in Fig 6.12 and it can be seen to exhibit the frequency dependence, like the negative capacitances obtained using the Linvill's NIC. Looking at the capacitance against frequency plot, it would be observed that the negative capacitance only occurs between 743MHz to 1500MHz. Below this range the coupled line NIC behaves like a negative inductor as shown in Fig. 6.12. This can also be observed from the other figures (Fig.6.9, 6.10). In Fig. 6.9, the locus of the simulated coupled line NIC starts out in the inductive region of the Smith chart before going into the capacitive region at 743MHz. The same can be observed in the reactance plot where a resonance is observed at this same frequency (Fig. 6.10).

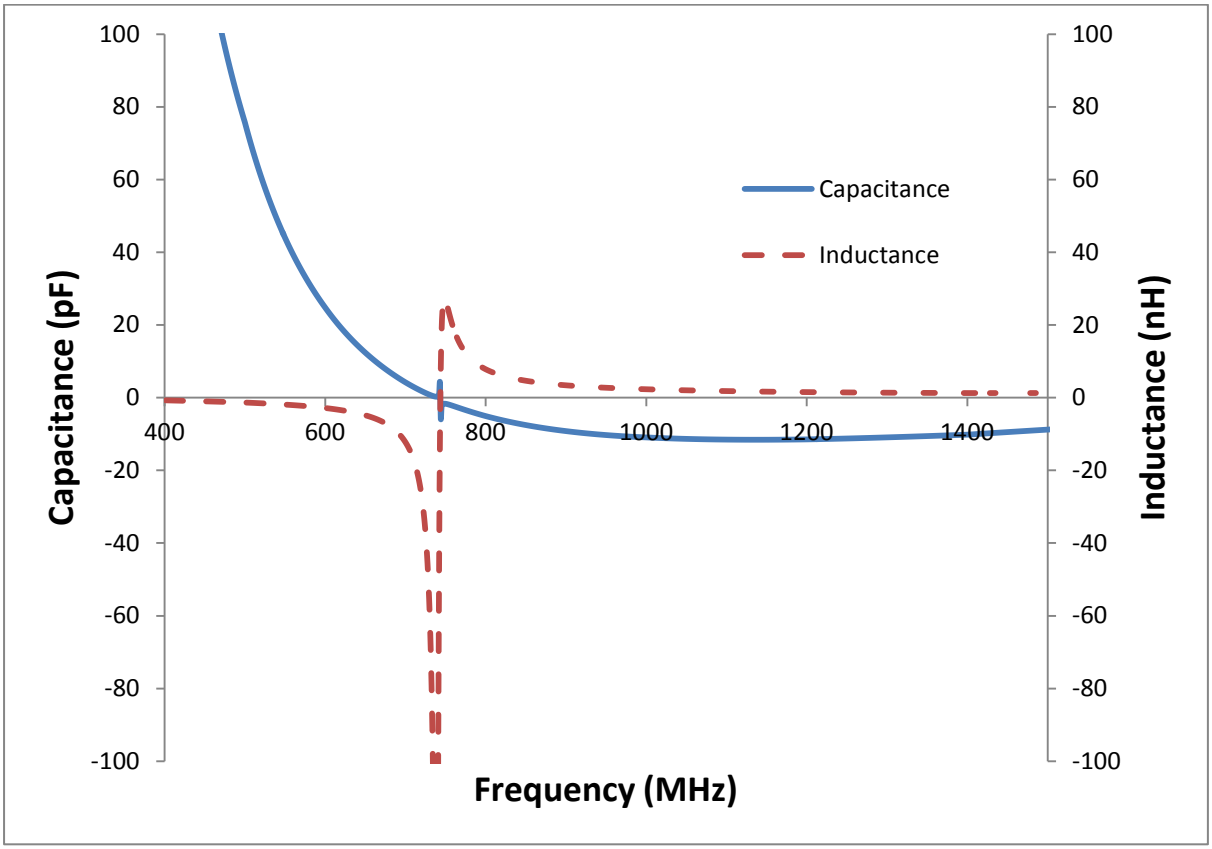

Fig. 6. 12 Simulated capacitance and inductance with coupled line NIC

6.4. Stability Analysis

Stability is still an important factor to consider in the coupled line NIC. To realise a stable and measureable NIC, it is necessary to have a means of predicting the stability of the coupled line NIC. The result of this analysis would also help with the choice of transistor used in the NIC. To perform a stability analysis, the T network representing the coupled line section is used.

As the coupled line NIC is not symmetrical, it is not possible to apply any form of simplification to the circuit, as was applied to Linvill's NIC. Fig. 6.13 below shows the equivalent circuit of the coupled line NIC. The capacitor C_{in} is the capacitor to invert and this also doubles as a DC blocking capacitor within the bias network. Resistor r_c is the collector resistance for the transistor in common base mode. Using the transfer function analysis similar to that in [3], a stability analysis was done. L_{s1}, L_{s2} and L_p are the impedance calculated using equations 6.1 – 6.6.

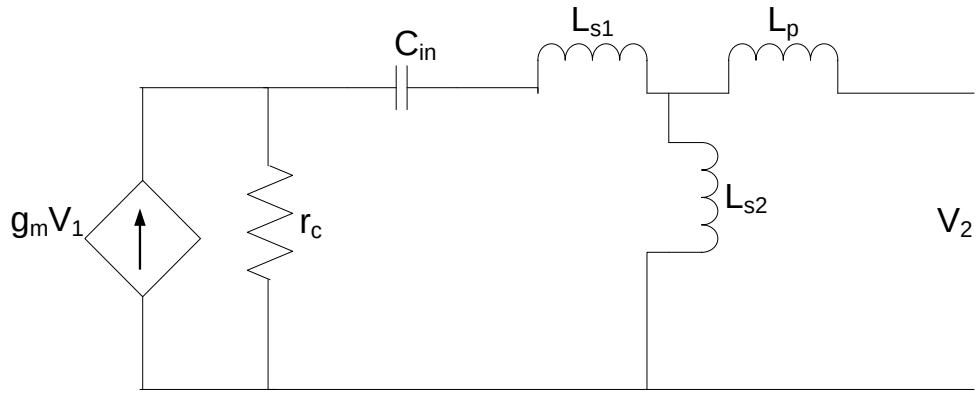

Fig. 6. 13 The Equivalent circuit of the coupled line NIC with current source.

Transforming the current source to its equivalent voltage source as shown in Fig.6.7, the coupled line NIC equivalent becomes Fig.6.14. Where the voltage is $g_m V_1 r_c$ and the current through the resistance r_c is $g_m V_1$.

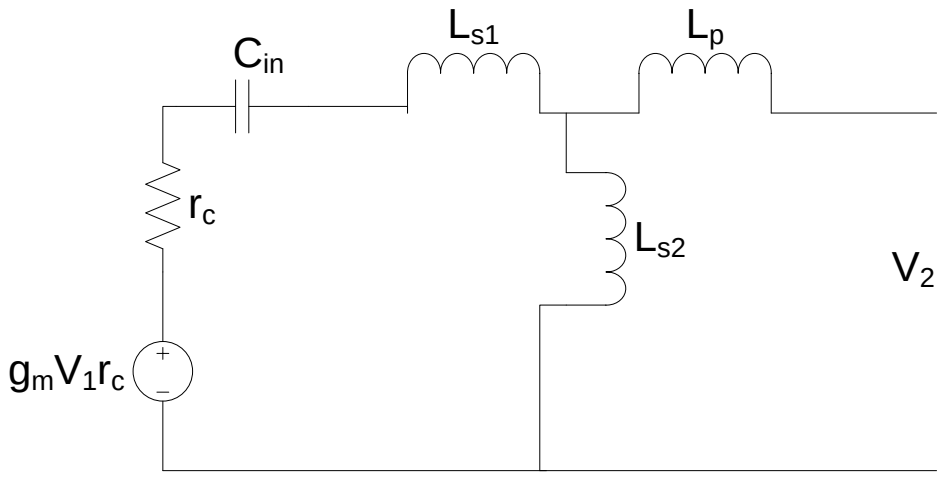

Fig. 6. 14 The Equivalent circuit of the coupled NIC with voltage source.

The total impedance, X_T, seen from the output V_2 can be obtained by replacing the voltage source with a short circuit and X_T can be obtained as shown in Fig.6.15.

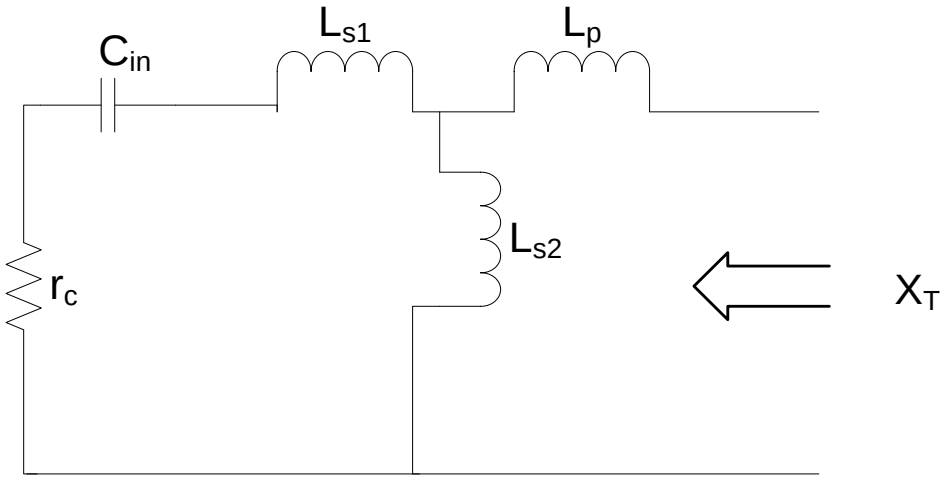

Fig. 6. 15 Total impedance of the coupled line NIC

Transforming the series combination of r_c, C_{in}, L_{s1} is X_1

$$X_1 = r_c + \frac{1}{sC_{in}} + sL_{s1} \tag{6.28}$$

$$X_1 = \frac{s^2L_{s1}C_{in} + sr_cC_{in} + 1}{sC_{in}} \tag{6.29}$$

X_2 is the parallel combination of X_1 and L_{s2}

$$\frac{1}{X_2} = \frac{1}{X_1} + \frac{1}{sL_s} \tag{6.30}$$

$$\frac{1}{X_2} = \frac{sC_{in}}{s^2L_{s1}C_{in} + sr_cC_{in} + 1} + \frac{1}{sL_{s2}} \tag{6.31}$$

$$\frac{1}{X_2} = \frac{s^2L_{s2}C_{in} + s^2L_{s1}C_{in} + sr_cC_{in} + 1}{(sL_{s2})(s^2L_{s1}C_{in} + sr_cC_{in} + 1)} \tag{6.32}$$

Since $L_{s1} = L_{s2}$, both are set to L_s from hereforth.

$$X_2 = \frac{s^3({L_s}^2C_{in}) + s^2r_cL_sC_{in} + sL_s}{2s^2L_sC_{in} + sr_cC_{in} + 1} \tag{6.33}$$

$$X_T = X_2 + sL_p \tag{6.34}$$

$$X_T = \frac{s^3(L_s{}^2C_{in}) + s^2r_cL_sC_{in} + sL_s}{2s^2L_sC_{in} + sr_cC_{in} + 1} + sL_p \tag{6.35}$$

$$X_T \tag{6.36}$$

$$= \frac{s^3(L_s{}^2C_{in}) + s^2r_cL_sC_{in} + sL_s + sL_P(2s^2L_sC_{in} + sr_cC_{in} + 1)}{2s^2L_sC_{in} + sr_cC_{in} + 1}$$

Fig.6.14 can thus be reduced to Fig.6.16 below

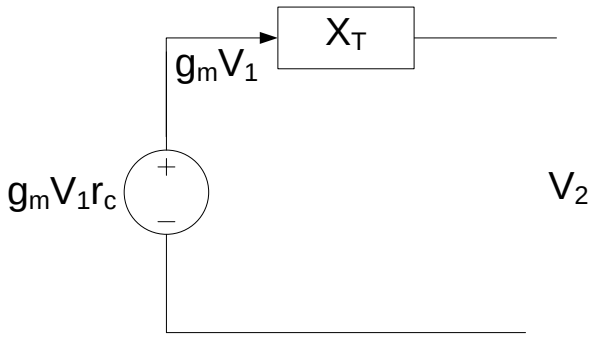

Fig. 6. 16 Equivalent coupled line NIC schematic with total impedance

$$V_2 = g_mV_1X_T \tag{6.37}$$

$$\frac{V_2}{V_1} = g_mX_T \tag{6.38}$$

$$\frac{V_2}{V_1}$$

$$= g_m\left(\frac{s^3(L_s{}^2C_{in}) + s^2r_cL_sC_{in} + sL_s + sL_P(2s^2L_sC_{in} + sr_cC_{in} + 1)}{2s^2L_sC_{in} + sr_cC_{in} + 1}\right) \quad (6.39)$$

The poles of the transfer function can be obtained by examining the roots of the denominator of equation 6.39. Because this is a quadratic equation and the coefficient of the second term, (s), being positive means that the poles of the transfer function would always be on the negative side of the complex s – plane. This therefore implies that the NIC would be unconditionally stable.

6.5. Realisation of Coupled Line NIC

The coupled line NIC was realised as a single layered structure, with a ground plane beneath. It has an overall size of 50mm × 20mm. The transistor, capacitor to invert, the bias network and the coupled line section are all on the top side of the board with a ground plane underneath. The complete structure is shown in Fig.6.17. The coupled line used for this design is grounded CPW which is 6mm long. The individual transmission lines that make up the coupled lines are 2mm wide. They are separated from each other and from the ground plane by 0.4mm. The substrate used is the Taconic TLY – 5 with thickness of 1.57mm, di-electric constant of 2.2 and loss tangent of 0.0009. The copper ground plane conductor has a thickness of 0.035mm.

The capacitor to invert is 0.1pF and this also doubles as a DC blocking capacitor and there is another 2pF DC blocking capacitor between the base terminal of the transistor and the other transmission line in the coupled line. The transistor used in the NXP BFS17 which has a

transition frequency of 1.5GHz biased at 5V and 20mA. Table 6.1 contains the details of all the elements used in realising this NIC.

Table 6. 1: Components used in the NIC

(Datasheets are given in Appendix)

Component	Manufacturer	Value
Transistor	AVAGO	BFS-17
Capacitor	AVX	0.1pF, 2pF
Inductor	Coilcraft	1.8nH, 22nH
Resistor	Panasonic	33Ω, 10Ω and 10KΩ
Substrate	Taconic	TLY-5

Fig. 6.17b shows the layout. As negative elements could contain negative resistance and hence would be inherently unstable and un-measurable, there is a need to add positive elements between the measurement ports and the terminals of the NIC. The NIC terminals are points A and B in Fig.6.17b. A finite length of the connecting transmission line (17.5mm), a 10Ω resistor in series and a 2pF capacitor in shunt between the measurement ports and points A and B means that the NIC performance must be de-embedded from the measured results of the structure.

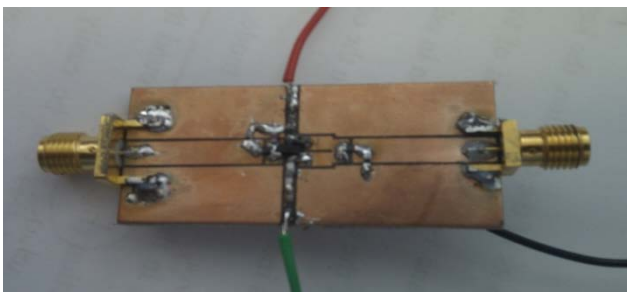

(a)

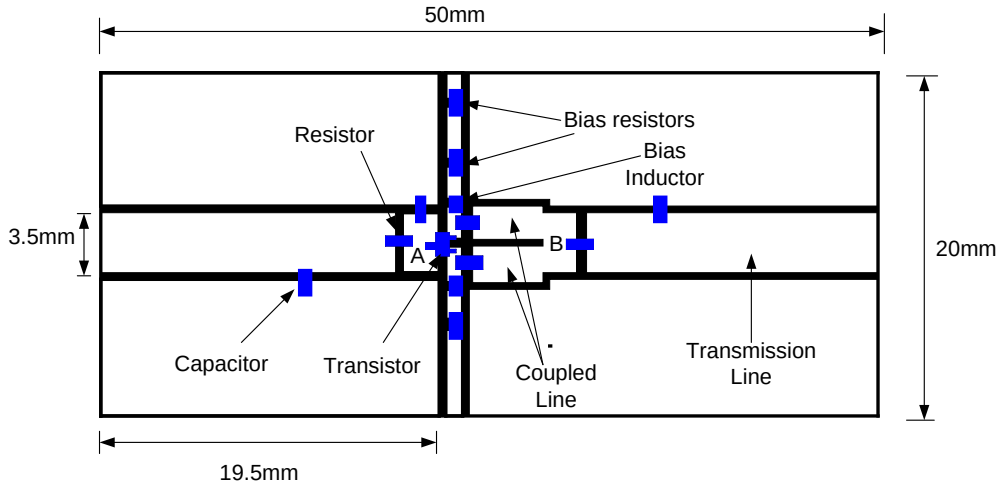

(b)

Fig. 6. 17 Coupled Line NIC prototype (a) Photograph (b) Layout schematics

6.6. Measured Results

The coupled line NIC structure described above in section 6.5 has been built and measured. Fig. 6.18 shows the S_{11} and S_{22} of the structure. It should be noticed that the S_{11} and S_{22} still exhibit the Foster element characteristics of clockwise rotation around the Smith chart. This is due to the other elements added between the NIC and the measurement ports. To obtain the performance of the NIC, its characteristics must be de-embedded from this result.

Fig. 6.19 shows the de-embedded results of the coupled line NIC. The non-Foster characteristics are clear to see by the anti-clockwise rotation of S_{11} and S_{22} around the Smith chart.

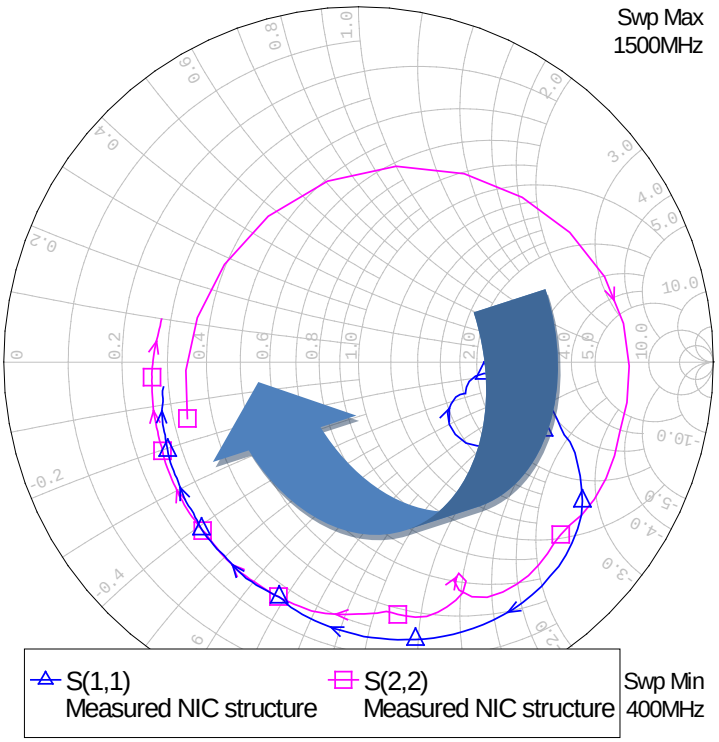

Fig. 6. 18. Measured result

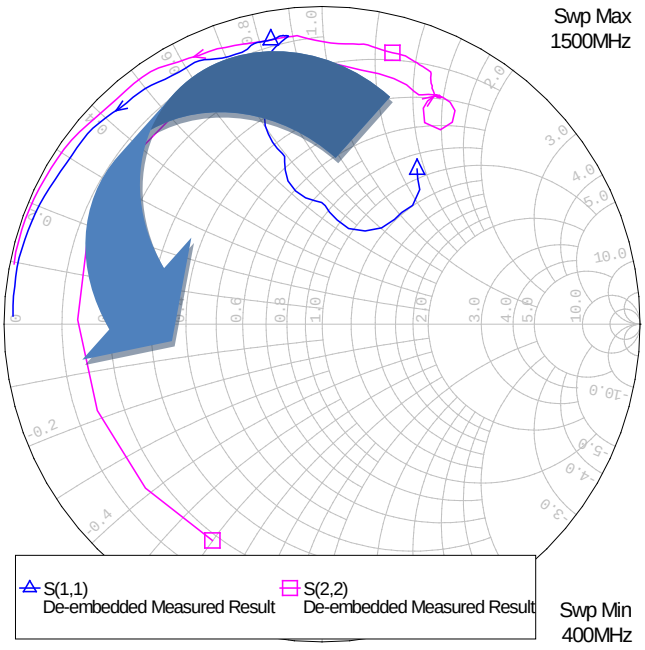

Fig. 6. 19. De-embedded Measured Result for Coupled Line NIC

In Fig. 6.19, the locus of S_{22} of the de-embedded result still shows some Foster element characteristics between 400MHz and 733MHz. This behaviour is better seen in Fig. 6.20 where the reactance seen through port 2 of the de-embedded NIC increases with increase in frequency. Beyond this point, the reactance seen from the two ports are non-Foster.

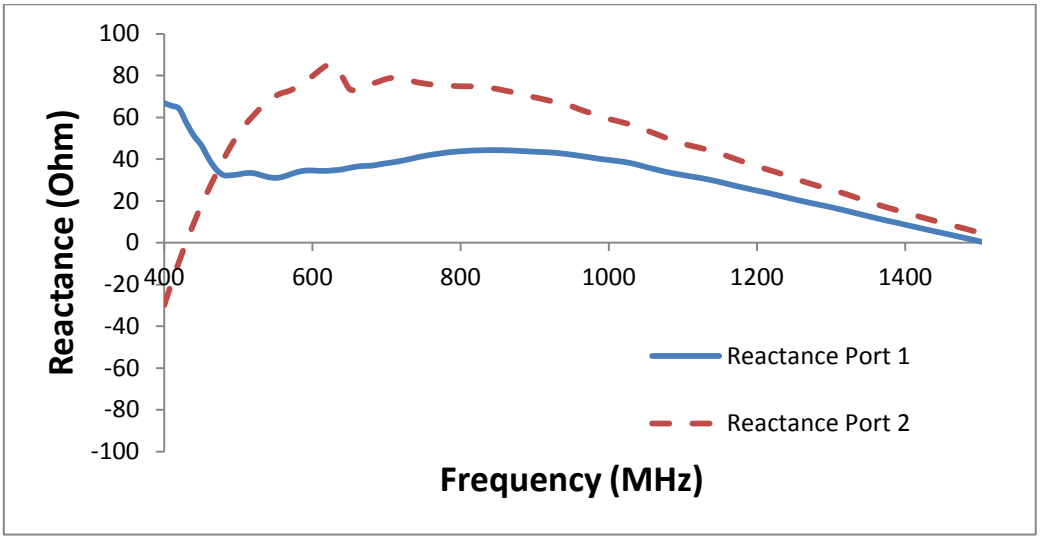

Fig. 6. 20. Measured reactance of coupled line NIC

The capacitance through port 1 of the coupled line NIC is shown in Fig. 6.21 and it can be seen to have negative capacitance from 0.4GHz to approximately 1.5GHz which is the frequency of interest. This result was computed from the de-embedded measured reactance of the coupled line NIC. It can also still be seen to exhibit the frequency dependence associated with non-Foster elements realised using NICs. A resonance is expected at 1.5GHz as indicated by the sharp drop in capacitance. This can also be observed in Fig. 6.20 where the net reactance is seen to approach zero. Also in Fig. 6.19, the locus on the Smith chart can also be observed to lie mainly in the negative capacitive region but it approaches the inductive region of the Smith chart with increasing frequency.

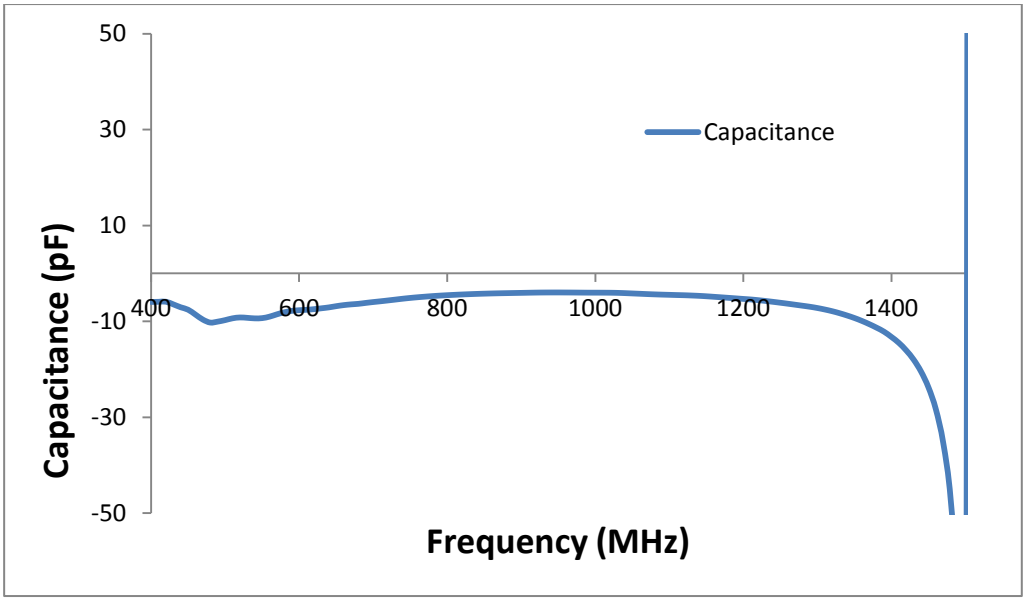

Fig. 6. 21. Measured capacitance of coupled line NIC

The gain through the coupled line NIC is shown in Fig. 6 .22. The gain is seen to be between -17dB and 6dB within the measured bandwidth. This is higher than what was obtained using the Linvill's NIC design. The resistance in the coupled line NIC is shown in Fig 6.23 and the Q of the negative capacitance is computed using equation 6.40 and shown in Fig. 6.24. The computed Q is higher than that of the Linvill NIC and this is due to the lower resistance in the coupled line NIC compared to the Linvill's NIC. This can be observed by comparing the real part of de-embedded NIC reactance in Fig. 5.7 to that in Fig.6.19.

$$Q = \frac{|X|}{R} \tag{6.40}$$

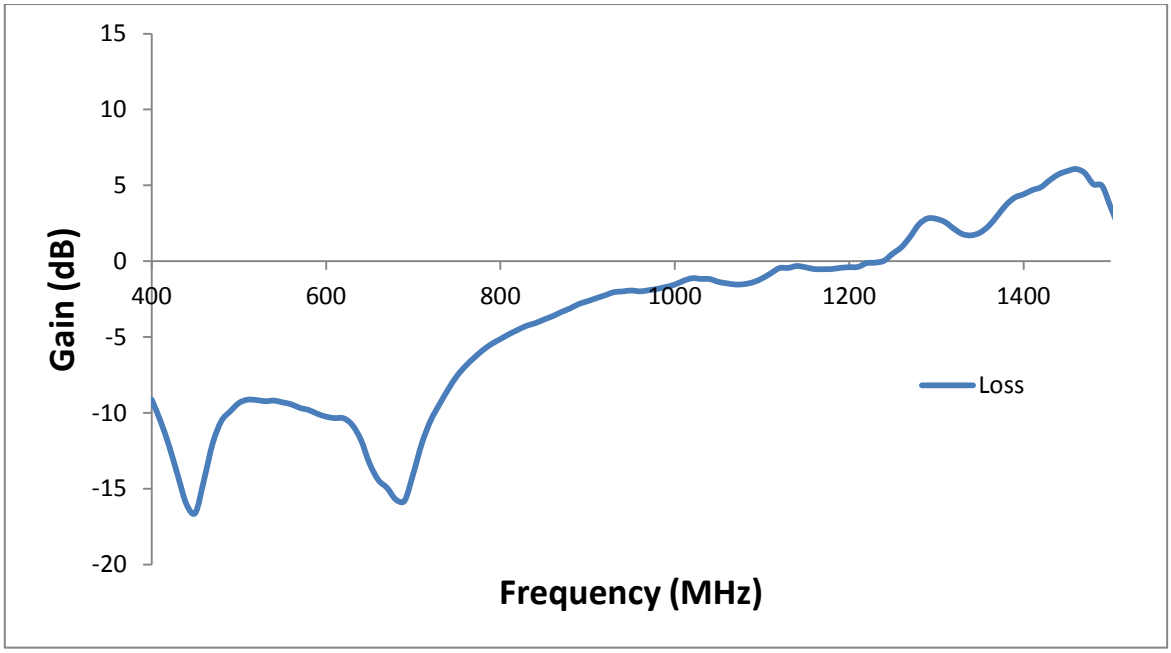

Fig. 6. 22. Gain in measured coupled line NIC

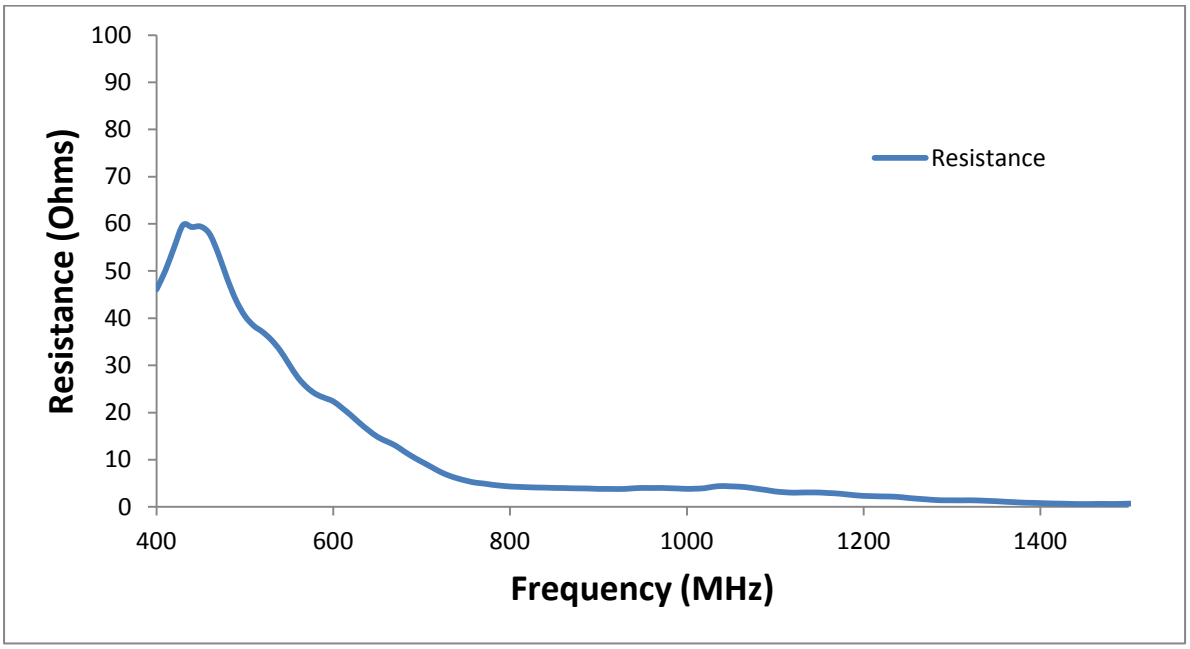

Fig. 6. 23. Resistance in coupled line NIC

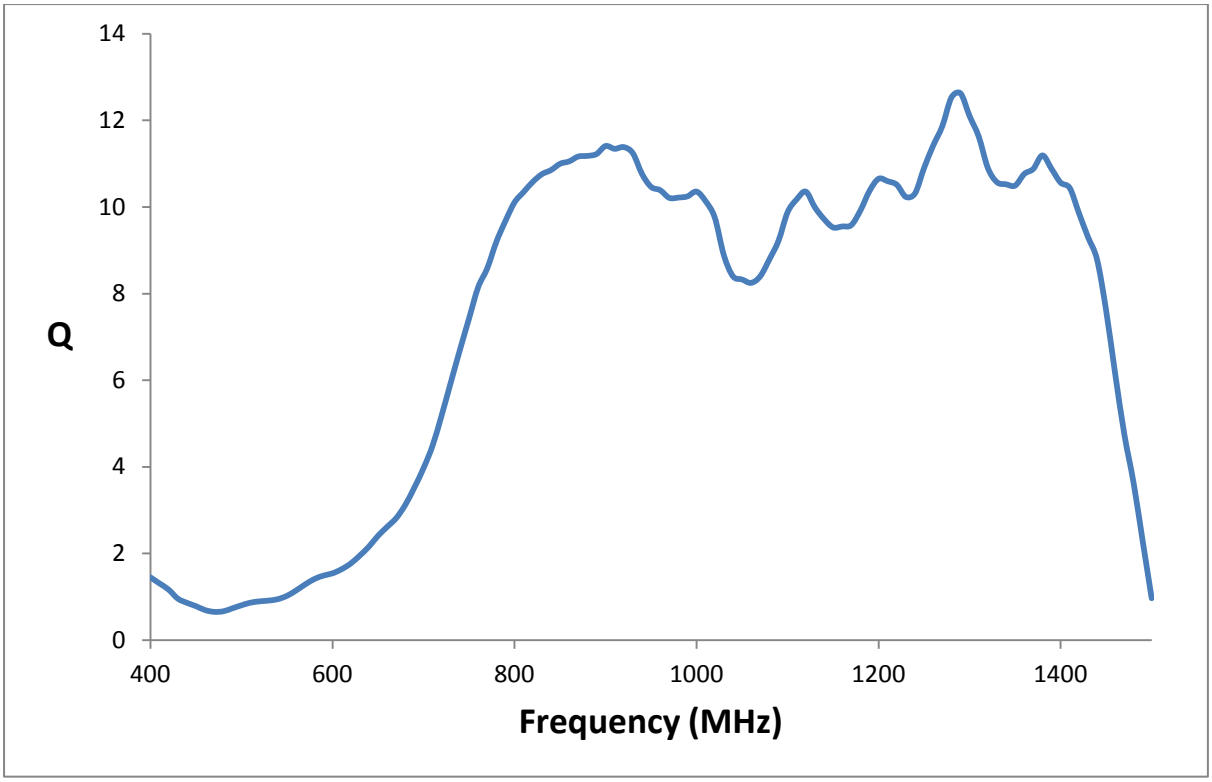

Fig. 6. 24. Q of the coupled line NIC

6.7. Linearity and Noise Measurements

6.7.1. Antenna

In order to measure the linearity and noise contribution of the coupled line NIC in matched antenna system, it was decided to design a simple equivalent circuit which could represent an antenna, a monopole, within the band within which the coupled line NIC was designed for. A 17.5mm long and 2mm wide grounded CPW transmission line in series with an 18pF capacitor has been used to transform the 50Ω port impedance into what is now seen and used as an equivalent antenna. This schematic is shown in Fig. 6.25. The S_{22} of the antenna equivalent circuit is shown in Fig. 6.26 and this represents the antenna return loss.

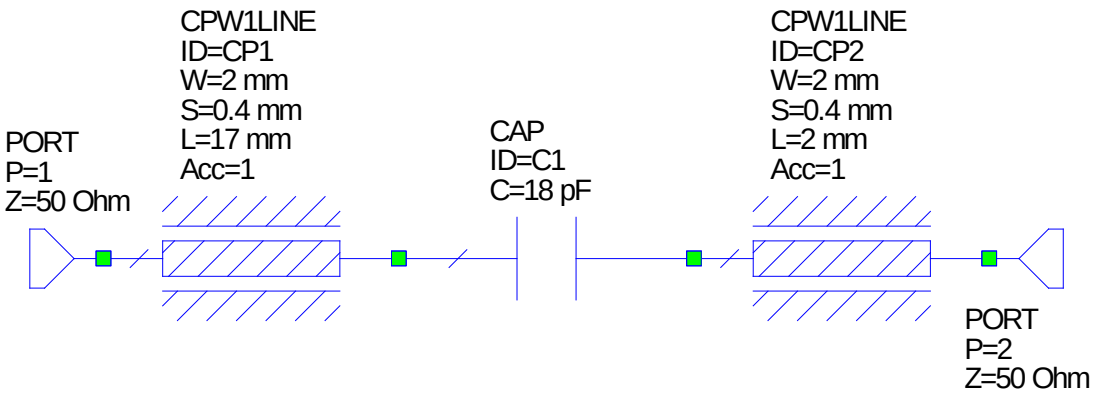

Fig. 6. 25. Schematic of antenna equivalent.

A two port circuit is used to represent the antenna because of the need to

1. Have a port via which two tones can be injected into the coupled line NIC system for linearity measurements and
2. Attach a 50Ω based noise tube for noise measurement.

The equivalent antenna circuit described above is then matched with the coupled line NIC. The NIC matched antenna is shown in Fig. 6.27. The overall structure is one PCB layer of size 26mm x 40mm. The coupled line NIC has a length of 6mm, width of 2mm and the gap between the conductors that form the coupled line is 0.4mm. A 2mm grounded CPW transmission line connects the NIC matched equivalent antenna to the SMA measurement port. The capacitor that is inverted is 7.5pF and there is a 2pF DC bias capacitor between the base of the transistor and the coupled transmission line. The complete equivalent structure is shown in Fig 6.27.

The measured S_{22} of the NIC matched antenna equivalent is shown in Fig. 6.26 and this is representative of a matched antenna reflection coefficient. It can be seen that the reactance of

the antenna equivalent has been completely cancelled within the frequency band of interest. This equivalent matched antenna is then use to characterise the coupled line NIC for noise and linearity.

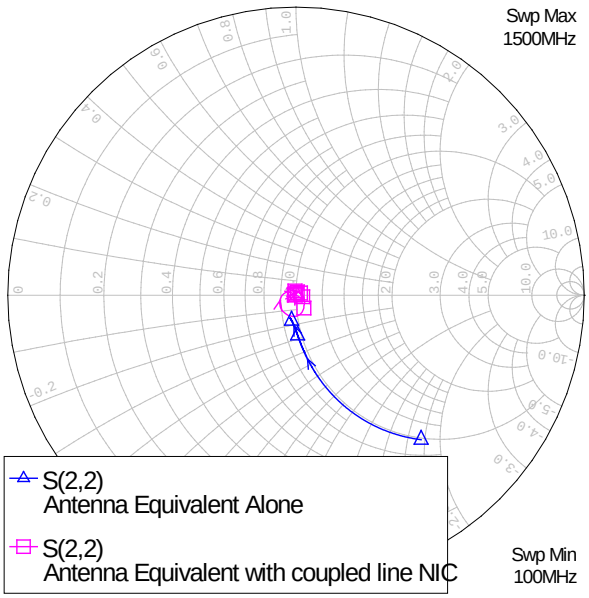

Fig. 6. 26. Measured antenna equivalent and antenna equivalent matched with coupled line NIC

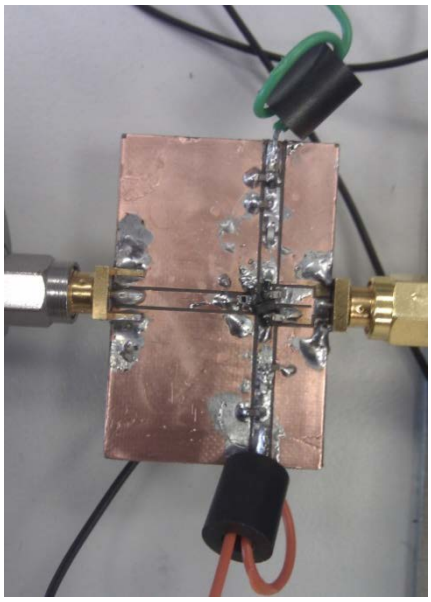

Fig. 6. 27. Antenna equivalent matched with coupled line NIC (a) Photograph and (b) Layout schematic

6.7.2. Linearity Measurement

To characterise the NIC's linearity, a two tone measurements was undertaken on the coupled line NIC matched antenna which is referred to as the device under test (DUT) from here forth. The setup is similar to the one described in chapter 5, with frequency separation between the two tones being 1MHz.

Fig. 6.28 shows the results for the fundamental tones, the received tone and the third order product of the NIC at 1GHz. The input power is varied from -25dBm to 15dBm. It can be seen that the NIC experiences a 1dB compression at 7dBm and this gives an indication of what the input power of the two tones should be in order to compute the IP3. When the power of the fundamental tones are below 0 dBm, the third order products are found to be within the noise floor of the VNA and hence any measurement of the third order products made at this point would be misleading. Between 0dBm and 5dBm it can be seen that the slope of the measured power of the intermodulation product is 3 times the gradient of the received power of the fundamental tones. This region is ideal for setting the input power of the fundamental tones for IMD measurements. Above 5dBm, it can be seen that NIC has gone into compression, because of the change in gradient of both the received power of the fundamental frequency and the IMD products. Hence measurements made above this input power level could be misleading.

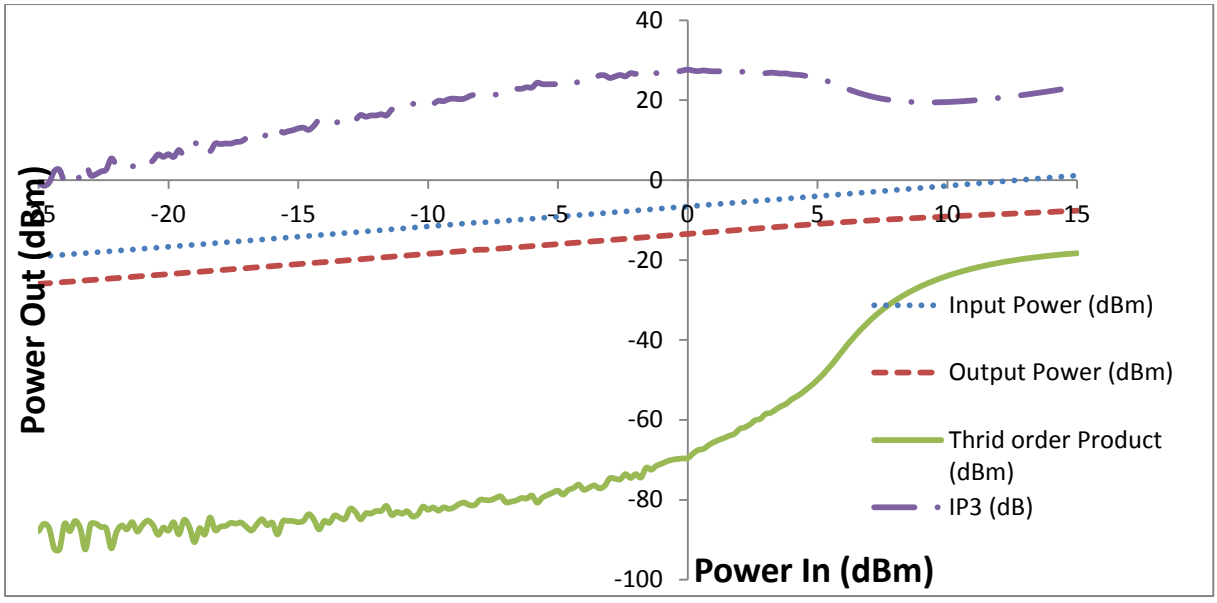

Fig. 6. 28. Power sweep for IMD measurement with antenna equivalent matched with coupled line NIC

The power output spectrum from the DUT is shown in Fig. 6.29, where the third order products as well as higher order products are clearly visible. Using the data from the levels of the third order products as well as the fundamental frequency, the IP3 can be calculated and the result is shown in Fig. 6.30. With an average level of 25dBm, the IP3 of the DUT is higher than what was obtained with the two transistor equivalent. A comparison of the output spectrum between the two NIC realisations methods (Linvill's and coupled line NIC) would reveal that the third and higher order products of intermodulation are lower with the coupled line NIC. This places lesser burden on the linearization methods that might be employed if higher linearity were required.

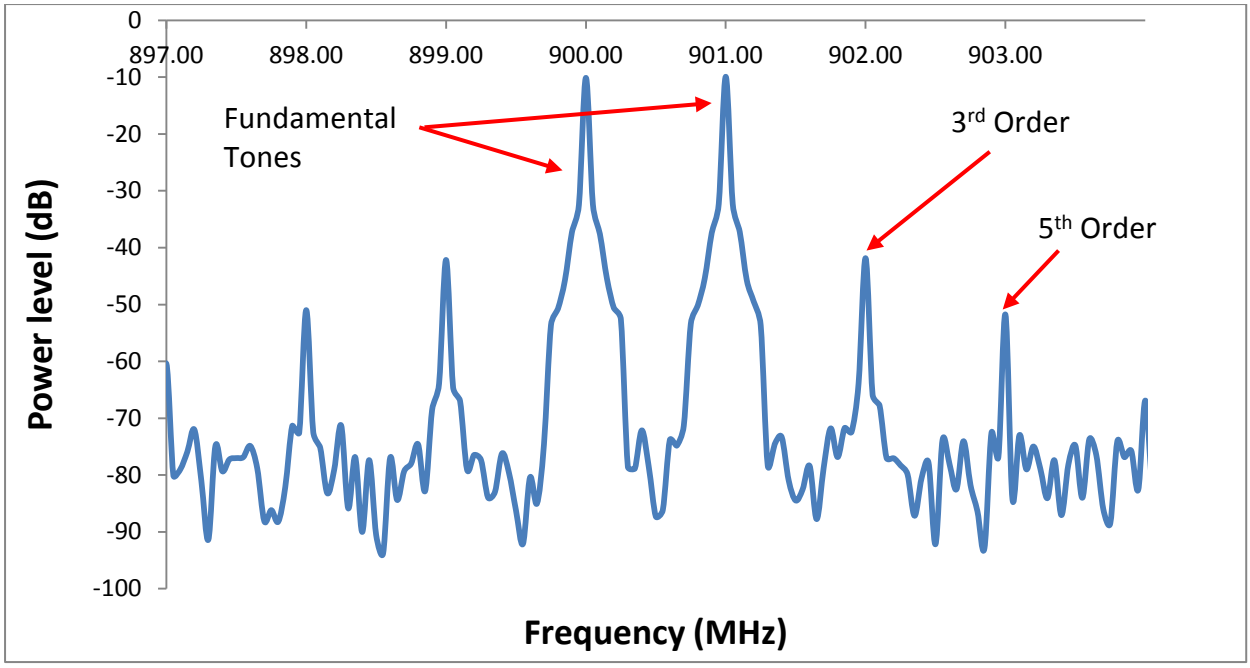

Fig. 6. 29. Output spectrum from two tone test on equivalent antenna matched with coupled line NIC

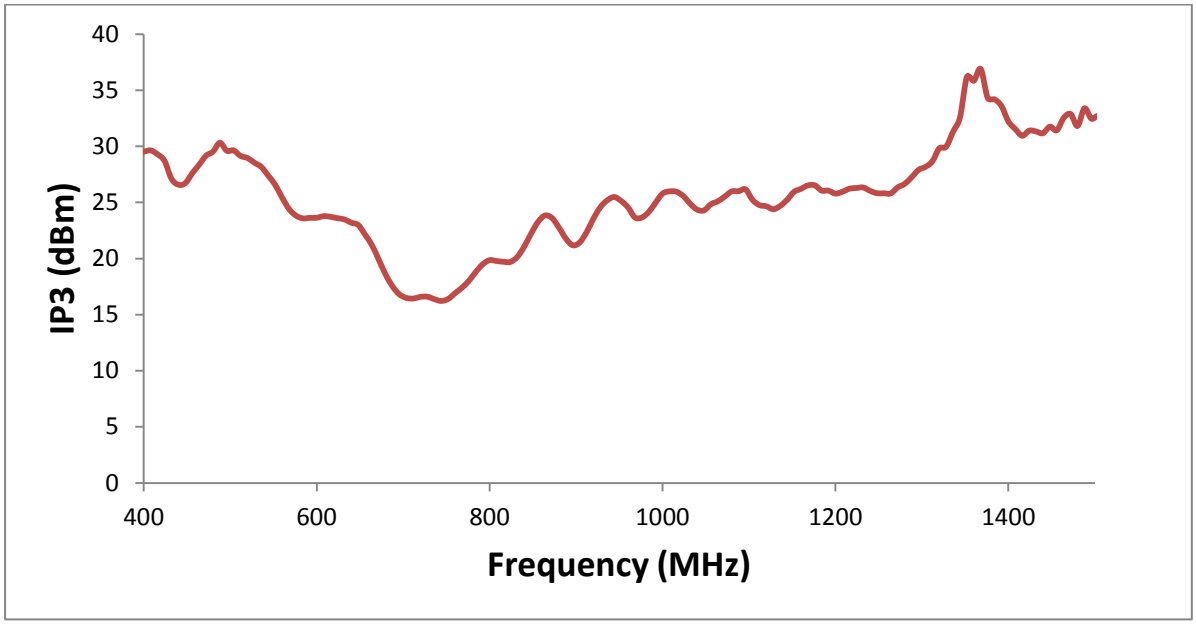

Fig. 6. 30. Measured IP3 of antenna equivalent matched with coupled line NIC.

6.7.3. Noise Measurement

To characterise the impact of a coupled line NIC matched antenna on the overall noise sensitivity of a receiver, a SNR advantage has been calculated for the coupled line NIC matched antenna against a lossy matched antenna.

The Y-factor measurement technique described in the previous chapter has been used to calculate the noise figure of the DUT and this has then been used to compute the SNR advantage by using equation 6.41 below.

$$SNR_{adv} = (S_{NIC} - S_{lossy}) - (NF_{NIC} - NF_{lossy}) \qquad 6.41$$

where S_{NIC} is the gain with NIC matching and S_{lossy} is the gain with purely resistive matching

It can be seen that the there is an SNR advantage of 10dB or more between 850MHz and 1.2GHz. It should be noticed that there is a dip below the 10dB advantage between 940MHz – 960MHz which coincides with the GSM900 bandwidth. There was an appreciable increase in the noise floor of the spectrum analyser within this frequency band and hence the measured noise level within the DUT is higher within this frequency range compared to what is measured across the rest of the bandwidth. The primary source of noise or interference is thought to be from the GSM 900 band.

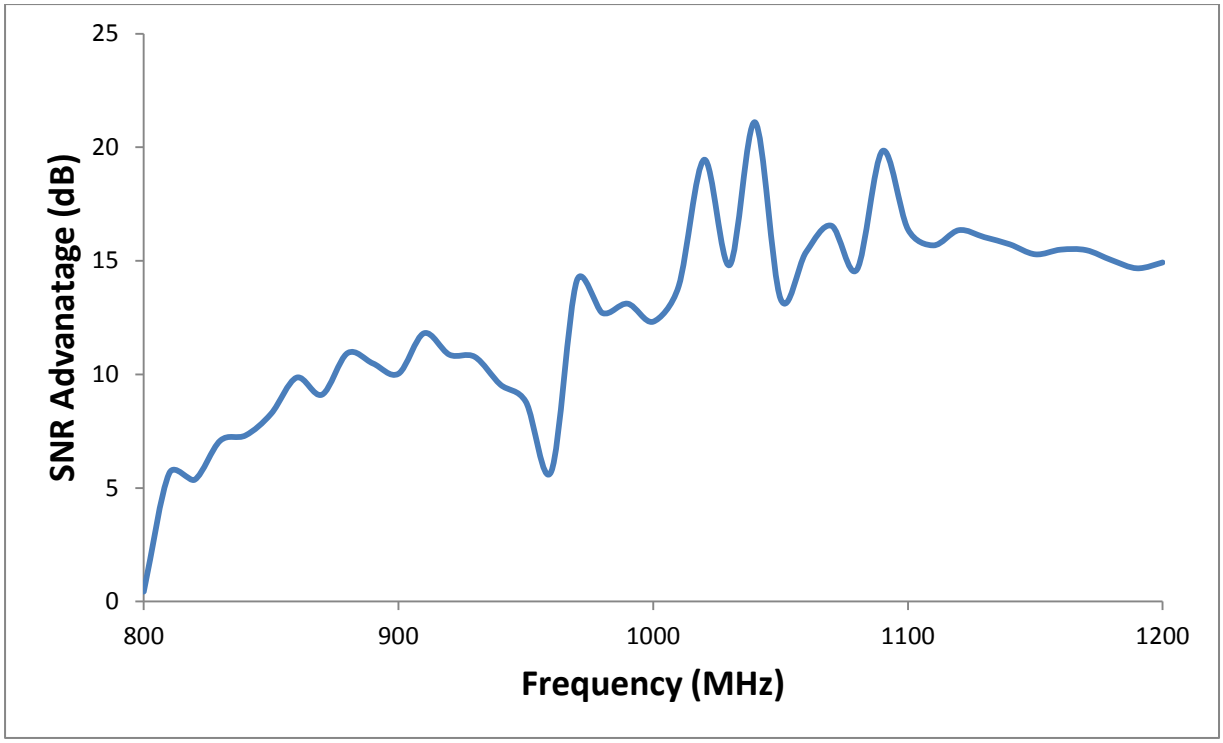

Fig. 6. 31. SNR advantage of antenna matched with coupled line NIC.

A comparison between the two tone tests of the coupled line NIC and the Linvill's NIC (chapter 5, prototype 2) is shown in Fig 6.32 and the SNR adv comparison of the two NIC prototypes are also shown in Fig 6.33. From this comparison it is clear that the coupled line NIC has a better linearity because the 3rd order inter-modulation products can be seen to be about 20dB lower than those of the Linvill's NIC. There is also an appreciable reduction in the noise floor of the coupled line NIC. Fig. 6.33 shows the comparison of the SNR advantage between the two NIC structures. It can be seen that the coupled line NIC starts to have a better SNR advantage from 900MHz and this advantage rises to 10dB at 1GHz. There is a dip at 960MHz which can be attributed to interference from the GSM 900 transmitters.

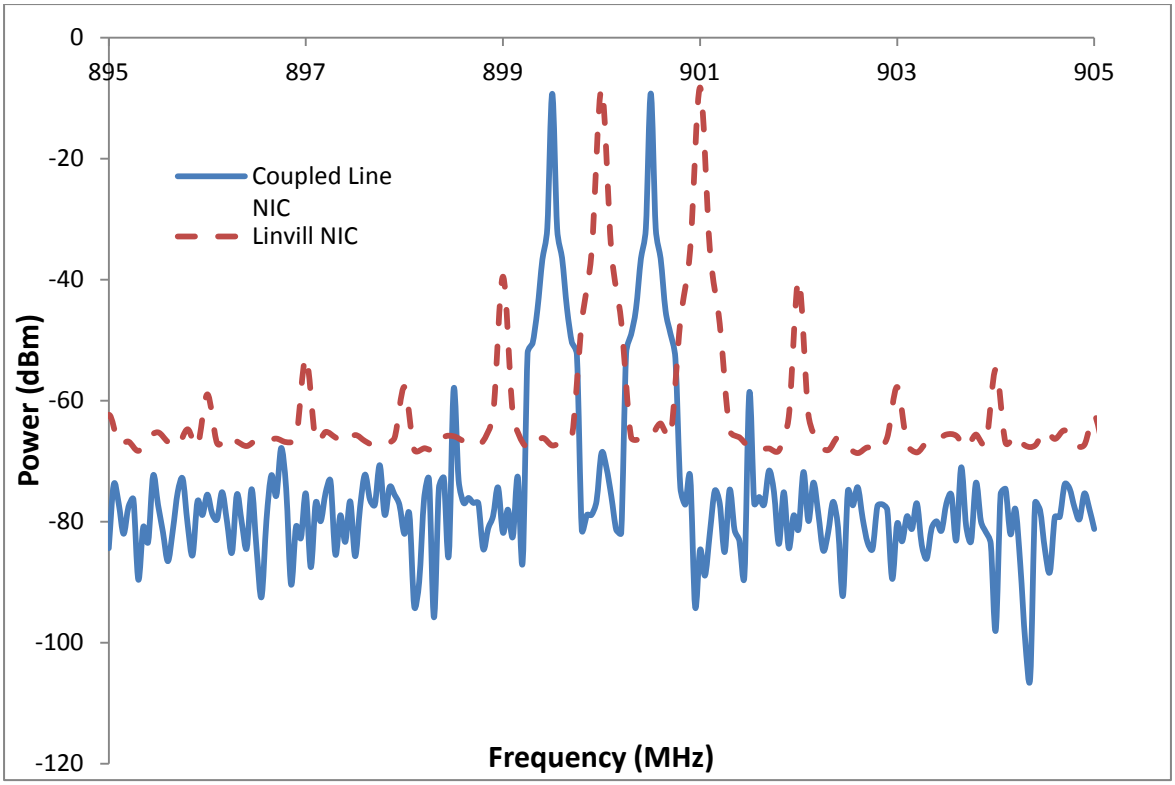

Fig.6.32 Two tone output spectrum comparison between coupled line NIC and Linvill's NIC

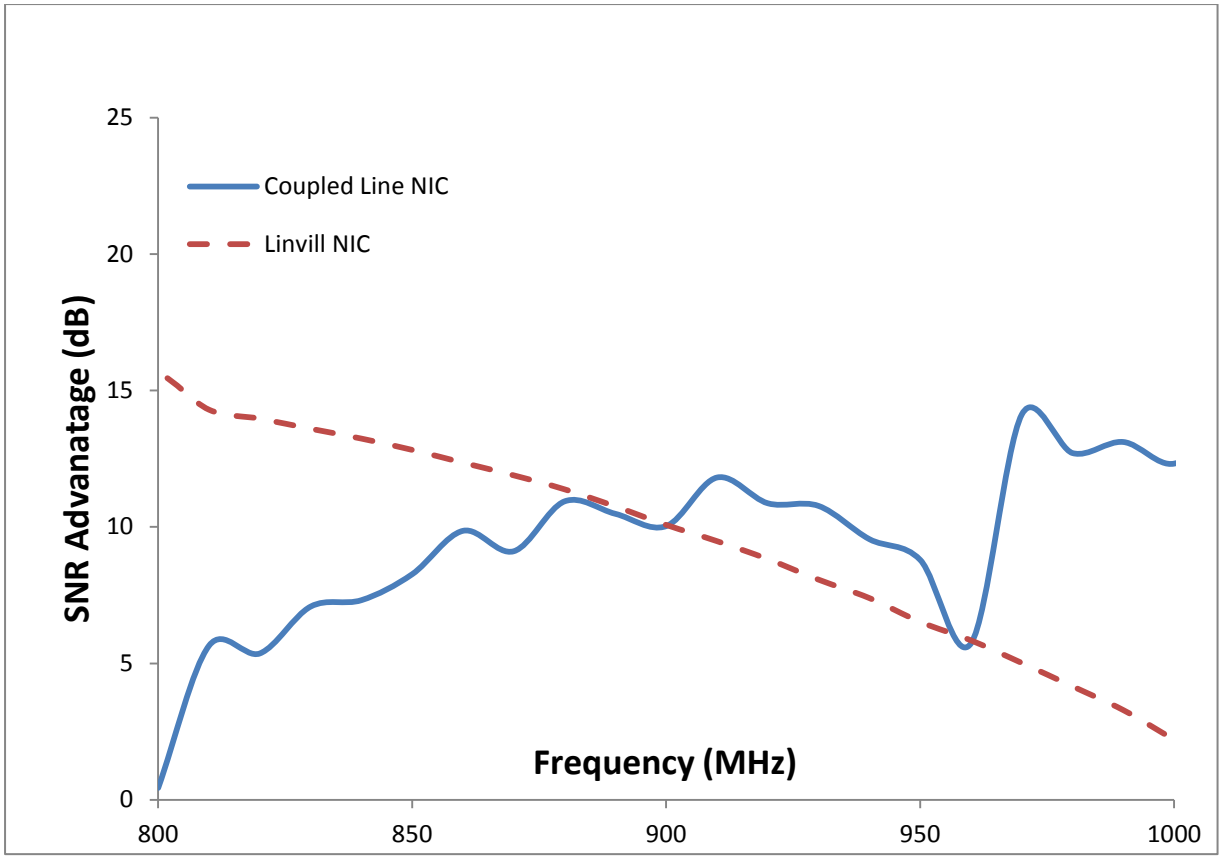

Fig.6.33 SNR advantage comparison between coupled line NIC and Linvill's NIC

6.8. Conclusion

In this chapter, an alternative means of realising non-Foster elements has been discussed. Its noise and linearity performance have been shown. Because it is achievable as a single layer PCB, it is therefore easier to fabricate. The use of a single transistor also helps with the stability problems typically associated with the Linvill's model. It is also less complicated and has a lower count on the number of elements required. Because there are no stability concerns as shown by the stability analysis, it is possible to demonstrate the NIC at even higher frequencies when compared with what is obtainable with the Linvill's model. It does however still have considerable loss through the NIC especially at the lower frequencies as can be seen with Q factor, although this is better than what is obtainable within this frequency

range with the Linvill's model. A comparison between the noise contributions of the two different topologies shows the expected results as the coupled line NIC with a single transistor has a better SNR advantage over the Linvill's NIC. Similar performances are also experienced during the linearity measurements.

References

[1] S. E. Sussman-Fort and R. M. Rudish, "Non-Foster Impedance Matching of Electrically-Small Antennas," Antennas and Propagation, IEEE Transactions on, vol. 57, pp. 2230-2241, 2009.

[2] D. M. Pozar, Microwave Engineering, 3Rd Ed: Wiley India Pvt. Limited, 2009.

[3] A. S. Sedra and K. C. Smith, Microelectronic Circuits Revised Edition: Oxford University Press, Inc., 2007.

CHAPTER 7

COUPLED LINE NIC MATCHED ANTENNA

7.1. Background

In this chapter, the coupled line NIC is integrated with a planar monopole antenna. The non-Foster element obtainable from the NIC makes it possible to obtain a wideband matching of the monopole at frequencies lower than the resonant frequency. The reduced complexity involved with the coupled line NIC makes it a good option for this integration. Having a single active device reduces the bias networks disruptions to the ground plane. Realisation on a single layer also makes it easier to integrate with the planar monopole. The stability analysis on the coupled line NIC in the previous chapter showed that the NIC would be unconditionally stable; hence there is less worry about instabilities and oscillations with the overall matched antenna.

Using the NIC to provide wideband matching to an antenna at lower frequency opens the antenna to different scenarios, such as its use in cognitive radio (CR), as a spectrum sensing antenna, and its use in transceivers operating within different frequency bands. Also because the antenna is now small at the frequency of operation, it is possible to have small antennas with wide bandwidths.

Simulations in this chapter are done in both AWR design environment and CST microwave studio. S – parameter files of transistors and surface mount elements are transferred from Microwave Office by AWR into CST microwave studio.

7.2. The antenna

The fabricated antenna which is a planar monopole and its printed schematic are shown in Fig.7.1. It is printed on a Taconic TLY – 5 substrate 40mm × 58mm with dielectric constant of 2.2, loss tangent of 0.0009 and thickness of 1.57mm. The copper on the substrate has a thickness of 0.035mm. The antenna ground plane is 40mm × 20.5mm. The printed monopole itself is 2mm × 18mm and it is fed via a 50Ω coplanar waveguide (CPW) line. It is resonant at 3.5GHz. The layout schematic and dimensions of the antenna are shown in Fig. 7.1b. This antenna has been fabricated and its measured return loss without matching is shown in Fig.7.2. There is a small dip in the return loss at 1.35GHz; this can be attributed to the ground plane of the antenna being excited.

(a)

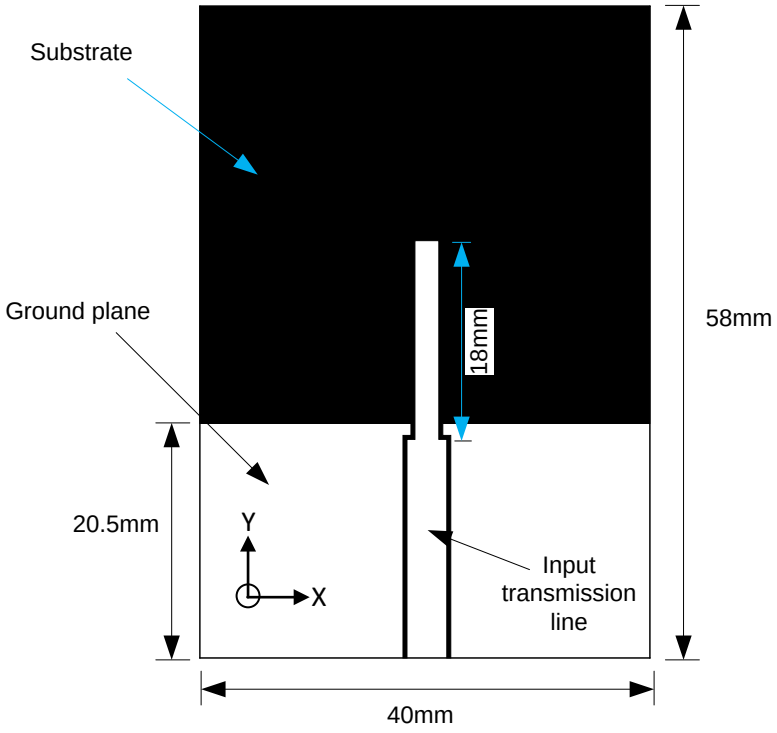

(b)

Fig. 7. 2. (a). Fabricated printed monopole and (b). The printed monopole schematic.

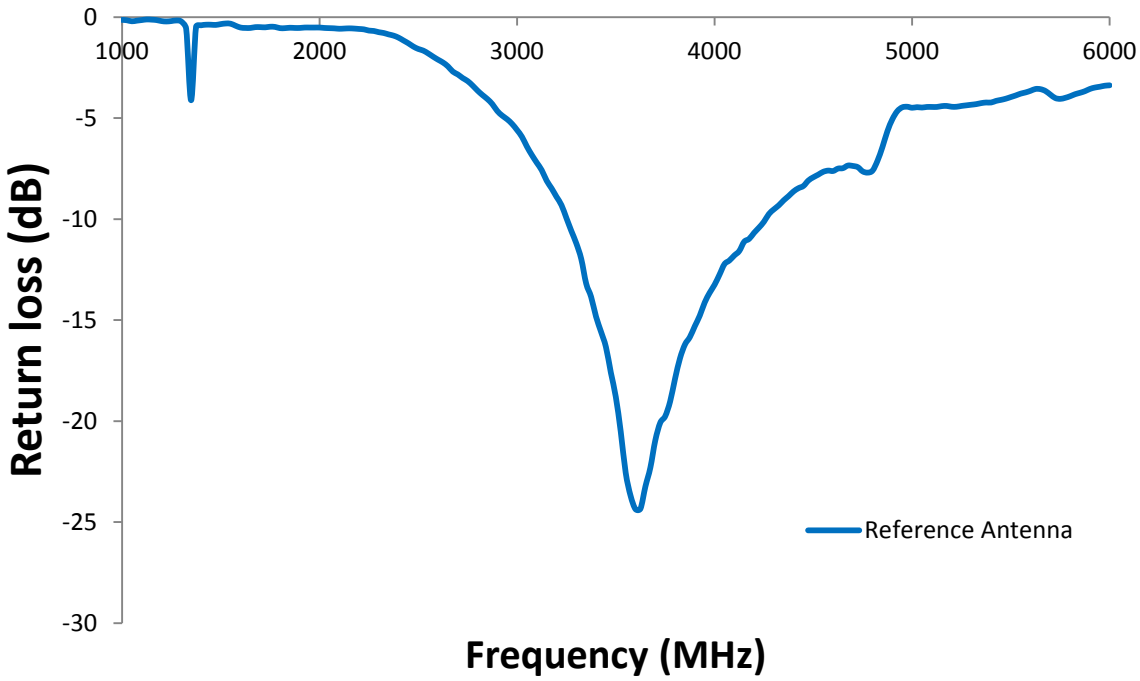

Fig. 7. 3. Measured Antenna return loss.

7.3. The 6 GHz Negative Impedance Converter

As the antenna is designed to resonate beyond the cut-off frequency of the coupled line NIC shown in chapter 6, therefore a new set of measurements were carried out with a different transistor whose transition frequency is above the frequency of interest of 4GHz. For this, an NXP transistor BFR93a with F_T of 6GHz was chosen (datasheet in appendix A). Using the same design and measurement techniques used in chapter 6, the de-embedded S_{11} and S_{22} are shown in Fig.7.3. The transistors are biased at 5V and 10mA. The de-embedded measured result can be seen to exhibit the expected non-Foster characteristics by the anti-clockwise rotation around the Smith chart up to 6GHz which is the cut off frequency of the transistor.

Fig.7.4 also shows the negative capacitance and inductance obtainable from the 6GHz NIC. It can be seen that there is a net negative capacitance between 1GHz – 1.7GHz and between 3.5GHz – 6GHz. In between these frequency regions, the NIC has a net negative inductance. This can also be seen in Fig.7.3, where the locus of S_{11} and S_{22} on the Smith chart goes between the negative capacitive region into the negative inductive region and back into the negative capacitive region. This explains why in Fig.7.4, there is a transition from negative capacitance to negative inductance and back to negative capacitance.

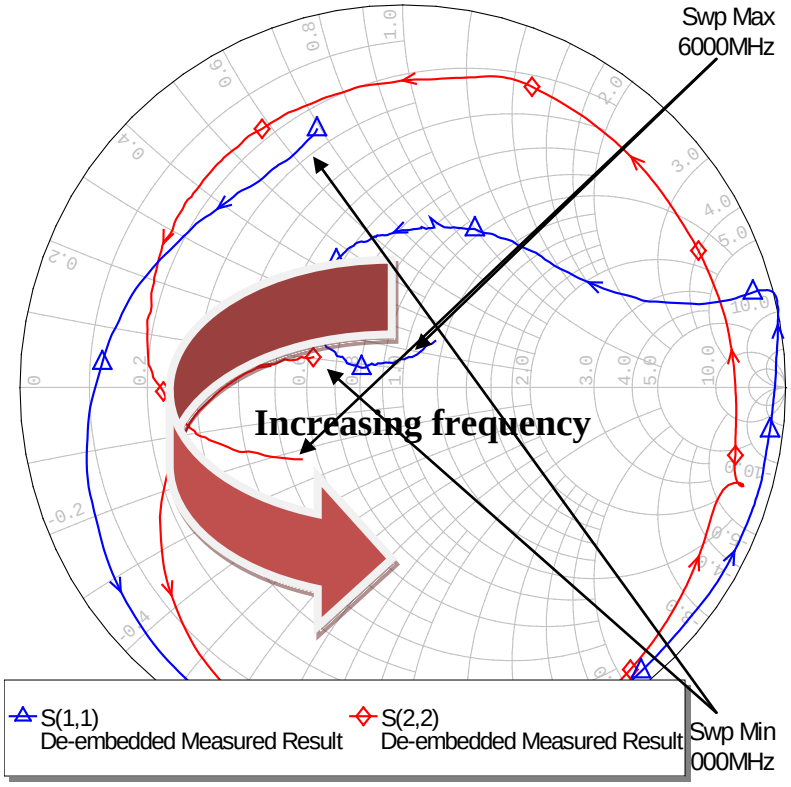

Fig. 7. 4 . The de-embedded measured S_{11} and S_{22} of the 6GHz Coupled line NIC

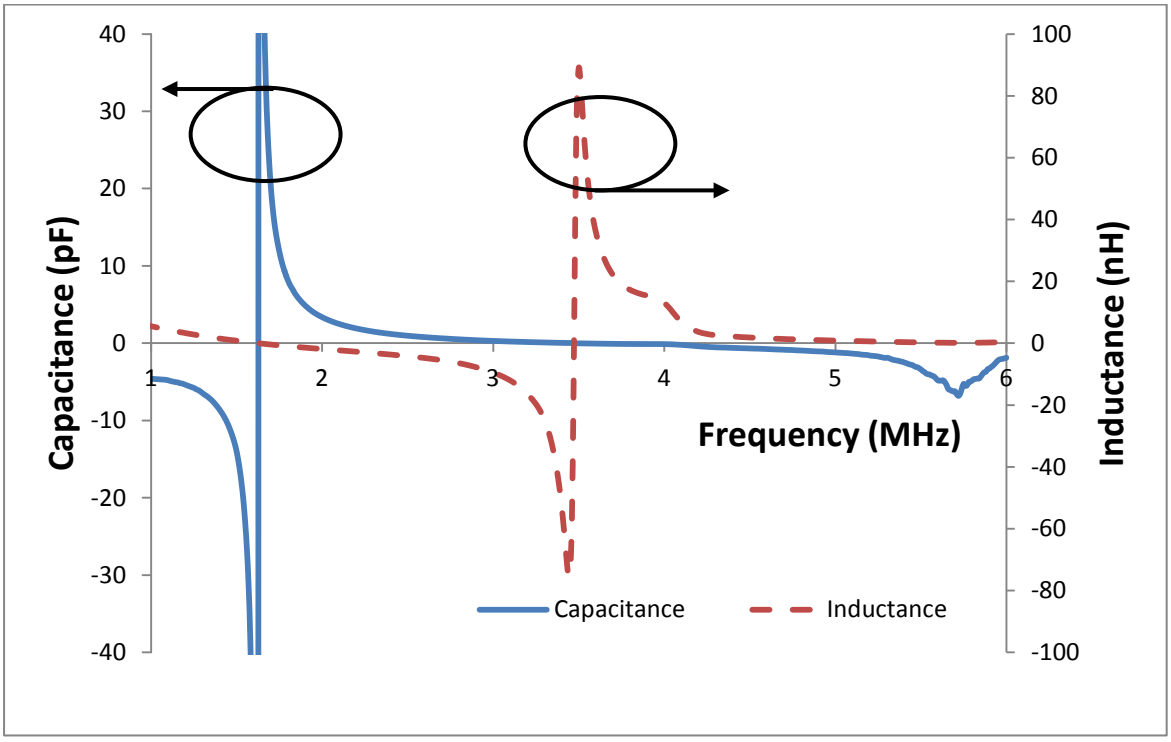

Fig. 7. 5. Measured capacitance and Inductance of the 6GHz coupled line NIC

7.4. Antenna matching

To demonstrate the NIC broadband matching capacity, the planar monopole described above was matched with a coupled line NIC in series with the antenna as shown in Fig.7.5. For comparison with conventional matching techniques, the reference antenna is also matched using a passive matching network consisting of an inductor and a capacitor (Fig. 7.6).

7.4.1. Negative Impedance Converter Matching Network

The NIC matched antenna is shown in Fig. 7.5a. The coupled line NIC is designed as previously shown in chapter 6. The coupled line is 6mm long, the individual conductors are 2mm wide and the gap between the conductors and between the conductor and ground plane is 0.4mm. The NXP BFR93a transistor is used with a F_T of 6GHz and it is biased at 5V and 10mA. The capacitor to invert is 0.1pF and there is 7.5pF DC blocking capacitor between the base terminal of the transistor and the coupled line. There is a 50Ω CPW transmission line between the ends of the coupled line and the measurement port. The schematic of the coupled line matched antenna is shown in Fig. 7.5b which includes the antenna and coupled line NIC dimensions.

The emitter of the transistor is connected to the base of the monopole. The simulated return loss is shown in Fig.7.7. The overall NIC matched antenna has a configuration of the antenna connected in series with the non-Foster element realised using the coupled line NIC.

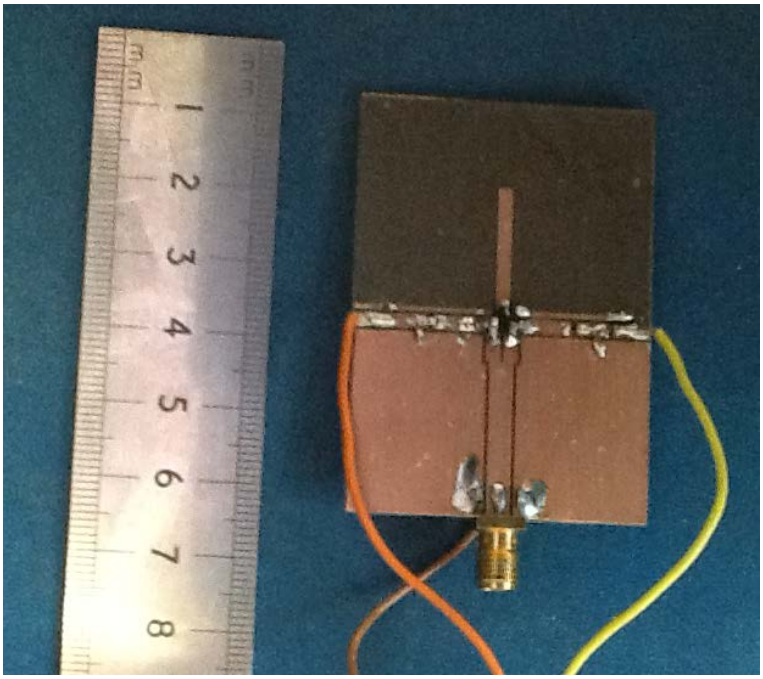

(a)

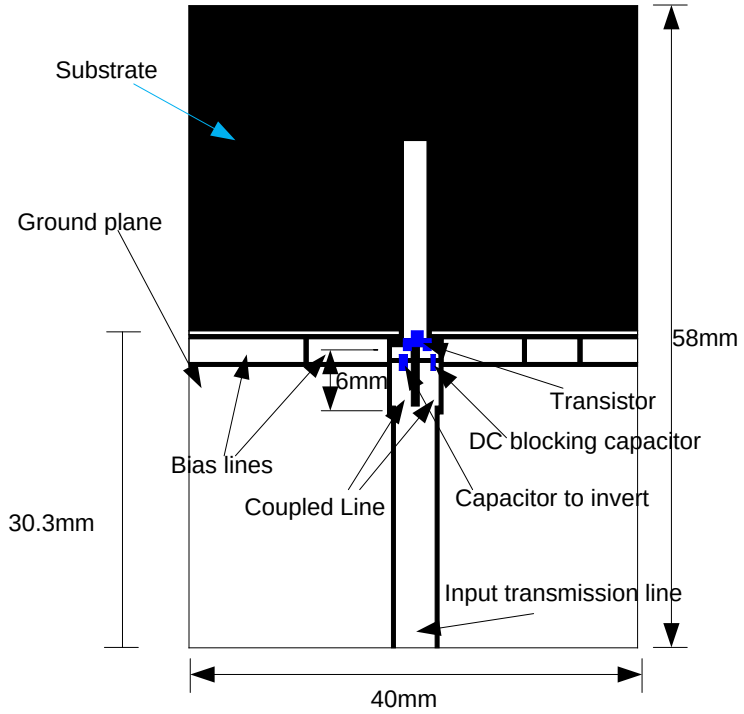

(b)

Fig. 7. 6. (a) The fabricated NIC matched antenna and (b) The layout schematic of the NIC matched antenna

7.4.2. Passive matching

In order have a comparison between the performance of the NIC matched antenna and alternative means of antenna matching, the reference antenna has been matched passively with a matching network comprised of surface mount inductors and capacitors. The matching network schematic and the passively matched antenna are shown in Fig.7.6 below. The matching network is made up of a series 2.2nH inductor and a shunt 10pF capacitor. The simulated return loss of the reference antenna passively matched is shown in Fig.7.7.

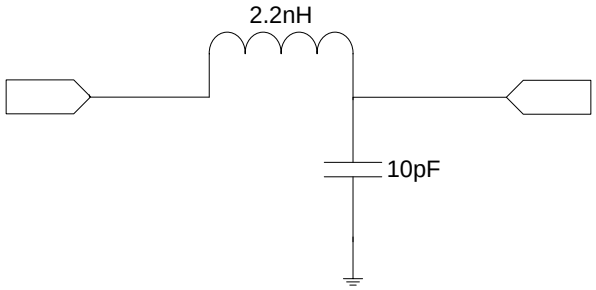

(a)

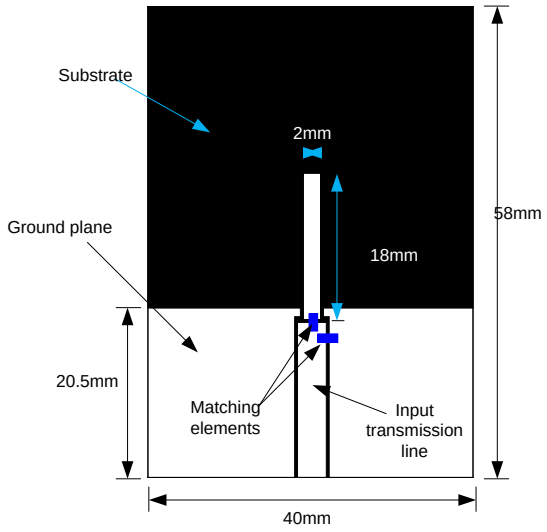

(b)

Fig. 7. 7. (a) The passive matching network and (b) The layout of the passively matched antenna.

7.5. Results

7.5.1. Simulated result

Fig. 7.7 shows the simulated return loss of the reference antenna (Fig.7.1), the NIC matched antenna (Fig.7.5) and the passively matched antenna (Fig.7.6). The reference antenna is resonant at 3.6GHz. It has a -10dB or better return loss bandwidth of 0.7GHz between 3.3GHz and 4GHz. With the NIC matching network, the antenna has a -10dB return loss or better bandwidth of 0.6GHz between 2.4GHz and 3GHz. With passive matching however, it is possible to match the reference antenna at 2.3GHz with a -10dB bandwidth of 0.2GHz between 2.2GHz and 2.4GHz. The NIC matching network has been able to match the antenna at a lower frequency when the antenna can be consider electrically small without significant loss in -10dB match bandwidth unlike the passive matching network which can only achieve very small matched bandwidth.

As antenna return loss alone is not enough to characterise an antenna, Table 7.1 shows the simulated realised gain and antenna efficiency. The dark coloured cells show gain and efficiency of each antenna at its resonant frequency. From Table 7.1, it can be seen that the NIC is able to provide broadband matching to the antenna and still maintain a good antenna gain and efficiency. The NIC matched antenna has a gain-bandwidth product of 3.13dBi compared to that of the passively matched antenna which is 1.18dBi. The gain and efficiency of the NIC matched antenna is only bettered by the reference antenna within the bandwidths where it is matched. The passively matched antenna does improve the antenna's gain and efficiency within the band within which it is matched but as this is only narrowband, the gain and efficiency improvements also occur within the narrow bandwidths

From these results, it is clear that the NIC matching network does provide broadband matching of antennas without significant adverse effects on the antenna gain and efficiency.

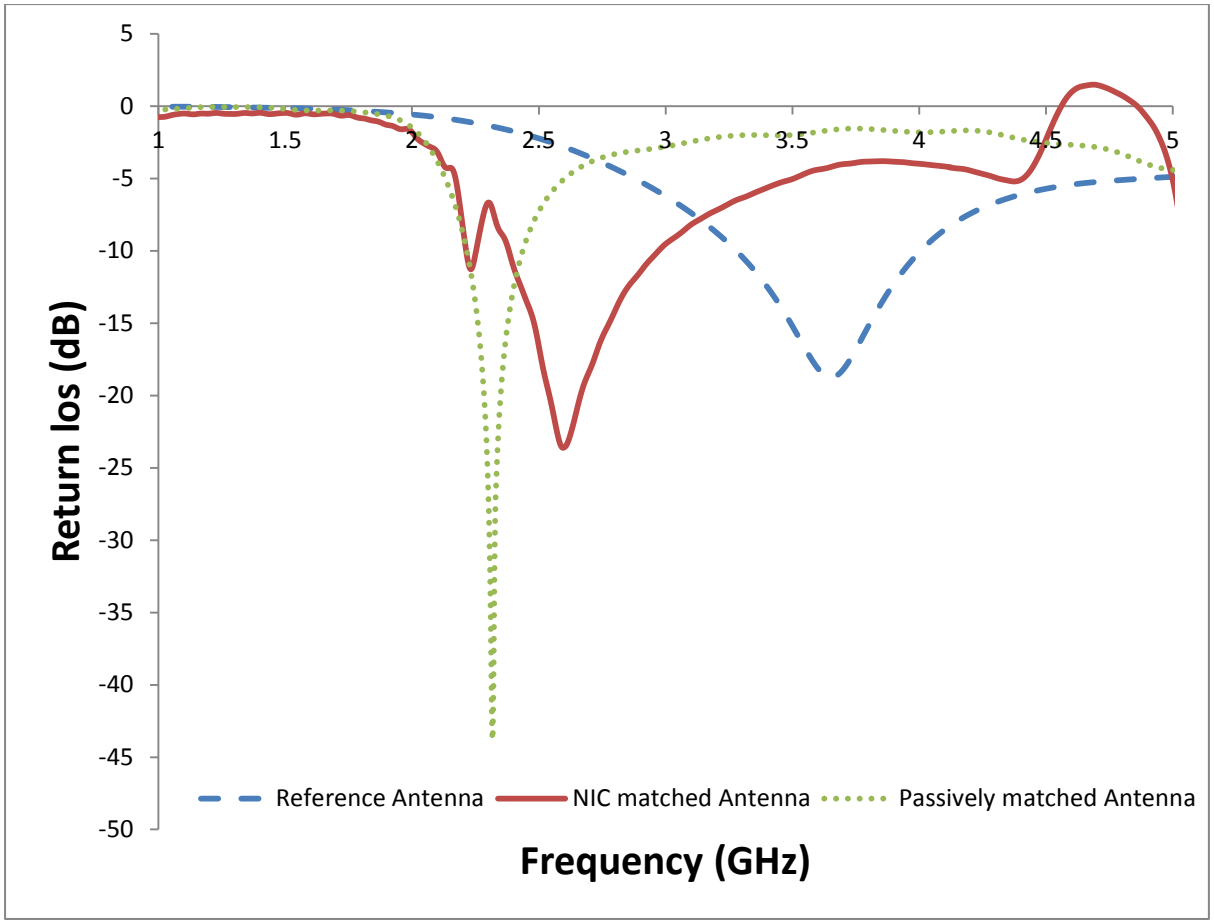

Fig. 7. 8. Simulated Antenna return loss.

Table 7. 1. Simulated antenna gain and efficiency.

Frequency (MHz)	Reference Antenna		NIC matched Antenna		Passively matched Antenna	
	Gain (dBi)	Efficiency (dB)	Gain (dBi)	Efficiency (dB)	Gain (dBi)	Efficiency (dB)
1800	-9.89	-11.93	-5.35	-7.49	-10.09	-12.12
2000	-7.19	-9.30	-0.93	-3.50	-3.64	-5.69
2300	-3.57	-5.91	1.77	-0.98	1.99	-0.2329
2400	-2.49	-4.93	3.28	-0.23	2.00	-0.33
2600	-0.65	-3.29	3.71	-0.16	0.83	-1.72
2800	0.83	-2.07	3.54	-0.05	-0.05	-2.76
3000	1.91	-1.23	3.62	0.00	-0.46	-3.41
3200	2.70	-0.67	3.64	-0.01	-1.05	-4.11
3400	3.24	-0.29	3.50	-0.52	-1.27	-4.40
3600	3.47	-0.10	3.27	-0.93	-1.82	-5.02
3800	3.50	-0.16	3.00	-1.26	-1.67	-5.10
4000	3.16	-0.48	2.77	-1.46	-1.70	-5.17
4200	3.06	-0.90	2.57	-0.98	-1.47	-4.87

7.5.2. Measured result

Prototypes of the antennas described in sections 7.2 and 7.4 have been built and measured. The measured return loss of these antenna prototypes are shown in Fig.7.8.

The reference antenna is well matched between 3.2GHz and 4.2GHz which represents a Q of 3.7. With the NIC matched antenna, a 10dB return loss or better was obtained between 1.7GHz to 2.9GHz, which gives a Q of 2. This frequency range allows the antenna to be used in GSM 1800, 1900, PCS, UMTS and Wi-Fi devices despite the fact that it was not designed to be resonant within these frequency bands. Also there is no need for multiple matching networks as would have been required if a passive matching network were to be used to cover these frequency bands. Varying the bias condition does not affect the broadband performance of the NIC matched antenna but a limited form of frequency tuning can be observed.

The passively matched antenna however, is able to have a better than 10dB return loss between 2584MHz and 2700MHz. This implies a Q of approximately 22. In order to be able to cover the broad bandwidths covered with the NIC matching network, multiple matching networks would be required and the simplicity of the matching network is lost because of the need for switches and its corresponding bias network. The narrow instantaneous bandwidth achievable with passive matching also prevents this antenna being used in some communication scenarios such as the spectrum sensing antenna in cognitive radio or any system that requires wide instantaneous bandwidths.

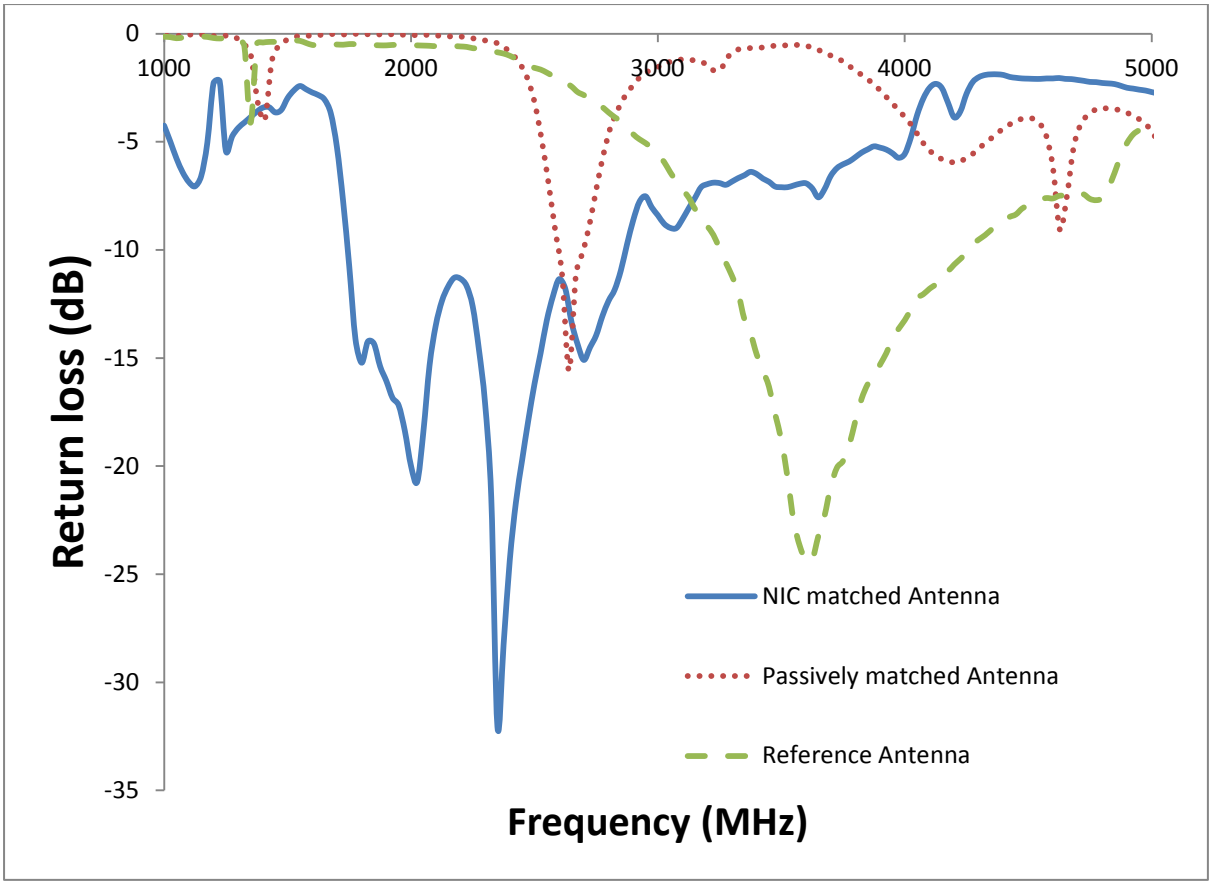

Fig. 7. 9. Measured antenna return loss

7.5.3. Radiation Pattern

The measured radiation patterns for the NIC matched antenna are shown in Figs. 7.9 and those for the reference antenna are shown in Figs 7.10 and 7.11.

Figure 7.9 shows the radiation patterns of the NIC matched antenna measured at 1.8GHz, 2.4GHz and 2.8GHz in both the co-polarisation and cross-polarisation. Looking at the XZ (H) plane radiation patterns, Figs 7.9 (b),(d) and (f), it is clear that the NIC matched antenna is omni-directional which is as expected with a monopole antenna. In the XY (E) plane, Figs. 7.9 (a), (c) and (e) the expected notches at 90^{o} and 270^{o} in the patterns are also seen. When only observing the three principal planes, the maximum gain for the NIC matched antenna is in the XZ plane and the same can be observed with the reference antenna. Within the NIC

matched antenna patterns, it can be observed that there are gaps and discontinuities within the XY plot at 2.4GHz and in the XZ plane at 1.8GHz. These discontinuities are due to the bias lines. When the turn-table on which the antenna is mounted is rotated, the DC bias lines to the power supply do get rotated and do not always return to the same starting point at the end of the 360^{o} rotation. This then leads to different fields around the antenna hence the discontinuity in the radiation fields. This absence of absolute control over the position of the bias lines contributes to the errors in measurement. In the XY plane, the radiation pattern at 1.8GHz shows a different pattern when compared to that which is obtained at other frequency points. The notches expected at 90^{o} and 270^{o} are not observable, this is because at the lowest matched frequency of the antenna, the surface mount components have a greater interaction and impact on the antenna behaviour.

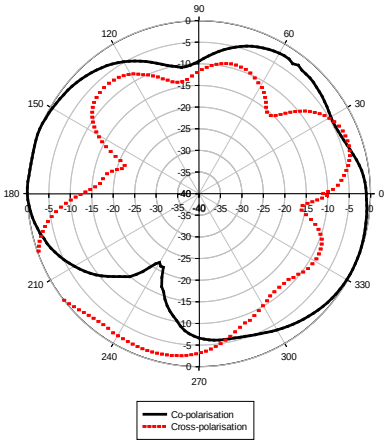

(a)

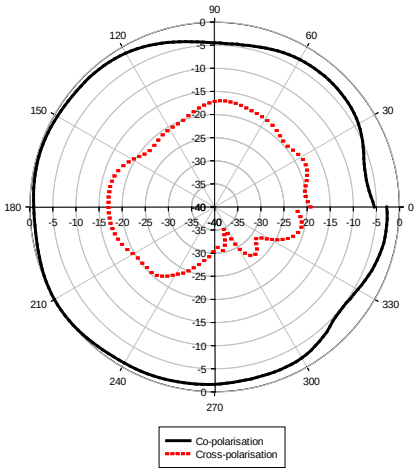

(b)

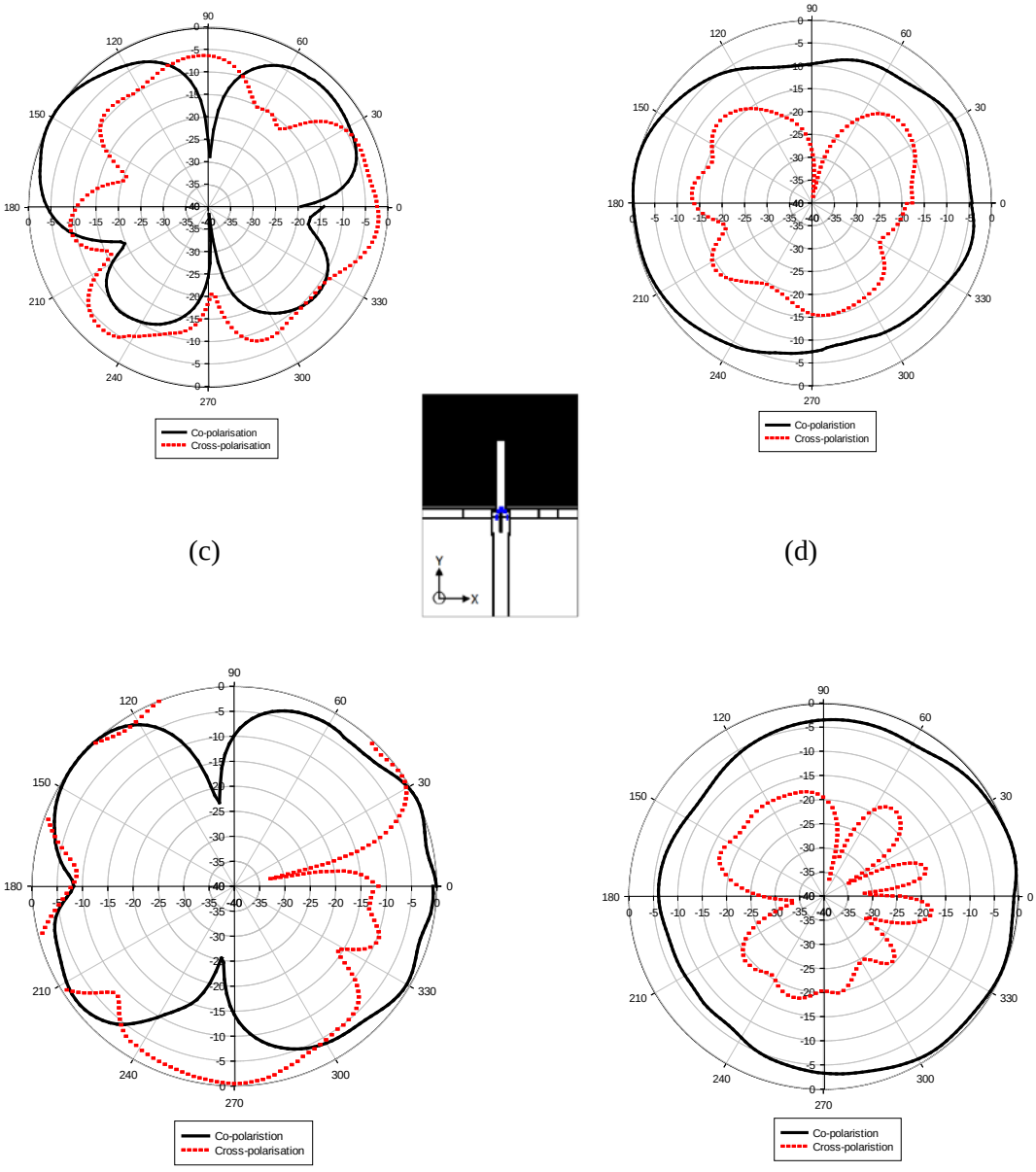

Fig. 7. 10. Measured normalised radiation patterns of the NIC matched antenna at three different frequencies: (a) XY (E) plane at 1.8GHz (b) XZ (H) plane at 1.8GHz (c) XY (E) plane at 2.4GHz (d) XZ (H) plane at 2.4GHz (e) XY (E) plane at 2.8GHz and (f) XZ (H) plane at 2.8GHz

For the reference antenna, the patterns were measured at 3GHz, 3.5GHz and 4GHz where the antenna is matched. From Fig.7.10, the radiation pattern also exhibits the expected omni-directional pattern in the XZ plane and the notches associated with monopoles in the XY plane at 90^{o} and 270^{o}. Fig.7.11 also shows the radiation patterns of the reference antenna at 1.8GHz. 2.4GHz and 2.8GHz in order to give some form of bench marker with which the radiation patterns of the NIC matched antenna can be compared. At 1.8GHz in the XY plane (Fig.7.11a), the expected butterfly pattern typical of monopoles with notches at 90^{o} and 270^{o} is not observable. This is similar to what is obtained with the NIC matched antenna.

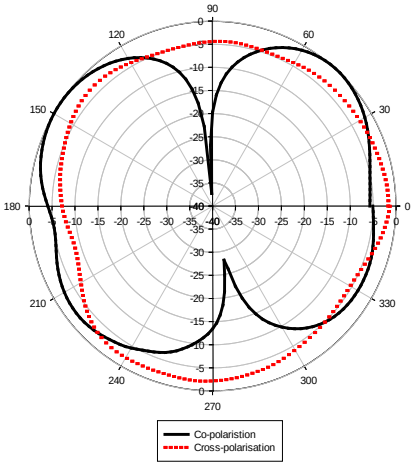

(a)

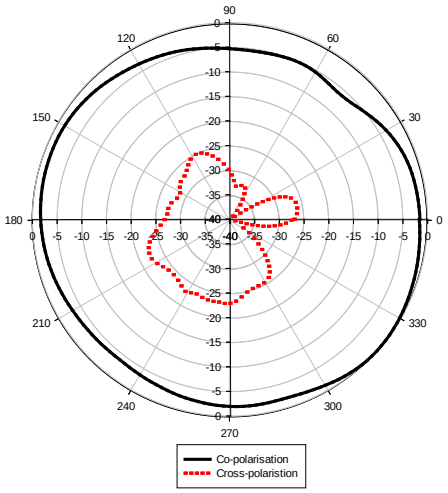

(b)

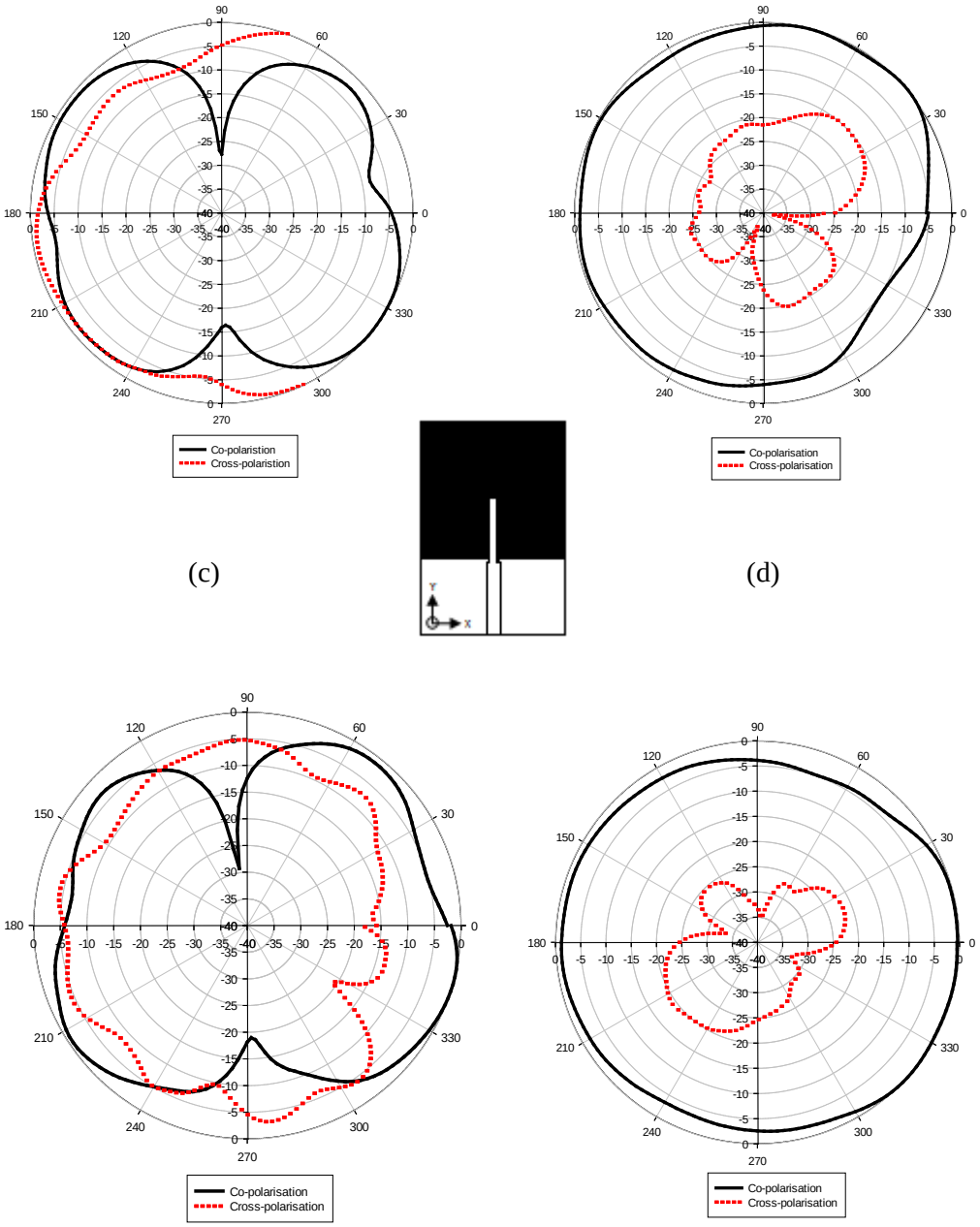

Fig. 7. 11Measured normalised radiation patterns of the reference antenna at three different frequencies: (a) XY (E) plane at 3GHz (b) XZ (H) plane at 3GHz (c) XY (E) plane at 3.5GHz (d) XZ (H) plane at 3.5GHz (e)XY (E) plane at 4GHz and (f) XZ (H) plane at 4GHz

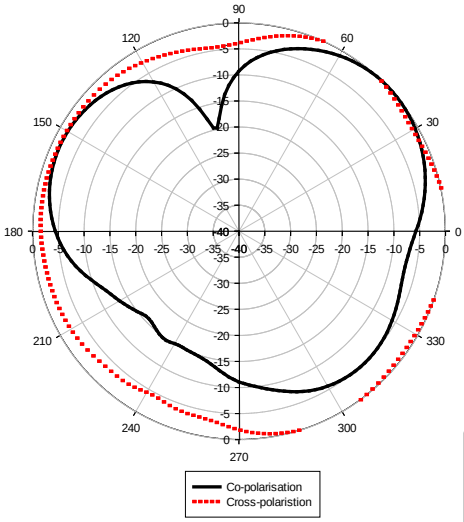
Co-polarisation
Cross-polaristion

(a)

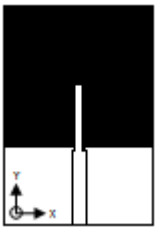

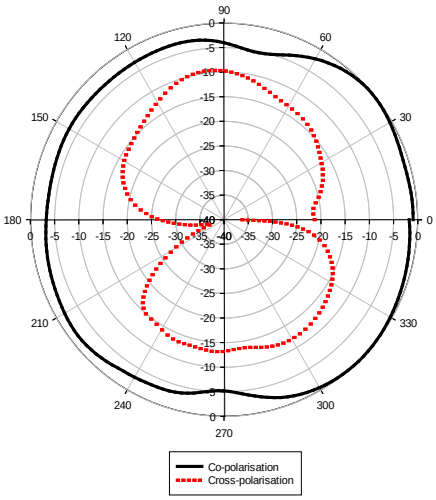
Co-polarisation
Cross-polarisation

(b)

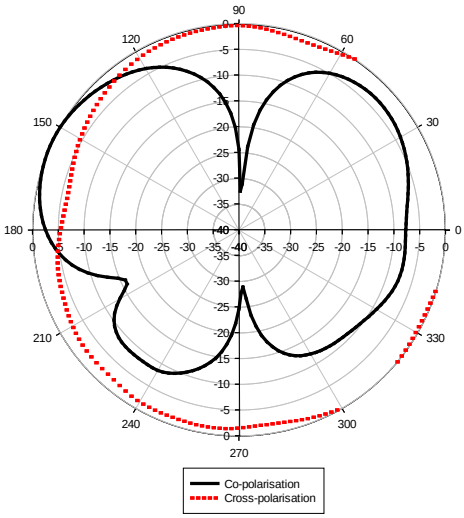
Co-polarisation
Cross-polarisation

(c)

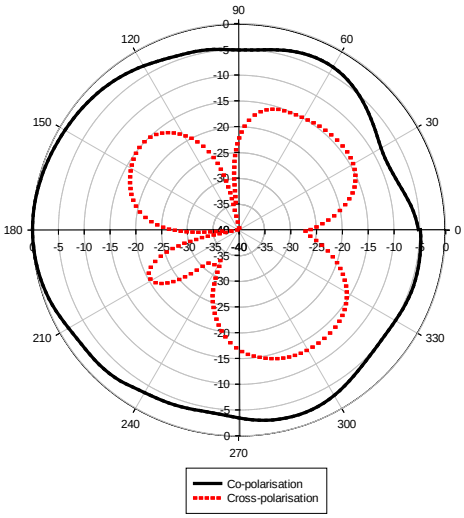
Co-polarisation
Cross-polarisation

(d)

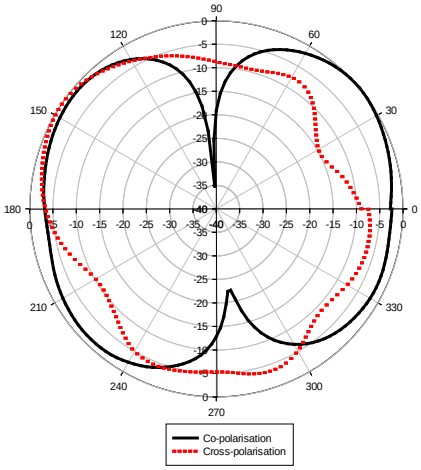

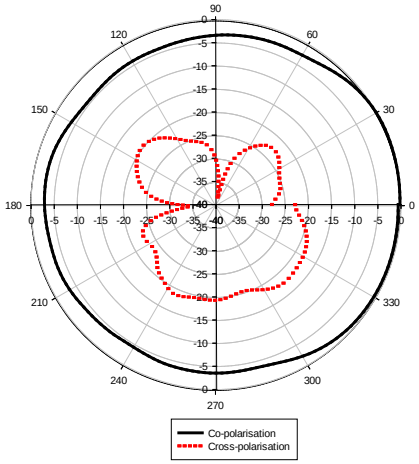

(e) (f)

Fig. 7. 12. Measured normalised radiation patterns of the reference antenna at three different frequencies: (a) XY (E) plane at 1.8GHz (b) XZ (H) plane at 1.8GHz (c) XY (E) plane at 2.4GHz (d) XZ (H) plane at 2.4GHz (e)XY (E) plane at 2.8GHz and (f) XZ (H) plane at 2.8GHz

7.5.4. Gain measurement

The measured gain in the XY plane of the NIC matched antenna, the passively matched antenna and the reference antenna are shown in Fig.7.12. The measurement set-up is described in the appendix D. From Fig.7.12, it is clear that the NIC improves the gain of the antenna within the matched frequency band of 1.7GHz to 2.9GHz and by about 20dB at 2GHz. After 2.9GHz when the return loss of the antenna is below 10dB, the gain of the NIC matched antenna starts to degrade and at 3.3GHz the gain from the reference antenna is higher than the NIC matched antenna. The gain-bandwidth product (equation 7.1) of the NIC matched antenna at 1dBi is 1 while that of the passively matched antenna is 0.35. This represents about a 300% increase with the NIC matched antenna.

$$\text{Gain-bandwidth product} = G \times \frac{\Delta f}{f_0} \qquad (7.1)$$

Where G = Gain in linear units (not in dBi) , f_0 is the centre frequency and Δf is the bandwidth

The passively matched antenna has a better gain within its matched bandwidth than the reference antenna. Outside its matched frequency band, the gain of the passively matched antenna drops below what is obtainable with the reference antenna.

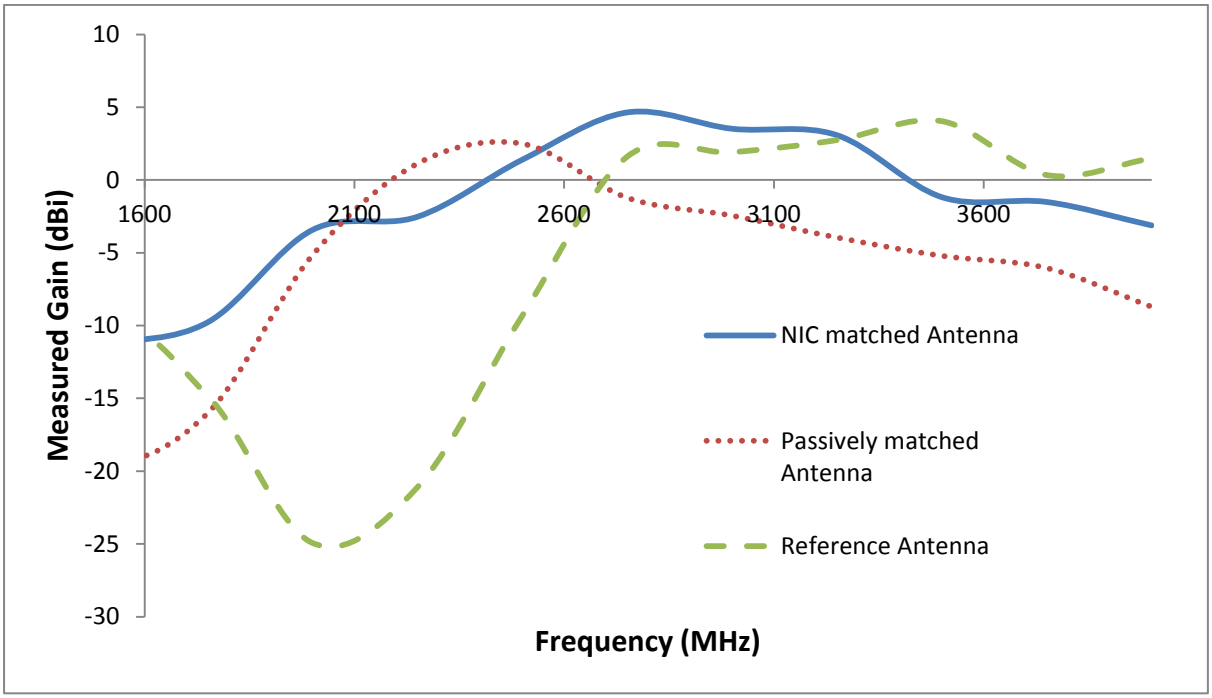

Fig. 7. 13. Measured gain of the antennas

7.6. Conclusion

In this chapter, a planar monopole has been integrated with a coupled line NIC. With the NIC, it was possible to match the antenna below its self resonant frequency. The NIC matching provided a wideband antenna between 1.7GHz and 2.9GHz. The NIC matched antenna is then compared with when the antenna is matched passively. With the passive matching network, it was possible to have a narrowband antenna which was resonant at 2.6GHz with a matched bandwidth of 0.1GHz. These two results when compared show the advantage of using NIC to provide non-Foster matching, as it has the capability to cancel the reactance of an antenna over a wider frequency range than when conventional Foster matching is done. The gain of the different antennas, the reference antenna, the NIC matched antenna and the passively matched antenna have also been compared. With the NIC matched antenna, the gain within the matched bandwidth is significantly higher than that of the reference antenna over a wide bandwidth with 20dB improvement at 2GHz. This shows that the wideband return loss obtained with the NIC is not from losses within the NIC but the actual cancellation of the reactance of the antenna within these frequency bands which results in a better power transfer. With the passively matched antenna however, the gain of the antenna over the reference antenna is only over a relatively narrow bandwidth and outside this frequency band, the gain of the passively matched antenna rolls off. The NIC matched antenna also shows a better gain-bandwidth product than what is obtainable with passive matching.

CHAPTER 8

SYSTEM IMPLEMENTATION OF NEGATIVE IMPEDANCE CONVERTER

8.1. Background

This chapter discusses the implication an NIC matching network would have on the RF system frontend design. This discussion is based on the measurement results and experiments from chapters 3 -7. The Negative Impedance Converter (NIC) has been shown to provide broadband matching of antennas. A review of the current RF system frontend shows that there is a need for matching networks to be reciprocal in other to utilize the frequency division duplex (FDD) on which most systems are based. The two different methods of realising NICs; the Linvill's model and the coupled line NIC, have been discussed in chapters 3, 4, 5 and 6. From the fabricated prototypes also described in these chapters, S_{21} and S_{12} have been measured. Figs. 8.1 and 8.2 both show that the magnitude and phase plots of the NICs and it can be seen that they are reciprocal especially within the frequency bands where the non-Foster properties are evident. Implementing an NIC matched antenna in a practical system would however require a change in RF system front-end design.

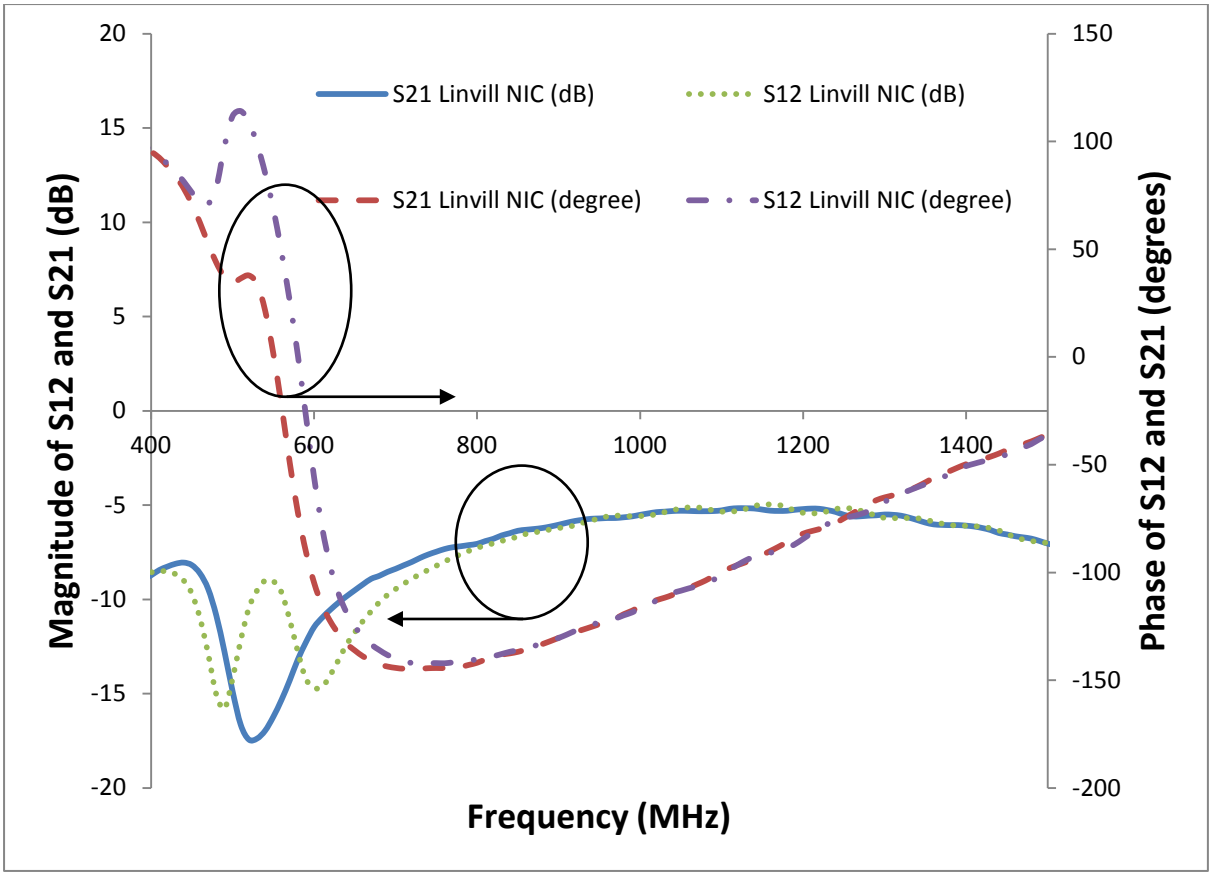

Fig.8. 1. Measured Linvill's NIC S_{21} and S_{12} (chapter 5 - Prototype 2)

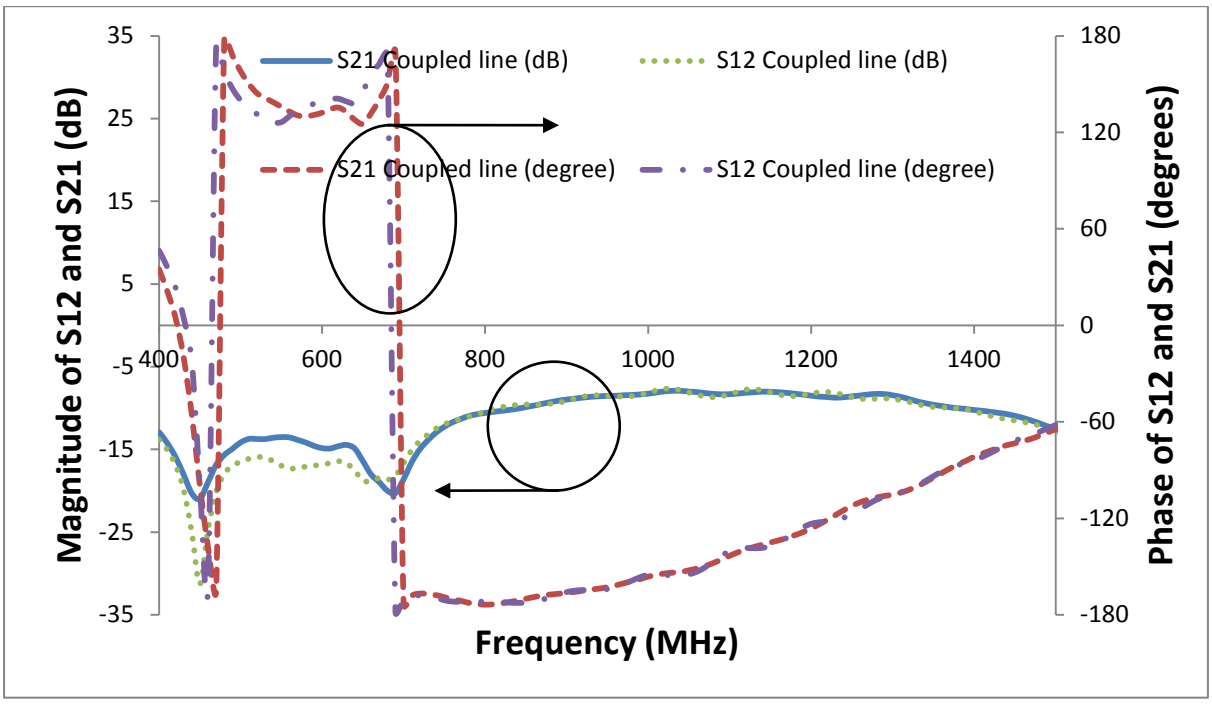

Fig.8. 2. Measured Coupled line NIC S_{21} and S_{12} (chapter 6)

The RF front-end of a wideband transceiver is shown in Fig.8.3 and it consists broadly of two chains, the Transmission (TX) chain and the Receiver (RX) chain. Both chains however have different requirements and characteristics. The TX chain as shown in Fig.8.3 includes a power amplifier (PA) and a wideband transmitter. The last system component before the antenna is the PA. This means that whatever matching network exists between the PA and the antenna matching network should have the capability to handle the high power generated by the PA. In the case of a mobile device 1W of output power should be expected. The NIC is therefore expected to be able to handle such power.

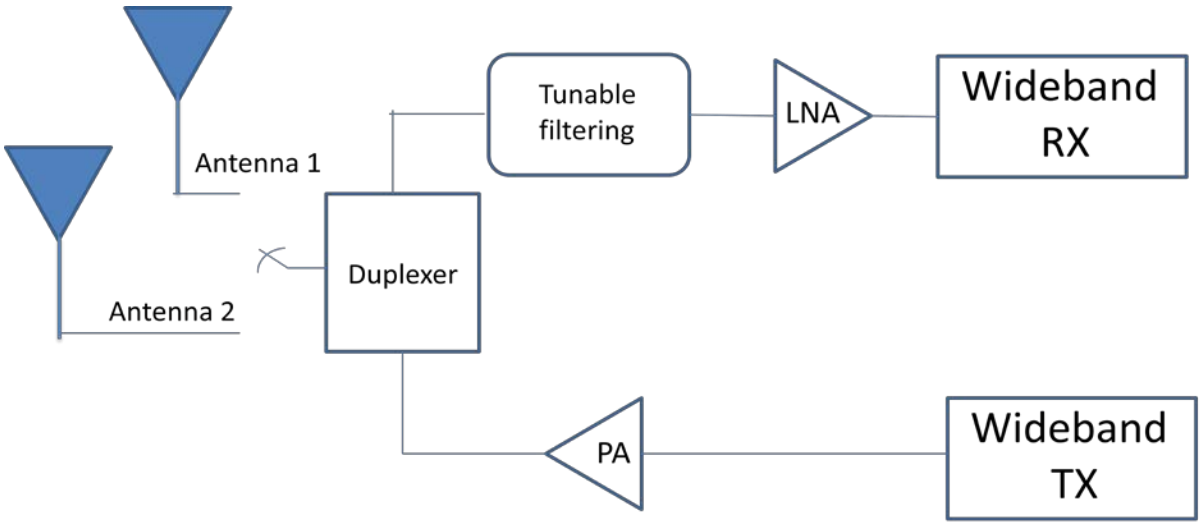

Fig.8. 3. Typical transceiver front-end

In terms of NIC design, this would mean transistors with high power handling capability typically about 30dBm at 1dB compression point (P1dB). High power transistors such as Avago ATF-511P8 would be able to handle the power requirements within the TX chain but it comes with a drawback with a noise figure of 1.4dB which is about a 123% increase in Noise factor as against what would be obtained if transistors with lower P1dB were used as in

the case of Avago ATF 54143 which has NF of 0.5dB and P1dB of 20.4dBm. Datasheets of the two transistors are included in the appendix A. Transistors with higher noise figures are not a major source of concern in the TX chain because the working power levels are significantly higher than the noise floor and the extra noise introduced by an NIC designed with these transistors would not have a great effect as it would be within the same range the noise contribution from the PA. Also Friis formula for noise factor [1] (equation 8.1) shows that the dominant noise contributors are the earliest stages in the TX chain. Therefore the noise contribution of the NIC in the transmit mode would be minimal when compared to earlier stages.

$$= F_1 + \sum_{i=2}^{n} \frac{F_i - 1}{G_1 G_2 \ldots\ldots G_{n-1}} \qquad 8.1$$

In the RX chain however, the main driver is the need to increase the sensitivity of the receiver. Therefore, care is taken to reduce every source of noise. In the RX chain, the signal flow is from the antenna to the Low Noise Amplifier (LNA). Any noise introduced by the antenna sub-system would be amplified by the LNA. There is therefore the need to ensure that the noise contributions from the NIC matched antenna are low. Hence the use of low noise transistors. These transistors usually have a lower P1dB.

Considering the noise factor equation, an NIC matched antenna would be the first sub-system in the RX chain therefore the overall noise figure of the system is heavily reliant on the noise characteristics of the antenna sub-system.

These two requirements are almost mutually exclusive; in that medium to high power transistors have high noise figures while low noise figure transistors have low power handling capability. Therefore there is a need to change from the front-end architecture whereby a single antenna is used in both transmit and receive to a different architecture

where two different antennas are used or to have an architecture whereby the matching networks are designed into the different transmitter and receiver chains and a switch is used to connect the antenna to the different matching networks.

Prior front-end designs, Fig.8.3, used multiple narrow band antennas to cover different frequency bands and multiple throw switches are used to connect the antennas to the duplex which is in turn connected to the TX and RX chain. Another alternative was to use an architecture that employs an Antenna Tuning Unit (ATU) shown in Fig.8.4. The ATU usually contains multiple matching networks (MN) which are used to match a single antenna at different frequency bands. These matching networks are either tuneable or switchable or a combination of both. Inside the ATU would have been an ideal location for the NIC circuit but for its inability to simultaneously have high power handling capability and a low noise figure. For this reason, an alternative architecture is being suggested.

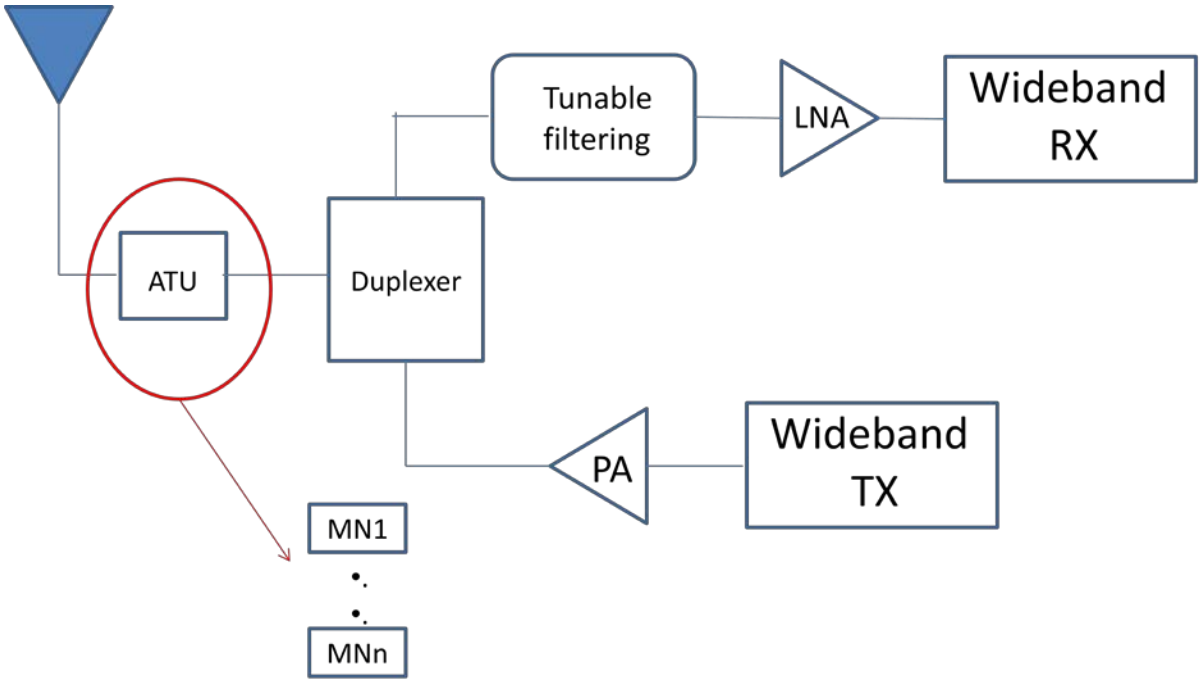

Fig.8. 4. Transceiver front-end with Antenna tuning unit

Fig.8.5 shows a system architecture which provides an opportunity to fit in the NIC matching network. It would require the use of two NICs, the TX NIC and the RX NIC. The main difference would be in the choice of transistors. These NICs would be designed into the different front-end chains and switches would be used to connect the antenna to the different front-end chains.

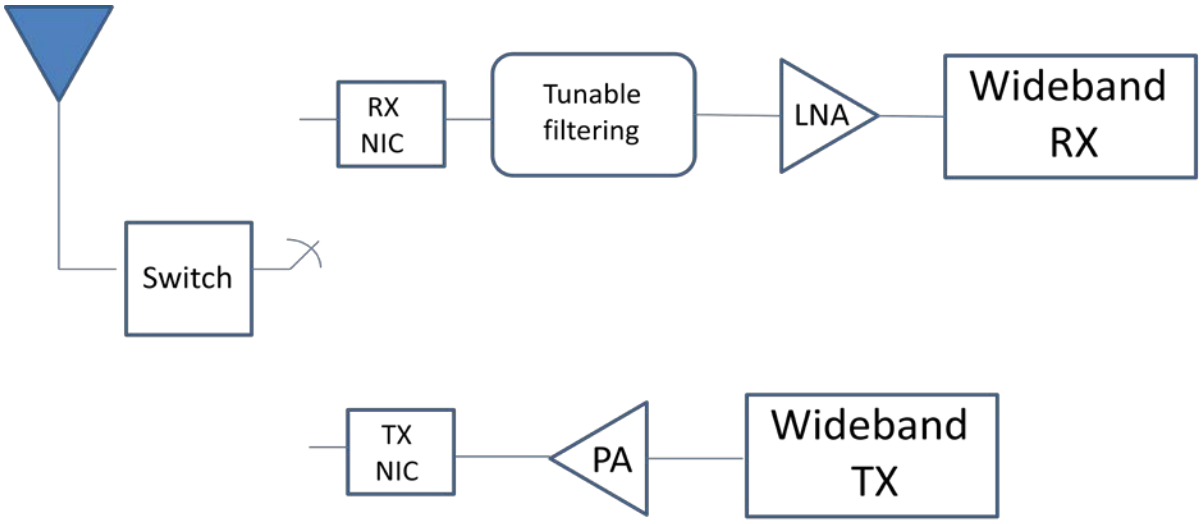

Fig.8. 5. Proposed transceiver front-end for NIC based antenna system.

This architecture also raises more concerns, because of the need to have an NIC in the TX chain and another in the RX chain, a frequency division duplex system would not be possible because a switch is required to connect the two chains to the antenna The need for switching limits the system to a time division duplex system only.

8.2. Conclusion

In this chapter, insights into the possible system implementation constraints that may arise from the use of NICs have been discussed and possible ways around these constraints have also been raised. The need to have different NIC circuitry in the both the TX chain and RX chain have been discussed because of the mutually exclusive requirements of high power capability and low noise. Typical I_{DSS} of a high power transistor is higher than those with lower power requirement. Therefore, to bias these transistor means that higher currents are required and this leads to higher noise contribution.

Reference

[1] H. T. Friis, "Noise Figures of Radio Receivers," Proceedings of the IRE, vol. 32, pp. 419-422, 1944.

CHAPTER 9

CONCLUSIONS AND FUTURE WORK

9.1. Conclusions

This thesis describes research into the use of non-Foster elements in providing broadband antenna matching. It shows and explains the use of non-Foster elements in matching networks and also shows how these elements can be realised using Negative Impedance Converters (NIC). Using the Linvill's NIC has its own peculiar challenges such as stability which was discussed and steps to be taken to achieve stability of NICs were given. Stability within the NIC is very important and has limited the top frequency of previous NICs. Other important system parameters include linearity and noise which were also quantified.

An alternative means of realising non-Foster element was also investigated and its results are shown and compared favourably with the Linvill's model. This NIC realised with coupled transmission lines was integrated with an antenna. The coupled line NIC matched antenna was characterised in terms of return loss and gain. This was compared with matching the antenna conventionally through the use of passive matching network.

From the results obtained, it is clear that NIC based matching networks provide good broadband matching. Though by using NICs within a communication system, there are new sources of concern like noise and linearity but measurements shows that the NIC contributions are all within acceptable limits or similar to contributions from other RF frontend devices. There are positives in terms of gain and antenna efficiency.

9.1.1. Potential of broadband antenna matching using Negative Impedance Converter

Chapter 3 discussed the need for non-Foster matching and its use in obtaining wideband matching. Non-Foster elements were realised by simulating the Linvill's NIC schematic. A simulated antenna has been matched with both Foster and non-Foster matching networks to demonstrate the potential of non-Foster elements and NICs. The use of NIC to achieve non-Foster elements have also been discussed and demonstrated with simulation. The frequency dependence of the inverted impedances using NICs as compared to ideal negative elements have also been shown.. Also non-Foster elements realised by NICs have been used to match an antenna and the resultant wide bandwidth match is shown. Another application of non-Foster elements in its use in increasing the tuning range of varactors has been discussed and demonstrated. The potential for instability was also pointed out with a matched S_{11} begin greater than 0dB.

9.1.2. Stability in Practical NIC Circuit

Chapter 4 shows the stability analysis on the NIC. The standard K factor and auxiliary B1 stability factor test performed using AWR did not predict the oscillation that was experienced when the NIC circuit was fabricated. This is because these tests are based on measurements made from the ports of the circuit; therefore hidden mode oscillations were not detected. Because of the inability of the standard test to predict the instability, a new stability analysis was derived. This analysis is based on the transfer function of the circuit. It has been possible to predict the oscillation frequency to within 16% of the value . The analysis also reveals the critical part of the NIC circuit that leads to oscillation, the feedback path between the transistors. With a parametric study, it is possible to realise a stable NIC given a fixed feedback path length.

9.1.3. Realisation of NIC and Antenna Matching

An NIC based on the Linvill's schematic with an upper frequency cut-off of 1.5GHz has been shown in Chapter 5. The measured NIC has been combined in a simulator with a chassis antenna and a wideband performance has been achieved. It also showed a better performance than a resistively and lossy matched antenna in terms of antenna efficiency. An equivalent circuit has been built to represent the antenna within a frequency band and with this NIC matched equivalent circuit, the noise and linearity performance of the NIC have been investigated. It can be seen that the NIC matched antenna shows a Signal to Noise ratio advantage when compared with a resistively matched antenna. It terms of linearity, it can also be seen that the NIC's IP3 of 18dBm is within range of commercially available RF front end components. In a cascaded system, the overall IP3 is dominated by the later stages, therefore the impact of the IP3 of the NIC matched antenna on the overall cascaded system is low.

9.1.4. Coupled line Negative Impedance Converter

In chapter 6, an alternative means of realising non-Foster elements has been discussed. Its noise and linearity performance have been shown. Because it is achievable as a single layer PCB, it is easier to fabricate. The use of a single transistor also helps with the stability problems typically associated with the Linvill's model. It is also less complicated and has a lower count on the number of elements required. Because there are no stability concerns as shown by the stability analysis, it is easier to demonstrate the NIC at even higher frequencies when compared with what is obtainable with the Linvill's model. It does however still have considerable losses through the NIC especially at the lower frequencies as can be seen with Q factor, although this is better than what is obtainable within this frequency range with the Linvill's model.

A comparison between the output spectra when two tones are injected into the different NIC architecture is shown in Fig.6.32. It can be seen that the 3rd order inter-modulation products from the coupled line NIC are about 20dB lower than those from the Linvill's NIC. Also there is an appreciable reduction in the noise floor of the coupled line NIC. Figure 6.33 shows the comparison between the SNR advantage from using the different NIC methods and it is clear that though the Linvill NIC performs better at lower frequency, the coupled line NIC starts to perform better at about 900MHz and the difference rises to 10dB at 1GHz. There is a dip in at 960MHz which is due to the interference from other transmitters (GSM 900) within range.

9.1.6. Coupled Line NIC matched Antenna

In chapter 7, a planar monopole has been integrated with a coupled line NIC. With the NIC, it was possible to match the antenna below its self resonant frequency of 3.5GHz. The NIC matching provided a wideband antenna between 1.7GHz and 2.9GHz. This NIC matched antenna is then compared with a passively matched antenna. With the passive matching network, it was possible to have a narrowband antenna which was resonant at 2.6GHz with a matched bandwidth of 0.1GHz. These two results when compared show the advantage of using NIC to provide non-Foster matching as it has the capability to cancel the reactance of an antenna of a wider frequency range than when a conventional Foster matching is done. There is also the comparison between the gains of the different antennas; the reference antenna, the NIC matched antenna and the passively matched antenna. With the NIC matched antenna, the gain within the matched bandwidth is significantly higher than that of the reference antenna over a wide bandwidth with 20dB improvement at 2GHz. This shows that

the wideband return loss obtained with the NIC is not from losses within the NIC but the actual cancellation of the reactance of the antenna within these frequency bands. With the passively matched antenna however, the gain improvement of the antenna over the reference antenna is only over a relatively narrow bandwidth and outside this frequency band, the gain of the passively matched antenna rolls off. The NIC matched antenna also shows a better gain-bandwidth product than what is obtainable with passive matching.

9.1.7. System Implementation of the Negative Impedance Converter

In chapter 8, insights into the possible system implementation constraints that may arise from the use of NICs have been discussed and possible ways around these constraints have also been raised. The need to have different NIC circuitry in the both the TX chain and RX chain have been discussed because of the mutually exclusive requirements of high power capability and low noise in the different RF frontend chains.

9.2. Future Work

This work has demonstrated work into NICs. One of the major limitations of the Linvill's NIC is stability which necessitates a stability analysis. From the parametric analysis, it is possible to have the Linvill's NIC working at higher frequency but this would require a change in the fabrication method such as the use of MMICs.

1. The realisation of the Linvill's NIC on MMIC would not only help increase the achievable top frequency but it will also help reduce the loss and the overall size of the NIC.

2. Size reduction would make it easier to integrate the Linvill NIC into the chassis antenna. It would also be possible to achieve multiple NICs and therefore the initial matching network proposed for the chassis antenna would be achievable.
3. Investigate the use of electrically tuneable varactors instead of capacitors within NICs. This would give another degree of freedom when matching the antenna and also make the NIC based matching network reconfigurable.

Investigate possibility of making antenna efficiency measurements of NIC matched antennas. There are different methods via which antenna efficiency can be measured. The Wheeler cap method is the easiest but this method breaks down when elements are integrated onto the antenna structure. Alternative methods such as the 3D radiation pattern integration might be better suited or other variants of the Wheeler cap measurements could give better results.

APPENDIX A

COMPONENTS DATA SHEETS

Avago ATF54143

ATF-54143
Low Noise Enhancement Mode Pseudomorphic HEMT in a Surface Mount Plastic Package

AVAGO TECHNOLOGIES

Data Sheet

Description

Avago Technologies' ATF-54143 is a high dynamic range, low noise, E-PHEMT housed in a 4-lead SC-70 (SOT-343) surface mount plastic package.

The combination of high gain, high linearity and low noise makes the ATF-54143 ideal for cellular/PCS base stations, MMDS, and other systems in the 450 MHz to 6 GHz frequency range.

Surface Mount Package SOT-343

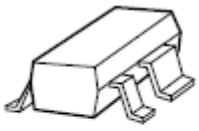

Pin Connections and Package Marking

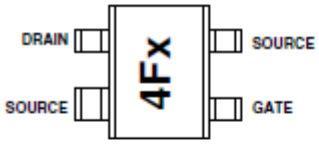

Note:
Top View. Package marking provides orientation and identification

"4F" = Device Code
"x" = Date code character
identifies month of manufacture.

Attention: Observe precautions for handling electrostatic sensitive devices.
ESD Machine Model (Class A)
ESD Human Body Model (Class 1A)
Refer to Avago Application Note A004R:
Electrostatic Discharge Damage and Control.

Features

- High linearity performance
- Enhancement Mode Technology [1]
- Low noise figure
- Excellent uniformity in product specifications
- 800 micron gate width
- Low cost surface mount small plastic package SOT-343 (4 lead SC-70)
- Tape-and-Reel packaging option available
- Lead-free option available.

Specifications

- 2 GHz; 3V, 60 mA (Typ.)
- 36.2 dBm output 3rd order intercept
- 20.4 dBm output power at 1 dB gain compression
- 0.5 dB noise figure
- 16.6 dB associated gain

Applications

- Low noise amplifier for cellular/PCS base stations
- LNA for WLAN, WLL/RLL and MMDS applications
- General purpose discrete E-PHEMT for other ultra low noise applications

Note:
1. Enhancement mode technology requires positive Vgs, thereby eliminating the need for the negative gate voltage associated with conventional depletion mode devices.

ATF-54143 Absolute Maximum Ratings [1]

Symbol	Parameter	Units	Absolute Maximum
V_{DS}	Drain - Source Voltage[2]	V	5
V_{GS}	Gate - Source Voltage[2]	V	-5 to 1
V_{GD}	Gate Drain Voltage[2]	V	-5 to 1
I_{DS}	Drain Current[2]	mA	120
P_{diss}	Total Power Dissipation[3]	mW	725
$P_{in\ max.}$ (ON mode)	RF Input Power (Vds=3V, Ids=60mA)	dBm	20[5]
$P_{in\ max.}$ (OFF mode)	RF Input Power (Vd=0, Ids=0A)	dBm	20
I_{GS}	Gate Source Current	mA	2[5]
T_{CH}	Channel Temperature	°C	150
T_{STG}	Storage Temperature	°C	-65 to 150
θ_{jc}	Thermal Resistance[4]	°C/W	162

Notes:
1. Operation of this device in excess of any one of these parameters may cause permanent damage.
2. Assumes DC quiescent conditions.
3. Source lead temperature is 25°C. Derate 6.2 mW/°C for $T_L > 33$°C.
4. Thermal resistance measured using 150°C Liquid Crystal Measurement method.
5. The device can handle +20 dBm RF Input Power provided I_{GS} is limited to 2 mA. I_{GS} at P_{1dB} drive level is bias circuit dependent. See application section for additional information.

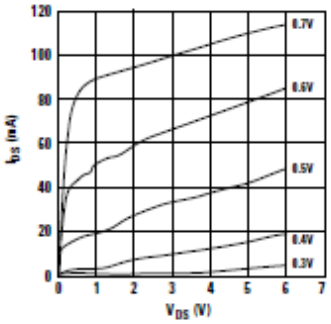

Figure 1. Typical I-V Curves. (V_{GS} = 0.1 V per step)

Product Consistency Distribution Charts [6, 7]

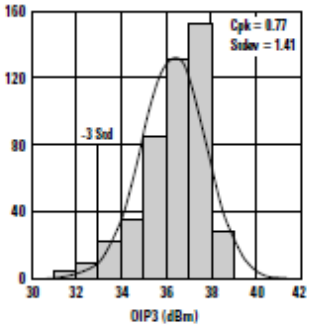

Figure 2. OIP3 @ 2 GHz, 3 V, 60 mA. LSL = 33.0, Nominal = 36.575

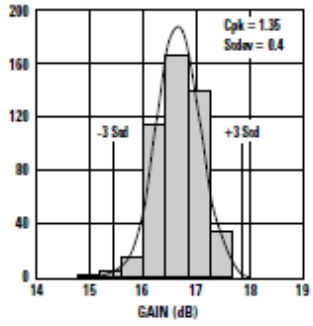

Figure 3. Gain @ 2 GHz, 3 V, 60 mA. USL = 18.5, LSL = 15, Nominal = 16.6

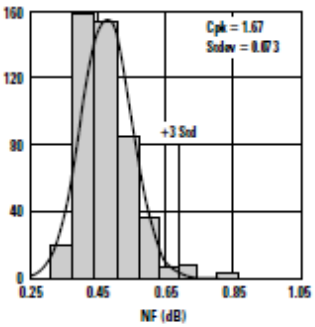

Figure 4. NF @ 2 GHz, 3 V, 60 mA. USL = 0.9, Nominal = 0.49

Notes:
6. Distribution data sample size is 450 samples taken from 9 different wafers. Future wafers allocated to this product may have nominal values anywhere between the upper and lower limits.
7. Measurements made on production test board. This circuit represents a trade-off between an optimal noise match and a realizeable match based on production test equipment. Circuit losses have been de-embedded from actual measurements.

ATF-54143 Electrical Specifications

T_A = 25°C, RF parameters measured in a test circuit for a typical device

Symbol	Parameter and Test Condition			Units	Min.	Typ.[2]	Max.
Vgs	Operational Gate Voltage		Vds = 3V, Ids = 60 mA	V	0.4	0.59	0.75
Vth	Threshold Voltage		Vds = 3V, Ids = 4 mA	V	0.18	0.38	0.52
Idss	Saturated Drain Current		Vds = 3V, Vgs = 0V	µA	—	1	5
Gm	Transconductance		Vds = 3V, gm = ΔIdss/ΔVgs; ΔVgs = 0.75 - 0.7 = 0.05V	mmho	230	410	560
Igss	Gate Leakage Current		Vgd = Vgs = -3V	µA	—	—	200
NF	Noise Figure[1]	f = 2 GHz	Vds = 3V, Ids = 60 mA	dB	—	0.5	0.9
		f = 900 MHz	Vds = 3V, Ids = 60 mA	dB	—	0.3	—
Ga	Associated Gain[1]	f = 2 GHz	Vds = 3V, Ids = 60 mA	dB	15	16.6	18.5
		f = 900 MHz	Vds = 3V, Ids = 60 mA	dB	—	23.4	—
OIP3	Output 3rd Order	f = 2 GHz	Vds = 3V, Ids = 60 mA	dBm	33	36.2	—
	Intercept Point[1]	f = 900 MHz	Vds = 3V, Ids = 60 mA	dBm	—	35.5	—
P1dB	1dB Compressed	f = 2 GHz	Vds = 3V, Ids = 60 mA	dBm	—	20.4	—
	Output Power[1]	f = 900 MHz	Vds = 3V, Ids = 60 mA	dBm	—	18.4	—

Notes:
1. Measurements obtained using production test board described in Figure 5.
2. Typical values measured from a sample size of 450 parts from 9 wafers.

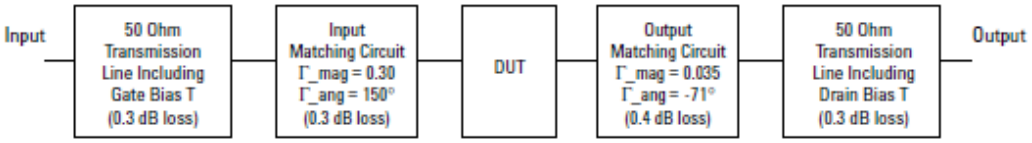

Figure 5. Block diagram of 2 GHz production test board used for Noise Figure, Associated Gain, P1dB, and OIP3 measurements. This circuit represents a trade-off between an optimal noise match and associated impedance matching circuit losses. Circuit losses have been de-embedded from actual measurements.

ATF-54143 Typical Performance Curves

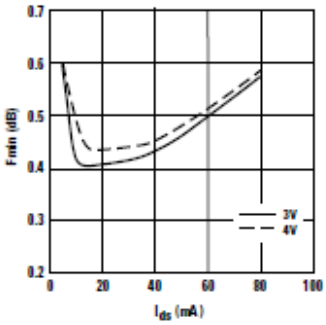

Figure 6. Fmin vs. I_{ds} and V_{ds} Tuned for Max OIP3 and Fmin at 2 GHz.

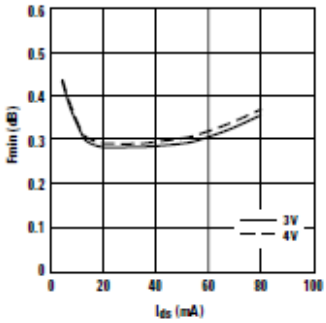

Figure 7. Fmin vs. I_{ds} and V_{ds} Tuned for Max OIP3 and Min NF at 900 MHz.

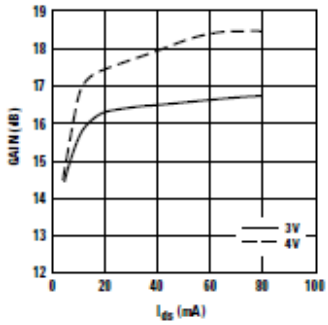

Figure 8. Gain vs. I_{ds} and V_{ds} Tuned for Max OIP3 and Fmin at 2 GHz.

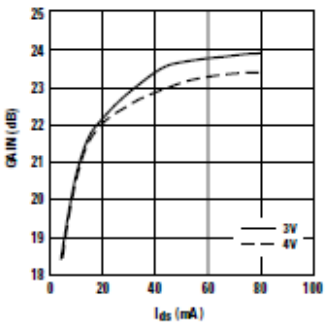

Figure 9. Gain vs. I_{ds} and V_{ds} Tuned for Max OIP3 and Fmin at 900 MHz.

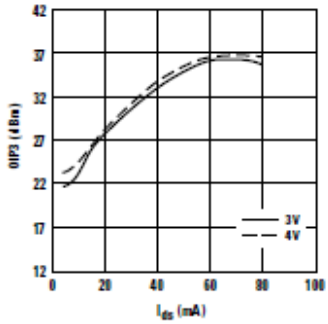

Figure 10. OIP3 vs. I_{ds} and V_{ds} Tuned for Max OIP3 and Fmin at 2 GHz.

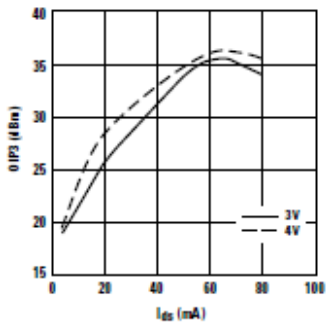

Figure 11. OIP3 vs. I_{ds} and V_{ds} Tuned for Max OIP3 and Fmin at 900 MHz.

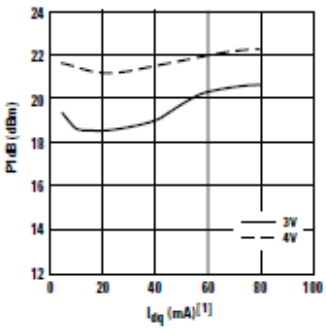

Figure 12. P1dB vs. I_{dq} and V_{ds} Tuned for Max OIP3 and Fmin at 2 GHz.

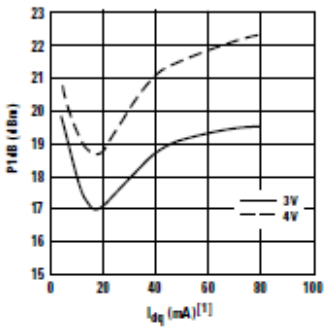

Figure 13. P1dB vs. I_{dq} and V_{ds} Tuned for Max OIP3 and Fmin at 900 MHz.

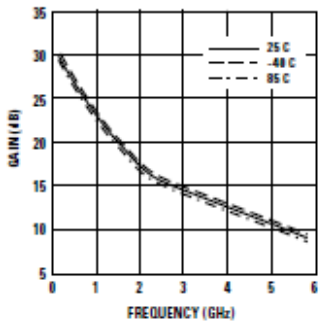

Figure 14. Gain vs. Frequency and Temp Tuned for Max OIP3 and Fmin at 3V, 60 mA.

Notes:

1. I_{dq} represents the quiescent drain current without RF drive applied. Under low values of I_{ds}, the application of RF drive will cause I_d to increase substantially as P1dB is approached.
2. Fmin values at 2 GHz and higher are based on measurements while the Fmins below 2 GHz have been extrapolated. The Fmin values are based on a set of 16 noise figure measurements made at 16 different impedances using an ATN NP5 test system. From these measurements a true Fmin is calculated. Refer to the noise parameter application section for more information.

ATF-54143 Typical Performance Curves, continued

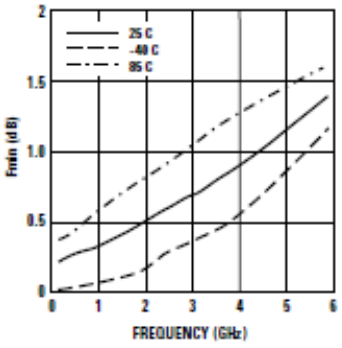

Figure 15. Fmin[2] vs. Frequency and Temp Tuned for Max OIP3 and Fmin at 3V, 60 mA.

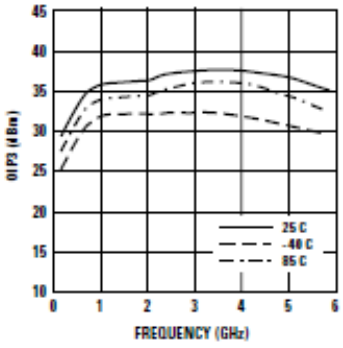

Figure 16. OIP3 vs. Frequency and Temp Tuned for Max OIP3 and Fmin at 3V, 60 mA.

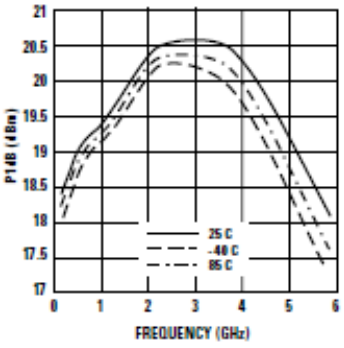

Figure 17. P1dB vs. Frequency and Temp Tuned for Max OIP3 and Fmin at 3V, 60 mA.

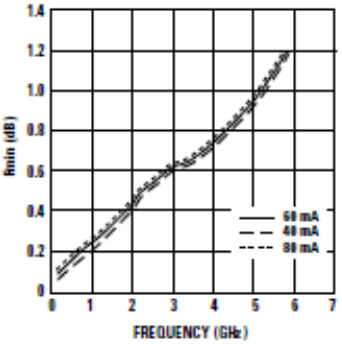

Figure 18. Fmin[1] vs. Frequency and I_{ds} at 3V.

ATF-54143 Reflection Coefficient Parameters tuned for Maximum Output IP3, V_{DS} = 3V, I_{DS} = 60 mA

Freq (GHz)	ΓOut_Mag.[1] (Mag)	ΓOut_Ang.[2] (Degrees)	OIP3 (dBm)	P1dB (dBm)
0.9	0.017	115	35.54	18.4
2.0	0.026	-85	36.23	20.38
3.9	0.013	173	37.54	20.28
5.8	0.025	102	35.75	18.09

Note:
1. Gamma out is the reflection coefficient of the matching circuit presented to the output of the device.
2. Fmin values at 2 GHz and higher are based on measurements while the Fmins below 2 GHz have been extrapolated. The Fmin values are based on a set of 16 noise figure measurements made at 16 different impedances using an ATN NP5 test system. From these measurements a true Fmin is calculated. Refer to the noise parameter application section for more information.

NXP BFS 17

NPN 1 GHz wideband transistor BFS17

DESCRIPTION

NPN transistor in a plastic SOT23 package.

APPLICATIONS

- A wide range of RF applications such as:
  - Mixers and oscillators in TV tuners
  - RF communications equipment.

PINNING

PIN	DESCRIPTION
1	base
2	emitter
3	collector

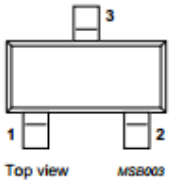

Marking code: E1p.

Fig.1 SOT23.

QUICK REFERENCED DATA

SYMBOL	PARAMETER	CONDITIONS	TYP.	MAX.	UNIT
V_{CBO}	collector-base voltage	open emitter	–	25	V
V_{CEO}	collector-emitter voltage	open base	–	15	V
I_C	DC collector current		–	25	mA
P_{tot}	total power dissipation	up to T_s = 70 °C; note 1	–	300	mW
f_T	transition frequency	I_C = 25 mA; V_{CE} = 5 V; f = 500 MHz; T_j = 25 °C	1	–	GHz
F	noise figure	I_C = 2 mA; V_{CE} = 5 V; R_S = 50 Ω; f = 500 MHz; T_j = 25 °C	4.5	–	dB

LIMITING VALUES

In accordance with the Absolute Maximum Rating System (IEC 134).

SYMBOL	PARAMETER	CONDITIONS	MIN.	MAX.	UNIT
V_{CBO}	collector-base voltage	open emitter	–	25	V
V_{CEO}	collector-emitter voltage	open base	–	15	V
V_{EBO}	emitter-base voltage	open collector	–	2.5	V
I_C	DC collector current		–	25	mA
I_{CM}	peak collector current		–	50	mA
P_{tot}	total power dissipation	up to T_s = 70 °C; note 1	–	300	mW
T_{stg}	storage temperature		–65	+150	°C
T_j	junction temperature		–	150	°C

Note to the Quick reference data and the Limiting values

1. T_s is the temperature at the soldering point of the collector pin.

THERMAL CHARACTERISTICS

SYMBOL	PARAMETER	CONDITIONS	VALUE	UNIT
$R_{th\ j\text{-}s}$	thermal resistance from junction to soldering point	up to T_s = 70 °C; note 1	260	K/W

Note

1. T_s is the temperature at the soldering point of the collector pin.

CHARACTERISTICS

T_j = 25 °C unless otherwise specified.

SYMBOL	PARAMETER	CONDITIONS	MIN.	TYP.	MAX.	UNIT
I_{CBO}	collector cut-off current	I_E = 0; V_{CB} = 10 V	–	–	10	nA
h_{FE}	DC current gain	I_C = 2 mA; V_{CE} = 1 V	25	90	–	
		I_C = 25 mA; V_{CE} = 1 V	25	90	–	
f_T	transition frequency	I_C = 2 mA; V_{CE} = 5 V; f = 500 MHz	–	1	–	GHz
		I_C = 25 mA; V_{CE} = 5 V; f = 500 MHz	–	1.6	–	GHz
C_c	collector capacitance	$I_E = i_e$ = 0; V_{CB} = 10 V; f = 1 MHz	–	0.8	1.5	pF
C_e	emitter capacitance	$I_C = i_c$ = 0; V_{EB} = 0.5 V; f = 1 MHz	–	–	2	pF
C_{re}	feedback capacitance	I_C = 1 mA; V_{CE} = 5 V; f = 1 MHz	–	0.65	–	pF
F	noise figure	I_C = 2 mA; V_{CE} = 5 V; R_S = 50 Ω; f = 500 MHz	–	4.5	–	dB

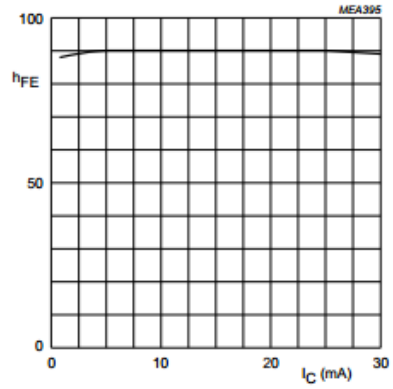

V_{CE} = 1 V; T_j = 25 °C.

Fig.2 DC current gain as a function of collector current.

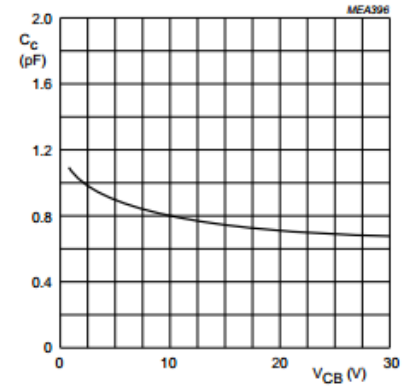

$I_E = i_e = 0$; f = 1 MHz; T_j = 25 °C.

Fig.3 Collector capacitance as a function of collector-base voltage.

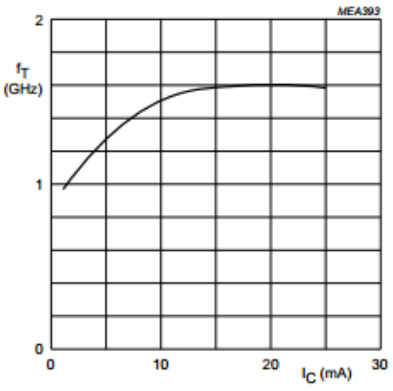

V_{CE} = 5 V; f = 500 MHz; T_j = 25 °C.

Fig.4 Transition frequency as a function of collector current.

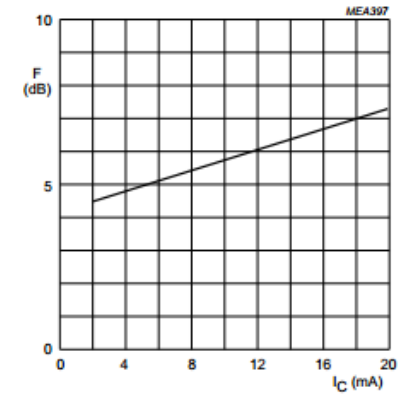

V_{CE} = 5 V; R_S = 50 Ω; f = 500 MHz; T_j = 25 °C.

Fig.5 Minimum noise figure as a function of collector current.

NPN 6 GHz wideband transistor BFR93A

FEATURES

- High power gain
- Low noise figure
- Very low intermodulation distortion.

APPLICATIONS

- RF wideband amplifiers and oscillators.

DESCRIPTION

NPN wideband transistor in a plastic SOT23 package.
PNP complement: BFT93.

PINNING

PIN	DESCRIPTION
1	base
2	emitter
3	collector

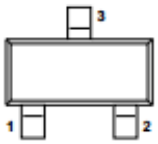

Marking code: R2p.

Fig.1 SOT23.

QUICK REFERENCE DATA

SYMBOL	PARAMETER	CONDITIONS	TYP.	MAX.	UNIT
V_{CBO}	collector-base voltage	open emitter	–	15	V
V_{CEO}	collector-emitter voltage	open base	–	12	V
I_C	collector current (DC)		–	35	mA
P_{tot}	total power dissipation	$T_s \leq 95$ °C	–	300	mW
C_{re}	feedback capacitance	$I_C = 0$; $V_{CE} = 5$ V; f = 1 MHz	0.6	–	pF
f_T	transition frequency	$I_C = 30$ mA; $V_{CE} = 5$ V; f = 500 MHz	6	–	GHz
G_{UM}	maximum unilateral power gain	$I_C = 30$ mA; $V_{CE} = 8$ V; f = 1 GHz; $T_{amb} = 25$ °C	13	–	dB
		$I_C = 30$ mA; $V_{CE} = 8$ V; f = 2 GHz; $T_{amb} = 25$ °C	7	–	dB
F	noise figure	$I_C = 5$ mA; $V_{CE} = 8$ V; f = 1 GHz; $\Gamma_s = \Gamma_{opt}$; $T_{amb} = 25$ °C	1.9	–	dB
V_O	output voltage	$d_{im} = -60$ dB; $I_C = 30$ mA; $V_{CE} = 8$ V; $R_L = 75\ \Omega$; $T_{amb} = 25$ °C; $f_p + f_q - f_r = 793.25$ MHz	425	–	mV

LIMITING VALUES

In accordance with the Absolute Maximum Rating System (IEC 134).

SYMBOL	PARAMETER	CONDITIONS	MIN.	MAX.	UNIT
V_{CBO}	collector-base voltage	open emitter	–	15	V
V_{CEO}	collector-emitter voltage	open base	–	12	V
V_{EBO}	emitter-base voltage	open collector	–	2	V
I_C	collector current (DC)		–	35	mA
P_{tot}	total power dissipation	$T_s \leq 95$ °C; note 1	–	300	mW
T_{stg}	storage temperature		–65	+150	°C
T_j	junction temperature		–	+175	°C

Note

1. T_s is the temperature at the soldering point of the collector pin.

THERMAL CHARACTERISTICS

SYMBOL	PARAMETER	CONDITIONS	VALUE	UNIT
$R_{th\ j\text{-}s}$	thermal resistance from junction to soldering point	$T_s \leq 95$ °C; note 1	260	K/W

Note

1. T_s is the temperature at the soldering point of the collector pin.

CHARACTERISTICS

$T_j = 25$ °C unless otherwise specified.

SYMBOL	PARAMETER	CONDITIONS	MIN.	TYP.	MAX.	UNIT
I_{CBO}	collector cut-off current	$I_E = 0$; $V_{CB} = 5$ V	–	–	50	nA
h_{FE}	DC current gain	$I_C = 30$ mA; $V_{CE} = 5$ V	40	90	–	
C_c	collector capacitance	$I_E = i_e = 0$; $V_{CB} = 5$ V; f = 1 MHz	–	0.7	–	pF
C_e	emitter capacitance	$I_C = i_c = 0$; $V_{EB} = 0.5$ V; f = 1 MHz	–	1.9	–	pF
C_{re}	feedback capacitance	$I_C = i_c = 0$; $V_{CE} = 5$ V; f = 1 MHz; $T_{amb} = 25$ °C	–	0.6	–	pF
f_T	transition frequency	$I_C = 30$ mA; $V_{CE} = 5$ V; f = 500 MHz	4.5	6	–	GHz
G_{UM}	maximum unilateral power gain (note 1)	$I_C = 30$ mA; $V_{CE} = 8$ V; f = 1 GHz; $T_{amb} = 25$ °C	–	13	–	dB
		$I_C = 30$ mA; $V_{CE} = 8$ V; f = 2 GHz; $T_{amb} = 25$ °C	–	7	–	dB
F	noise figure (note 2)	$I_C = 5$ mA; $V_{CE} = 8$ V; f = 1 GHz; $\Gamma_s = \Gamma_{opt}$; $T_{amb} = 25$ °C	–	1.9	–	dB
		$I_C = 5$ mA; $V_{CE} = 8$ V; f = 2 GHz; $\Gamma_s = \Gamma_{opt}$; $T_{amb} = 25$ °C	–	3	–	dB
V_O	output voltage	notes 2 and 3	–	425	–	mV
d_2	second order intermodulation distortion	notes 2 and 4	–	–50	–	dB

Notes

1. G_{UM} is the maximum unilateral power gain, assuming S_{12} is zero and $G_{UM} = 10 \log \frac{|S_{21}|^2}{(1-|S_{11}|^2)(1-|S_{22}|^2)}$ dB .
2. Measured on the same die in a SOT37 package (BFR91A).
3. $d_{im} = -60$ dB (DIN 45004B); $I_C = 30$ mA; $V_{CE} = 8$ V; $R_L = 75\ \Omega$; $T_{amb} = 25$ °C;
   $V_p = V_O$ at $d_{im} = -60$ dB; $f_p = 795.25$ MHz;
   $V_q = V_O - 6$ dB at $f_q = 803.25$ MHz;
   $V_r = V_O - 6$ dB at $f_r = 805.25$ MHz;
   measured at $f_p + f_q - f_r = 793.25$ MHz.
4. $I_C = 30$ mA; $V_{CE} = 8$ V; $R_L = 75\ \Omega$; $T_{amb} = 25$ °C;
   $V_p = 200$ mV at $f_p = 250$ MHz;
   $V_q = 200$ mV at $f_q = 560$ MHz;
   measured at $f_p + f_q = 810$ MHz.

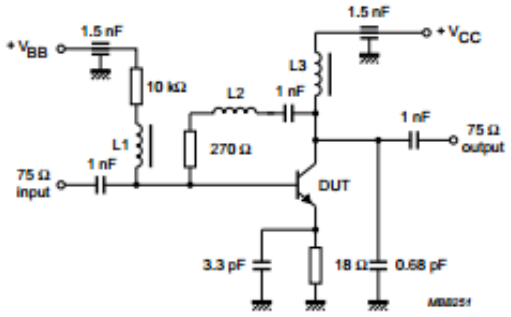

L1 = L3 = 5 μH choke.
L2 = 3 turns 0.4 mm copper wire; winding pitch 1 mm; internal diameter 3 mm.

Fig.2 Intermodulation distortion and second harmonic distortion MATV test circuit.

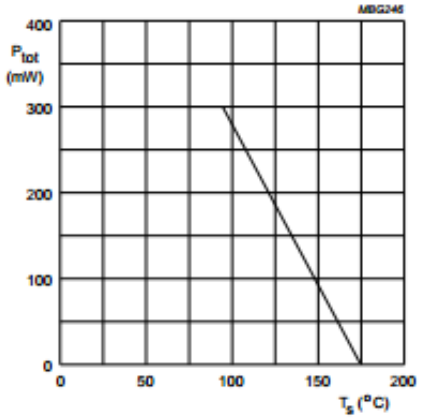

Fig.3 Power derating curve.

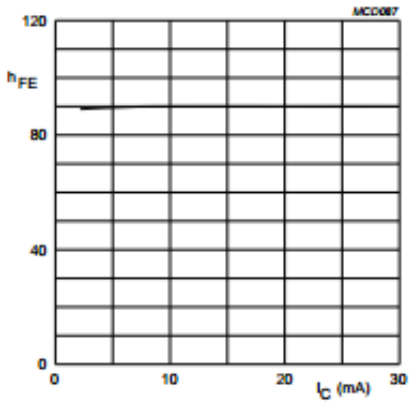

V_{CE} = 5 V; T_j = 25 °C.

Fig.4 DC current gain as a function of collector current.

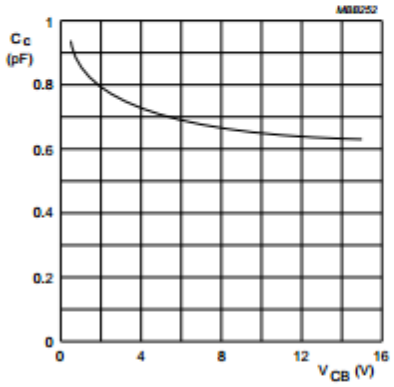

$I_E = i_e = 0$; f = 1 MHz; T_j = 25 °C.

Fig.5 Collector capacitance as a function of collector-base voltage; typical values.

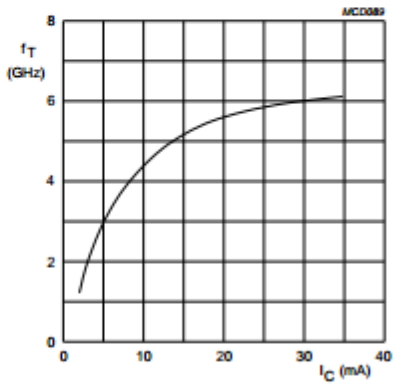

V_{CE} = 5 V; f = 500 MHz; T_j = 25 °C.

Fig.6 Transition frequency as a function of collector current; typical values.

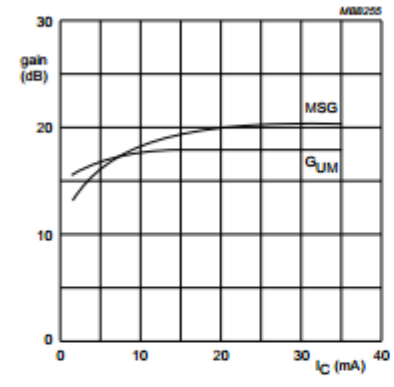

V_{CE} = 8 V; f = 500 MHz.

Fig.7 Gain as a function of collector current; typical values.

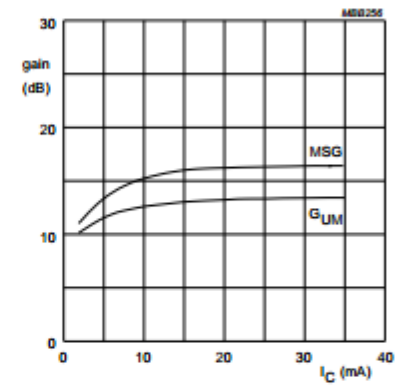

V_{CE} = 8 V; f = 1 GHz.

Fig.8 Gain as a function of collector current; typical values.

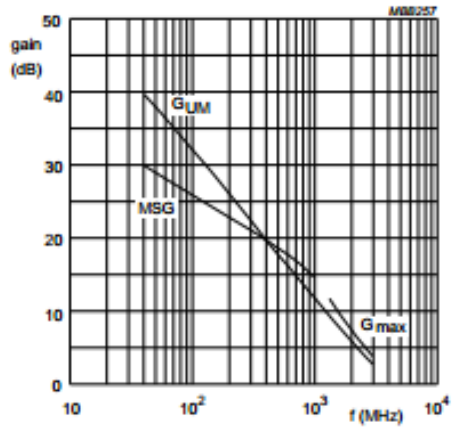

I_C = 10 mA; V_{CE} = 8 V.

Fig.9 Gain as a function of frequency; typical values.

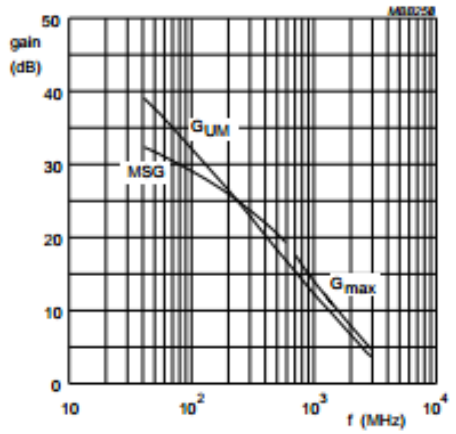

I_C = 30 mA; V_{CE} = 8 V.

Fig.10 Gain as a function of frequency; typical values.

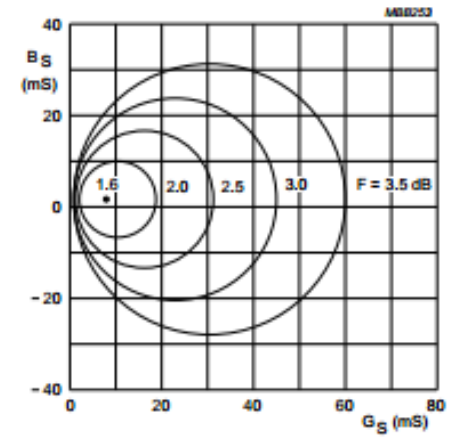

I_C = 4 mA; V_{CE} = 8 V; f = 800 MHz; T_{amb} = 25 °C.

Fig.11 Circles of constant noise figure; typical values.

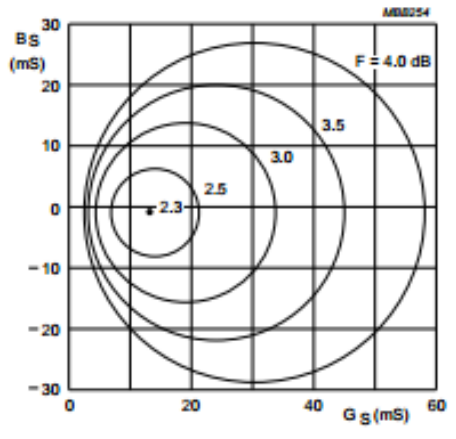

I_C = 4 mA; V_{CE} = 8 V; f = 800 MHz; T_{amb} = 25 °C.

Fig.12 Circles of constant noise figure; typical values.

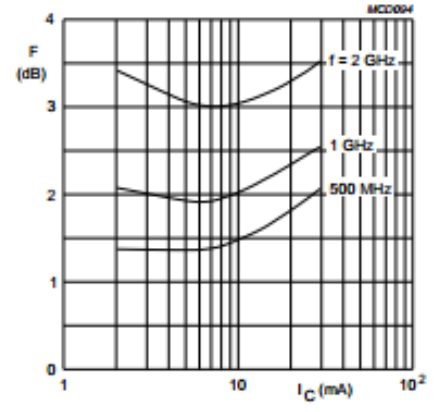

V_{CE} = 8 V.

Fig.13 Minimum noise figure as a function of collector current; typical values.

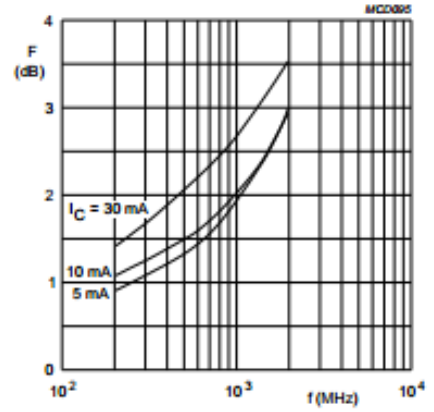

V_{CE} = 8 V.

Fig.14 Minimum noise figure as a function of frequency; typical values.

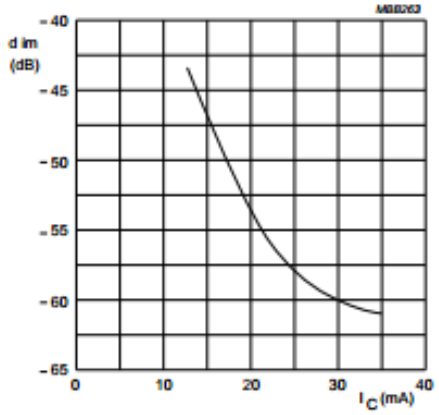

V_{CE} = 8 V; V_O = 425 mV (52.6 dBmV);
$f_p + f_q - f_r$ = 793.25 MHz; T_{amb} = 25 °C.
Measured in MATV test circuit (see Fig.2)

Fig.15 Intermodulation distortion; typical values.

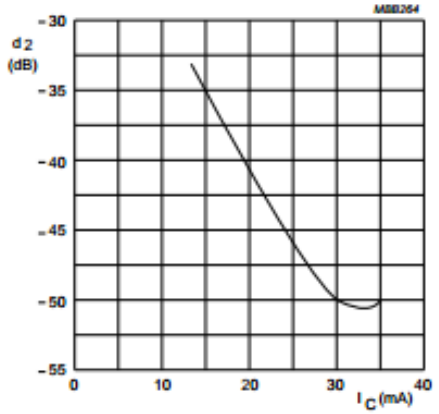

V_{CE} = 8 V; V_O = 200 mV (46 dBmV);
$f_p + f_q - f_r$ = 810 MHz; T_{amb} = 25 °C.
Measured in MATV test circuit (see Fig.2)

Fig.16 Second order intermodulation distortion; typical values.

Avago ATF 511P8

ATF-511P8

High Linearity Enhancement Mode[1] Pseudomorphic HEMT in 2x2 mm² LPCC[3] Package

Data Sheet

Description

Avago Technologies's ATF-511P8 is a single-voltage high linearity, low noise E-pHEMT housed in an 8-lead JEDEC-standard leadless plastic chip carrier (LPCC[3]) package. The device is ideal as a high linearity, low-noise, medium-power amplifier. Its operating frequency range is from 50 MHz to 6 GHz.

The thermally efficient package measures only 2 mm x 2 mm x 0.75 mm. Its backside metalization provides excellent thermal dissipation as well as visual evidence of solder reflow. The device has a Point MTTF of over 300 years at a mounting temperature of +85°C. All devices are 100% RF & DC tested.

Notes:
1. Enhancement mode technology employs a single positive V_{gs}, eliminating the need of negative gate voltage associated with conventional depletion mode devices.
2. Refer to reliability datasheet for detailed MTTF data.
3. Conforms to JEDEC reference outline MO229 for DRP-N.
4. Linearity Figure of Merit (LFOM) is essentially OIP3 divided by DC bias power.

Pin Connections and Package Marking

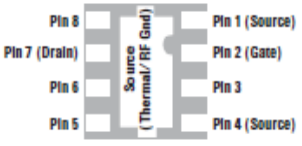

Bottom View

Top View

Note:
Package marking provides orientation and identification:
"1P" = Device Code
"x" = Date code indicates the month of manufacture.

Features

- Single voltage operation
- High linearity and P1dB
- Low noise figure
- Excellent uniformity in product specifications
- Small package size: 2.0 x 2.0 x 0.75 mm
- Point MTTF > 300 years[2]
- MSL-1 and lead-free
- Tape-and-reel packaging option available

Specifications

2 GHz; 4.5V, 200 mA (Typ.)

- 41.7 dBm output IP3
- 30 dBm output power at 1 dB gain compression
- 1.4 dB noise figure
- 14.8 dB gain
- 12.1 dB LFOM[4]
- 69% PAE

Applications

- Front-end LNA Q2 and Q3 driver or pre-driver amplifier for Cellular/PCS and WCDMA wireless infrastructure
- Driver amplifier for WLAN, WLL/RLL and MMDS applications
- General purpose discrete E-pHEMT for other high linearity applications

ATF-511P8 Absolute Maximum Ratings[1]

Symbol	Parameter	Units	Absolute Maximum
V_{DS}	Drain–Source Voltage[2]	V	7
V_{GS}	Gate–Source Voltage[2]	V	-5 to 1
V_{GD}	Gate Drain Voltage[2]	V	-5 to 1
I_{DS}	Drain Current[2]	A	1
I_{GS}	Gate Current	mA	46
P_{diss}	Total Power Dissipation[3]	W	3
$P_{in\,max.}$	RF Input Power[4]	dBm	+30
T_{CH}	Channel Temperature	°C	150
T_{STG}	Storage Temperature	°C	-65 to 150
Θ_{ch_b}	Thermal Resistance[5]	°C/W	33

Notes:
1. Operation of this device in excess of any one of these parameters may cause permanent damage.
2. Assumes DC quiescent conditions.
3. Board (package belly) temperature T_B is 25°C. Derate 30 mW/°C for T_B > 50°C.
4. With 10 Ohm series resistor in gate supply and 3:1 VSWR.
5. Channel-to-board thermal resistance measured using 150°C Liquid Crystal Measurement method.
6. Device can safely handle +30dBm RF Input Power provided I_{GS} limited to 46mA. I_{GS} at P_{1dB} drive level is bias circuit dependent.

Product Consistency Distribution Charts at 2 GHz, 4.5V, 200 mA[6,7]

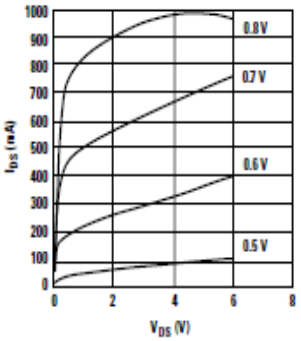

Figure 1. Typical I-V Curves (V_{gs} = 0.1 per step).

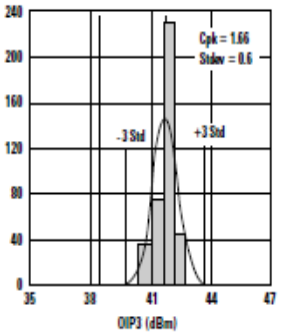

Figure 2. OIP3 LSL = 38.5, Nominal = 41.7.

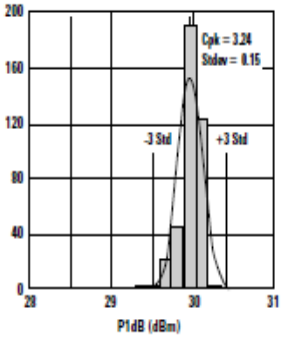

Figure 3. P1dB LSL = 28.5, Nominal = 30.

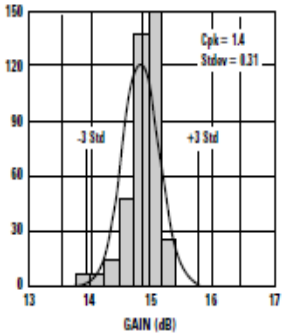

Figure 4. Gain LSL = 13.5, Nominal = 14.8, USL = 16.5.

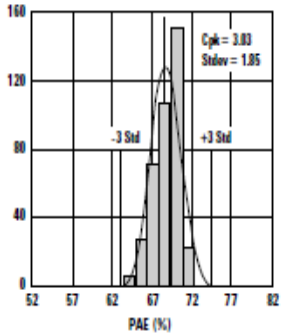

Figure 5. PAE LSL = 52, Nominal = 68.9.

Notes:
6. Distribution data sample size is 400 samples taken from 4 different wafers and 3 different lots. Future wafers allocated to this product may have nominal values anywhere between the upper and lower limits.
7. Measurements are made on production test board, which represents a trade-off between optimal OIP3, P1dB and VSWR. Circuit losses have been de-embedded from actual measurements.

ATF-511P8 Electrical Specifications

T_A = 25°C, DC bias for RF parameters is Vds = 4.5V and Ids = 200 mA unless otherwise specified.

Symbol	Parameter and Test Condition		Units	Min.	Typ.	Max.
Vgs	Operational Gate Voltage	Vds = 4.5V, Ids = 200 mA	V	0.25	0.51	0.8
Vth	Threshold Voltage	Vds = 4.5V, Ids = 32 mA	V	—	0.28	—
Idss	Saturated Drain Current	Vds = 4.5V, Vgs = 0V	µA	—	16.4	—
Gm	Transconductance	Vds = 4.5V, Gm = ΔIdss/ΔVgs; ΔVgs = Vgs1 – Vgs2 Vgs1 = 0.55V, Vgs2 = 0.5V	mmho	—	2178	—
Igss	Gate Leakage Current	Vds = 0V, Vgs = -4.5V	µA	-27	-2	—
NF	Noise Figure[1]	f = 2 GHz	dB	—	1.4	—
		f = 900 MHz	dB	—	1.2	—
G	Gain[1]	f = 2 GHz	dB	13.5	14.8	16.5
		f = 900 MHz	dB	—	17.8	—
OIP3	Output 3rd Order Intercept Point[1,2]	f = 2 GHz	dBm	38.5	41.7	—
		f = 900 MHz	dBm	—	43	—
P1dB	Output 1dB Compressed[1]	f = 2 GHz	dBm	28.5	30	—
		f = 900 MHz	dBm	—	29.6	—
PAE	Power Added Efficiency	f = 2 GHz	%	52	68.9	—
		f = 900 MHz	%	—	68.6	—
ACLR	Adjacent Channel Leakage Power Ratio[1,3]	Offset BW = 5 MHz	dBc	—	-58.9	—
		Offset BW = 10 MHz	dBc	—	-62.7	—

Notes:

1. Measurements obtained using production test board described in Figure 6 and PAE tested at P1dB condition.
2. I) 2 GHz OIP3 test condition: F1 = 2.0 GHz, F2 = 2.01 GHz and Pin = -5 dBm per tone.
   II) 900 MHz OIP3 test condition: F1 = 900 MHz, F2 = 910 MHz and Pin = -5 dBm per tone.
3. ACLR test spec is based on 3GPP TS 25.141 V5.3.1 (2002-06)
   - Test Model 1
   - Active Channels: PCCPCH + SCH + CPICH + PICH + SCCPCH + 64 DPCH (SF=128)
   - Freq = 2140 MHz
   - Pin = -5 dBm
   - Channel Integrate Bandwidth = 3.84 MHz
4. Use proper bias, board, heatsink and derating designs to ensure maximum channel temperature is not exceeded. See absolute maximum ratings and application note for more details.

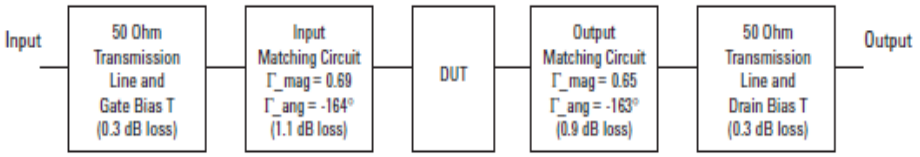

Figure 6. Block diagram of the 2 GHz production test board used for NF, Gain, OIP3 , P1dB and PAE and ACLR measurements. This circuit achieves a trade-off between optimal OIP3, P1dB and VSWR. Circuit losses have been de-embedded from actual measurements.

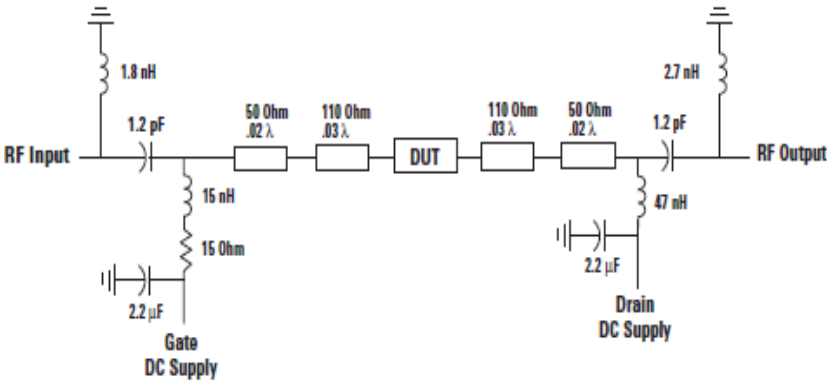

Figure 7. Simplified schematic of production test board. Primary purpose is to show 15 Ohm series resistor placement in gate supply. Transmission line tapers, tee intersections, bias lines and parasitic values are not shown.

Gamma Load and Source at Optimum OIP3 and P1dB Tuning Conditions

The device's optimum OIP3 and P1dB measurements were determined using a load pull system at 4.5V, 200 mA quiesent bias:

Optimum OIP3

Freq	Gamma Source		Gamma Load		OIP3	Gain	P1dB	PAE
(GHz)	Mag	Ang	Mag	Ang	(dBm)	(dB)	(dBm)	(%)
0.9	0.776	152	0.549	-178	43.3	17.94	29.63	63.8
2.0	0.872	-171	0.683	-179	43.1	15.06	30.12	66.8
2.4	0.893	-162	0.715	-174	42.8	14.03	29.90	64.5
3.9	0.765	-132	0.574	-144	41.7	9.47	29.02	52

Optimum P1dB

Freq	Gamma Source		Gamma Load		OIP3	Gain	P1dB	PAE
(GHz)	Mag	Ang	Mag	Ang	(dBm)	(dB)	(dBm)	(%)
0.9	0.773	153	0.784	-173	38.0	19.28	31.9	54.23
2.0	0.691	147	0.841	-166	36.4	10.34	31.4	38.15
2.4	0.797	164	0.827	-166	36.2	8.43	31.2	37.38
3.9	0.602	-163	0.794	-155	35.4	7.03	31	32.72

ATF-511P8 Typical Performance Curves (at 25°C unless specified otherwise)
Tuned for Optimal OIP3 at 4.5V 200 mA

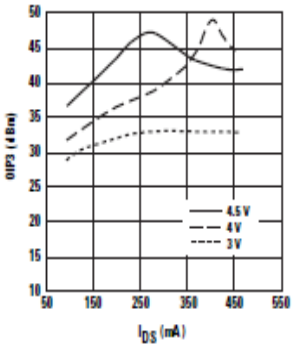

Figure 8. OIP3 vs. I_{DS} and V_{DS} at 2 GHz.

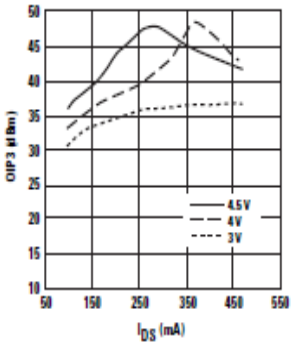

Figure 9. OIP3 vs. I_{DS} and V_{DS} at 900 MHz.

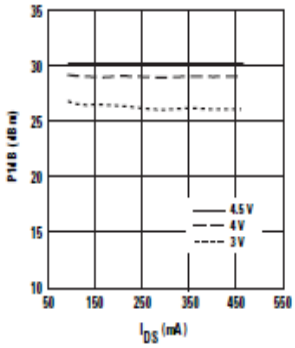

Figure 10. P1dB vs. I_{DS} and V_{DS} at 2 GHz.

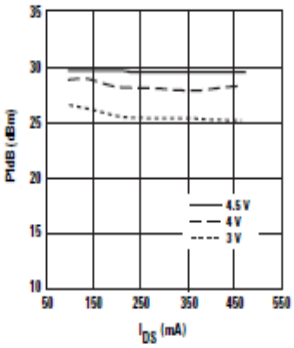

Figure 11. P1dB vs. I_{DS} and V_{DS} at 900 MHz.

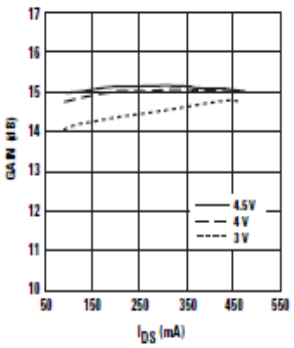

Figure 12. Gain vs. I_{DS} and V_{DS} at 2 GHz.

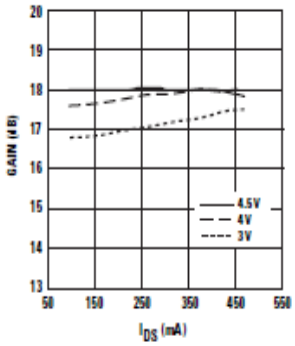

Figure 13. Gain vs. I_{DS} and V_{DS} at 900 MHz.

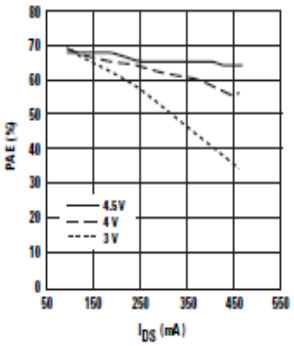

Figure 14. PAE vs. I_{DS} and V_{DS} at 2 GHz.

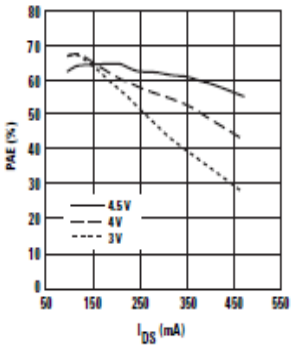

Figure 15. PAE vs. I_{DS} and V_{DS} at 900 MHz.

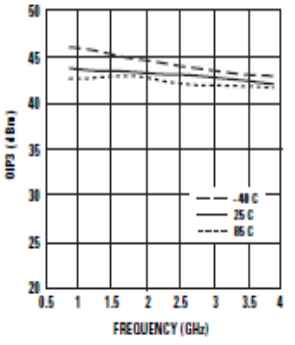

Figure 16. OIP3 vs. Temp and Freq.

Note:
Bias current for the above charts are quiescent conditions. Actual level may increase or decrease depending on amount of RF drive.

ATF-511P8 Typical Performance Curves, continued (at 25°C unless specified otherwise)
Tuned for Optimal OIP3 at 4.5V, 200 mA

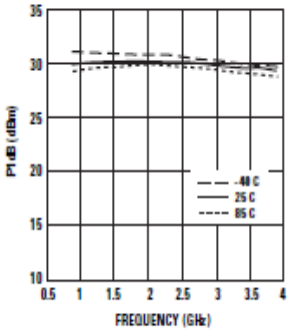

Figure 17. P1dB vs. Temp and Freq.

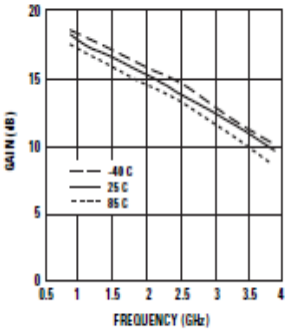

Figure 18. Gain vs. Temp and Freq.

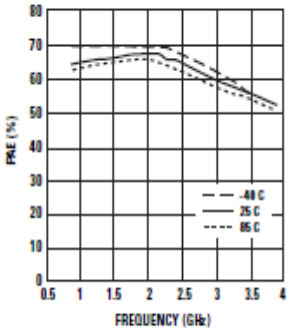

Figure 19. PAE vs. Temp and Freq.

ATF-511P8 Typical Performance Curves (at 25°C unless specified otherwise)
Tuned for Optimal P1dB at 4.5 V, 200 mA

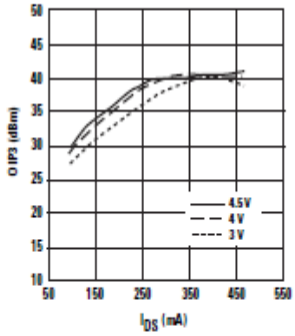

Figure 20. OIP3 vs. I_{DS} and V_{DS} at 2 GHz.

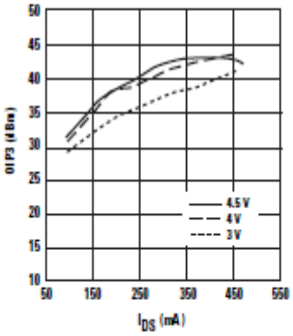

Figure 21. OIP3 vs. I_{DS} and V_{DS} at 900 MHz.

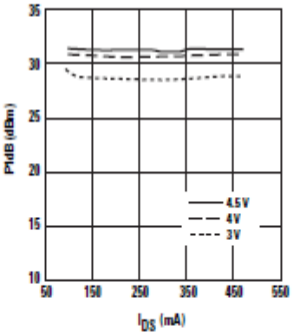

Figure 22. P1dB vs. I_{DS} and V_{DS} at 2 GHz.

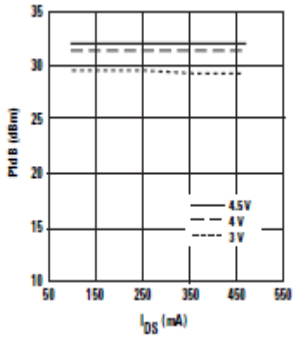

Figure 23. P1dB vs. I_{DS} and V_{DS} at 900 MHz.

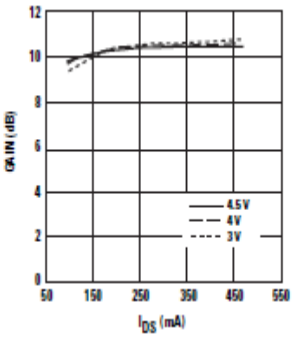

Figure 24. Gain vs. I_{DS} and V_{DS} at 2 GHz.

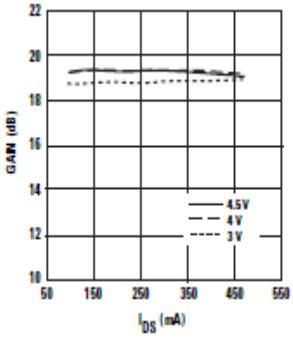

Figure 25. Gain vs. I_{DS} and V_{DS} at 900 MHz.

Note:
Bias current for the above charts are quiescent conditions. Actual level may increase or decrease depending on amount of RF drive.

ATF-511P8 Typical Performance Curves, continued (at 25°C unless specified otherwise)
Tuned for Optimal P1dB at 4.5V, 200 mA

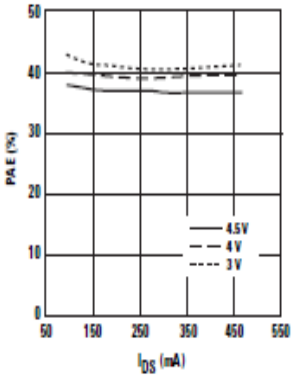

Figure 26. PAE vs. I_{DS} and V_{DS} at 2 GHz.

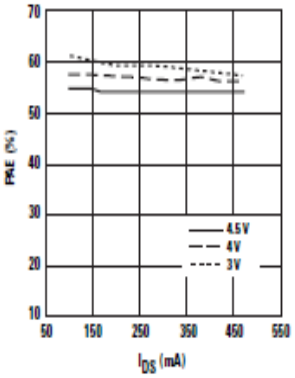

Figure 27. PAE vs. I_{DS} and V_{DS} at 900 MHz.

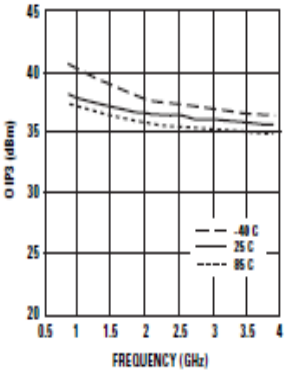

Figure 28. OIP3 vs. Temp and Freq.

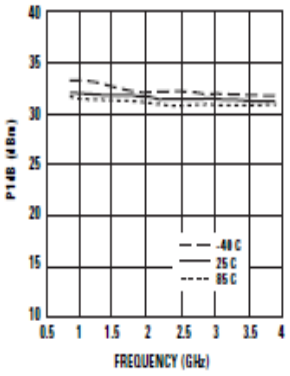

Figure 29. P1dB vs. Temp and Freq.

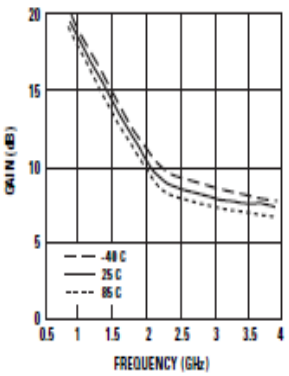

Figure 30. Gain vs. Temp and Freq.

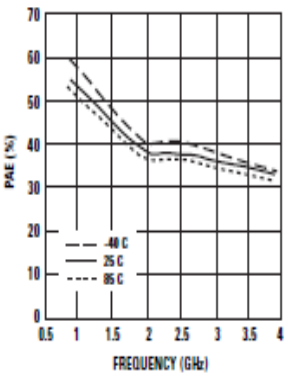

Figure 31. PAE vs. Temp and Freq.

Note:
Bias current for the above charts are quiescent conditions. Actual level may increase or decrease depending on amount of RF drive.

ATF-511P8 Typical Scattering Parameters, V_{DS} = 4.5V, I_{DS} = 300 mA

Freq.	S_{11}		S_{21}			S_{12}			S_{22}		MSG/MAG
GHz	Mag.	Ang.	dB	Mag.	Ang.	dB	Mag.	Ang.	Mag.	Ang.	dB
0.1	0.94	-134.9	31.16	36.15	111.2	-38.53	0.01	29.7	0.73	-164.5	34.79
0.2	0.93	-157.7	25.64	19.14	99.2	-37.87	0.01	21.8	0.76	-173.7	31.68
0.3	0.93	-166.6	22.26	12.97	94.2	-37.61	0.01	21.1	0.78	-176.8	29.99
0.4	0.93	-171.8	19.78	9.74	90.9	-37.09	0.01	23.4	0.78	-179.9	28.43
0.5	0.92	-173.9	18.70	8.60	88.9	-36.15	0.01	25.4	0.75	178.9	27.31
0.6	0.93	-176.9	17.12	7.18	86.1	-35.80	0.01	27.0	0.75	176.9	26.52
0.7	0.92	-178.8	15.78	6.15	84.3	-35.41	0.01	29.5	0.75	175.5	25.59
0.8	0.93	178.7	14.61	5.37	82.3	-35.11	0.01	32.5	0.76	174.0	24.75
0.9	0.92	177.1	13.58	4.77	80.6	-35.00	0.01	33.1	0.75	172.8	24.24
1	0.93	175.7	12.64	4.28	79.1	-34.46	0.01	35.0	0.76	171.6	23.53
1.5	0.93	168.7	8.99	2.81	71.4	-32.70	0.02	40.0	0.76	166.0	20.88
2	0.93	163.0	6.36	2.08	64.2	-31.27	0.02	42.3	0.76	160.6	17.20
2.5	0.92	157.8	4.40	1.66	57.2	-29.90	0.03	42.5	0.76	155.5	14.71
3	0.92	152.5	2.73	1.36	50.4	-28.59	0.03	41.6	0.75	149.7	12.65
4	0.92	142.8	0.03	1.00	37.6	-26.69	0.04	35.7	0.74	138.6	9.96
5	0.91	133.2	-2.17	0.77	24.2	-25.30	0.05	29.8	0.71	127.2	7.23
6	0.91	124.6	-4.21	0.61	14.1	-24.32	0.06	23.7	0.65	117.2	4.97
7	0.91	115.7	-5.80	0.51	5.6	-23.48	0.06	19.5	0.59	111.3	3.02
8	0.91	106.0	-6.82	0.45	-2.6	-22.49	0.07	14.1	0.56	108.2	1.86
9	0.91	95.5	-7.36	0.42	-10.2	-21.39	0.08	8.5	0.58	103.7	1.19
10	0.90	85.2	-7.98	0.40	-22.2	-20.50	0.09	0.4	0.60	96.0	0.53
11	0.89	74.3	-8.69	0.38	-29.1	-19.72	0.10	-8.4	0.63	87.2	-0.04
12	0.89	63.0	-9.25	0.35	-40.1	-19.42	0.10	-17.1	0.65	77.6	-0.61
13	0.89	54.1	-9.80	0.32	-51.7	-19.12	0.11	-23.9	0.67	68.2	-1.04
14	0.90	46.3	-10.25	0.31	-55.2	-18.65	0.11	-29.7	0.69	58.7	-1.13
15	0.90	40.6	-10.86	0.30	-57.3	-18.57	0.11	-35.8	0.69	50.1	-1.88
16	0.89	33.3	-11.16	0.32	-71.1	-18.02	0.12	-42.3	0.71	41.8	-2.26
17	0.83	25.4	-11.81	0.24	-75.3	-17.65	0.13	-47.1	0.73	35.1	-3.17
18	0.86	20.0	-12.07	0.24	-90.5	-17.43	0.13	-53.1	0.76	27.7	-3.76

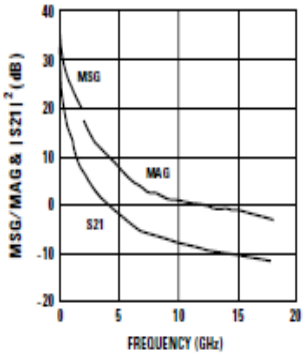

Figure 32. MSG/MAG & $|S21|^2$ (dB) @ 4.5V, 300 mA.

Notes:
1. S parameter is measured on a microstrip line made on 0.025 inch thick alumina carrier. The input reference plane is at the end of the gate lead. The output reference plane is at the end of the drain lead.

Accu-P®

Thin-Film Chip Capacitors for RF Signal and Power Applications

AVX RF

1

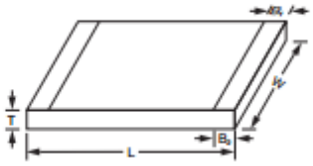

ACCU-P® (Signal and Power Type Capacitors)

	01005*	0201*	0402*	0603*	0805*	1210
L	0.405±0.020 (0.016±0.001)	0.60±0.05 (0.023±0.002)	1.00±0.1 (0.039±0.004)	1.60±0.1 (0.063±0.004)	2.01±0.1 (0.079±0.004)	3.02±0.1 (0.119±0.004)
W	0.215 ± 0.020 (0.0085 ± 0.001)	0.325±0.050 (0.0128±0.002)	0.55±0.07 (0.022±0.003)	0.81±0.1 (0.032±0.004)	1.27±0.1 (0.050±0.004)	2.5±0.1 (0.100±0.004)
T	0.145 ± 0.020 (0.006 ± 0.001)	0.225±0.050 (0.009±0.002)	0.40±0.1 (0.016±0.004)	0.63±0.1 (0.025±0.004)	0.93±0.2 (0.036±0.008)	0.93±0.2 (0.036±0.008)
B_1	0.00 $^{+0.1}_{-0.0}$ (0.000 $^{+0.004}_{-0.000}$)	0.10±0.10 (0.004±0.004)	0.00 $^{+0.1}_{-0.0}$ (0.000 $^{+0.004}_{-0.000}$)	0.35±0.15 (0.014±0.006)	0.30±0.1 (0.012±0.004)	0.43±0.1 (0.017±0.004)
B_2	0.10 ± 0.03 (0.004 ± 0.001)	0.15±0.05 (0.006±0.002)	0.20±0.1 (0.008±0.004)	0.35±0.15 (0.014±0.006)	0.30±0.1 (0.012±0.004)	0.43±0.1 (0.017±0.004)

*Mount Black Side Up

DIMENSIONS: millimeters (inches)

HOW TO ORDER

0402 | 3 | J | 4R7 | A | B | S | TR

Size
C005
0201
0402
0603
0805
1210*

Voltage
2 = 200V
1 = 100V
5 = 50V
3 = 25V
Y = 16V
Z = 10V

Temperature Coefficient (1)
J = 0±30ppm/°C (-55°C to +125°C)
K = 0±60ppm/°C (-55°C to +125°C)

Capacitance
Capacitance expressed in pF. (2 significant digits + number of zeros)
for values <10pF, letter R denotes decimal point.
Example:
68pF = 680
8.2pF = 8R2

Tolerance for C≤2.0pF*
Z = ±0.01pF
P = ±0.02pF
Q = ±0.03pF
A = ±0.05pF
B = ±0.1pF
C = ±0.25pF

for C≤3.0pF
Q = ±0.03pF
A = ±0.05pF
B = ±0.1pF
C = ±0.25pF

for C≤5.6pF
A = ±0.05pF
B = ±0.1pF
C = ±0.25pF

for 5.6pF<C<10pF
B = ±0.1pF
C = ±0.25pF
D = ±0.5pF

for C≥10pF
F = ±1%
G = ±2%
J = ±5%

Specification Code
B = Accu-P® technology

Termination Code
W = Nickel/Solder Coated *Accu-P® 0402* Sn90, Pb10***
T = Nickel/High Temperature Solder Coated *Accu-P® 0805**, 1210**** Sn96, Ag4
Nickel/Solder Coated *Accu-P® 0603**** Sn63, Pb37
**S = Nickel/Lead Free Solder Coated *Accu-P® 01005, 0201, 0402, 0603* Sn100

Packaging Code
TR = Tape & Reel

(1) TC's shown are per EIA/IEC Specifications.

Engineering Kits Available
see pages 114-115

* Tolerances as tight as ±0.01pF are available. Please consult the factory.

**RoHS compliant
*** Not RoHS Compliant

LEAD-FREE
LEAD-FREE COMPATIBLE COMPONENT

RoHS COMPLIANT

For RoHS compliant products, please select correct termination style.

ELECTRICAL SPECIFICATIONS

Operating and Storage Temperature Range	-55°C to +125°C
Temperature Coefficients(1)	0 ± 30ppm/°C dielectric code "J" / 0 ± 60ppm/°C dielectric code "K"
Capacitance Measurement	1 MHz, 1 Vrms
Insulation Resistance (IR)	≥10^{11} Ohms (≥10^{10} Ohms for 0201 and 0402 size)
Proof Voltage	2.5 U_R for 5 secs.
Aging Characteristic	Zero
Dielectric Absorption	0.01%

Accu-P®

0603 Typical Electrical Tables

AVX RF

1

Capacitance @ 1MHz and Tolerance		Self Resonance Frequency (GHz) Typ.	Q Standard Value @ 1GHz		Frequency 900MHz			Frequency 1900MHz			Frequency 2400MHz		
C (pF)	Tol.		Typ.	Min.	C(eff) (pF) Typ.	Q Typ.	ESR (mOhm) Typ.	C(eff) (pF) Typ.	Q Typ.	ESR (mOhm) Typ.	C(eff) (pF) Typ.	Q Typ.	ESR (mOhm) Typ.
0.05	±0.02	25.6	1200	660	0.00	1333	945	0.00	556	832	0.00	397	880
0.1	±0.02	18.1	1156	636	0.00	1284	675	0.00	535	628	0.00	382	667
0.15	±0.02	14.8	1111	611	0.00	1235	555	0.00	514	533	0.00	367	567
0.2	±0.02	12.8	1067	587	0.00	1185	483	0.00	494	474	0.00	353	505
0.25	±0.02	11.4	1022	562	0.00	1136	433	0.00	473	433	0.00	338	462
0.3	±0.02	10.4	978	538	0.31	1086	397	0.32	453	402	0.32	323	430
0.35	±0.02	9.7	933	513	0.00	1037	368	0.00	432	378	0.00	309	404
0.4	±0.02	9.0	889	489	0.00	988	345	0.00	412	358	0.00	294	383
0.45	±0.02	8.5	844	464	0.00	938	326	0.00	391	341	0.00	279	365
0.5	±0.02	8.1	800	440	0.00	889	310	0.00	370	327	0.00	265	350
0.55	±0.02	7.7	788	434	0.00	875	296	0.00	363	315	0.00	261	337
0.6	±0.02	7.4	777	427	0.00	860	283	0.00	356	304	0.00	258	326
0.65	±0.02	7.1	765	421	0.00	846	273	0.00	348	294	0.00	255	315
0.7	±0.02	6.8	754	414	0.72	832	263	0.72	341	285	0.73	252	306
0.75	±0.02	6.6	742	408	0.00	817	254	0.00	334	277	0.00	248	298
0.8	±0.02	6.4	730	402	0.00	803	247	0.00	326	270	0.00	245	290
0.85	±0.02	6.2	719	395	0.00	789	239	0.00	319	264	0.00	242	283
0.9	±0.02	6.0	707	389	0.00	775	233	0.00	312	258	0.00	239	277
0.95	±0.02	5.9	696	383	0.00	760	227	0.00	304	252	0.00	235	271
1	±0.02	5.7	684	376	1.019	746	216	1.061	297	242	1.101	232	260
1.05	±0.02	5.6	667	367	1.076	731	213	1.126	290	239	1.171	226	256
1.1	±0.02	5.4	649	357	1.134	717	210	1.190	282	236	1.241	220	253
1.15	±0.02	5.3	632	347	1.192	702	206	1.254	275	233	1.311	214	250
1.2	±0.02	5.2	614	338	1.250	687	203	1.318	267	230	1.381	209	247
1.25	±0.02	5.1	605	333	1.307	677	200	1.382	262	227	1.451	203	244
1.3	±0.02	5.0	596	328	1.365	667	197	1.446	257	224	1.521	197	241
1.35	±0.02	4.9	587	323	1.423	658	194	1.511	252	221	1.591	191	238
1.4	±0.02	4.8	578	318	1.481	648	190	1.575	247	218	1.661	185	235
1.45	±0.02	4.8	569	313	1.538	638	187	1.639	242	215	1.731	179	232
1.5	±0.02	4.7	560	308	1.596	628	184	1.703	237	212	1.801	173	229
1.55	±0.02	4.6	551	303	1.645	620	181	1.760	233	209	1.866	170	226
1.6	±0.02	4.5	542	298	1.694	611	178	1.817	228	206	1.930	166	222
1.65	±0.02	4.5	534	293	1.743	603	175	1.874	224	203	1.995	163	219
1.7	±0.02	4.4	525	289	1.792	595	172	1.931	219	200	2.060	159	216
1.75	±0.02	4.3	516	284	1.841	587	169	1.988	215	197	2.124	156	213
1.8	±0.02	4.2	507	279	1.890	578	166	2.045	211	194	2.189	153	209
1.85	±0.02	4.2	498	274	1.939	570	163	2.102	206	191	2.253	149	206
1.9	±0.02	4.1	490	269	1.988	562	160	2.158	202	188	2.318	146	203
1.95	±0.02	4.1	481	264	2.037	553	157	2.215	197	185	2.383	142	199
2	±0.03	4.0	472	260	2.086	545	154	2.272	193	182	2.447	139	196
2.1	±0.03	3.9	462	254	2.190	535	151	2.402	187	180	2.604	134	193
2.2	±0.03	3.8	452	249	2.295	524	148	2.532	181	177	2.761	129	191
2.3	±0.03	3.8	442	243	2.400	514	145	2.662	175	175	2.917	124	188
2.4	±0.03	3.7	433	238	2.504	503	143	2.793	168	172	3.074	118	186
2.5	±0.03	3.6	423	232	2.609	493	140	2.923	162	170	3.230	113	183
2.6	±0.03	3.6	413	227	2.714	482	137	3.053	156	167	3.387	108	181
2.7	±0.03	3.5	403	222	2.818	472	134	3.183	150	165	3.543	103	178
2.8	±0.03	3.4	395	217	2.933	463	133	3.336	147	164	3.742	100	177
2.9	±0.03	3.4	388	213	3.047	453	131	3.489	144	162	3.940	97	175
3	±0.03	3.3	380	209	3.162	444	130	3.642	140	161	4.139	95	174
3.1	±0.05	3.2	372	205	3.276	435	129	3.795	137	160	4.337	92	172
3.2	±0.05	3.2	365	201	3.391	425	127	3.947	134	159	4.536	89	171
3.3	±0.05	3.1	357	196	3.506	416	126	4.100	131	157	4.734	86	169
3.4	±0.05	3.1	349	192	3.620	407	125	4.253	128	156	4.933	84	168
3.5	±0.05	3.1	342	188	3.735	397	123	4.406	125	155	5.131	81	166
3.6	±0.05	3.0	334	184	3.849	388	122	4.559	121	154	5.330	78	165
3.7	±0.05	3.0	326	179	3.964	379	121	4.712	118	152	5.528	75	164
3.8	±0.05	3.0	318	175	4.078	369	119	4.865	115	151	5.727	73	162
3.9	±0.05	2.9	311	171	4.193	360	118	5.018	112	150	5.925	70	161

Accu-P®

0603 Typical Electrical Tables

Capacitance @ 1MHz and Tolerance		Self Resonance Frequency (GHz) Typ.	Q Standard Value @ 1GHz		Frequency 900MHz			Frequency 1900MHz			Frequency 2400MHz		
C (pF)	Tol.		Typ.	Min.	C(eff) (pF) Typ.	Q Typ.	ESR (mOhm) Typ.	C(eff) (pF) Typ.	Q Typ.	ESR (mOhm) Typ.	C(eff) (pF) Typ.	Q Typ.	ESR (mOhm) Typ.
4	±0.05	2.9	307	169	4.301	355	117	5.188	110	149	6.188	68	160
4.1	±0.05	2.8	303	167	4.410	351	116	5.358	108	148	6.450	67	159
4.2	±0.05	2.8	299	164	4.518	347	116	5.528	106	148	6.713	65	158
4.3	±0.05	2.7	295	162	4.627	342	115	5.698	104	147	6.975	64	157
4.4	±0.05	2.7	291	160	4.735	338	114	5.867	102	146	7.238	62	157
4.5	±0.05	2.7	287	158	4.843	333	113	6.037	100	146	7.500	61	156
4.6	±0.05	2.6	283	156	4.952	329	112	6.207	98	145	7.763	59	155
4.7	±0.05	2.6	279	154	5.060	324	112	6.377	96	144	8.025	58	154
5.1	±0.05	2.5	263	145	5.494	307	109	7.057	88	142	9.075	52	151
5.6	±0.05	2.4	244	134	6.035	285	105	7.906	78	138	10.39	44	147
6.2	±0.1	2.3	228	126	6.865	267	102	9.517	72	133	13.66	40	141
6.8	±0.1	2.2	213	117	7.694	250	100	11.13	66	128	16.93	35	135
7.5	±0.1	2.1	196	107	8.367	227	98	12.63	57	125	20.91	28	132
8.2	±0.1	2.0	176	97	9.041	205	96	14.14	49	123	24.88	21	129
9.1	±0.1	1.9	161	89	10.20	188	96	18.09	42	122	40.00	16	128
10	±1%	1.8	146	80	11.37	171	95	22.05	36	121	70.00	12	127
11	±1%	1.7	129	71	12.66	153	95	26.44	29	120	140.0	6	126
12	±1%	1.6	112	62	13.95	134	94	30.83	22	119	231.3	1	125
13	±1%	1.6	102	56	15.31	122	93	40.37	18	118	n/a	n/a	n/a
14	±1%	1.5	92	51	16.67	111	92	49.91	15	118	n/a	n/a	n/a
15	±1%	1.5	82	45	18.03	99	90	59.44	11	117	n/a	n/a	n/a
16	±1%	1.4	79	43	19.61	96	90	80.00	8	117	n/a	n/a	n/a
17	±1%	1.4	76	42	21.18	92	90	120.0	6	116	n/a	n/a	n/a
18	±1%	1.3	73	40	22.76	89	90	190.0	4	116	n/a	n/a	n/a
19	±1%	1.3	69	38	24.37	84	89	n/a	n/a	n/a	n/a	n/a	n/a
20	±1%	1.2	65	36	25.98	80	89	n/a	n/a	n/a	n/a	n/a	n/a
22	±1%	1.2	57	31	29.21	72	87	n/a	n/a	n/a	n/a	n/a	n/a
24	±1%	1.2	48	26	34.44	62	87	n/a	n/a	n/a	n/a	n/a	n/a
27	±1%	1.1	43	24	41.87	56	86	n/a	n/a	n/a	n/a	n/a	n/a
30	±1%	1.0	37	21	49.29	49	85	n/a	n/a	n/a	n/a	n/a	n/a
33	±1%	1.0	32	18	56.72	43	84	n/a	n/a	n/a	n/a	n/a	n/a
36	±1%	1.0	27	15	64.15	37	83	n/a	n/a	n/a	n/a	n/a	n/a
39	±5%	1.0	21	12	71.57	30	82	n/a	n/a	n/a	n/a	n/a	n/a

Document 537-1

Chip Inductors – 0603HP Series (1608)

- Higher Q and lower DCR than other 0603 inductors
- Highest SRF values – as high as 16 GHz
- Excellent current handling capability – up to 2100 mA
- 54 inductance values from 1.8 to 390 nH

Typical Q vs Frequency

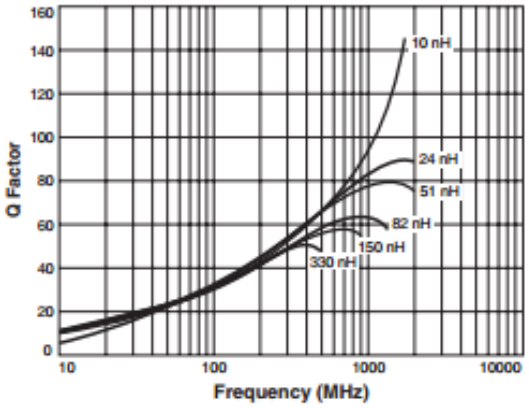

Typical L vs Frequency

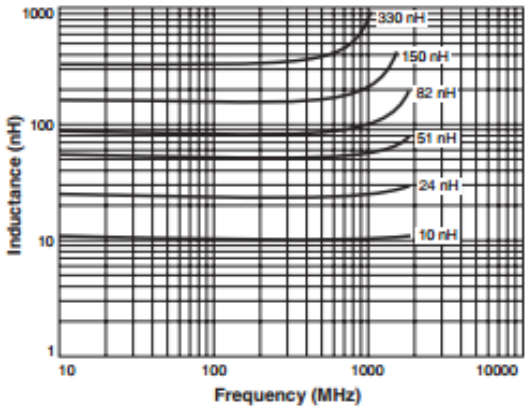

Current Derating

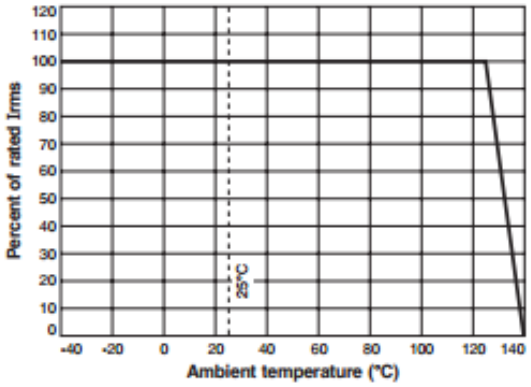

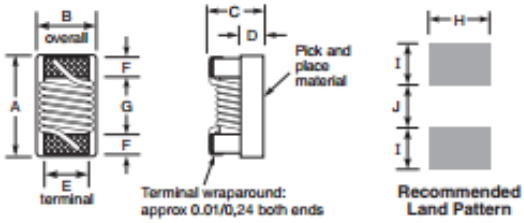

A max	B (min–max)	C max	D	E	F	G	H	I	J	
0.069	0.034–0.043	0.037	0.015	0.029	0.013	0.038	0.040	0.027	0.028	inches
1,75	0,86–1,09	0,94	0,38	0,74	0,33	0,96	1,02	0,69	0,71	mm

Note: Height dimension (C) is before optional solder application. For maximum height dimension including solder, add 0.006 in / 0,152 mm.

Core material Ceramic

Environmental RoHS compliant, halogen free optional

Terminations RoHS compliant silver-palladium-platinum-glass frit. Other terminations available at additional cost.

Weight 2.0 – 3.2 mg

Ambient temperature –40°C to +125°C with Irms current, +125°C to +140°C with derated current

Storage temperature Component: –40°C to +140°C. Tape and reel packaging: –40°C to +80°C

Resistance to soldering heat Max three 40 second reflows at +260°C, parts cooled to room temperature between cycles

Temperature Coefficient of Inductance (TCL) +25 to +125 ppm/°C

Moisture Sensitivity Level (MSL) 1 (unlimited floor life at <30°C / 85% relative humidity)

Failures in Time (FIT) / Mean Time Between Failures (MTBF) One per billion hours / one billion hours, calculated per Telcordia SR-332

Packaging 2000 per 7" reel. Paper tape: 8 mm wide, 1 mm thick, 4 mm pocket spacing

PCB washing Tested with pure water or alcohol only. For other solvents, see Doc787_PCB_Washing.pdf.

Coilcraft
www.coilcraft.com

US +1-847-639-6400 sales@coilcraft.com
UK +44-1236-730595 sales@coilcraft-europe.com
Taiwan +886-2-2264 3646 sales@coilcraft.com.tw
China +86-21-6218 8074 sales@coilcraft.com.cn
Singapore + 65-6484 8412 sales@coilcraft.com.sg

Document 537-1 Revised 03/25/13

0603HP Series (1608)

Designer's Kits C406A and B contain 10 each of all 5% values
Designer's Kits C406A-2 and B-2 contain 10 each of all 2% values

Part number[1]	Inductance[2] (nH)	Percent tol	L test freq (MHz)	Q typ at 250 MHz	900 MHz L typ	900 MHz Q typ[3]	1.7 GHz L typ	1.7 GHz Q typ[3]	SRF typ[4] (GHz)	DCR max[5] (Ohms)	Irms[6] (mA)	Color code
0603HP-1N8XJL_	1.8	**5**	250	23	1.77	40	1.77	65	16.0	0.033	2100	Black
0603HP-2N2XJL_	2.2	**5**	250	13	2.14	25	2.12	35	15.0	0.180	900	Yellow
0603HP-3N3X_L_	3.3	**5,3,2**	250	32	3.28	67	3.32	104	9.60	0.024	1900	Blue
0603HP-3N6X_L_	3.6	**5,3,2**	250	40	3.59	70	3.62	116	9.70	0.031	1900	Red
0603HP-3N9X_L_	3.9	**5,3,2**	250	35	3.88	68	3.95	108	7.50	0.039	1600	Brown
0603HP-4N3X_L_	4.3	**5,3,2**	250	30	4.29	58	4.31	91	7.50	0.080	1300	Orange
0603HP-4N7X_L_	4.7	**5,3,2**	250	26	4.65	48	4.71	75	7.90	0.100	1100	Violet
0603HP-5N1X_L_	5.1	**5,3,2**	250	40	5.08	84	5.12	140	8.90	0.036	1700	Green
0603HP-5N6X_L_	5.6	**5,3,2**	250	48	5.60	87	5.73	145	6.60	0.036	1700	Black
0603HP-6N0X_L_	6.0	**5,3,2**	250	49	5.92	94	6.12	154	6.00	0.036	1700	White
0603HP-6N8X_L_	6.8	**5,3,2**	250	42	6.83	88	7.05	143	5.80	0.042	1400	Red
0603HP-7N2X_L_	7.2	**5,3,2**	250	48	7.25	96	7.38	139	5.40	0.052	1400	Green
0603HP-7N5X_L_	7.5	**5,3,2**	250	41	7.55	81	7.85	112	5.30	0.080	1300	Brown
0603HP-8N2X_L_	8.2	**5,3,2**	250	46	8.21	96	8.39	148	5.90	0.054	1400	Orange
0603HP-8N7X_L_	8.7	**5,3,2**	250	46	8.73	97	9.00	149	5.50	0.054	1400	Yellow
0603HP-9N1X_L_	9.1	**5,3,2**	250	40	9.18	76	9.64	109	5.10	0.037	1400	Black
0603HP-9N5X_L_	9.5	**5,3,2**	250	49	9.56	98	9.99	149	4.90	0.053	1400	Blue
0603HP-10NX_L_	10	**5,3,2**	250	49	10.16	90	10.64	142	4.30	0.048	1400	Orange
0603HP-11NX_L_	11	**5,3,2**	250	41	11.06	78	11.82	108	4.10	0.058	1400	Gray
0603HP-12NX_L_	12	**5,3,2**	250	37	12.26	69	13.20	91	4.10	0.088	1100	Yellow
0603HP-15NX_L_	15	**5,3,2**	250	48	15.41	83	17.20	124	3.60	0.078	1200	Green
0603HP-16NX_L_	16	**5,3,2**	250	45	16.37	77	18.70	116	3.50	0.085	1100	White
0603HP-18NX_L_	18	**5,3,2**	250	41	18.56	76	20.90	100	3.30	0.066	1200	Blue
0603HP-22NX_L_	22	**5,3,2**	250	44	22.7	77	25.90	88	3.15	0.140	850	Violet
0603HP-23NX_L_	23	**5,3,2**	250	40	24.0	69	29.53	80	3.00	0.183	850	Orange
0603HP-24NX_L_	24	**5,3,2**	250	42	24.9	77	28.90	91	2.95	0.074	1100	Black
0603HP-27NX_L_	27	**5,3,2**	250	44	28.4	74	34.00	84	2.80	0.150	780	Gray
0603HP-30NX_L_	30	**5,3,2**	250	49	31.5	82	37.90	82	2.80	0.130	920	Brown
0603HP-33NX_L_	33	**5,3,2**	250	45	34.9	76	42.90	80	2.70	0.170	680	White
0603HP-36NX_L_	36	**5,3,2**	250	44	38.5	69	50.00	64	2.50	0.225	720	Red
0603HP-39NX_L_	39	**5,3,2**	250	48	41.5	78	51.90	74	2.45	0.19	680	Black
0603HP-43NX_L_	43	**5,3,2**	250	45	45.7	83	58.10	76	2.45	0.17	810	Orange
0603HP-47NX_L_	47	**5,3,2**	200	47	50.6	77	66.90	72	2.30	0.24	680	Brown
0603HP-51NX_L_	51	**5,3,2**	200	49	54.6	73	71.30	62	2.30	0.28	660	Blue
0603HP-56NX_L_	56	**5,3,2**	200	50	60.3	74	79.90	56	2.20	0.30	610	Red
0603HP-68NX_L_	68	**5,3,2**	200	46	75.5	73	113.3	49	2.00	0.33	600	Orange
0603HP-72NX_L_	72	**5,3,2**	150	46	80.8	69	—	—	1.90	0.42	550	Yellow
0603HP-75NX_L_	75	**5,3,2**	150	46	84.6	71	—	—	1.90	0.52	500	Violet
0603HP-82NX_L_	82	**5,3,2**	150	45	94.0	62	—	—	1.80	0.46	510	Green
0603HP-91NX_L_	91	**5,3,2**	150	45	103.0	64	—	—	1.65	0.58	440	White
0603HP-R10X_L_	100	**5,3,2**	150	49	114.0	69	—	—	1.70	0.54	470	Blue
0603HP-R11X_L_	110	**5,3,2**	150	47	126.2	63	—	—	1.60	0.58	440	Violet
0603HP-R12X_L_	120	**5,3,2**	150	47	142.4	61	—	—	1.55	0.72	420	Gray
0603HP-R15X_L_	150	**5,3,2**	150	47	188.8	57	—	—	1.35	0.82	390	White
0603HP-R18X_L_	180	**5,3,2**	100	48	232.2	50	—	—	1.30	1.50	310	Black
0603HP-R20X_L_	200	**5,3,2**	100	47	265.0	47	—	—	1.25	2.00	280	Green
0603HP-R21X_L_	210	**5,3,2**	100	48	288.0	45	—	—	1.20	2.00	280	Gray
0603HP-R22X_L_	220	**5,3,2**	100	47	315.0	41	—	—	1.10	2.00	280	Brown
0603HP-R25X_L_	250	**5,3,2**	100	45	—	—	—	—	1.05	3.00	240	Violet
0603HP-R27X_L_	270	**5,3,2**	100	46	—	—	—	—	1.05	2.25	260	Red
0603HP-R30X_L_	300	**5,3,2**	100	47	—	—	—	—	0.99	2.80	220	Green
0603HP-R33X_L_	330	**5,3,2**	100	46	—	—	—	—	0.93	3.60	180	Blue
0603HP-R36X_L_	360	**5,3,2**	100	47	—	—	—	—	0.93	4.00	170	Gray
0603HP-R39X_L_	390	**5,3,2**	100	47	—	—	—	—	0.88	4.00	170	Yellow

1. When ordering, please specify tolerance, termination and packaging codes:

0603HP-R39XJLW

Tolerance: G = 2% H = 3% J = 5%
(Table shows stock tolerances in bold.)

Termination: L = RoHS compliant silver-palladium-platinum-glass frit.
E = Halogen free component. RoHS compliant silver-palladium-platinum-glass frit terminations.
Special order: T = RoHS tin-silver-copper (95.5/4/0.5) or S = non-RoHS tin-lead (63/37).

Packaging: W = 7" machine-ready reel. EIA-481 punched paper tape (2000 parts per full reel).
U = Less than full reel. In tape, but not machine ready. To have a leader and trailer added ($25 charge), use code letter W instead.

2. Inductance tested at listed frequency using an Agilent/HP 4286A impedance analyzer with a Coilcraft SMD-A fixture and Coilcraft-provided correlation pieces.
3. Q measured using an Agilent/HP 16197 test fixture in an Agilent/HP 4291 impedance analyzer.
4. SRF measured using an Agilent/HP 8722ES network analyzer and a Coilcraft SMD-D test fixture.
5. DCR measured on a micro-ohmmeter and a Coilcraft CCF858 test fixture.
6. Current that causes a 15°C temperature rise from 25°C ambient.
7. Electrical specifications at 25°C.

Refer to Doc 362 "Soldering Surface Mount Components" before soldering.

Coilcraft
www.coilcraft.com

US +1-847-639-6400 sales@coilcraft.com
UK +44-1236-730595 sales@coilcraft-europe.com
Taiwan +886-2-2264 3646 sales@coilcraft.com.tw
China +86-21-6218 8074 sales@coilcraft.com.cn
Singapore + 65-6484 8412 sales@coilcraft.com.sg

Document 537-2 Revised 03/25/13

Panasonic Thick Film Chip Resistors

■ Construction

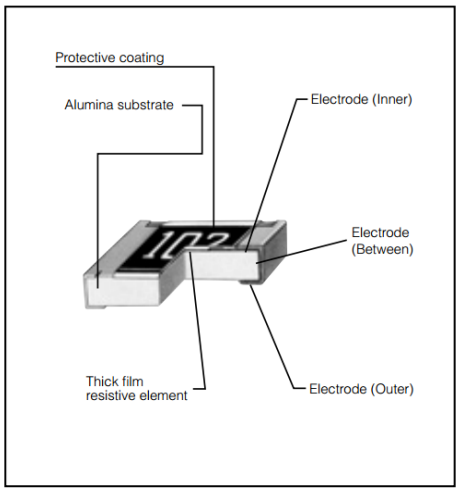

■ Dimensions in mm (not to scale)

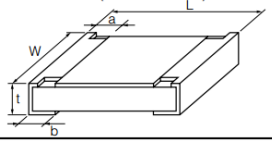

Type (inch size)	Dimensions (mm) L	W	a	b	t	Mass (Weight) (g/1000 pcs.)
ERJXG (01005)	$0.40^{\pm0.02}$	$0.20^{\pm0.02}$	$0.10^{\pm0.03}$	$0.10^{\pm0.03}$	$0.13^{\pm0.02}$	0.04
ERJ1G (0201)	$0.60^{\pm0.03}$	$0.30^{\pm0.03}$	$0.10^{\pm0.05}$	$0.15^{\pm0.05}$	$0.23^{\pm0.03}$	0.15
ERJ2G (0402)	$1.00^{\pm0.05}$	$0.50^{\pm0.05}$	$0.20^{\pm0.10}$	$0.25^{\pm0.05}$	$0.35^{\pm0.05}$	0.8
ERJ3G (0603)	$1.60^{\pm0.15}$	$0.80^{+0.15}_{-0.05}$	$0.30^{\pm0.20}$	$0.30^{\pm0.15}$	$0.45^{\pm0.10}$	2
ERJ6G (0805)	$2.00^{\pm0.20}$	$1.25^{\pm0.10}$	$0.40^{\pm0.20}$	$0.40^{\pm0.20}$	$0.60^{\pm0.10}$	4
ERJ8G (1206)	$3.20^{+0.05}_{-0.20}$	$1.60^{+0.05}_{-0.15}$	$0.50^{\pm0.20}$	$0.50^{\pm0.20}$	$0.60^{\pm0.10}$	10
ERJ14 (1210)	$3.20^{\pm0.20}$	$2.50^{\pm0.20}$	$0.50^{\pm0.20}$	$0.50^{\pm0.20}$	$0.60^{\pm0.10}$	16
ERJ12 (1812)	$4.50^{\pm0.20}$	$3.20^{\pm0.20}$	$0.50^{\pm0.20}$	$0.50^{\pm0.20}$	$0.60^{\pm0.10}$	27
ERJ12Z (2010)	$5.00^{\pm0.20}$	$2.50^{\pm0.20}$	$0.60^{\pm0.20}$	$0.60^{\pm0.20}$	$0.60^{\pm0.10}$	27
ERJ1T (2512)	$6.40^{\pm0.20}$	$3.20^{\pm0.20}$	$0.65^{\pm0.20}$	$0.60^{\pm0.20}$	$0.60^{\pm0.10}$	45

■ Ratings

<For Resistor>

Type (inch size)	Power Rating at 70 °C (W)	Limiting Element Voltage(1) (V)	Maximum Overload Voltage(2) (V)	Resistance Tolerance (%)	Resistance Range (Ω)	T.C.R. ($\times10^{-6}$/°C)	Category Temperature Range (°C)
ERJXG (01005)	0.031	15	30	±5	4.7 to 1 M (E24)	<10 Ω : −100 to +600 10 Ω to 100 Ω : ±300 100 Ω< : ±200	−55 to +125
ERJ1G (0201)	0.05	25	50	±5	1 to 10 M (E24)	<10 Ω: −100 to +600 10 Ω to 1 MΩ: ±200 1 MΩ<: −400 to +150	−55 to +125
ERJ2G (0402)	0.1	50	100	±5	1 to 10 M (E24)		−55 to +155
ERJ3G (0603)	0.1	75	150	±5	1 to 10 M (E24)		−55 to +155
ERJ6G (0805)	0.125	150	200	±5	1 to 10 M (E24)		−55 to +155
ERJ8G (1206)	0.25	200	400	±5	1 to 10 M (E24)		−55 to +155
ERJ14 (1210)	0.5	200	400	±5	1 to 10 M (E24)		−55 to +155
ERJ12 (1812)	0.75	200	500	±5	1 to 10 M (E24)		−55 to +155
ERJ12Z (2010)	0.75	200	500	±5	1 to 10 M (E24)		−55 to +155
ERJ1T (2512)	1	200	500	±5	1 to 1 M (E24)		−55 to +155

(1) Rated Continuous Working Voltage (RCWV) shall be determined from RCWV=$\sqrt{\text{Power Rating} \times \text{Resistance Values}}$, or Limiting Element Voltage listed above, whichever less.
(2) Overload (Short-time Overload) Test Voltage (SOTV) shall be determined from SOTV=2.5 (Only ERJ2G=2.0) × Power Rating or max. Overload Voltage listed above whichever less.

<For Jumper>

Type (inch size)	Rated Current (A)	Maximum Overload Current (A)
ERJXG (01005)	0.5	1
ERJ1G (0201)		
ERJ2G (0402)	1	2
ERJ3G (0603)		
ERJ6G (0805)	2	4
ERJ8G (1206)		
ERJ14 (1210)		
ERJ12 (1812)		
ERJ12Z (2010)		
ERJ1T (2512)		

Power Derating Curve

For resistors operated in ambient temperatures above 70 °C, power rating shall be derated in accordance with the figure below.

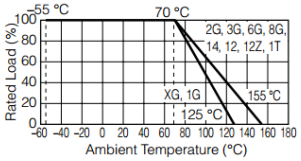

02 Aug. 2012

Substrate TLY – 5

TLY-5 TYPICAL VALUES					
Property	Test Method	Units	Value	Units	Value
Dielectric Constant @ 10 GHz	IPC-TM 650 2.5.5.5		2.20		2.20
Dissipation Factor @ 10 GHz	IPC-TM 650 2.5.5.5		0.0009		0.0009
Moisture Absorption	IPC-TM 650 2.6.2.1	%	<0.02	%	<0.02
Dielectric Breakdown	IPC-TM 650 2.5.6	kV	>60	kV	>60
Volume Resistivity	IPC-TM 650 2.5.17.1	Mohm/cm	10^7	Mohm/cm	10^7
Surface Resistivity	IPC-TM 650 2.5.17.1	Mohm	10^7	Mohm	10^7
Arc Resistance	IPC-TM 650 2.5.1	seconds	>180	seconds	>180
Flexural Strength Lengthwise	IPC-TM 650 2.4.4	lbs./in.	>12,000	N/mm^2	>83
Flexural Strength Crosswise	IPC-TM 650 2.4.4	lbs./in.	>10,000	N/mm^2	>69
Peel Strength (1oz copper)	IPC-TM 650 2.4.8	lbs./linear in.	12.0	N/mm	2.1
Thermal Conductivity	ASTM F 433	W/m/K	0.22	W/m/K	0.22
x-y CTE	ASTM D 3386 (TMA)	ppm/°C	20	ppm/°C	20
z CTE	ASTM D 3386 (TMA)	ppm/°C	280	ppm/°C	280
UL-94 Flammability Rating	UL-94		V-0		V-0

Type	Dk
TLY-5A	2.17
TLY-5	2.20
TLY-3	2.33
TLT-0 | TLX-0	2.45
TLT-9 | TLX-9	2.50
TLT-8 | TLX-8	2.55
TLT-7 | TLX-7	2.60
TLT-6 | TLX-6	2.65
TLE-95	2.95
TLC-27	2.75
TLC-30	3.00
TLC-32	3.20
RF-30	3.00
RF-35 | RF-35P	3.50
RF-60	6.15
CER-10	10

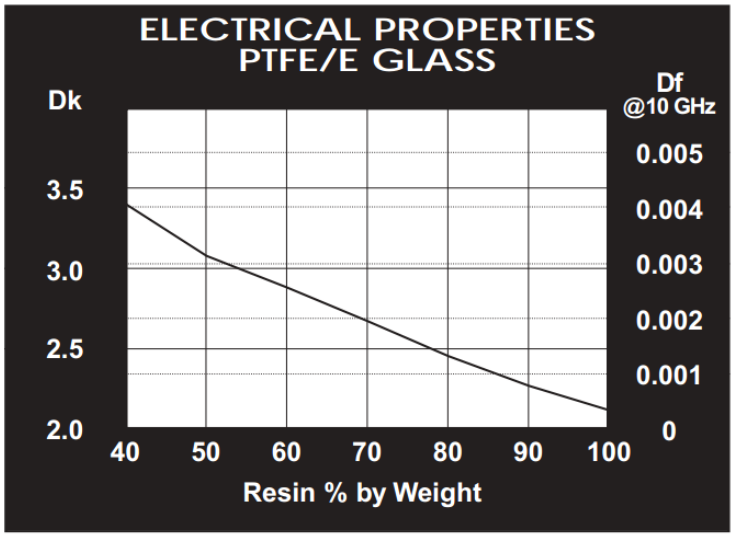

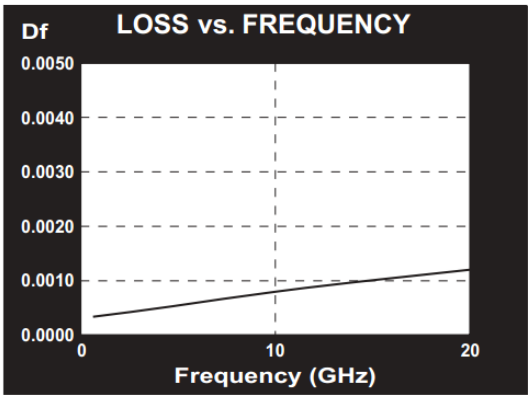

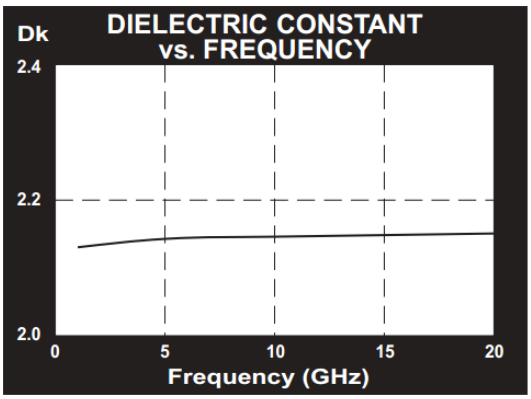

Noise Tube NC 346B

Noisecom

Data Sheet

NC346
10 MHz to 55 GHz

Broadband Calibrated Noise Sources for Noise Figure Measurements

The Noisecom NC346 Series is designed for precision noise figure measurement applications. The VSWR has been improved, reducing multiple reflections of the test signals and significantly increasing the measurement accuracy of most noise figure set-ups.

The NC346 Series noise sources have broadband coverage and extremely good temperature and voltage stability, for the finest noise figure meter-compatible laboratory standards. Outputs of 6, 15.5 and 22 dB ENR are available, allowing the units to accurately measure noise figures up to 20, 30 and 36 dB respectively.

The return loss of the noise sources is measured in both the on and off states and is included in the calibration report provided with each noise source up to 40 GHz. Each noise source is also supplied with calibration data traceable to NIST.

Specifications

Calibration	1 GHz steps
Temperature coefficient	Less than 0.009 dB/°C
Operating temperature	0°C to +55°C
Input power	+28 VDC ±2 VDC at 15 mA typical for NC346 A, B & D
VSWR	Less than 1.15:1 from 10 MHz – 5 GHz for units with 5 – 7 dB or 14 –16 dB ENR
Regulator	Built-in
Voltage coefficient	< 0.002 dB/%ΔV

VSWR **Typical VSWR for NC346C**

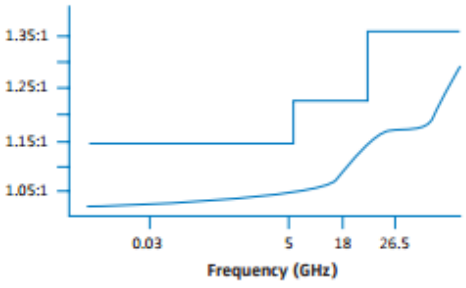

Count on the Noise Leader

NC346 Coaxial Series

Model	RF Connector	Frequency (GHz)	Output ENR (dB)	VSWR (maximum @ on/off) 0.01 - 5 GHz	5 - 18 GHz	18 - 26.5 GHz	26.5 - 40 GHz	40 - 60 GHz	I (max) (mA)
NC346A	SMA Male	0.01 - 18.0	5 - 7	1.15:1	1.25:1				30
NC346A Precision	APC3.5 Male	0.01 - 18.0	5 - 7	1.15:1	1.25:1				30
NC346A Option 1	N Male	0.01 - 18.0	5 - 7	1.15:1	1.25:1				30
NC346A Option 2	APC7	0.01 - 18.0	5 - 7	1.15:1	1.25:1				30
NC346A Option 4	N Female	0.01 - 18.0	5 - 7	1.15:1	1.25:1				30
NC346B	SMA Male	0.01 - 18.0	14 - 16	1.15:1	1.25:1				30
NC346B Precision	APC3.5 Male	0.01 - 18.0	14 - 16	1.15:1	1.25:1				30
NC346B Option 1	N Male	0.01 - 18.0	14 - 16	1.15:1	1.35:1				30
NC346B Option 2	APC7	0.01 - 18.0	14 - 16	1.15:1	1.25:1				30
NC346B Option 4	N Female	0.01 - 18.0	14 - 16	1.15:1	1.35:1				30
NC346C	APC3.5 Male	0.01 - 26.5	13 - 17	1.15:1	1.25:1	1.35:1			30
NC346D	SMA Male	0.01 - 18.0	19 - 25*	1.50:1	1.50:1				30
NC346D Precision	APC3.5 Male	0.01 - 18.0	19 - 25*	1.50:1	1.50:1				30
NC346D Option 1	N Male	0.01 - 18.0	19 - 25*	1.50:1	1.75:1				30
NC346D Option 2	APC7	0.01 - 18.0	19 - 25*	1.50:1	1.50:1				30
NC346D Option 3	N Female	0.01 - 18.0	19 - 25*	1.50:1	1.75:1				30
NC346E	APC3.5 Male	0.01 - 26.5	19 - 25*	1.50:1	1.50:1	1.50:1			30
NC346Ka	K Male**	0.10 - 40.0	10 - 17	v1.25:1	1.30:1	1.40:1	1.50:1		30
NC346V	V Male	0.10 - 55.0	7 - 21	1.50:1	1.50:1	1.75:1	2.00:1	2.50:1	30

* Flatness better than ±2 dB ** Compatible with SMA and APC3.5

NC346 Waveguide Series (inches)

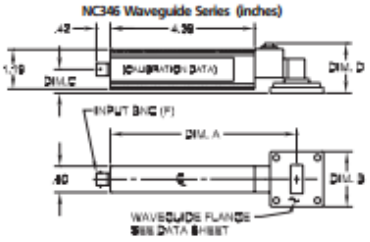

NC346 Coaxial Series Dimensions (inches)

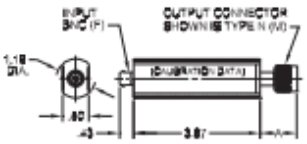

Waveguide Flange Chart

Waveguide Type	DIM A(in.)	DIM B(in.)	DIM C(in.)	DIM D(in.)
WR75	5.25	1.50 SQ	.98	1.60
WR90	5.68	1.68 SQ	72	1.50
WR229	6.02	3.87	1.10	2.09

CONNECTOR	DIM A (in.)
SMA Male	0.50
APC 3.5 Male	0.50
N Male	1.14
APC 7	1.30
N Female	0.94
K Male	0.46
V Male	0.85

Mounting bracket available, order option NC346optMB

NC346 Waveguide Series (Built-In Isolator*)

Model	Flange	Frequency (GHz)	ENR (dB)	VSWR (on/off)	I (max) (mA)
NC346B-WR229	CPR229F	3.7 - 4.2	14 - 16**	1.20:1	30
NC346B-WR90	UG39/U	8.5 - 9.6	14 - 16**	1.20:1	30
NC346B-WR75	UBR120	10.5 - 13.0	14 - 16**	1.20:1	30

*Inquire for other flanges or waveguide sizes **Flatness better than ±0.15 dB

Wireless Telecom Group
Boonton Microlab Noisecom

Wireless Telecom Group Inc.
25 Eastmans Rd
Parsippany, NJ
United States
Tel: +1 973 386 9696
Fax: +1 973 386 9191
www.noisecom.com

N/NC346/0611/EN

APPENDIX B

MICROWAVE OFFICE FROM AWR

Microwave Office RF/microwave design software encompasses all the tools essential for high frequency IC, PCB and module design, including:

- Linear and Non-linear circuit simulators
- Electromagnetic (EM) analysis tools
- Integrated schematic and layout
- Built-in elements s-parameter library
- Parametric cell libraries with built-in design-rule check (DRC)

. The version used during this PhD research study was 2010 and 2011.

B. 1. Instruction to use Microwave Office from AWR

Microwave Office has simple interface. The linear circuit simulator is the main tool used for this work. The first step is to set the global project units and parameters from the Options tab, Project Option as shown in Fig. B.1. From the new window, it is possible to set the frequency range, the frequency step size and the global units. Next is to create a new schematic, from the project tab, add schematic as shown in Fig. B.2

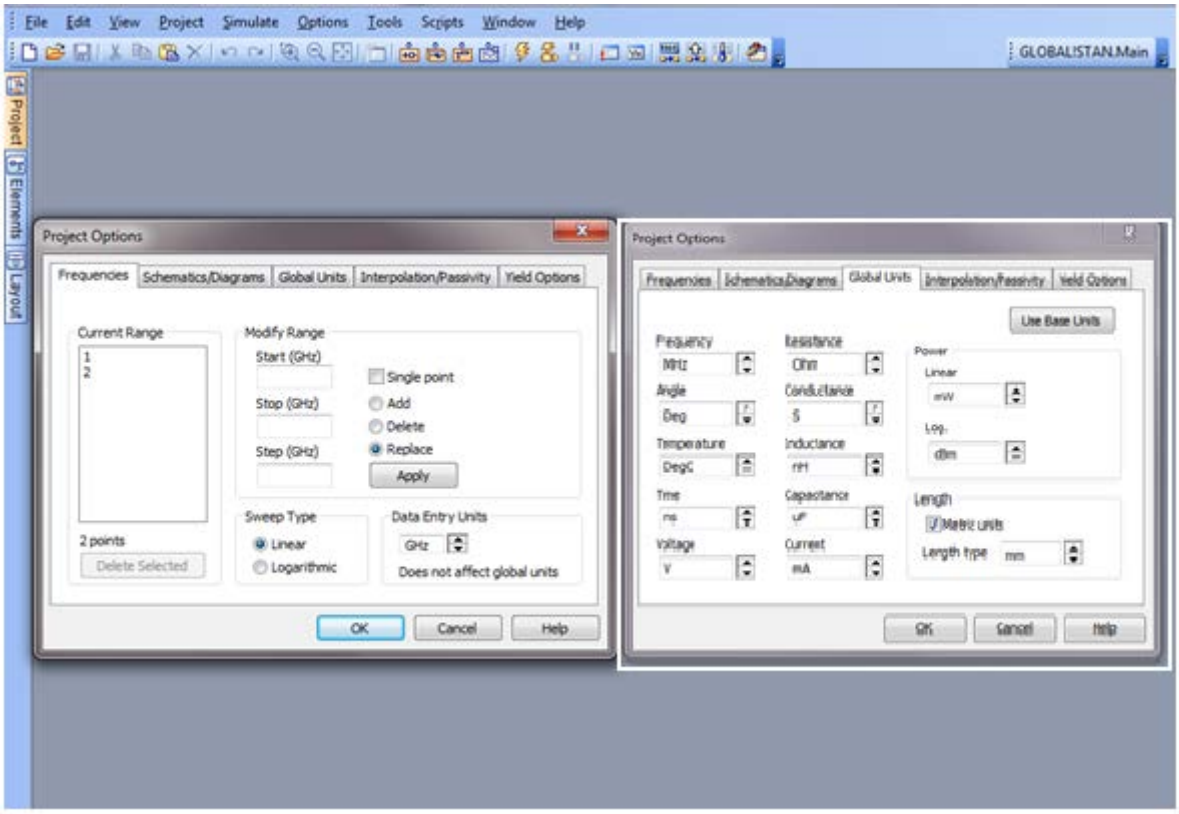

Fig.B.1 Project Options

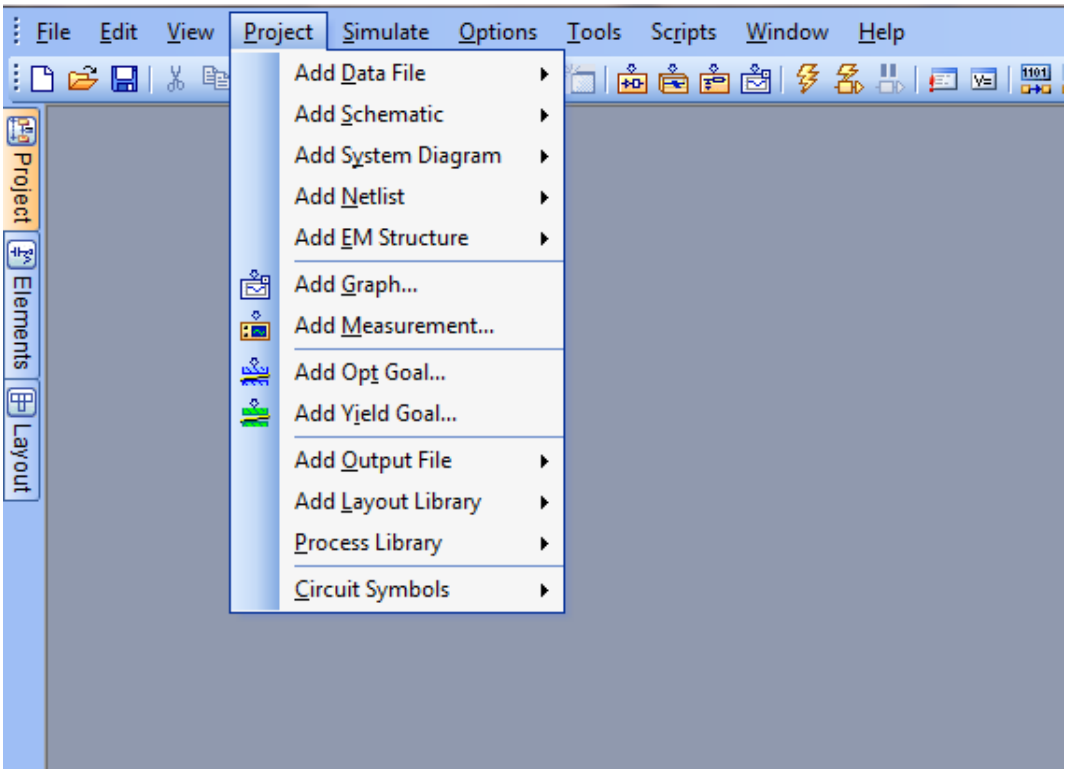

Fig. B.2 Schematic test

There are additional tools that can be used to help optimise design parameters such as the tuner and the optimiser. These tools need setting up and appropriate goals and targets set. The location of the tuner and optimiser tools are shown in Fig.B.3.

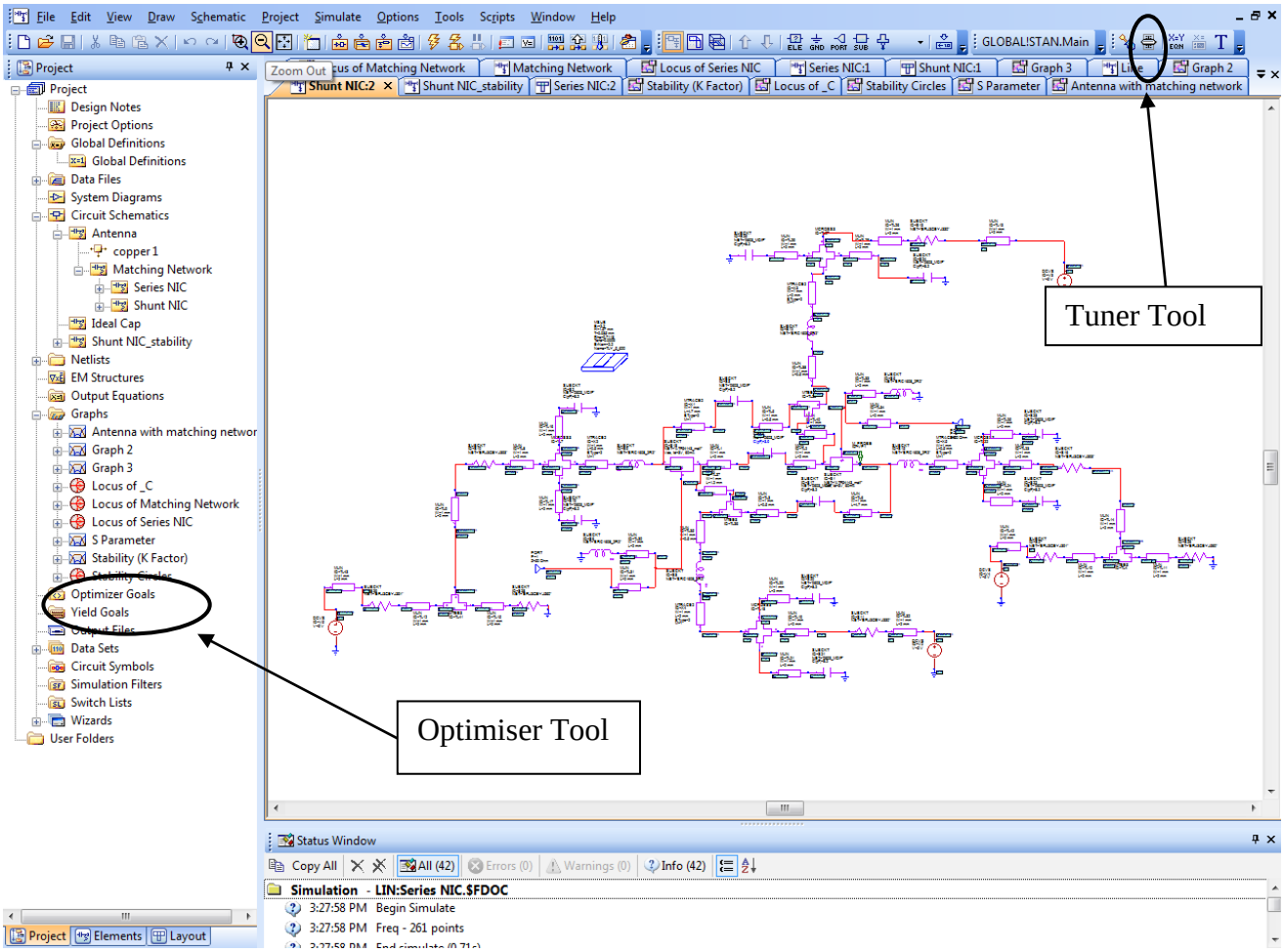

Fig.B.3 AWR tools: Optimiser and Tuner

AWR design environment also provides access to S- parameter files of components from manufacturers as well as providing ideal components. This can be found under the elements tab, searches can be done either by type or vendor as shown in Fig.B.4.

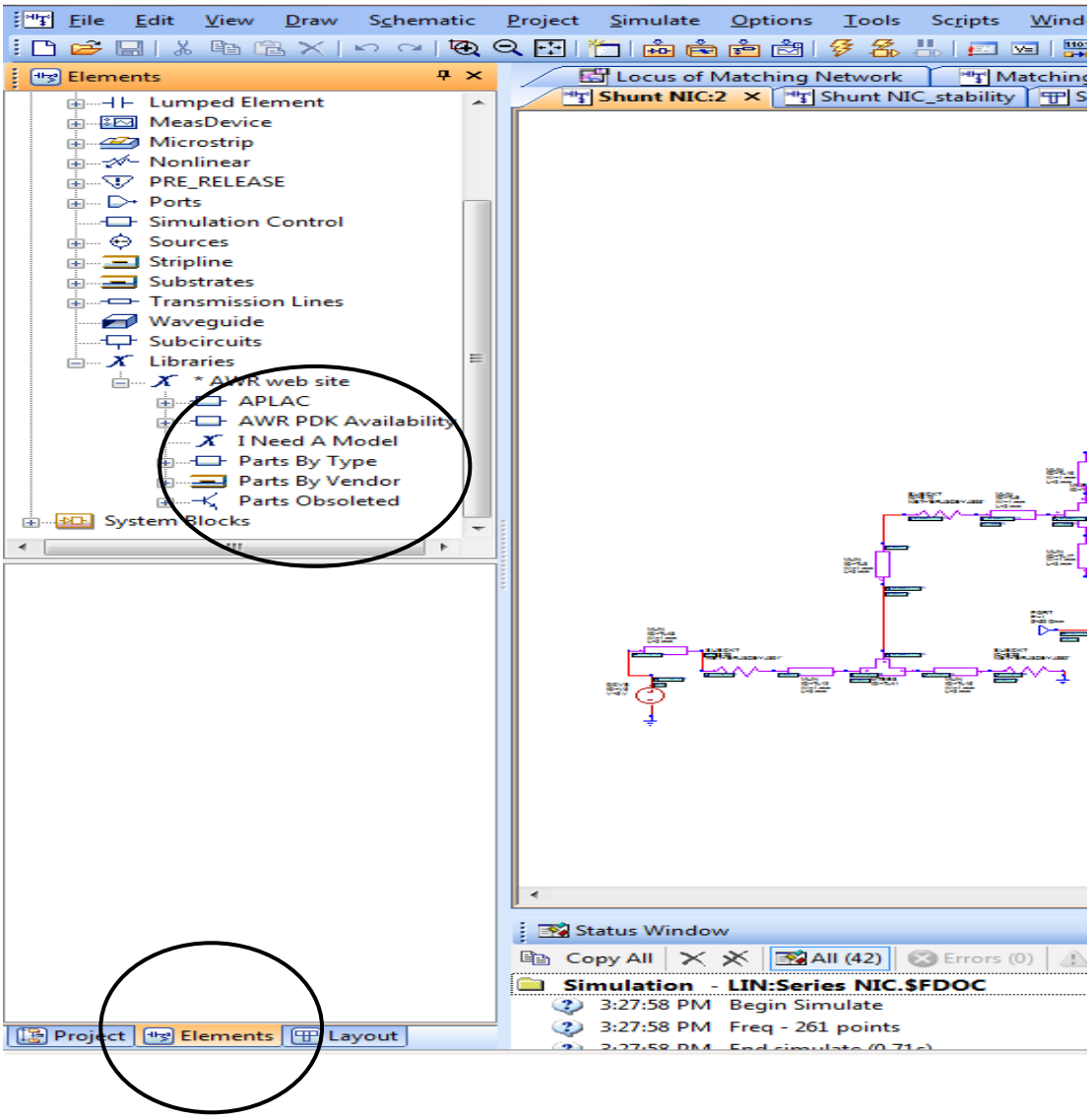

Fig.B.4 Manufacturer element's S - parameters

Appendix C

CST Microwave Studio

CST Microwave Studio is a three dimensional finite integral full wave simulator. It has a frequency domain solver that is fast, accurate and efficient. It offers EM simulations for structures with results ranging from S-parameters for simple designs and far-field plots for antennas. The versions used for this PhD research are 2009, 2010, 2011 and 2012.

C.1. The Use of CST Microwave Studio

Within CST there are some templates, as shown in Fig. C.1, that helps specify the basic conditions for the simulating antenna and other structures. The specified criteria are the units, the background material, the boundary conditions and the mesh sizes. These conditions can be changed within the simulator to mean individual demands.

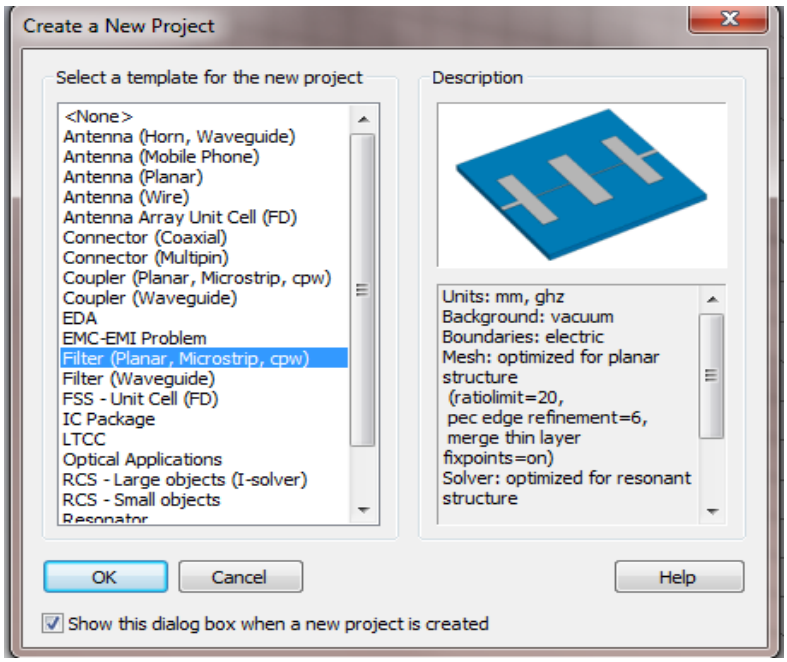

Fig. C.1. CST template

CST also offers the simple 3D shapes also referred to as primitives from which other complex shapes can be obtained by various Boolean operations like subtract, intersect, trim, add and insert. The NIC structures and antenna were formed from these primitives. Fighdhd shows the location of these primitives in the CST design screen. From the solve menu, it is possible to set the simulation parameters such as the frequency range, background materials etc.

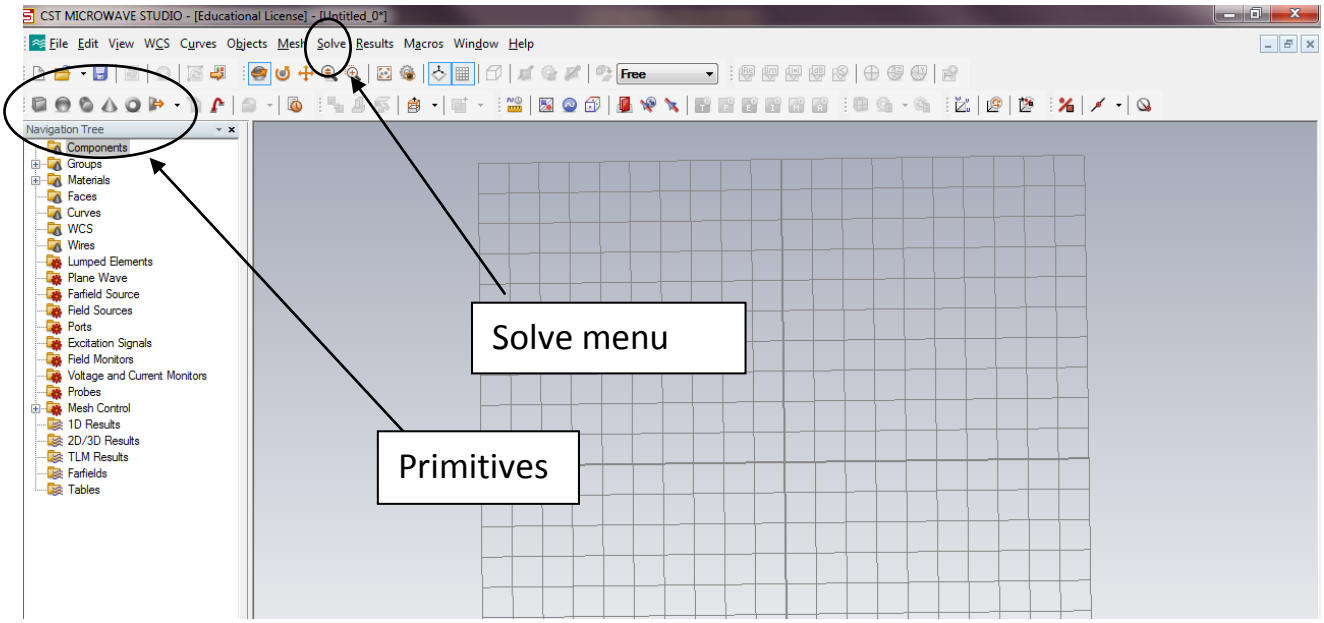

Fig. C.2. CST design screen highlighting the primitives and the solve menu

Appendix D

D.1. S Parameters

S parameters, or scattering parameters [1], are the reflection and transmission coefficients between the incident and reflection voltage waves mostly operating at radio frequency and microwave frequencies. S parameters change with frequency and each parameter is typically characterized by a magnitude and phase.

D.2. Measurement Equipments

S parameters can be measured using vector network analyzer (VNA), shown in Fig. D.1.

Fig. D. 1. Picture of vector network analyzer

The radiation patterns (amplitude and phase), polarization, and gain of antenna, which are used to characterize the radiation capabilities of an antenna, are measured using the typical instrumentation, shown in Fig. D. 2. Such antenna range instrumentation must be designed to cover a wide range of frequency operation band, and it usually can be classified into five categories [3] as below:

1. source antenna and transmitting system
2. receiving system
3. positioning system
4. recording system
5. data-processing system

For all the antennas design during this work, their radiation patterns and gain were measured inside an anechoic chamber.

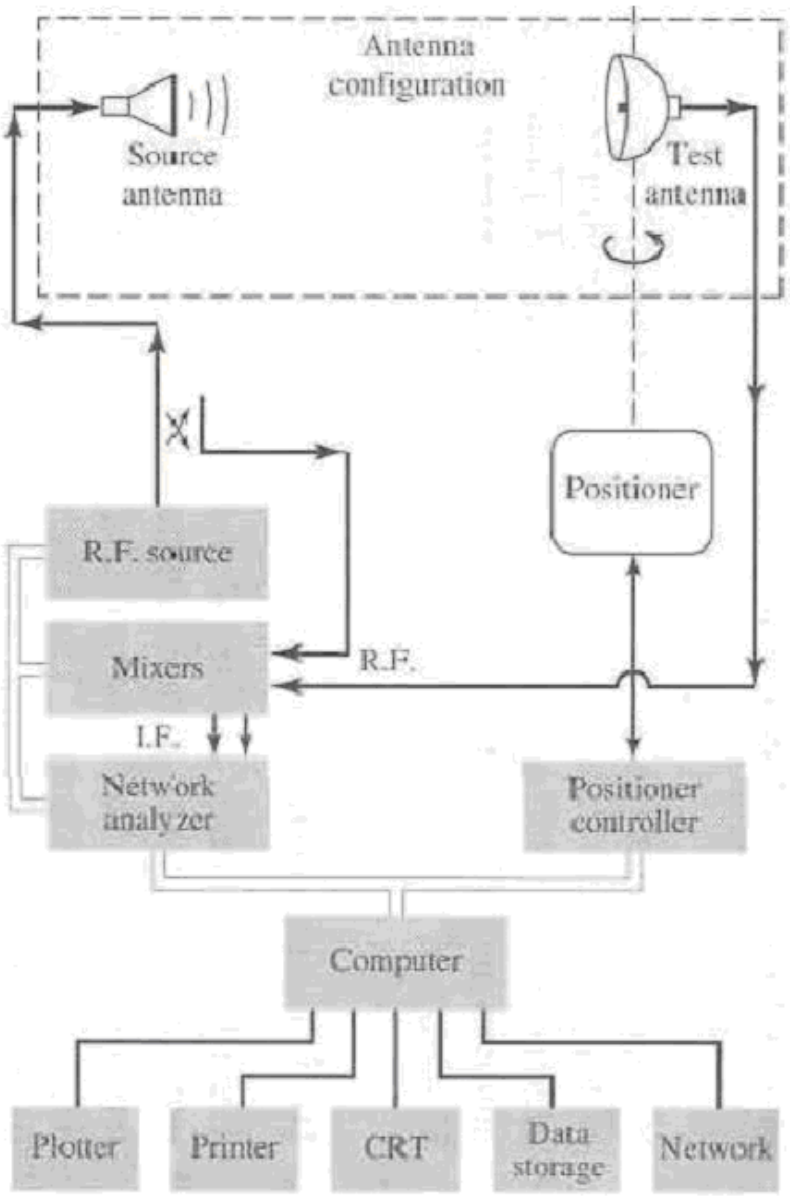

Fig. D. 2. Block diagrams of typical instrumentations for measuring antenna patterns [2]

D.3. Antenna Parameters

Directivity

The directivity of an antenna can be defined as the ration of the radiation intensity of the antenna in a given direction to the radiation intensity averaged over all directions [1]. The average radiation intensity is equal to the total power radiated by the antenna divided by 4π.

Equation D.1 shows the equation for calculating the directivity of a non-isotropic antenna. When direction is not specified the maximum directivity implies the direction of maximum radiation intensity.

$$D = \frac{U}{U_0} = \frac{4\pi U}{P_{rad}} \quad \text{D.1}$$

$$D_{max} = \frac{4\pi U_{max}}{P_{rad}} \quad \text{D.2}$$

Where D is directivity

D_0 is maximum directivity

U is the radiation intensity

U_{max} is maximum radiation intensity

U_0 is radiation intensity of an isotropic source

P_{rad} is total radiated power

Gain

The absolute gain of an antenna is the ratio of the radiation intensity of the antenna in a specified direction to the radiation intensity of the antenna if it were isotropic. These can be expressed as shown in equation D.3.

$$Gain = 4\pi \frac{radiation\ intensity}{total\ input\ power} = 4\pi \frac{U(\theta, \varphi)}{P_{in}} \quad \text{D.3}$$

However, the commonly quoted gain is the relative gain, which is also what is quoted within this thesis is the ratio of the power gain in a given direction to the power gain of a reference

antenna. In doing this measurements / calculations, it is assumed that the power inputs are the same for both antennas. The reference antenna is usually an antenna whose gain can be calculated or known. For this thesis the reference antenna is the ETS-LINDGREN Quad ridge guide antenna with model number 3164-03 and serial number 00062674..

However, power in (Pin) in equation D.3 is assumed to be from a lossless isotropic source. The radiated power, Prad, can be calculated from the Pin by using equation D.4

$$P_{rad} = e_{cd} P_{in} \qquad \text{D.4}$$

Where,

P_{rad} is the radiated power

e_{cd} is the radiation efficiency and

P_{in} is the total power in (power into the antenna from an isotropic source)

Antenna Efficiency

Antenna total efficiency e_0 is used to account for the losses through and at the terminals of the antenna and also the losses within the antenna structure. These losses can be broadly categorised into two

1. Reflection or mismatch losses and
2. Material or antenna structural losses

There total efficiency of an antenna can be written as

$$e_0 = e_r e_c e_d \qquad \text{D.5}$$

e_r is the reflection efficiency (mismatch) = $(1 - |\Gamma|^2)$

e_c is the conduction efficiency

e_d is the dielectric efficiency

Usually, e_c and e_d are combined to represent the antenna radiation efficiency (e_{cd}).

Therefore antenna total efficiency can be represented as

$$\text{Total efficiency} = \text{Radiation efficiency} \times (1 - |\Gamma|^2) \qquad \text{D.6}$$

The radiation efficiency of an antenna can be related to its gain and directivity by equation D.7

$$G(\theta, \varphi) = e_{cd} D(\theta, \varphi) \qquad \text{D.7}$$

It should also be noted here that the gain discussed above doesn't include the loss due to mismatch.

D.4. S-Parameters

The scattering matrix provides a complete description of the network as seen from its N ports. It relates the voltage incident on the ports to those reflected from the ports. Scattering matrix parameters are easily measured from a VNA and these parameters can be easily converted into other matrix parameters if required.

$$\begin{bmatrix} V^-_1 \\ \vdots \\ V^-_N \end{bmatrix} = \begin{bmatrix} S_{11} & \cdots & S_{1N} \\ \vdots & \ddots & \vdots \\ S_{N1} & \cdots & S_{NN} \end{bmatrix} \begin{bmatrix} V^+_1 \\ \vdots \\ V^+_N \end{bmatrix}$$

Specific elements with the S matrix can be determined as

$$S_{ij} = \left.\frac{V^-{}_i}{V^+{}_j}\right|_{V_k{}^+=0\ for\ k\neq j}$$

D.5. Gain Measurement procedure

For gain measurements, the following equipment are required within the anechoic chamber

1. Vector Network Analyser (VNA)
2. Two wideband antennas working within the same frequency as the Device Under Test (DUT)

Follow the steps below to measure the gain of the DUT

1. The two wideband antennas are setup at the two ends of the anechoic chamber
2. The VNA is calibrated to measure S21 and normalise the measurement set up.
3. One of the wideband antennas is substituted with the DUT and the resultant S21 is measured
4. The measured S21 with the DUT is then added to the gain of the substituted wideband antenna to obtain the gain of the antenna.
5. The difference between the measured S21 of the wideband antenna and the measured S21 of the DUT is the gain of the DUT.

In this thesis, the wideband antenna used is the ETS-LINDGREN Quad ridge guide antenna with model number 3164-03 and serial number 00062674.

Reference:

[1] D. M. Poza, Microwave Engineering, 2nd ed: John Wiley & Sons, Inc, 1998

[2] C. A. Balanis, Antenna Theory, Analysis and Design, 3rd ed: John Wiley & Sons, Inc, 2005

[3] IEEE Standard Test Procedures for Antennas, IEEE Std 149-1979, Published by IEEE, Inc., 1979, Distributed by Wiley-Interscience.

APPENDIX E

MANUFACTURE OF PRINTED CIRCUIT BOARD

E.1. Printed Circuit Broad (PCB)

In recent times, printed antennas have attracted increasing interest due to their simple manufacture. The most economic way to build a printed circuit broad (PCB) is photoengraving, which uses a photo mask and etchant to selectively remove a photo resist coating. The remaining photo resist protects the copper foil. Subsequent etching removes the unwanted copper. If you are using “Pre Coated FR4” as the PCB material, then you will need to create a Photo Positive master. However, if a Duroid is used or a similar uncoated substrate, then the process to coat this material is different, in that a “Photo Negative” artwork is required and you will need to ensure you design your layout accordingly.

For multilayer designs like the Linvill’s NIC, each layer is fabricated separately and the via holes are made into each layer and these vias connect the two layers together. Fig.E.1 shows the top layer layout of the Linvill’s NIC with the location of the vias. The holes are drilled into the PCB and rivets 0.8mm diameter are inserted into these holes.

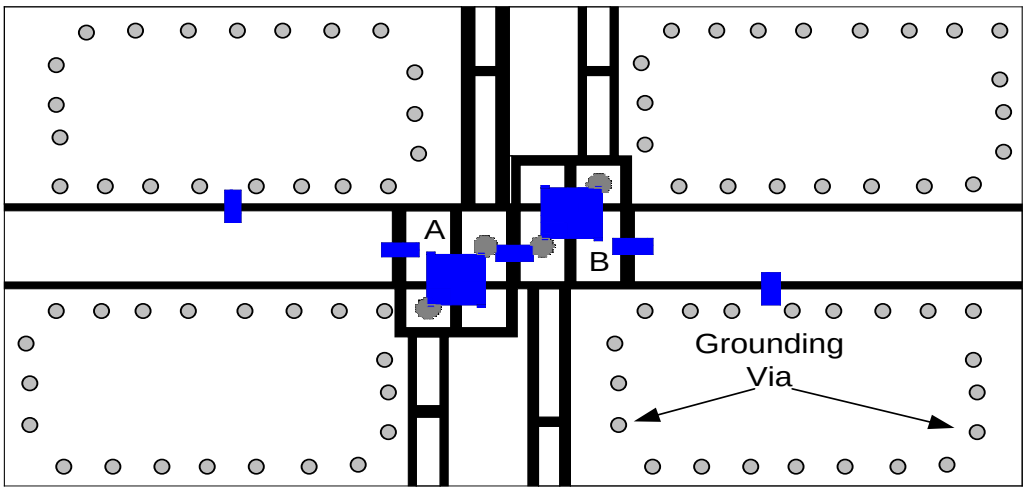

Fig.E.1. Via Layout on Linvill NIC